



**US Army Corps
of Engineers®**
Engineer Research and
Development Center



Mississippi River Hydrodynamic and Delta Management Study: Delta Management Modeling

AdH/SEDLIB Multi-Dimensional Model Validation and Scenario Analysis Report

Gary L. Brown, Jennifer N. McAlpin, Kimberly C. Pevey,
Phu V. Luong, Cherie R. Price, and Barbara A. Kleiss

March 2019



The U.S. Army Engineer Research and Development Center (ERDC) solves the nation's toughest engineering and environmental challenges. ERDC develops innovative solutions in civil and military engineering, geospatial sciences, water resources, and environmental sciences for the Army, the Department of Defense, civilian agencies, and our nation's public good. Find out more at www.erdclibrary.usace.army.mil.

To search for other technical reports published by ERDC, visit the ERDC online library at <http://acwc.sdp.sirsi.net/client/default>.

Mississippi River Hydrodynamic and Delta Management Study: Delta Management Modeling

AdH/SEDLIB Multi-Dimensional Model Validation and Scenario Analysis Report

Gary L. Brown, Jennifer N. McAlpin, Kimberly C. Pevey,
and Phu V. Luong

*Coastal and Hydraulics Laboratory
U.S. Army Engineer Research and Development Center
3909 Halls Ferry Road
Vicksburg, MS 39180-6199*

Cherie R. Price

*USACE New Orleans District
7400 Leake Ave
New Orleans, LA 70118*

Barbara A. Kleiss

*USACE Mississippi Valley Division
1400 Walnut Street
Vicksburg, MS 39180*

Final report

Approved for public release; distribution is unlimited.

Prepared for U.S. Army Corps of Engineers, New Orleans District
7400 Leake Ave.
New Orleans, LA 70118

Under Project No. 142871, "Mississippi River Hydrodynamic and Delta Management Study"

Abstract

This report details the process of developing and validating a multi-dimensional hydrodynamic, salinity, sediment transport, and coastal wetland morphology model of the Lower Mississippi River Delta. This model has been developed to run various sediment diversion scenarios. The results of these scenario analyses are documented in this report.

The morphologic modeling results for the diversion scenario analyses show net land gain in the near vicinity of the diversion outlets and net land loss farther away from the outlets. The areas of land gain roughly correspond with the zones of sand deposition whereas the areas of largest land loss correspond with areas where there is diversion-induced inundation but not significant deposition of sediment from the diversion. The modeling results indicate that diversion-induced inundation results in a reduction in plant productivity, which induces an acceleration of land loss.

Significant uncertainty exists with respect to the response of the existing wetland vegetation to diversion-induced inundation. The magnitude of this uncertainty can only be narrowed with further consensus building within wetland science.

With respect to salinity, the receiving waters tend to freshen significantly during diversion operations. However, when operations cease, the recovery of salinity is almost entirely determined by prevailing offshore and/or riverine conditions.

DISCLAIMER: The contents of this report are not to be used for advertising, publication, or promotional purposes. Citation of trade names does not constitute an official endorsement or approval of the use of such commercial products. All product names and trademarks cited are the property of their respective owners. The findings of this report are not to be construed as an official Department of the Army position unless so designated by other authorized documents.

DESTROY THIS REPORT WHEN NO LONGER NEEDED. DO NOT RETURN IT TO THE ORIGINATOR.

Contents

Abstract	ii
Figures and Tables.....	vi
Preface.....	x
Unit Conversion Factors	xi
1 Introduction.....	1
Background of the study.....	1
Objective	1
Scope of the study.....	2
Approach of the study	3
2 Model Characteristics and Model Improvements.....	4
Adaptive Hydraulics (AdH) and SEDLIB	4
Modeling diversions using quasi-3D capability of AdH/SEDLIB	5
Limitations of quasi-3D capability of AdH/SEDLIB.....	7
Model improvement: the wetland vegetation module.....	7
<i>Introduction</i>	<i>8</i>
<i>Primary productivity module algorithm for wetland vegetation.....</i>	<i>9</i>
<i>Demonstration.....</i>	<i>11</i>
<i>Feedback to AdH hydrodynamics.....</i>	<i>12</i>
Model improvement: time scaling using modified porosity	12
3 Model Development	15
Model mesh development	15
Boundary conditions and initialization.....	16
<i>Hydrodynamics and salinity.....</i>	<i>16</i>
<i>Boundary conditions for morphologic modeling.....</i>	<i>25</i>
<i>Noncohesive sediment boundary conditions and bed initialization.....</i>	<i>26</i>
<i>Cohesive sediment properties and boundary conditions</i>	<i>28</i>
<i>Bed sediment characteristics and marsh vegetation characteristics.....</i>	<i>30</i>
4 Hydrodynamic and Salinity Calibration and Validation	32
Hydrodynamic calibration	32
<i>Hydraulic roughness</i>	<i>32</i>
<i>Modeled discharge through existing distributaries.....</i>	<i>35</i>
<i>Water surface elevation calibration and validation</i>	<i>36</i>
<i>Discharge observations in Breton Sound</i>	<i>43</i>
Salinity calibration and validation	45
5 Morphology and Vegetation Validation	53
Vegetation validation.....	53
Morphologic model validation: the Caernarvon delta	54

Morphologic modeling validation: the West Bay delta	57
6 Sediment Diversion Scenario Analysis: Preliminary Screening Analysis and Initial Model Simulations	60
Introduction	60
Screening analysis	61
Initial model simulations.....	66
<i>Hydrodynamics (water surface elevation)</i>	67
<i>Morphology (land building)</i>	68
<i>Salinity</i>	70
7 Sediment Diversion Scenario Analysis: Mid-Breton and Mid-Barataria Diversions; Selected Simulations and Morphologic Modeling Boundary Conditions.....	72
Selected simulations.....	72
Morphologic modeling boundary conditions	74
<i>Mississippi River inflow hydrograph</i>	74
<i>Tidal boundary condition</i>	74
<i>Applied subsidence</i>	75
<i>Applied annual idealized storm wind</i>	76
<i>Applied sediment inflow boundary conditions</i>	77
8 Sediment Diversion Scenario Analysis: Mid-Breton and Mid-Barataria Diversions; Water Surface Elevation and Morphologic Analyses.....	79
Water surface elevation impacts: Year 0	79
Water surface elevation impacts: Year 50.....	80
Qualitative analysis of sediment erosion and deposition and wetland vegetation	81
Quantitative analysis of the efficiency of optimization operations.....	86
Land gained and lost as a result of diversion operations.....	87
<i>Land change maps</i>	87
<i>Quantification of land change by regional polygon</i>	90
Discussion	97
9 Sediment Diversion Scenario Analysis: Mid-Breton and Mid-Barataria Diversions; Salinity Analysis	102
Model boundary conditions	102
Without project salinity: influence of relative sea level rise.....	102
Scenario analysis results for Year 0 (2020)	104
Discussion	107
10 Summary and Conclusions	109
Calibration and validation.....	109
Morphologic modeling.....	110
Salinity modeling.....	112
References	114
Appendix A: DAMLAY Theoretical Development	118

Appendix B: Physics of Diversions.....	133
Appendix C: Optimization of Diversion Operations	140
Appendix D: SEDLIB-VEG Cohort Analysis: Influence of Vegetation Species Switching on Inundation Response in the Breton and Barataria Basins and the Birdsfoot	147
Report Documentation Page	

Figures and Tables

Figures

Figure 1-1. Mississippi River Hydrodynamic/Delta Management Study area.....	2
Figure 2-1. Demonstration of the wetland vegetation module.....	11
Figure 2-2. Demonstration of porosity scaling for a wetland formed by a steady inflow of water and sediment.....	13
Figure 3-1. AdH morphologic model mesh.....	16
Figure 3-2. Applied inflows.....	17
Figure 3-3. Locations of largest existing Mississippi River diversions (upstream of the Birdsfoot Delta).....	18
Figure 3-4. Leakage discharge rating curve for the Bonnet Carre spillway.....	19
Figure 3-5. Discharge hydrograph for Bonnet Carre Diversion: 2010–2011.....	20
Figure 3-6. Discharge hydrograph for Davis Pond Diversion: 2010–2011.....	21
Figure 3-7. Discharge hydrograph for Caernarvon Diversion: 2010–2011.....	22
Figure 3-8. Applied tidal boundary condition.....	23
Figure 3-9. Location map for the wind stations.....	24
Figure 3-10. Downstream bed sediment initialization.....	28
Figure 3-11. Comparison of modeled and observed bed bulk density as a function of organic content.....	31
Figure 4-1. The Fort St. Philip distributary.....	35
Figure 4-2. Comparison between modeled and observed water discharge at the Bohemia Spillway/Fort St. Philips uncontrolled diversion.....	36
Figure 4-3. Observation locations for hydrodynamic and salinity calibration and validation.....	37
Figure 4-4. Selected water surface calibration time series plots for Breton Sound.....	38
Figure 4-5. Selected water surface calibration time series plots for Barataria Bay.....	38
Figure 4-6. Statistical analysis of water surface elevation calibration for all observation locations, by rank order (green is acceptable agreement; red is poor agreement).....	40
Figure 4-7. Selected water surface validation time series plots for Breton Sound.....	41
Figure 4-8. Selected water surface validation time series plots for Barataria Bay.....	41
Figure 4-9. Statistical analysis of water surface elevation validation for all observation locations, by rank order (green is acceptable agreement; red is poor agreement).....	42
Figure 4-10. Discharge comparison at Site 2.....	43
Figure 4-11. Discharge comparison at Site 3.....	44
Figure 4-12. Discharge comparison at Site 5.....	44
Figure 4-13. Discharge comparison at Site 9.....	45
Figure 4-14. Color contour of spring (high river discharge) salinity.....	46
Figure 4-15. Color contour of summer (falling river discharge) salinity.....	46
Figure 4-16. Color contour of fall (low river discharge) salinity.....	47
Figure 4-17. Selected salinity calibration time series plots for Breton Sound.....	48
Figure 4-18. Selected salinity calibration time series plots for Barataria Bay.....	48

Figure 4-19. Statistical analysis of salinity calibration for all observation locations, by rank order (green is acceptable agreement, red is poor agreement).....	49
Figure 4-20. Selected salinity validation time series plots for Breton Sound.....	50
Figure 4-21. Selected salinity validation time series plots for Barataria Bay.....	51
Figure 4-22. Statistical analysis of salinity validation for all observation locations, by rank order (green is acceptable agreement; red is poor agreement).....	52
Figure 5-1. Modeled vegetation biomass in Breton Sound.....	53
Figure 5-2. Comparison between modeled and observed sediment fluxes through Caernarvon Diversion.....	54
Figure 5-3. Observed growth of the Caernarvon delta (source: Lake Pontchartrain Foundation).....	55
Figure 5-4. Modeled vegetation biomass at the Caernarvon Delta in 2012, assuming a subsidence of 5 mm/year.....	55
Figure 5-5. Modeled vegetation biomass at the Caernarvon Delta in 2012, assuming a subsidence of 9 mm/year.....	56
Figure 5-6. Comparison between modeled and observed areal extent of the Caernarvon delta, assuming subsidence = 5 mm/year.....	56
Figure 5-7. Comparison between modeled and observed areal extent of the Caernarvon delta, assuming subsidence = 9 mm/year.....	57
Figure 5-8. Observed West Bay delta in October 2012.....	57
Figure 5-9. Modeled West Bay delta in October 2012.....	58
Figure 5-10. Quantitative comparison between modeled and observed values of the growth of the West Bay delta between 2009 and 2011.....	59
Figure 6-1. Locations of diversions evaluated in preliminary screening analysis.....	61
Figure 6-2. DAMLAY results: estimated net available head for the proposed diversions.....	63
Figure 6-3. DAMLAY results: estimated operational lifespan of the proposed diversions.....	64
Figure 6-4. DAMLAY results: estimated acres of created land for the proposed diversions.....	64
Figure 6-5. Water surface elevation difference associated with the Upper Breton Diversion at 7079 cms.....	65
Figure 6-6. Water surface elevation impacts associated with the Mid-Breton and Lower Breton Diversions (contoured from 0 to 1 m of water surface elevation impact).....	68
Figure 6-7. Modeled land gain and land loss associated with the Mid-Breton and Lower Breton Diversions.....	69
Figure 6-8. Modeled land gain and land loss associated with the Mid-Breton and Lower Breton Diversions.....	69
Figure 6-9. Average April through June salinity for analysis year 2020, without project.....	70
Figure 6-10. Average April through June salinity for analysis year 2020, Mid-Barataria Diversion operated at 75 kcfs.....	71
Figure 6-11. Average April through June salinity for analysis year 2020, Mid-Breton Diversion operated at 35 kcfs.....	71
Figure 7-1. Base operations for diversion scenario simulations.....	73
Figure 7-2. Optimized operations for diversion scenario simulations.....	73
Figure 7-3. Applied tidal boundary condition for first 5 years of simulation.....	75
Figure 7-4. Applied spatially varying subsidence surface.....	76

Figure 7-5. Applied storm (wind) condition for first 2 years of simulation.....	77
Figure 7-6. Applied sediment inflow boundary conditions.	78
Figure 8-1. Water surface elevation difference with and without diversion operations for Year 2020 of the model simulation (Year 0 of the analysis).....	80
Figure 8-2. Bed elevation change associated with sands for base diversion operations after 50 years of operation.	82
Figure 8-3. Bed elevation change associated with sands for optimized diversion operations after 50 years of operation.	82
Figure 8-4. Bed elevation change associated with fines for base diversion operations after 50 years of operation.	83
Figure 8-5. Bed elevation change associated with fines for optimized diversion operations after 50 years of operation.	83
Figure 8-6. Root mass distribution for without project conditions after 50 years of simulation.....	84
Figure 8-7. Root mass distribution for base diversion operation conditions after 50 years of simulation.	85
Figure 8-8. Refractory organics distribution for without project conditions after 50 years of simulation.	85
Figure 8-9. Refractory organics distribution for base diversion operation conditions after 50 years of simulation.	86
Figure 8-10. Modeled land change after 50 years – without project.	88
Figure 8-11. Modeled land change after 50 years relative to without project conditions – base operations.....	89
Figure 8-12. Modeled land change after 50 years relative to without project conditions – base operations With Bohemia Spillway and Fort St. Philip closure.....	89
Figure 8-13. Modeled land change after 50 years relative to without project conditions – optimized operations.	90
Figure 8-14. Polygons used for WVA.....	91
Figure 8-15. Acres of land gained and lost after 50 years of diversion operation.....	92
Figure 8-16. Time-history of wetland acres relative to without project conditions – Breton polygon.....	93
Figure 8-17. Time-history of wetland acres relative to without project conditions – Bataratia polygon.	93
Figure 8-18. Time-history of wetland acres relative to without project conditions – Birdsfoot and NWR polygons.	94
Figure 8-19. Time-history of wetland acres relative to without project conditions – all polygons (except Pontchartrain).....	94
Figure 8-20. Location of observation point for time-history analysis of vegetation response to diversion-induced inundation.....	95
Figure 8-21. Time-history analysis of vegetation response to diversion-induced inundation – first 3 years.	96
Figure 8-22. Time-history analysis of vegetation response to diversion-induced inundation – 50 years.	96
Figure 8-23. Comparison of Observed (Snedden et al. 2015) and SEDLIB-VEG modeled correlation between inundation frequency and vegetation root biomass.....	98

Figure 9-1. Modeled average annual salinity without project for Year 0 (2020).	103
Figure 9-2. Modeled average annual salinity without project for Year 30 (2050).	103
Figure 9-3. Modeled average annual salinity without project for Year 50 (2070).	104
Figure 9-4. Salinity scenario results for Year 0 (2020).	106

Tables

Table 3-1. Wind stations.	24
Table 3-2. Sediment grain classes.	26
Table 3-3. Applied bed gradations.	28
Table 3-4. Cohesive sediment grain properties.	29
Table 3-5. Bed sediment characteristics.	30
Table 3-6. Marsh vegetation parameters.	30
Table 4-1. Calibrated friction parameters.	34
Table 4-2. Modeled and observed fraction of total flow at existing distributaries.	36
Table 5-1. Comparison between modeled and observed vegetation biomass at selected locations in Breton Sound.	53
Table 6-1. Water discharges associated with each diversion in preliminary screening analysis.	62
Table 6-2. Water surface elevation difference at a distance of 0.6 miles (1 km) from the diversion outlet.	66
Table 6-3. Diversions and design discharges for initial model simulations.	67
Table 8-1. Optimization efficiency indices for the Mid-Breton and Mid-Barataria optimization simulations.	87
Table 8-2. Criteria for determination of land change categories for land change maps.	87

Preface

This study was conducted for the U.S. Army Corps of Engineers (USACE), New Orleans District (MVN), in partnership with the Louisiana Coastal Protection and Restoration Authority (CPRA) for the Louisiana Coastal Area (LCA) program Project No. 142871, entitled “Mississippi River Hydrodynamic and Delta Management Study” (MRHDMS). The program manager for MVN was Ms. Cherie R. Price.

The knowledge and technology developed by the MRHDMS, and documented here, can be used to inform the development of coastal restoration plans, designs, and environmental impact statements, as well as quantifying possible impacts in the river and receiving basin. However, it should be noted that CPRA notified MVN by letter dated 15 May 2017 its intent to advance both the Mid-Barataria and Mid-Breton sediment diversions through the Department of the Army Section 10/404 permitting process and, since there were no additional alternatives left to consider in the MRHDMS, requested an orderly shutdown of the study. Pursuant to the objective of advancing the Mid-Barataria and Mid-Breton sediment diversions, CPRA has since invested significant efforts in seeking to address many of the outstanding issues that are discussed in this report. The results of these subsequent efforts are not documented here; this report only documents work undertaken as part of the MRHDMS.

The work was performed by personnel in the River and Estuarine Engineering Branch of the Flood and Coastal Division, U.S. Army Engineer Research and Development Center (ERDC), Coastal and Hydraulics Laboratory (CHL), in addition to personnel at the USACE MVN and personnel at the USACE Mississippi Valley Division.

At the time of publication of this report, the Branch Chief for the River and Estuarine Engineering Branch was Mr. Keith Flowers, and the Division Chief for the Flood and Coastal Division was Dr. Cary Talbot. The technical director was Dr. Julie Rosati, the Deputy Director of CHL was Mr. Jeffrey R. Eckstein, and the Director of CHL was Dr. Ty V. Wamsley.

COL Ivan P. Beckman was Commander of ERDC, and Dr. David W. Pittman was Director of ERDC.

Unit Conversion Factors

Multiply	By	To Obtain
acres	4,046.873	square meters
cubic feet	0.02831685	cubic meters
cubic yards	0.7645549	cubic meters
miles (U.S. statute)	1,609.347	meters
miles per hour	0.44704	meters per second
pounds (force) per square foot	47.88026	pascals
pounds (mass)	0.45359237	kilograms
slugs	14.59390	kilograms
square feet	0.09290304	square meters
tons (2,000 pounds, mass)	907.1847	kilograms
yards	0.9144	meters

1 Introduction

Background of the study

The Louisiana Coastal Area recommended a Mississippi Hydrodynamic Study and a Mississippi Delta Management Study, two parts of six long-term, large-scale recommended studies (Louisiana Coastal Area 2004). The State of Louisiana and The New Orleans District (MVN) of the U.S. Army Corps of Engineers agreed to combine these two parts into a single study, referred to as the Mississippi River Hydrodynamic and Delta Management Study. According to the Project Management Plan for the Mississippi River Hydrodynamic/Delta Management Study, the purpose of the study was to evaluate the existing Mississippi River system below the Old River Control Structure (ORCS) and to properly assess the operation of the lower-most Mississippi River system with respect to water and sediment transport, flood control, and navigation. The study area encompasses the Mississippi River from the ORCS to the Gulf of Mexico.

Objective

The study had as its initial focus the development of tools that can evaluate both the existing conditions of the river and any potential local and system-wide impacts of proposed changes to the system (such as additional diversions). The study included two general components. The Mississippi Hydrodynamic Component focused on data, models and analytic techniques applicable to the river. The Delta Management component focused on data, models and analytic techniques applicable to the receiving area (the Delta).

One specific component of the study entailed the development of multi-dimensional models. These models were developed in parallel efforts, one by the Water Institute of the Gulf (TWIG) for the State of Louisiana Coastal Protection and Restoration Authority (CPRA), one by MVN, by way of the U.S. Army Engineer Research and Development Center (ERDC).

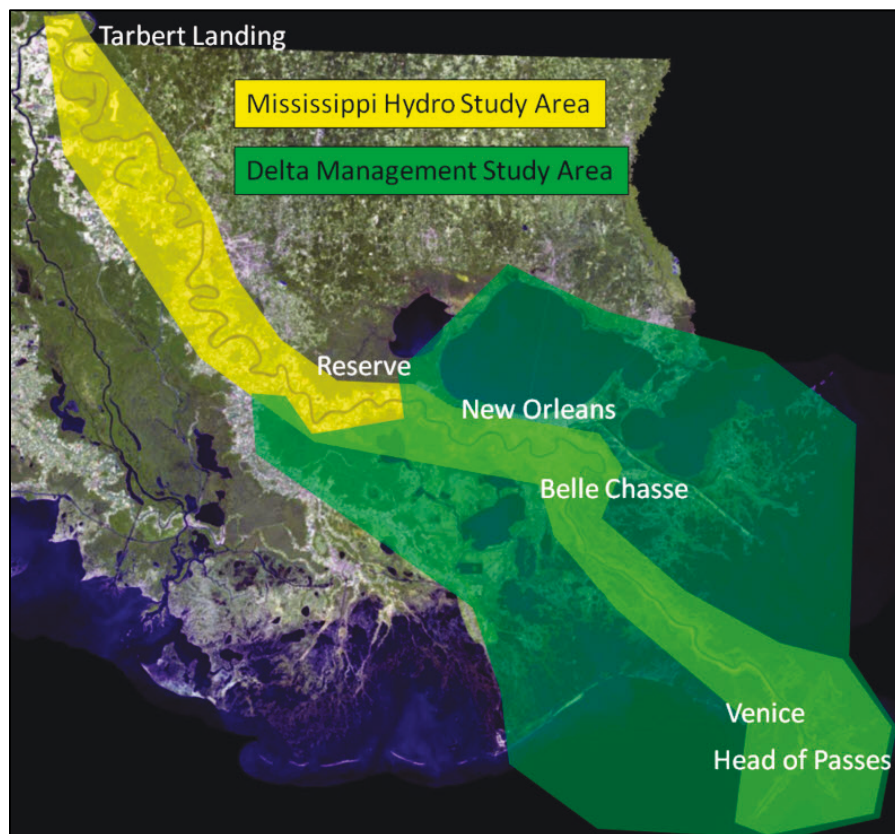
These models were then applied to address a specific proposed alteration of the system: perform scenario analyses to evaluate several proposed

combinations of sediment diversions to assess their effects on both the River and the Delta. This report details the results of the Delta modeling.

Scope of the study

The multi-dimensional model that is presented in this report is a model application developed using the Adaptive Hydraulics (AdH) numerical model code, which is developed and supported at the ERDC Coastal and Hydraulics Laboratory (CHL). AdH is linked to SEDLIB, a sediment transport library that is also developed and supported at CHL. The model is developed to simulate hydrodynamic, salinity, sedimentation, and morphodynamic processes (including the growth and interaction with wetland vegetation) in the Mississippi River and Delta. The full project study area extends from Tarbert Landing (River Mile [RM] 306.3 Above Head of Passes [AHP]) to the Gulf of Mexico, Figure 1-1. The Delta Management model extends from Reserve, LA (RM 138.7 AHP), to the Gulf of Mexico and includes all of the wetlands influenced by the river. The full domain of the Delta Management model is depicted in Chapter 3 of this report.

Figure 1-1. Mississippi River Hydrodynamic/Delta Management Study area.



This AdH/SEDLIB model of the Mississippi River Delta is developed to be used for use in any future river management issues. The immediate use of this model, however, is to evaluate the benefits and impacts associated with sediment diversions. Hence, the validation efforts discussed herein are focused on these efforts.

Approach of the study

The approach for development and validation of the model used for this study was as follows:

- Assemble and analyze all data pertinent to numerical model development (e.g., bathymetry, infrastructure, roughness characteristics, wetland vegetation characteristics, boundary condition data)
- Develop necessary model improvements (i.e., the wetland vegetation module and modified porosity morphologic acceleration technique)
- Develop the computational mesh
- Calibrate and validate hydrodynamics
- Calibrate and validate salinity
- Calibrate and validate wetland morphodynamics.

The results of these tasks are contained in this report.

Once the model was developed and validated, the model was applied to assess the effects of various proposed combinations of sediment diversions on the hydrodynamics, salinity, and morphology of the receiving waters (the Delta). The results of these scenario analyses are also contained in this report.

2 Model Characteristics and Model Improvements

Adaptive Hydraulics (AdH) and SEDLIB

The AdH model is a finite element model that is capable of simulating three-dimensional (3D) Navier-Stokes equations, two-dimensional (2D) and 3D shallow water equations, and groundwater equations. It can be used in a serial or multiprocessor mode on personal computers, UNIX, Silicon Graphics, and CRAY operating systems. For this study, AdH is applied in 2D depth-averaged mode. The 2D depth-averaged model, together with specific quasi-3D modifications appropriate for sediment transport applications (discussed below), was used for this study because this level of dimensional resolution resulted in a model that was able to adequately resolve the relevant physics without the burdensome computational expense that would have been incurred with a fully 3D model.

The adaptive aspect of AdH is its ability to dynamically refine the domain mesh in areas where more resolution is needed at certain times due to changes in the flow and/or transport conditions. AdH can simulate the transport of conservative constituents, such as salinity, as well as sediment transport that is coupled to bed and hydrodynamic changes. The ability of AdH to allow the domain to wet and dry as the tide and/or river stage changes is important for simulating the Lower Mississippi River and Delta. This tool was developed at CHL and has been used to model sediment transport in such varied environments as the Mississippi River, San Francisco Bay, and vessel traffic in the Houston Ship Channel.

More details about AdH and its computational philosophy and equations can be found at this website: <https://chl.erdcdren.mil/chladh/>.

SEDLIB is a sediment transport library developed at ERDC. (Brown 2012a,b). It is capable of solving problems consisting of multiple grain sizes, cohesive and cohesionless sediment types, and multiple layers. It calculates erosion and deposition processes simultaneously and simulates such bed processes as armoring, consolidation, and discrete depositional strata evolution.

The SEDLIB library system is designed to link to any appropriate hydrodynamic code. The hydrodynamic code must be capable of

performing advection-diffusion calculations for a constituent. SEDLIB interacts with the parent code by providing sources and sinks to the advection diffusion solver in the parent code. The solver is then used to calculate both bedload and suspended load transport for each grain class. The sources and sinks are passed to the parent code via an explicit bed sediment flux for each grain class.

The AdH /SEDLIB sediment model contributes several capabilities to the analysis, including the following:

- Quasi-3D flow and transport formulations, which use analytical and semi-empirical methods of approximating the 3D character of the flow and sediment transport phenomena (Brown 2008, 2012a).
- These include the ability to model the effects of helical flow through a river bendway on the suspended and bedload sediment transport by utilizing the bendway vorticity transport algorithm given by Bernard (1992).
- The SEDLIB module is equipped to simulate multi-grain class suspended load and bedload sediment transport phenomena. It is also equipped to handle generalized multi-grain class bed processes, including armoring, sorting, erosion to a solid boundary, and the storage of discrete depositional strata.
- The unstructured model mesh employed by AdH permits very high resolution in areas of interest and high-fidelity resolution of shoreline geometry.
- The ability to extend the boundaries sufficiently far from the project area so as not to prescribe the answer ensures that the results are not biased by judgments concerning boundary conditions.

Modeling diversions using quasi-3D capability of AdH/SEDLIB

As was stated previously, any model used to investigate diversions must be able to model the physical phenomena that determine the relative efficiency of the diversion (i.e., the sediment diversion coefficient). In general, the diversion of water and sediment is a 3D flow and transport phenomenon. However, for diversions that satisfy certain criteria, the quasi-3D capabilities associated with SEDLIB can be used to model the diversions with sufficient fidelity to characterize the diversion behavior. These criteria and the relevant 2D or quasi-3D process that is used to model each of the relevant physical processes are given below:

- *Lateral variation in the sediment concentration of the river* – this can be modeled with 2D transport, coupled with the bendway corrections to the hydrodynamics and transport included in the quasi-3D logic (Brown 2012a).
- *Vertical variation in the sediment concentration of the river* – for quasi-steady flows in large rivers, the vertical variation of suspended sediment is well-approximated with the nonequilibrium suspended sediment profile included in the quasi-3D logic (Brown 2008).
- *Bendway effects in the river (helical flow effects)* - this can be modeled with 2D transport, coupled with the bendway corrections to the hydrodynamics and transport included in the quasi-3D logic (Bernard 1992).
- *Influence of the angle of the diversion* – the diversion angle influences sediment capture due to the relative influences of the change in momentum, the induced helical flow, and flow separation inside the diversion. All of these behaviors are represented in the 2D model with bendway correction. The detailed flow structure is not modeled, but the gross effects on sediment behavior are captured.
- *Influence of the elevation of the invert of the diversion* – if the diversion is designed as a skimming diversion (i.e., a shallow diversion on a steep banking with relatively small discharge), then the 2D model will not capture this skimming behavior for sediments that are significantly stratified in the water column (i.e., sand-sized sediments). The Caernarvon and Davis Pond Diversions are examples of this type of diversion. However, large, deep diversions along banklines with milder slopes do not exhibit skimming behavior. These diversions are typically not isokinetic (i.e., the energy gradient toward the diversion is steeper than the river). This steep energy gradient tends to distort streamlines in the river, pulling water from depth into the diversion. Since all of the proposed diversions satisfy the criteria given here for non-skimming diversions, the 2D model should be adequate to model their behavior.
- *Influence of the water discharge through the diversion* – This can be modeled with a 2D model

The above arguments are general and qualitative in nature, but experience with the model, and the performance of the model with laboratory test cases, suggests that they are valid. A recent example of this is the application of the model to investigate the ORCS (Heath et al. 2015). The model was able to simulate the sediment diversion coefficients of the three diversion structures, matching both qualitatively and (to some degree)

quantitatively the behavior of the structures as assessed by field experience and (for the lower two structures) by an existing coal-bed physical model study.

Limitations of quasi-3D capability of AdH/SEDLIB

Note that the quasi-3D formulation discussed here is developed with the assumption that a logarithmic (or near-logarithmic) vertical velocity profile exists in the prototype. Where this is not the case, the quasi-3D assumptions are not valid.

For this application, a near-logarithmic vertical velocity profile does not exist in the lowermost Mississippi River at low river discharge, where a salinity wedge is observed to propagate upstream in the Mississippi River, resulting in a vertically stratified velocity profile. This salinity wedge can have significant impacts on silt and clay sediment deposition as both the hydrodynamics and the rate of deposition of the sediments are influenced by its presence (silt and clay sized sediments tend to flocculate in saline conditions, greatly accelerating their fall velocity and thus inducing deposition).

Therefore, since the model configuration used here (the quasi-3D formulation of AdH) is not appropriate to address stratified flow effects, there is no attempt made to model salt-wedge dynamics in the Mississippi River in this report.

Model improvement: the wetland vegetation module

To simulate the impacts associated with both delta building associated with diversions and the impacts of diversions on existing wetlands, it was necessary to develop a means of modeling the growth and mortality of wetland vegetation. To this end, a primary productivity model has been developed and implemented into SEDLIB. This is a generic wetland vegetation model for which the rate of growth of vegetation is exclusively a function of local water depth. Hence, the true complexity of wetland vegetation processes across multiple species is not simulated; rather, it is anticipated that this complexity will be addressed via sensitivity analyses.

Introduction

This model is based largely on the work of Fagherazzi et al. (2012). The primary differences between this model and the referenced model arise from the differences in the operational time-step. The referenced model can operate on relatively large time scales, using tidally averaged or even monthly averaged input parameters. However, the vegetation model developed for this study is being incorporated into an existing sediment model (SEDLIB), so it is designed to make computations that are dependent on local, near-instantaneous conditions (e.g., water depth). This allows the interaction between the organic matter associated with the productivity of the wetland vegetation and the erosion and deposition of mineral sediments to occur at the same time scales, thereby ensuring that the interactions are not constrained by simplifications associated with the integration of different time scales.

The model is integrated into the SEDLIB sediment module by simply assigning two of the sediment classes to be organic classes. The first is the root class; it represents the behavior of the root material. The second is the refractory class; it represents the storage of compacted refractory organic material.

These sediment classes behave exactly as other sediment classes, with three significant exceptions:

1. The mass of the root class can grow, as determined by Equations 1–4 (below).
2. The mass of the refractory class can grow, as determined by Equation 5 (below).
3. When the organic classes erode, they are assumed to disintegrate; that is, they are not transported.

As with other sediment classes in SEDLIB, each organic class is assigned a characteristic bulk density and erosional characteristics. The root material class is assigned a very low bulk density, commensurate with the bulk density of the rooting zone. The refractory class is assigned a higher bulk density, associated with compacted refractory organics (note that this module does not compute compaction; it assumes that the refractory fractions of both litterfall and root decay are immediately compacted).

The bulk density and erosional characteristics of each bed layer are then computed as the grain-class-fraction weighted average of the properties assigned to the sediment classes that comprise that layer.

All other bed sorting and storage functions that operate on the mineral sediment classes also apply to the organic classes. Hence, mixing with mineral sediments is handled implicitly within the regular function of SEDLIB.

The only difference between these organic *sediment* classes and the other inorganic classes is that the masses of each of these classes are modified at each time-step as a result of vegetative growth and decay.

Primary productivity module algorithm for wetland vegetation

The equation for the mass of wetland vegetation at a given time-step is given as a basic implicit source/sink mass balance.

$$m_{veg} = \frac{m_{veg.o} + v_{src}\Delta t}{1 + v_{snk}\Delta t} \quad (1)$$

The source term is given as a function of local, instantaneous depth.

$$v_{src} = v_{src.m} \left(1 - \frac{h}{h_{ldep}} \right) : 0 \leq h \leq h_{ldep} \quad (2)$$

The sink term is found by setting m_{veg} and $m_{veg.o}$ equal to $m_{veg.eq}$ in (1) and solving for v_{snk} .

$$v_{snk} = \frac{v_{src.m}}{m_{veg.eq}} \quad (3)$$

Once m_{veg} has been determined, m_{root} is given as a simple function of the root-to-shoot ratio.

$$m_{root} = m_{veg} r_{rs} \quad (4)$$

The refractory mass is a cumulative mass. It is updated at each time-step with the contribution of both decaying vegetation and decaying roots, less the labile material.

$$m_{refr} = m_{refr.o} + m_{veg} v_{snk} \Delta t (1 - f_{lab}) \quad (5)$$

The root mass and the refractory source term are applied in the sediment layers immediately beneath the bed surface. The mass of each term is assumed to decay exponentially, from a maximum value at the surface, to a (near) zero value at a user-defined limiting root thickness (t_{rl}).

Each of the terms used in this development are defined below. Terms with an asterisk are user-defined terms.

- f_{lab}^* = the labile fraction: the fraction of dead vegetative material that decays quickly
- h_{ldep}^* = the limiting depth (meter): the maximum water depth for which wetland vegetation will grow
- m_{refr} = the mass per unit area of the refractory organic material in the sediment bed (kilograms per square meter)
- $m_{refr.o}$ = the mass per unit area of the refractory organic material in the sediment bed at the previous time-step (kilograms per square meter)
- m_{root} = the root mass per unit area in the sediment bed (kilograms per square meter)
- m_{veg} = the mass per unit area of wetland vegetation (kilograms per square meter)
- $m_{veg.eq}^*$ = the equilibrium mass per unit area of vegetation (kilograms per square meter) this is the mass for which vegetation mortality is equal to vegetation growth
- $m_{veg.o}$ = the mass per unit area of wetland vegetation at the previous time-step (kilograms per square meter)
- r_{rs}^* = the root-to-shoot ratio: this is the ratio of root mass to wetland vegetation mass
- t_{rl}^* = the rooting thickness limit (meter): this is the maximum distance below the surface of the sediment bed where roots can be found
- Δt = the time-step (seconds)
- v_{snk} = the rate of wetland vegetation mortality (1/second)

V_{src} = the rate of wetland vegetation growth ((kilograms per square meter per second)

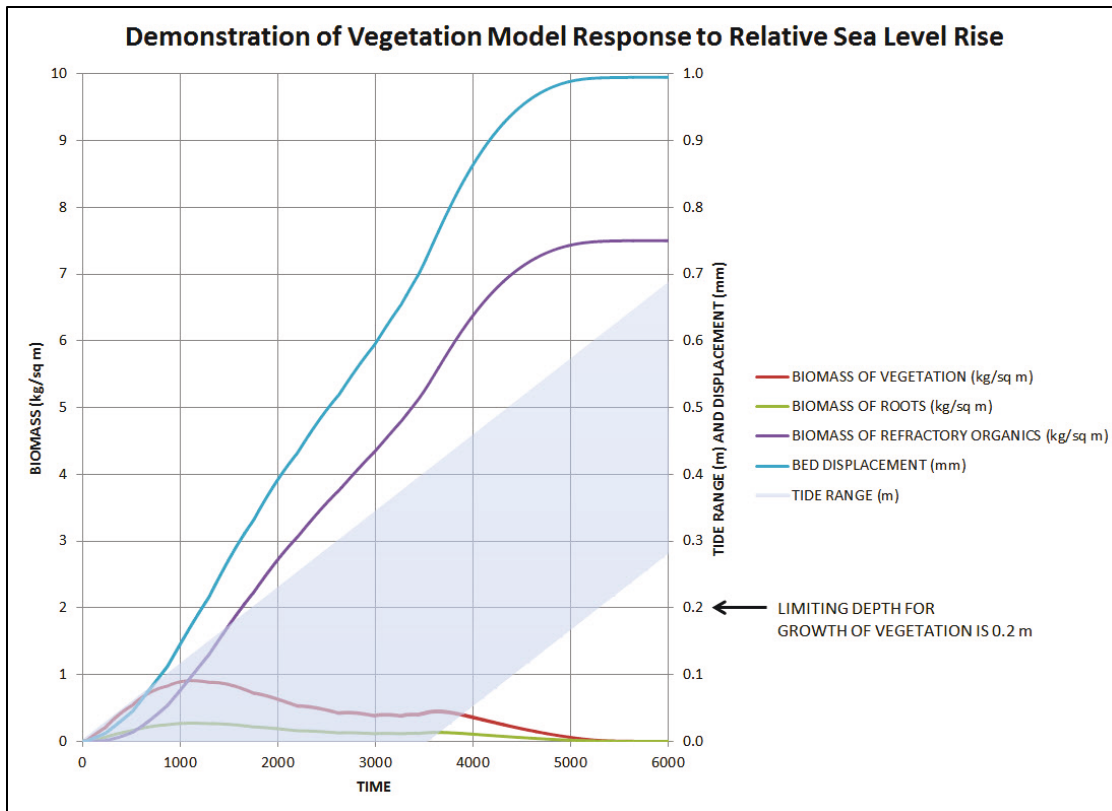
$V_{src,m}^*$ = the maximum rate of wetland vegetation growth (kilograms per square meter per second) .

Demonstration

Figure 2-1 shows how the wetland vegetation model works. The sediment bed is subjected to a tidal signal, with a mean elevation that increases over time (simulating a sea level rise rate that exceeds the maximum rate of marsh accretion). Initially, as the marsh inundates, the vegetation grows until it reaches a maximum (where growth and mortality are in balance). The root mass associated with this vegetation increases the bed elevation. Decaying vegetation is added to the refractory mass, further increasing the bed elevation over time.

As the tide range increases further, the mortality exceeds the rate of growth and the vegetation mass is reduced. Eventually, all organic production ceases as the threshold depth for growth is exceeded for all phases of the tide.

Figure 2-1. Demonstration of the wetland vegetation module.



Feedback to AdH hydrodynamics

One other aspect of the wetland vegetation module is how the growth of vegetation feeds back into the hydrodynamic simulation. This is done by scaling the density of vegetation associated with the drag assigned to the wetland areas of the mesh by the ratio of the vegetation biomass present at a given node to the equilibrium vegetative biomass for that node. For example, if a given node has 60% of the equilibrium vegetative biomass, the density of the vegetation associated with the drag will be 60% of the maximum value.

Model improvement: time scaling using modified porosity

To investigate the long-term (multi-decadal) effects of sediment diversions, it is necessary to develop a means whereby morphologic change can be *accelerated* within the model. For quasi-steady conditions (i.e., slowly varying conditions), a simple and straightforward method of estimating this acceleration is to scale the porosity of the sediment. Consider the basic equation of mass conservation for a sediment bed (for simplicity, this is shown for a bed consisting of one grain class only).

$$D - E = \rho s(1 - p) \frac{\partial \eta}{\partial t} \quad (6)$$

Where D is the deposition flux, E is the erosion flux, ρ is the water density, s is the specific gravity of the sediment, p is the porosity of the sediment bed, and η is the bed elevation.

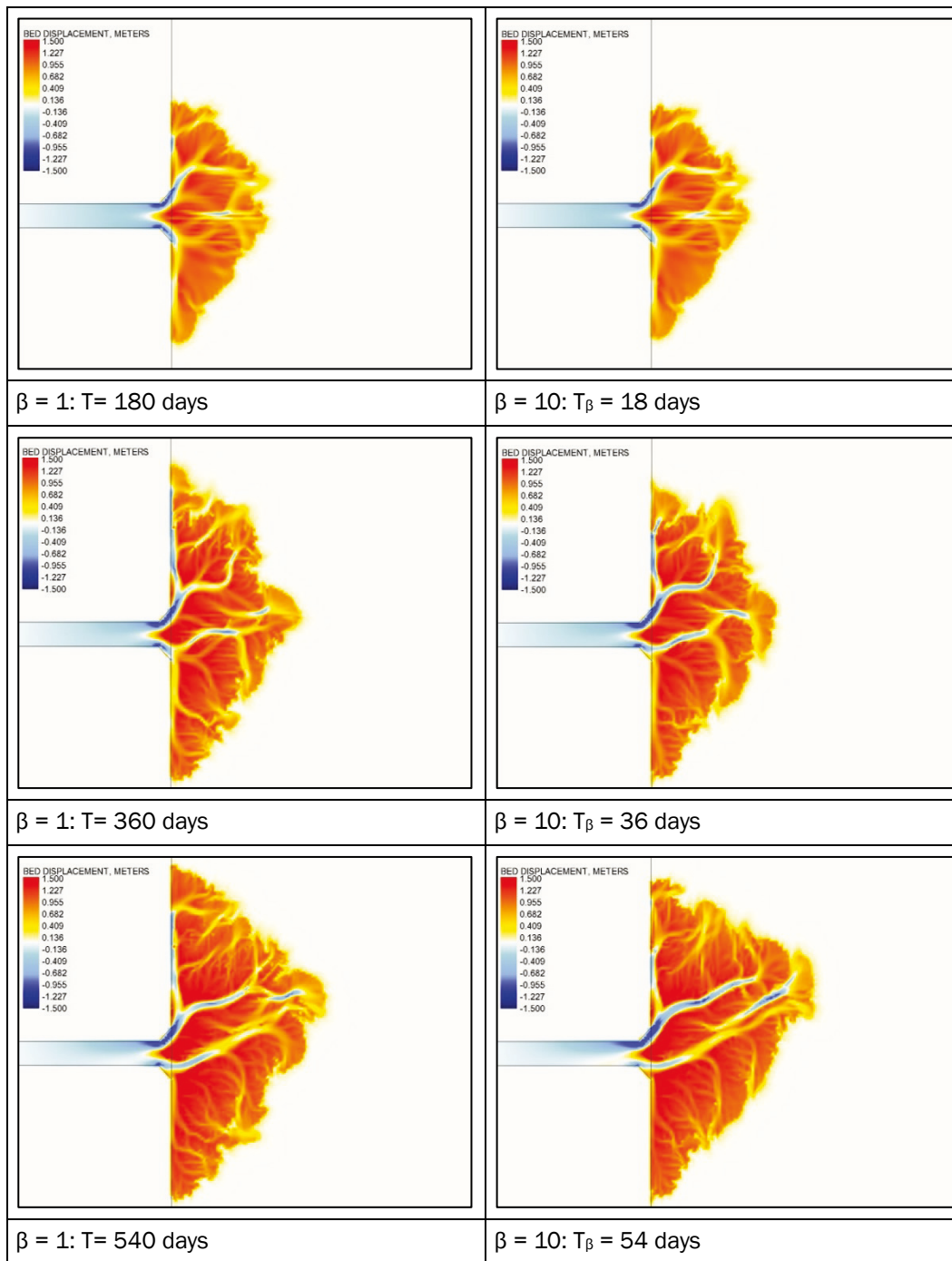
If wishing to accelerate the rate at which the same net flux (deposition minus erosion) will change the bed elevation by some acceleration factor β , substitute into (6) and solve for the porosity necessary to achieve this acceleration (p_β).

$$D - E = \rho s(1 - p) \frac{\partial \eta}{\partial t} = \rho s(1 - p_\beta) \beta \frac{\partial \eta}{\partial t} \quad (7)$$

$$p_\beta = 1 - \frac{1}{\beta}(1 - p) \quad (8)$$

Figure 2-2 shows how porosity scaling works for a wetland formed under steady inflow conditions.

Figure 2-2. Demonstration of porosity scaling for a wetland formed by a steady inflow of water and sediment.



Note that porosity scaling is only strictly valid for steady flow conditions. When unsteady conditions are present, time scaling will scale the relative magnitude of the temporal terms in the mass and momentum equations by the same scale factor (β).

For typical river discharge conditions, any significant scaling would result in significant changes in the velocities due to rapid rise and fall of the hydrograph in the scaled condition. These changes would alter the erosion and deposition patterns of the river, and hence the porosity scaling method of time acceleration would be inappropriate.

However, in the lowermost Mississippi River, the river stage is largely controlled by backwater conditions (due to the proximity of the Gulf of Mexico), and hence the stage difference between low and high water is severely constrained. Also, the river cross section does not change significantly between low and high water because of the backwater control (which keeps the lateral sediment bars submerged) and the levees, which prevent overbank flooding. These conditions all work to limit the contribution of the temporal terms to the mass and momentum equations to such an extent that significant porosity scaling can be achieved without loss of similitude.

This means that porosity scaling can be used in the lowermost Mississippi River if the scaling is first tested within the model to ensure similitude.

Note that this scaling cannot be applied to tidal conditions because the frequency of the tide is so high that scaling this signal would dramatically alter the resulting velocities. However, if it is assumed that the influence of the tide is largely periodic, the tidal signal can be modeled without scaling if the *number* of tides within a simulation is scaled. For example, if $\beta=10$, $T=10$ years, and there are 360 tides in 1 year (assuming approximately 24-hour tides), the river and tide can be modeled within the same model as follows:

- River: $\beta=10$, $T_\beta = 1$ year
- Tide: $\beta=1$, $T_\beta = 1$ year, total number of tides modeled = 36.

Again, testing of these methods should be performed for any specific application before they are used to assess scenarios.

3 Model Development

Model mesh development

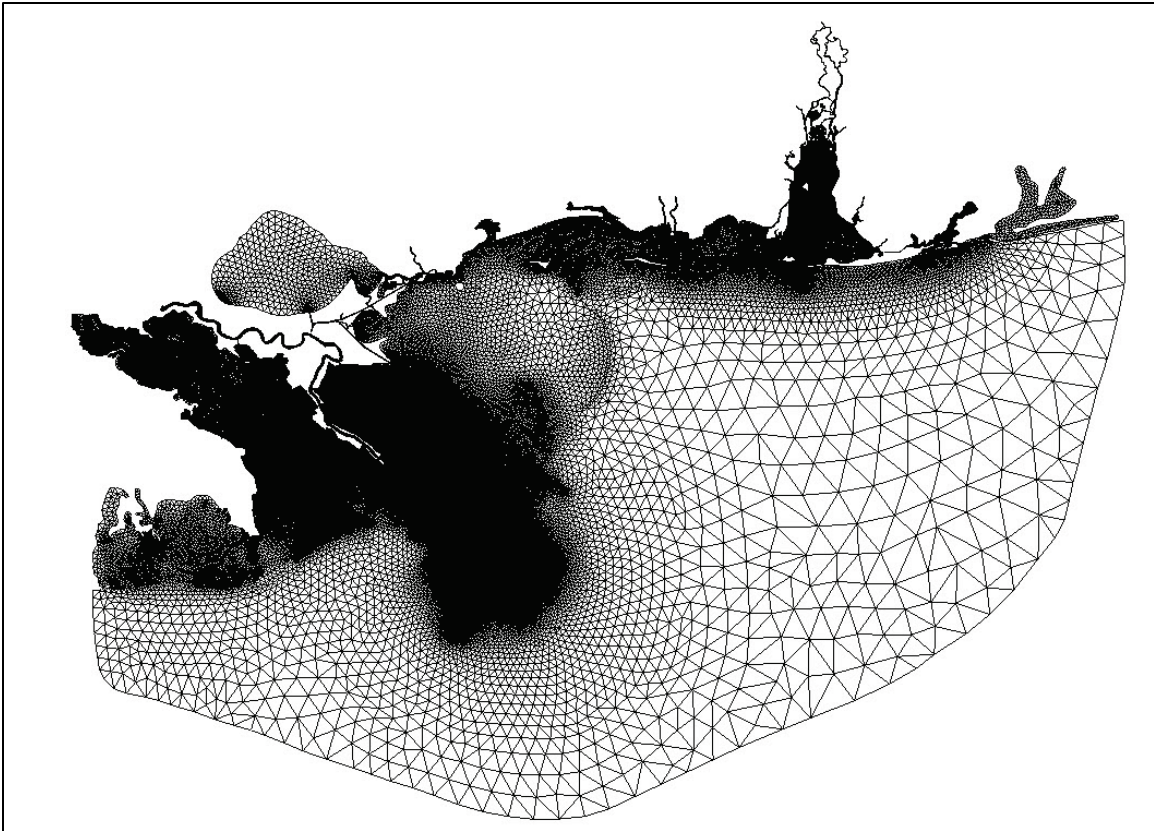
There are two model meshes that have been used for this study: one for salinity modeling and one for morphologic modeling. Both model meshes share the same general domain; they extend from Reserve, LA, to the Gulf of Mexico. The Gulf Boundary extends from Pensacola, FL, to the west side of Terrebonne Bay. The main differences lie in the increased resolution of the morphology mesh in Breton Sound and Barataria Bay.

The coarser mesh (the hydrodynamic and salinity mesh) contains 334,679 nodes and 656,226 elements. The finer mesh (the morphology mesh) contains 377,408 base and 739,319 base elements. The mesh resolution is set such that the river channel has 100-meter (m) spacing on average, and the element size increases toward the mesh boundaries. The finest resolution in the base mesh is approximately 10 m. However, since AdH is an adaptive code, the resolution has been set to increase in the model at any location where the error indicator determines that more resolution is required to ensure convergence of the solution within the specified error tolerance. Hence, at certain times during model simulation, when river discharge and/or winds induce significant currents, the number of nodes in the model is on the order of 50% more than the base resolution.

River training structures and revetments are identified and resolved explicitly in the model. Several existing diversions are included in the model: Bonnet Carre Spillway, Davis Pond, Caernarvon, and the Bohemia/Fort St. Philip series of crevasses. Figure 3-1 shows the complete model domain for the morphologic model. The horizontal coordinate system is Universal Trans-Mercator zone 16, meters. The vertical coordinate system is North American Vertical Datum of 1988 (NAVD88), meters.

Bathymetry data were taken from a variety of sources. Elevations in the river were taken from comprehensive surveys from MVN, channel condition surveys from MVN, and multi-beam surveys from MVN, ERDC, and the State of Louisiana (CPRA). Bathymetry and topography of the coastal wetlands and offshore were taken from National Oceanic and Atmospheric Administration (NOAA) digital elevation data, supplemented with high-resolution, single-beam and multi-beam data collected by ERDC and CPRA, that define the bathymetry of most of the major conveyance pathways within the Breton and Barataria marsh systems and the Fort St. Philip distributary.

Figure 3-1. AdH morphologic model mesh.



Boundary conditions and initialization

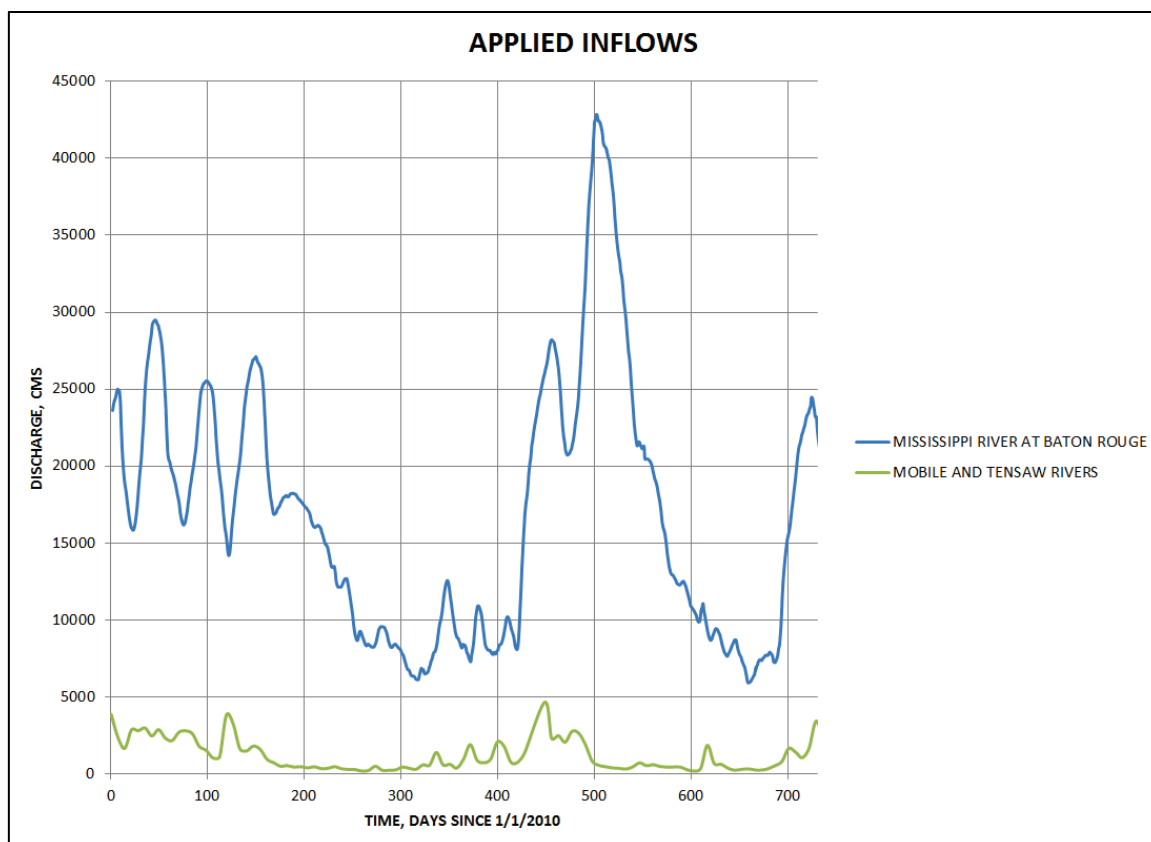
Hydrodynamics and salinity

The hydrodynamic and salinity model is driven by inflows for the Mississippi River and the Mobile/Tensaw Rivers, tides at the Gulf of Mexico, diversion discharges at Bonnet Carre, Davis Pond, and Caernarvon, winds, and Gulf salinity. Boundary condition data are obtained from several different sources and checked for quality prior to use in the numerical model. Boundary condition data were processed for 2010–2011.

Mississippi River inflow and Mobile/Tensaw River inflow

The Mississippi River inflow was taken from the U.S. Geological Survey (USGS) observations at Baton Rouge (Station 07374000). The Mobile and Tensaw River data were taken from the USGS observations of the Mobile River at Bucks (Station 0240269) and USGS observations of the Tensaw River at Mount Vernon (0247109). These inflows are given in Figure 3-2.

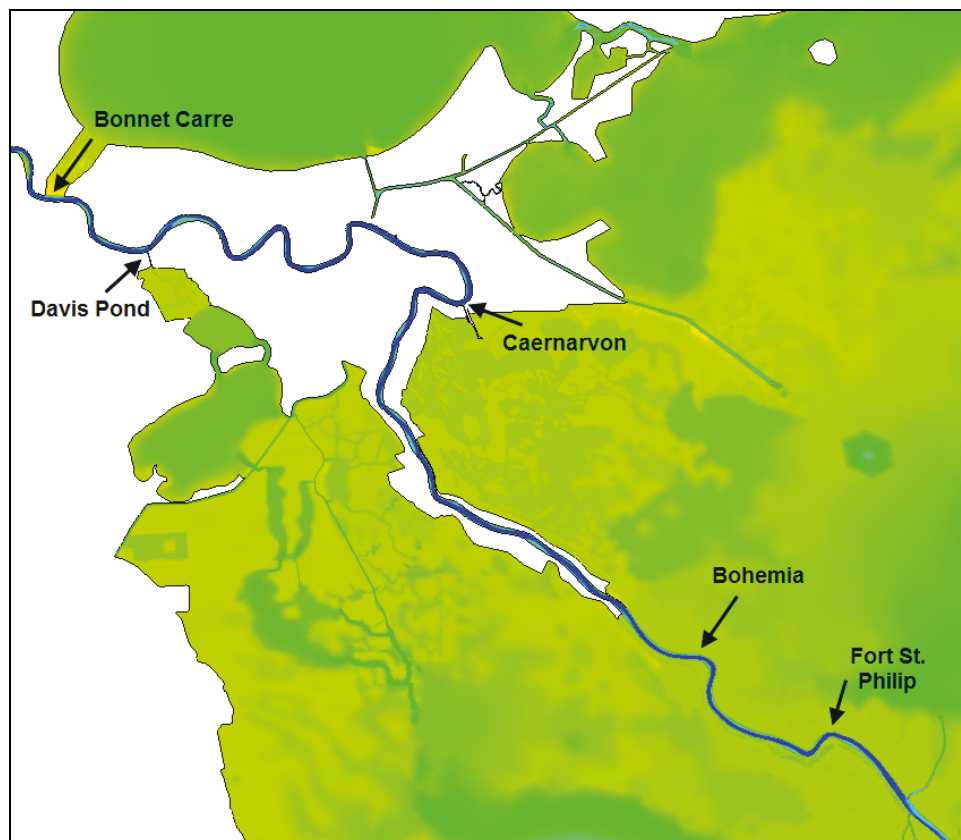
Figure 3-2. Applied inflows.



Existing diversions upstream of Baptiste Collette

Additional outflows from the Mississippi River occur at several diversion locations upstream of Baptiste Collette (Baptiste Collette and all flow outlets downstream are modeled directly). The regulated diversions are designed to divert fresh water into marsh areas to regulate salinity values or to simply divert water from the Mississippi River during high flows for flood protection. The largest of these regulated diversions are the Bonnet Carre Spillway, the Davis Pond Diversion, and the Caernarvon Diversion. In addition, two significant unregulated diversions are present along the east bank of the lower river, just upstream of Venice: The Bohemia Spillway and the Fort St. Philip Crevasse. Figure 3-3 shows the locations of these diversions.

Figure 3-3. Locations of largest existing Mississippi River diversions (upstream of the Birdsfoot Delta).

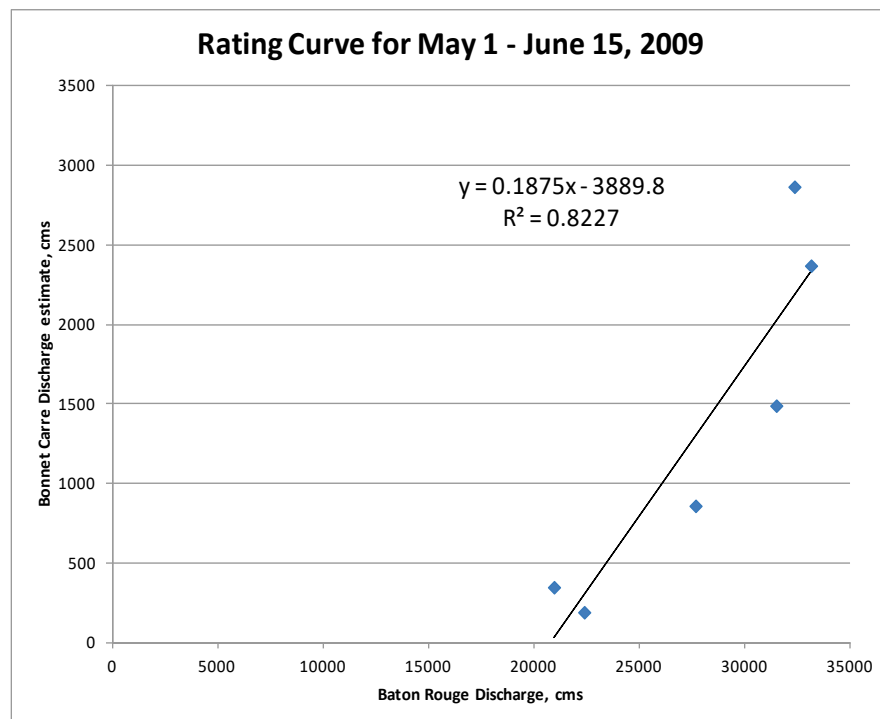


Bonnet Carre: The Bonnet Carre Spillway is located at RM 130, approximately 33 RM upstream of New Orleans. This diversion is 2,130 meters (m) long with 350 bays and has a rated capacity of 7,080 cubic meters per second (cms) (although there is evidence that this discharge was exceeded in the 2011 opening event). When opened, the diverted water from the Mississippi River passes through the Bonnet Carre spillway and enters into Lake Pontchartrain. The diversion was completed in 1931 and has been opened 10 times from 1937 to 2011. The Bonnet Carre diversion and spillway is an integral part of the Mississippi River and Tributaries Project for flood control. (Lane et al. 2001).

Although the diversion structure is intended to be closed unless Mississippi River flows are high enough to require the release of flows into the spillway, leakage through the timber piles closing the bays occurs when the water surface elevation on the river reaches the elevation of the structure. Leakage through the structure has been estimated to be at least 280 cms at high water.

The flows included in the model for the Bonnet Carre spillway are based on both the structure opening and the leakage. 2011 is the only year during the simulation period that the diversion was in operation. The leakage through the structure bays is estimated based on a rating curve using flow data from Baton Rouge (USGS 07374000 Mississippi River at Baton Rouge, LA), Davis Pond (USGS 295501090190400 Davis Pond Freshwater Diversion near Boutte, LA), Caernarvon (USGS 295124089542100 Caernarvon Outfall Channel at Caernarvon, LA), and Belle Chasse (USGS 07374525 Mississippi River at Belle Chasse, LA). The flows out of Bonnet Carre are set equal to the flows at Baton Rouge minus the sum of the flow out of the river at the three other locations. However, there is noise in some of these data, and it is known that the leakage only occurs under high flow conditions. A 7-day average flow signal was computed for all four locations, primarily to remove the tidal signal that is evident in the downstream gages. The rating curve was developed on a 41-day period of high flow from May into June 2009 and provides a relationship between the flows at Baton Rouge and the computed flows at Bonnet Carre. This linear fit is then used with the daily Baton Rouge flows to estimate the Bonnet Carre flows over the entire simulation period, such that Bonnet Carre flows are set to zero when the Baton Rouge flows are less than that required for the leakage to occur. Figure 3-4 shows the rating curve.

Figure 3-4. Leakage discharge rating curve for the Bonnet Carre spillway.

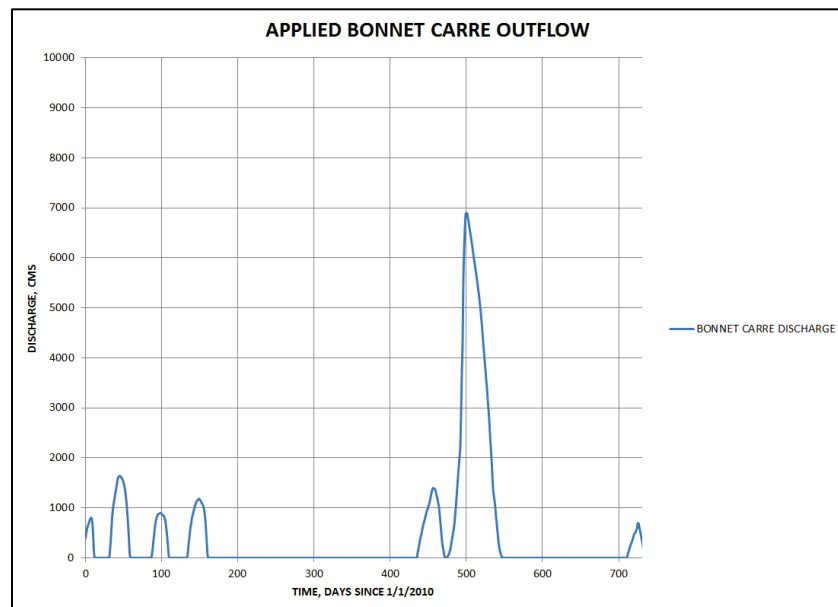


Note that the rating curve that arises from this mass balance analysis yields leakage flows that are much higher than those that have been observed in the spillway (which are on the order of 250 cms). It follows that the leakage discharge applied at Bonnet Carre Spillway in the model serves as a means of reconciling discharge measurements in the river at Baton Rouge and Belle Chasse, which have not yet been reconciled by other means (i.e., at the time that this work was conducted, the apparent mass *loss* between these discharge ranges had not been accounted for by any direct observational evidence). Since the modeling efforts contained in this report focus on changes to the lowermost river and receiving basins (below Belle Chasse), it was necessary to account for these differences in some fashion.

Subsequent to this modeling effort, a study was conducted to investigate this apparent mass loss by comparing multiple synoptic discharge measurements along the river for three separate flood events. This study yielded no direct evidence of any systematic loss of water between Baton Rouge and Belle Chasse (Lewis et al. 2017). Therefore, the apparent leakage obtained from time-integrating the discharge records at Baton Rouge and Belle Chasse is unsubstantiated by direct observation.

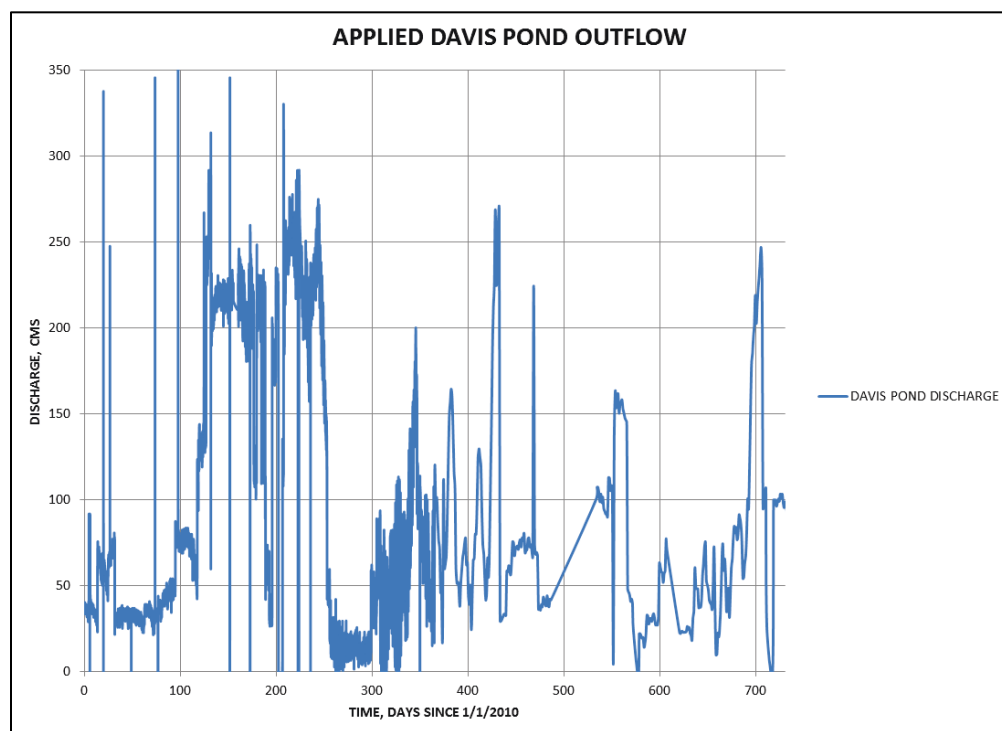
The actual gate opening period must also be included in these Bonnet Carre flow estimates. MVN has recorded the observed discharges for the 2011 opening, and the observed values are included in the applied boundary condition. The applied Bonnet Carre discharge is given in Figure 3-5.

Figure 3-5. Discharge hydrograph for Bonnet Carre Diversion: 2010–2011.



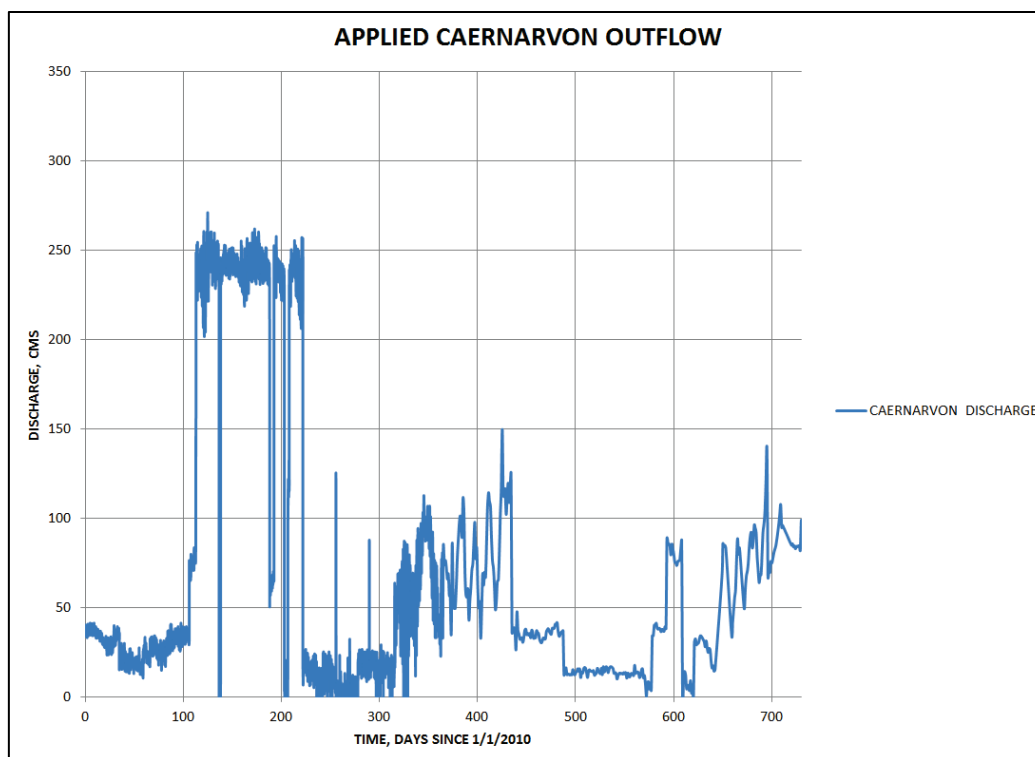
Davis Pond: The Davis Pond Diversion is located at RM 120 and was constructed to establish favorable salinity conditions in Barataria Bay. The diversion began operation in 2001 and has a maximum flow capacity of 300 cms, regulated by salinity monitoring in the pond area (Lindquist and Summer 2007). The flowrate at the Davis Pond Diversion is measured by USGS (USGS 295501090190400 Davis Pond Freshwater Diversion near Boutte, LA) and is applied as measured to the model (see Figure 3-6).

Figure 3-6. Discharge hydrograph for Davis Pond Diversion: 2010–2011.



Caernarvon Diversion: The Caernarvon Diversion is located at RM 82 and was completed in early 1991 with a design discharge of 225 cms. This diversion was constructed to regulate salinity in the Breton Sound and Caernarvon marsh areas on the east bank of the Mississippi River and to improve fish and wildlife habitat (Lane et al. 1999). The flowrate at the Caernarvon Diversion is measured by USGS (USGS 295124089542100 Caernarvon Outfall Channel at Caernarvon, LA) and is applied as measured to the model (see Figure 3-7).

Figure 3-7. Discharge hydrograph for Caernarvon Diversion: 2010–2011.



Bohemia Spillway-Fort St. Philip: The Bohemia Spillway is a degraded overflow structure along the eastern bank of the Mississippi River upstream of Venice, LA. The spillway width extends eastward approximately 3 miles from the river to Breton Sound. This diversion extends lengthwise along the river approximately 12 miles from the end of the Mississippi River levees at RM 40 to Bayou Lamoque, RM 28. Fort St. Phillip is a crevasse resulting from breaches in an existing concrete sill that is in disrepair. It is on the eastern bank of the Mississippi River and is located at approximately RM 20. This site is the location of an old masonry fort used in the early 1800s to protect southern Louisiana and Mississippi from invasion. Neither of these diversions are controlled. Therefore, the geometries of these reaches are included in the model to allow the model physics to determine the outflow. These modeled outflows are compared to measured values in the calibration and validation section of this report.

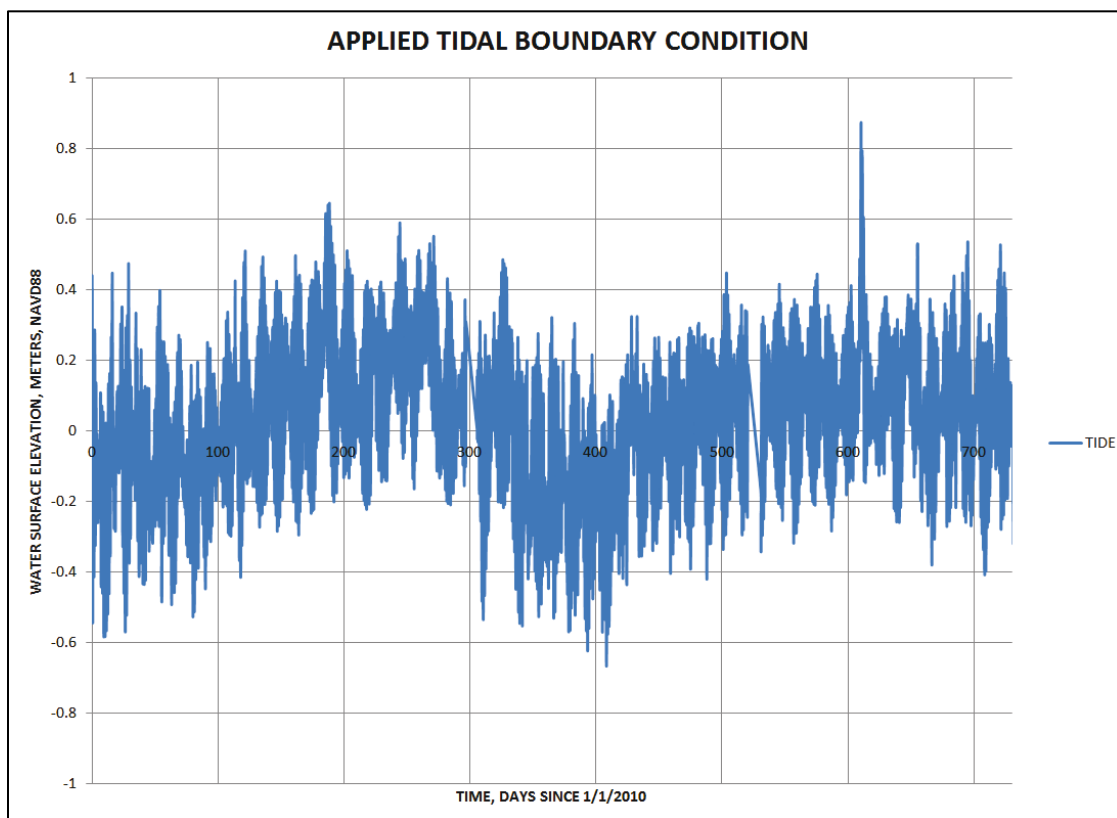
Tidal boundary condition

The Gulf of Mexico boundary condition is a tidal boundary condition based on measured data. The NOAA station at Port Fourchon (NOAA 8762075) was used to drive the boundary. Note that earlier applications of

the model utilized a complex combination of several tidal observations and tidal harmonics. However, the inherent uncertainty in this process did not guaranty that the results were any more representative of the true variability of the tidal boundary than the simple utilization of a spatially constant signal. Also, this interpolation introduced spurious currents at the boundary, which are undesirable.

The tidal data were smoothed by filtering to remove signals with a frequency of less than 4 hours. The data were adjusted for vertical offset and amplitude to ensure that the data applied along the entire boundary would return to match the observations at Port Fourchon. The vertical adjustment was -0.08 m, and the amplitude multiplier was 1.05. The applied tidal boundary condition is given in Figure 3-8.

Figure 3-8. Applied tidal boundary condition.



Wind forcing

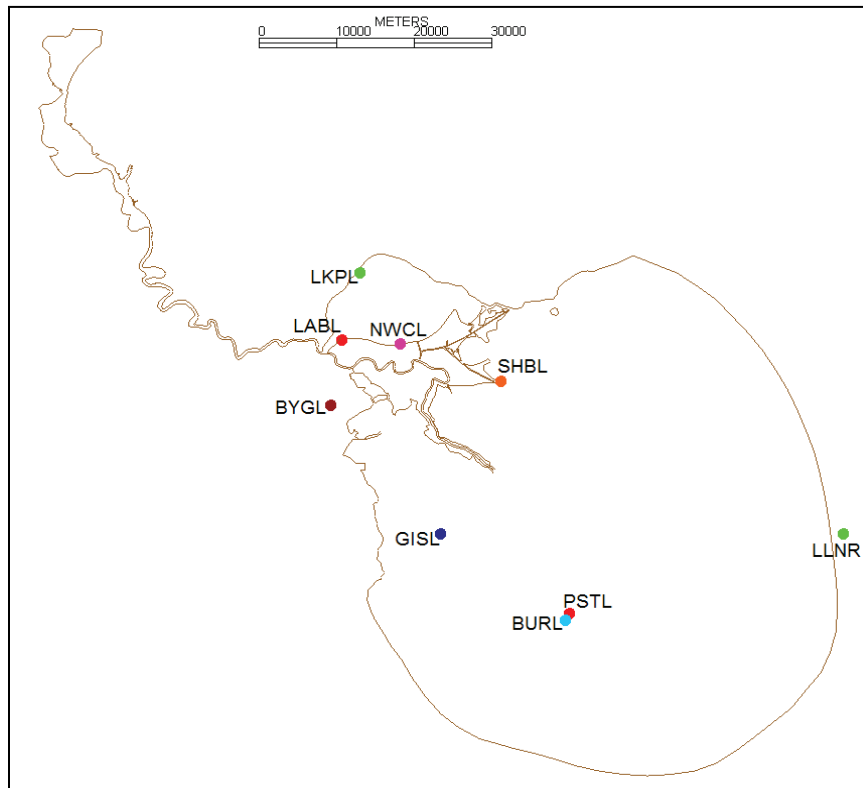
Wind data were obtained from the NOAA National Data Buoy Center for nine locations in the model domain vicinity. Given that the effect of the wind is largest in the estuarine portion of the model domain, the wind

stations are concentrated in this area. Any data gaps greater than 4 hours were filled with data from the closest station. The data were then filtered to remove any signals less than 4 hours such that noise in that data was removed. Table 3-1. Wind stations gives the wind station information, and Figure 3-9 shows the location of the nine wind stations.

Table 3-1. Wind stations.

Station Name	Station Symbol	Station Location (latitude/longitude)
Southwest Pass, LA	BURL1	28.905/-89.428
Bayou Gauche, LA	BYGL1	29.789/-90.420
Grand Isle, LA	GISL1	29.263/-89.957
Bayou LaBranch, LA	LABL1	30.050/-90.368
Western Lake Pontchartrain, LA	LKPL1	30.315/-90.281
Luke Offshore Test Platform	LLNR 293 (42040)	29.212/-88.207
New Canal, LA	NWCL1	30.027/-90.113
Pilot's Station East, Southwest Pass, LA	PSTL1	28.932/-89.407
Shell Beach, LA	SHBL1	29.868/-89.673

Figure 3-9. Location map for the wind stations.



Boundary conditions for morphologic modeling

The morphologic modeling boundary conditions require a much longer time series of boundary condition data since the morphologic model runs at decadal time scales. The limited verification of the morphologic modeling was performed by comparison to the observed evolution of the deltas at the Caernarvon Diversion and the West Bay Diversion. These diversions were simulated from 1993 to 2012 and 2003 to 2012, respectively. Hence, they require much longer duration boundary conditions.

The Mississippi River Discharge and existing diversion discharges are given using the same USGS observations described in the previous section.

For the purposes of morphologic modeling, it was assumed that the dominant influences on the morphology of the deltas associated with both Caernarvon and West Bay are water and sediment discharge through the diversion and the subsequent vegetation of the emergent deposits. Wind and tide are assumed to play a much smaller role. At the West Bay diversion, this is because much of the emergent substrate associated with the deposition of river sediments consists of the deposition of sand. Although wind and wave action do affect these deposits, the influence of these forces on the morphology of the deposits is small relative to the influence of the currents and sediment emerging from the diversion. For the Caernarvon Diversion, the tidal amplitude is very small (owing to its location in the north end of Breton Sound), and the fetch length for wind waves is limited by the surrounding marsh.

Hence, for these reasons, a simplifying assumption was made to omit tide and wind boundary conditions from these verification simulations.

The sediment is modeled in terms of discrete grain classes. The full range of classes that is found in the bed material, even in minute quantities, is represented in the model. This is done to ensure proper armoring of the river thalweg. The grain classes and their sizes are given in Table 3-2.

Table 3-2. Sediment grain classes.

Sediment Class	Abbreviation	Diameter (millimeter)
Clay	CLAY	.003
Very Fine Mud	VFM	.006
Fine Mud	FM	.011
Medium Mud	MM	.023
Coarse Mud	CM	.045
Very Fine Sand	VFS	.088
Fine Sand	FS	.177
Medium Sand	MS	.354
Coarse Sand	CS	.707
Very Coarse Sand	VCS	1.41
Very Fine Gravel	VFG	2.83
Fine Gravel	FG	5.66

Noncohesive sediment boundary conditions and bed initialization

The sand and gravel sediments (noncohesive sediments) are modeled using the following transport functions:

- Bedload transport - van Rijn (1984), modified for multiple grain classes by Kleinhans and van Rijn (2002)
- Suspended load – Wright and Parker (2004)
- Hiding factor – Egiazaroff (1965).

For the Caernarvon application, the sand load is specified at the Caernarvon outfall, according to rating curve relationships derived from a previous model study using the same AdH model (Brown et al. 2015).

For the West Bay application, the inflowing boundary condition is represented by applying a total sand load rating curve developed for Belle Chasse, LA (Allison et al. 2012) and then multiplying the resulting load by the observed fraction of each grain present in the sediment bed. This type of boundary condition is necessary because of the duration of the simulations, but there is inherent uncertainty associated with its application, for the following reasons:

- The rating curve based on observations is not segregated into discrete grain classes; therefore, it requires an approximation of this partitioning.
- Inconsistencies between observed concentrations and the concentrations calculated by the transport functions can result in significant erosion or deposition of sediment at the inflow boundary.
- For this reason, the model upstream of Caernarvon is run with a fixed bed elevation; this allows the model to adjust to any spurious sediment loads introduced at the boundary without influencing the conveyance capacity of the river.

The sediment bed is initialized as follows:

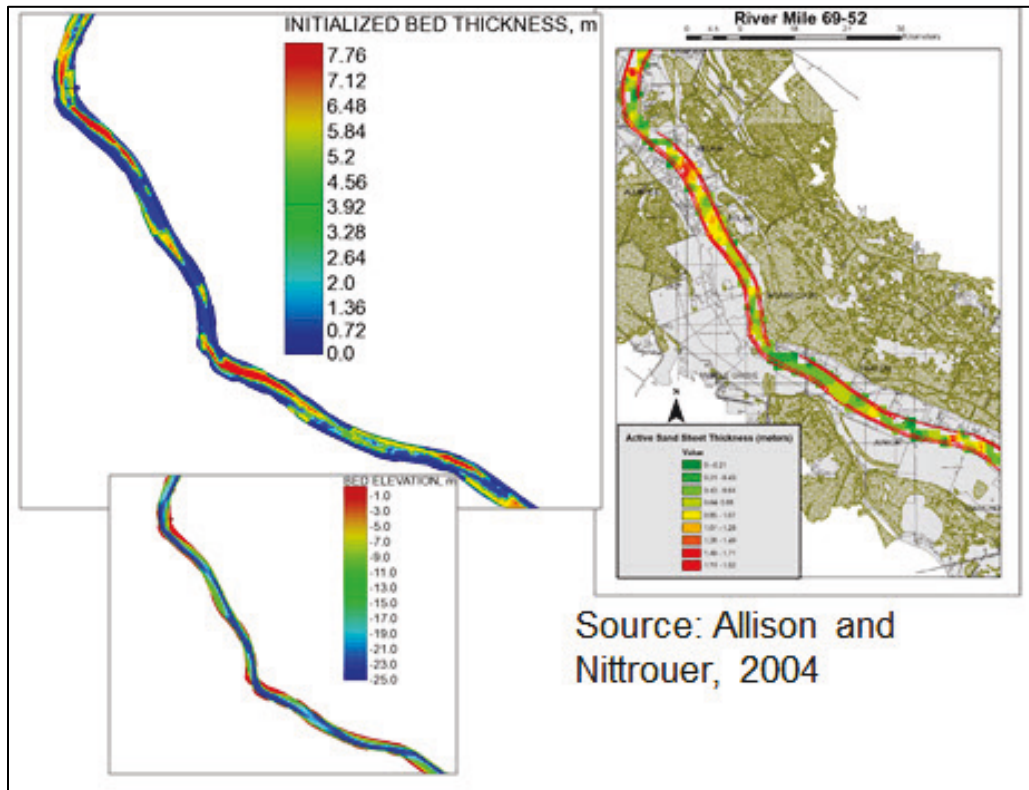
- The initial bed consists of six bed layers.
- The top four bed layers are *zero-thickness* layers; these are used to store depositional layers.
- The bottom two layers are defined by an elevation horizon; that is, their thickness varies spatially and is defined by the difference between the defined elevation of the top of the bed layer and the local elevation of the bed.
- The grain composition of the layers was taken from data collected in the river (Brown et al. 2015). They represent typical gradation in the river for lateral bars and point bars (top layer sediment) and deep thalweg sediments (bottom layer sediment).
- The elevation horizons and corresponding grain composition of the bed layers are given in Table 3-3.
- To initialize the bed, the model is run over several annual hydrographs without allowing bed elevation to change. Since the bed layer thicknesses and bed gradations are still permitted to change, this technique initializes the bed gradation (building up deposits of finer material in the lateral bars and scouring the thalweg down to relict material) without influencing the hydrodynamics with changes to the bed elevation.

Table 3-3. Applied bed gradations.

Layer	Elevation Horizon (meters, NAVD88)	Clay	VFM	FM	MM	CM	VFS	FS	MS	CS	VCS	VFG	MG
Top layer (lateral bars and point bars)	-18	0	0	0	0	0	.09	.76	.14	.01	0	0	0
Bottom layer (deep thalweg)	-23	0	0	0	0	0	.09	.128	.6	.18	.001	.0009	.0001

The results of this initialization in the lower river are depicted in Figure 3-10. This figure shows that the tendency to scour down to relict material is consistent with the observations of Allison and Nittrouer (2004).

Figure 3-10. Downstream bed sediment initialization.



Cohesive sediment properties and boundary conditions

Observations of cohesive sediment settling characteristics at the Caernarvon Diversion outfall indicate that the settling speeds are on the same order of magnitude as the free settling speeds on the individual,

unfloculated grains. Hence, the behavioral characteristics of the cohesive sediments are assigned to simulate these free settling characteristics. Also, since the primary consideration for cohesive sediments in this modeling effort is associated with deposition of the sediments, the erosional characteristics of these sediments are assumed to be those associated with recently settled sediments (i.e., sediment that can be easily resuspended). In other words, for this study, no effort was made to include the influence of consolidation on the erosion characteristics of newly deposited sediments; the erosion characteristics of existing consolidated beds are modeled, but new deposits in the model do not consolidate over time. The cohesive sediment grain characteristics are given as follows:

- Cohesive sediments are assigned properties appropriate for unconsolidated, free settling fine sediment.
- Sediment is assumed to settle grain by grain; settling speeds taken from Stokes Law.
- Critical shear for erosion assumed constant for all grains; near the same value as very fine sand.
- Erosion rate prescribed by Alishahi and Krone (1964). Erosion rate constant given as a function of the critical shear for erosion (according to Lick [2009]).
- Critical shear for deposition assumed proportional to grain size, scaled by critical shear of very fine sand. Deposition given by Krone (1962)

The cohesive sediment grain properties are given in Table 3-4.

Table 3-4. Cohesive sediment grain properties.

Class	Diameter (mm)	Settling Velocity (mm/sec)	Dry Bulk Density (kg/m ³)	Critical Shear for Erosion (Pa)	Erosion Rate Constant (kg/m ² /sec)	Critical Shear for Deposition (Pa)
CLAY	0.003	0.009	848	0.125	0.002	0.005
VFM	0.006	0.036	848	0.125	0.002	0.01
FM	0.011	0.121	848	0.125	0.002	0.02
MM	0.023	0.529	848	0.125	0.002	0.04

mm = millimeter
 sec = second
 kg = kilogram
 Pa = Pascal

For the Caernarvon application, the fine sediment load is specified at the Caernarvon outfall, according to rating curve relationships derived from a previous model study using the same AdH model (Brown et al. 2015).

Bed sediment characteristics and marsh vegetation characteristics

The sediment characteristics in AdH/SEDLIB are specified both by grain class and sediment bed layer. The grain class specifications are used to determine the properties of any material deposited during the simulation. These are given in the previous section (above). The bed layer specifications represent the initial conditions of the sediment bed. These characteristics are given in Table 3-5.

Table 3-5. Bed sediment characteristics.

Parameter	Value
Dry bulk density of sandy beds (kg/m ³)	1590
Dry bulk density of cohesive beds (kg/m ³)	1060
Critical Shear for Erosion for cohesive beds (Pa)	0.5
Erosion Rate Constant for cohesive beds (kg/m ² /sec)	0.01

The marsh vegetation model requires specification of the parameters given in Chapter 2. It also requires specification of the erosional characteristics of sediment beds. The values and references are given in Table 3-6.

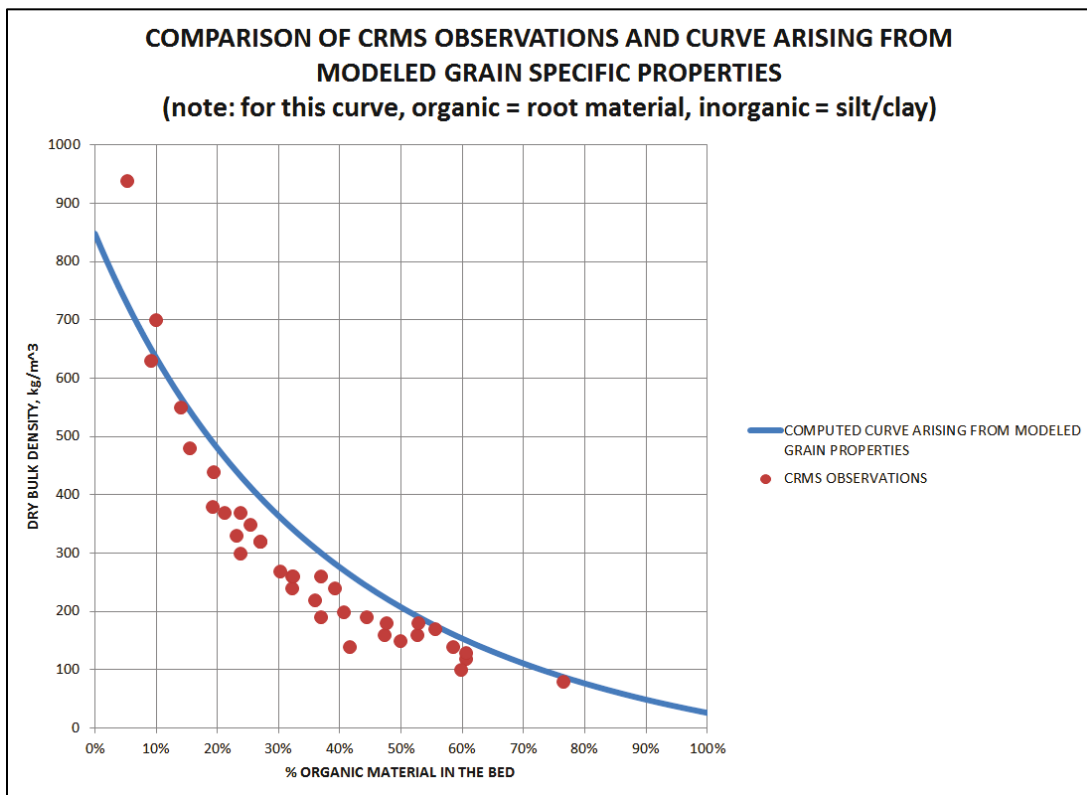
Table 3-6. Marsh vegetation parameters.

Parameter	Value	Primary Source
Maximum above-ground primary productivity (kg/m ² /sec)	4E-08	Darby (2006)
Limiting water depth for plant growth (m)	0.2	Kirwen and Guntenspergen (2012)
Root to shoot ratio	3	Darby (2006); Snedden et al. (2015)
maximum depth of root penetration (m)	1.0	
labile fraction	0.1	
Maximum equilibrium vegetation mass (kg/m ²)	1.6	Kirwen and Guntenspergen (2012)
Specific gravity of organics	1.3,1.6	Glinski et al. (2011); Huang et al. (2009)
Dry bulk density of refractory organics (kg/m ³)	160	Wamsley (2013)
Dry bulk density of roots (kg/m ³)	26	McKay et al. (2010)
Critical shear for erosion for vegetated beds (Pa)	1.0	
Erosion rate constant for vegetated beds (kg/m ² /sec)	.02	

These vegetation characteristics maximum organic accretion rates of approximately 0.8 centimeter (cm)/year, which is consistent with the long-term average value for multiple observations of the accretion rates in Louisiana marshes (Jarvis 2010).

Note that for layers that contain organic sediment (i.e., layers where roots grow and/or refractory organics are stored), the layers are assigned bulk density values and erosion characteristics that are based on the grain fraction weighted average of the characteristics associated with the constituent grains (within the context of the model, the roots and refractory organics are inventoried as grains). This permits the properties of the bed to change in proportion to the organic content. Figure 3-11 demonstrates this with respect to bulk density.

Figure 3-11. Comparison of modeled and observed bed bulk density as a function of organic content.



4 Hydrodynamic and Salinity Calibration and Validation

Hydrodynamic calibration

The hydrodynamic calibration consisted largely of the following tasks:

- Adjusting the friction parameters
- Adjusting the horizontal turbulent mixing parameters
- Ensuring that the model bathymetry and geometry are correct
- Ensuring that the model resolution is converged, especially in marsh conveyance channels (by allowing the mesh to adapt).

Hydraulic roughness

The hydraulic roughness of the submerged features (i.e., the river, channels, open water) is given by a general expression for boundary shear stress. The formulation given here is derived from a modified form of the classic logarithmic velocity profile. This modified profile was physically justified by Christensen (1972). The traditional profile yields a velocity of $-\infty$ at the bed whereas the modified profile forces the velocity to 0 at the bed. Note that this equation collapses to Manning's Equation for roughness to depth ratios within the Manning range; hence, this is effectively the same as Manning's Equation.

$$\tau_{b,x} = \frac{1}{2} C_D \rho u \sqrt{u^2 + v^2} \quad (9)$$

$$\tau_{b,y} = \frac{1}{2} C_D \rho v \sqrt{u^2 + v^2} \quad (10)$$

$$C_D = 2 \left(\frac{\kappa \beta}{\left[(\beta + 1) \{ \ln(\beta + 1) - 1 \} + 1 \right]} \right)^2 \quad (11)$$

$$\beta = 29.7 \frac{d}{k} \quad (12)$$

$$\kappa = 0.4 \quad (13)$$

Where C_D is the bed shear stress drag coefficient, $\tau_{b.x}$ is the x -component of the bed shear stress, $\tau_{b.y}$ is the y -component of the bed shear stress, u is the x -component of the depth-averaged velocity, v is the y -component of the depth-averaged velocity, ρ is the density of water, d is the water depth, k is the equivalent sand roughness height, and κ is the Von Kármán constant.

The hydraulic roughness of emergent features is specified as the bottom shear stress resulting from a steady (or quasi-steady) current through rigid, unsubmerged vegetation. The formulation given here is taken from Walton and Christensen (1980). This formulation includes both the form drag induced by flow through the obstructions and the skin drag induced by flow over the bed.

$$\tau_{b.x} = \frac{1}{2} C_D \rho u \sqrt{u^2 + v^2} \quad (14)$$

$$\tau_{b.y} = \frac{1}{2} C_D \rho v \sqrt{u^2 + v^2} \quad (15)$$

$$C_D = \frac{0.32 \left(1 - m \frac{\pi}{4} \delta^2 \right)}{\left[\ln \left(\frac{10.94d}{k} + 1 \right) \right]^2} + C_{D,s} d m \delta \quad (16)$$

$$C_{D,s} = 0.4 \quad (17)$$

Where C_D is the bed shear stress drag coefficient, $\tau_{b.x}$ is the x -component of the bed shear stress, $\tau_{b.y}$ is the y -component of the bed shear stress, u is the x -component of the depth-averaged velocity, v is the y -component of the depth-averaged velocity, ρ is the density of water, d is the water depth, k is the equivalent sand roughness height, $C_{D,s}$ is the drag coefficient for the stems, δ is the average stem diameter, and m is the average stem density.

The calibrated roughness parameters are given in Table 4-1.

Table 4-1. Calibrated friction parameters.

Material Type	Friction Equation	Bottom Roughness height (m)	Vegetation Stem Diameter (m)	Vegetation Stem Density (stems/m ²)
Channel Bottom	9-13	0.01		
Revetments	9-13	0.07		
Marsh Vegetation	14-17	0.02	0.01	50
Forested Vegetation	14-17	0.05	0.5	0.04

One other aspect of vegetative roughness that must be recalled here is how the change in vegetation coverage feeds back into the hydrodynamic simulation. This is done by scaling the density of vegetation associated with the drag assigned to the wetland areas of the mesh by the ratio of the vegetation biomass present at a given node to the equilibrium vegetative biomass for that node. For example, if a given node has 60% of the equilibrium vegetative biomass, the density of the vegetation associated with the drag will be 60% of the maximum value.

The horizontal turbulent mixing in the wetlands and the Mississippi River is specified using Smagorinsky turbulent closure (Smagorinsky 1961).

$$\varepsilon_{SM} = 0.04 A_s \left(\frac{\partial u}{\partial x} + \frac{\partial v}{\partial y} + \frac{1}{2} \left(\frac{\partial u}{\partial y} + \frac{\partial v}{\partial x} \right) \right) \quad (18)$$

The horizontal turbulent mixing in the open bays and the offshore is specified using a modification of the Smagorinsky turbulence closure that scales the mixing length by the local depth rather than the surface area of the element (Stansby 2004). This is necessary to ensure that the mixing values it calculates are physically sensible even when applies to elements with very large surface area (as is the case in the offshore)

$$\varepsilon_{M.SM} = (0.54h)^2 \left(\frac{\partial u}{\partial x} + \frac{\partial v}{\partial y} + \frac{1}{2} \left(\frac{\partial u}{\partial y} + \frac{\partial v}{\partial x} \right) \right) \quad (19)$$

A minimum eddy viscosity of 0.1 m²/sec is enforced regardless of what value the turbulence model yields.

Modeled discharge through existing distributaries

Figure 4-1 depicts the Fort St. Philip distributary. The Bohemia Spillway extends upstream of this location. The discharge through the Bohemia Spillway and Fort St. Philip distributaries plays a crucial role in both the distribution of freshwater and in the distribution of stream power available for transporting sand. To ensure that the model is capturing the correct volume of discharge, it was necessary to ensure that the channels were resolved sufficiently such that the conveyance was properly represented. This was done by allowing the mesh to dynamically adapt. Also, one of the primary sites where model bathymetry (and geometry) was found to be of significance was associated with the effort to ensure that the discharge through the Bohemia Spillway/Fort St. Philip Diversion matched the field observations.

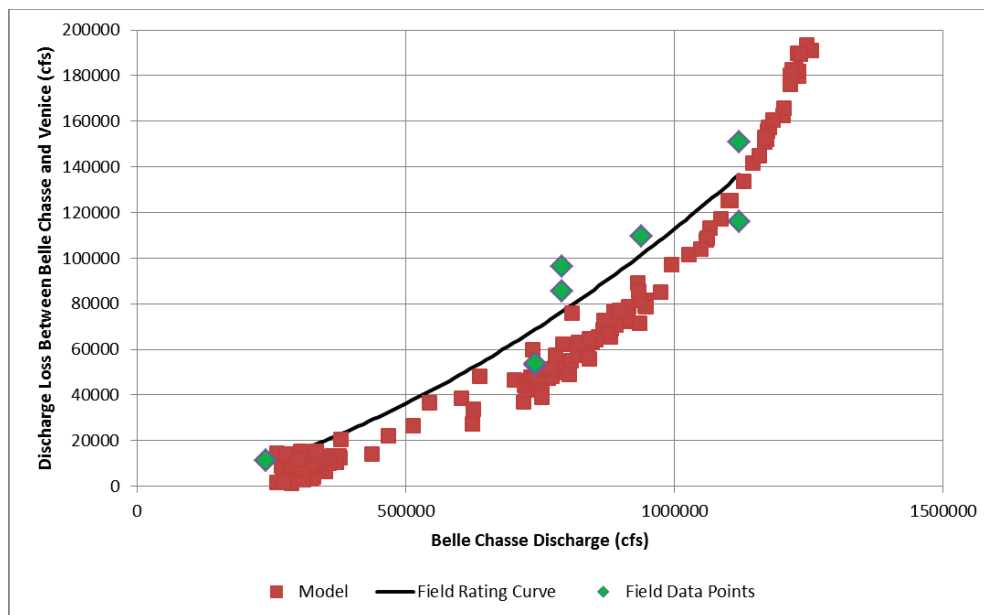
Figure 4-1. The Fort St. Philip distributary.



Figure 4-2 shows the comparison between the modeled (red) and measured (green, with the back line depicting a rating curve based on observations) flux through the Bohemia Spillway/Fort St. Philip complex, as a function of Mississippi River discharge at Belle Chasse. Although the general agreement is good, the model appears to underpredict the observations for the median flow range. However, there is considerable

uncertainty inherent in the observations (they are inferred from a difference of flux measurements), and there are only seven observations in this comparison. Therefore, since the model agrees with the observations to within the (approximate) uncertainty of the measurements, further adjustment of the model is not merited.

Figure 4-2. Comparison between modeled and observed water discharge at the Bohemia Spillway/Fort St. Philips uncontrolled diversion.



The modeled distribution of discharge through the existing diversions is compared to the observed distribution. The model accurately reflects the observed distribution, at least in this average sense.

Table 4-2. Modeled and observed fraction of total flow at existing distributaries.

	Baptiste Collette	Grand Pass	West Bay	Cubits Gap	Southwest Pass	South Pass	Pass A Loutre
Modeled Mean	0.124	0.113	0.084	0.103	0.362	0.124	0.087
Observed Mean	0.104	0.116	0.075	0.111	0.367	0.115	0.108

Water surface elevation calibration and validation

Water surface elevation and salinity data were assembled for multiple locations throughout the study area. Figure 4-3 depicts these locations and the data sources.

Figure 4-3. Observation locations for hydrodynamic and salinity calibration and validation.

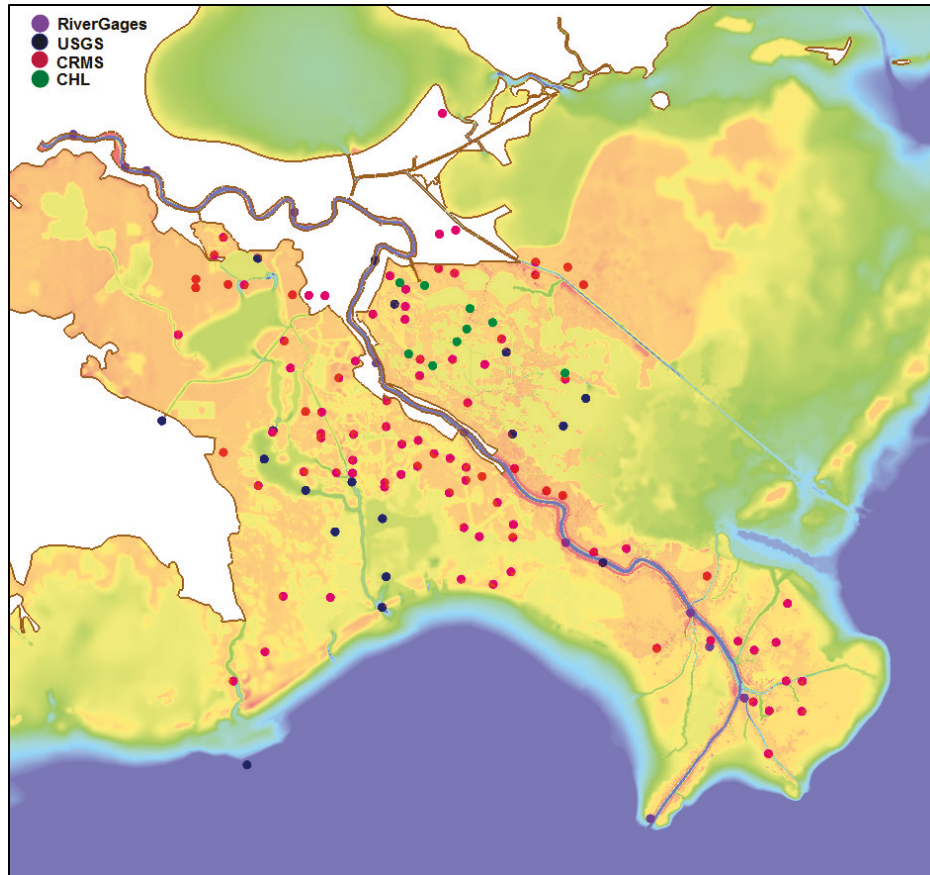


Figure 4-4 and Figure 4-5 depict some examples of time history plots of water surface elevation in Breton Sound and Barataria Bay, respectively. The ability to simulate the tidal amplitude indicates that the vegetative roughness and conveyance capacity of major channels are simulated correctly. There is a vertical offset in water surface elevation that is evident throughout Barataria Bay. It is possible that this may be due to a systematic offset in the vertical elevation of the observation stations in Barataria Bay since it is difficult to establish the vertical elevation accurately, especially in a subsiding environment. During the calibration processes, there was an adjustment of +0.07 m made to the datum of the applied tidal boundary to account for an observed systematic vertical offset in the comparisons between modeled and observed results for the entire model domain. However, the implementation of this corrected tidal boundary datum did not fully compensate for the observed offset in Barataria Bay. This implies that there may be an additional local correction that is required, possibly associated with established benchmarks in the field. However, as of the writing of this report, there is no direct evidence that can be used to confirm any specific hypothesis.

Figure 4-4. Selected water surface calibration time series plots for Breton Sound.

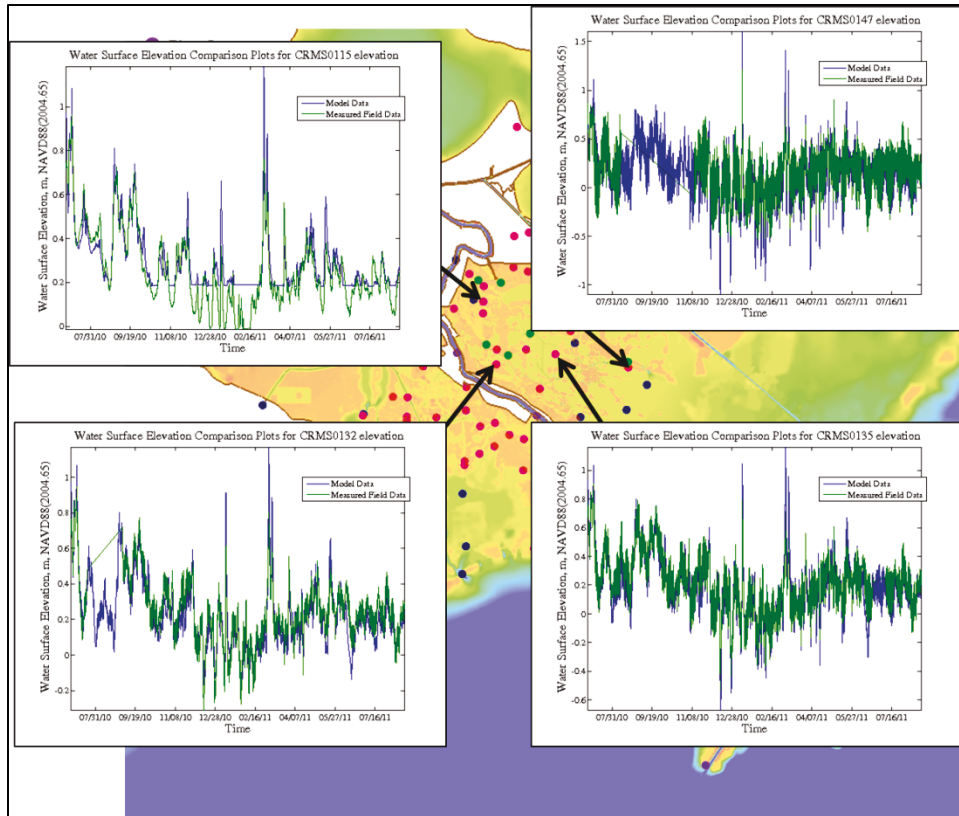
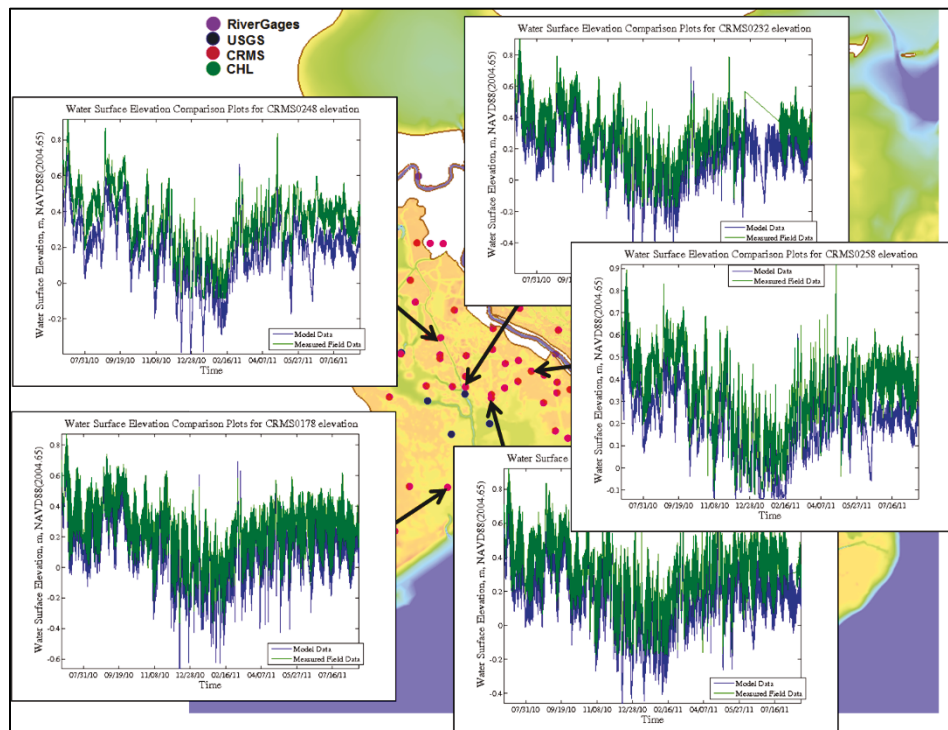


Figure 4-5. Selected water surface calibration time series plots for Barataria Bay.



For this project, quantitative statistical measures were established and published by Meselhe and Rodrigue (2013). These measures include the Normalized Root Mean Square Error, the Pearson Product-Moment Correlation Coefficient, and the Percent Bias, and the Correlation Coefficient are plotted in rank order. Plots of the statistical analyses using each of these measures between model and field observations for all available gages are given in Figure 4-6. Green and red zones on each plot indicate the thresholds of acceptable and poor statistical performance (respectively) as defined by Meselhe and Rodrigue (2013).

These statistics were computed using daily averaged data for the model and field data; hence, they are used to analyze the propagation of sub-tidal signals throughout the domain. Also, to produce useful analyses for these statistics, it is necessary for the vertical datum to be such that all of the values are either positive or negative. Therefore, for the purposes of the statistical analyses, all of the modeled and observed water surface elevation data were shifted up by 1 m.

The statistics indicate that roughly half of the modeled gages have acceptable comparisons to the field observations. The remaining poor comparisons could be influenced by several factors. One of these is the aforementioned observed vertical offset in the Baratavia Bay comparisons, and the field data have some gaps and outlier data that skew the results.

The water surface elevation validation data are given in Figure 4-7 through Figure 4-9. The results are very similar to those associated with the calibration data. Of note, however, is the storm-induced increase in water surface elevation that appears in each of the data sets. The good agreement between the model and field is further verification that the vegetative roughness is well calibrated for inundation events as well. This is important, as the roughness will partly determine the spatial extent of inundation associated with the introduction of diversions.

Figure 4-6. Statistical analysis of water surface elevation calibration for all observation locations, by rank order (green is acceptable agreement; red is poor agreement).

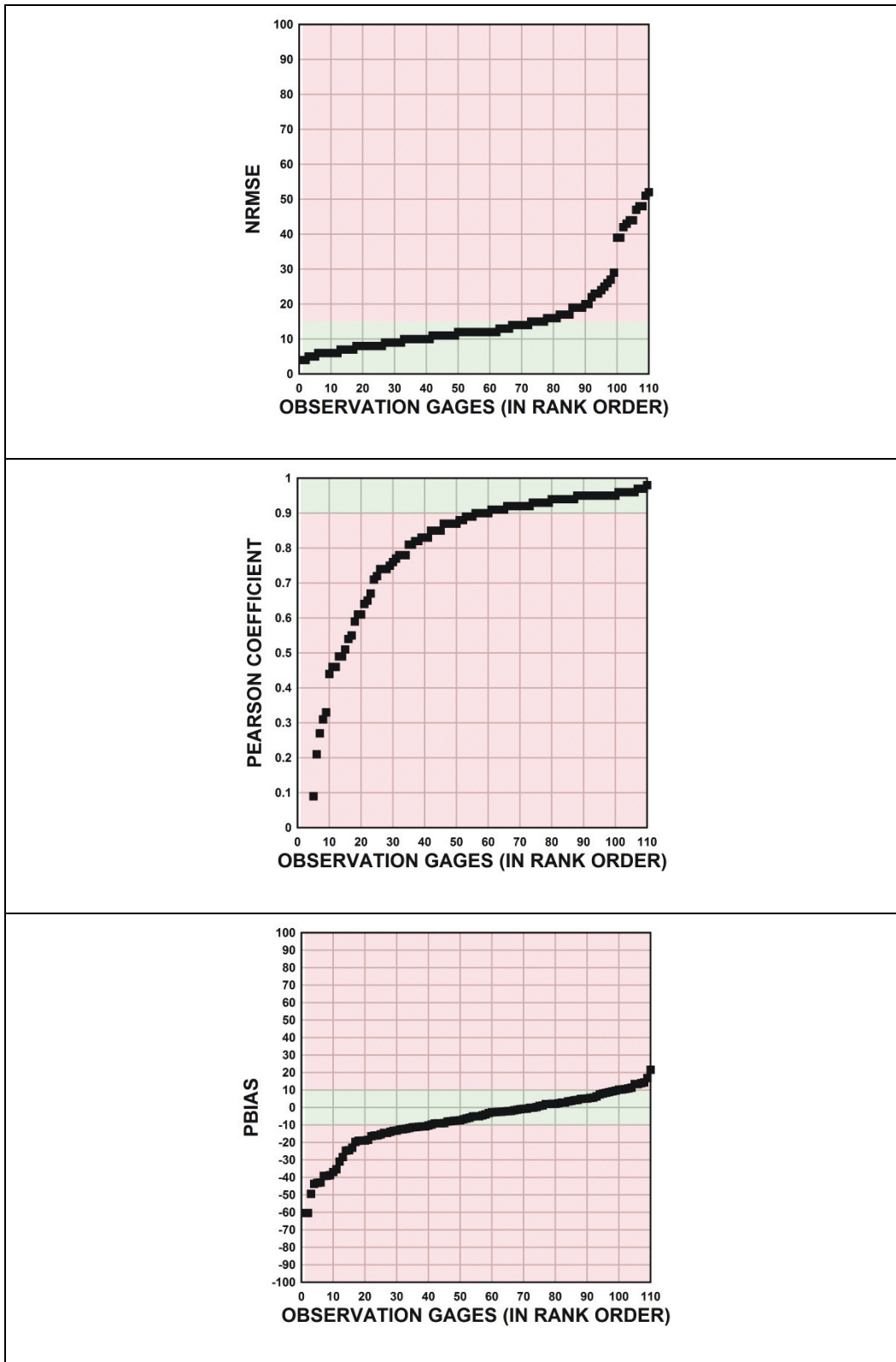


Figure 4-7. Selected water surface validation time series plots for Breton Sound.

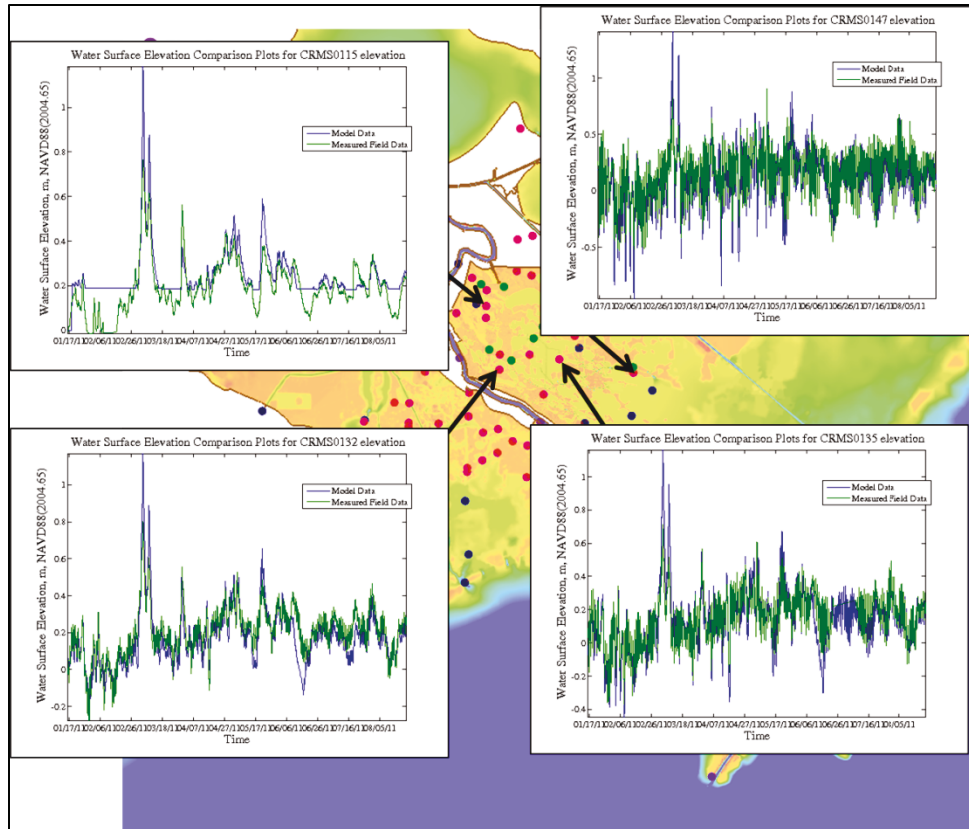


Figure 4-8. Selected water surface validation time series plots for Barataria Bay.

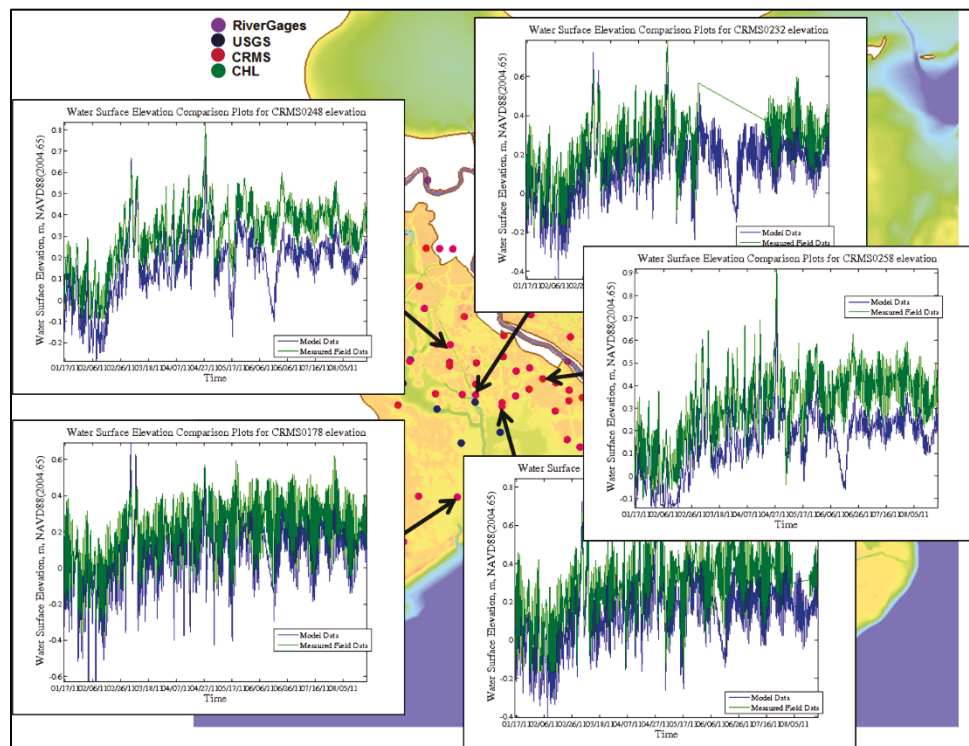
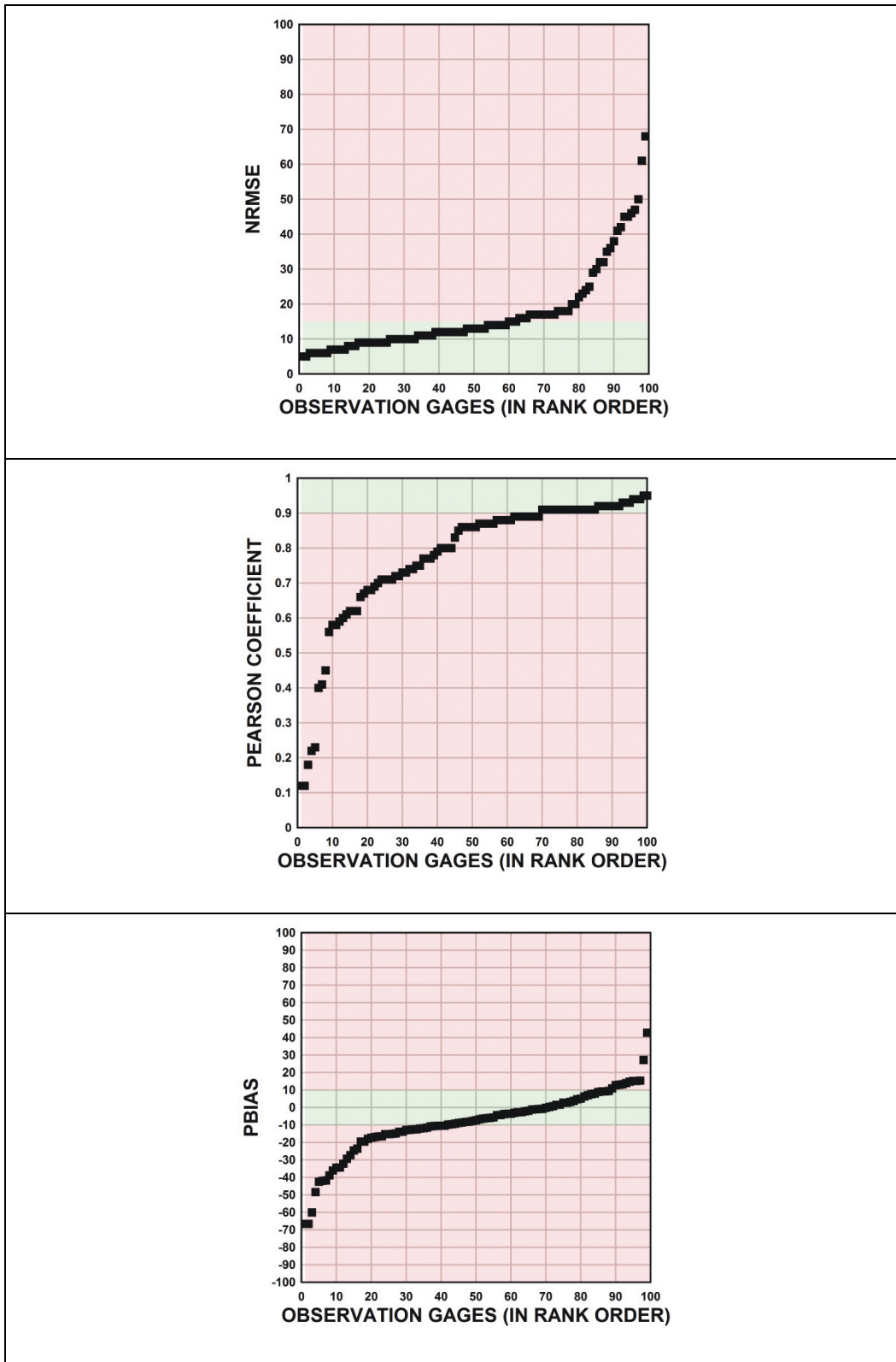


Figure 4-9. Statistical analysis of water surface elevation validation for all observation locations, by rank order (green is acceptable agreement; red is poor agreement).



Discharge observations in Breton Sound

In 2010, ERDC placed side-looking acoustic Doppler velocimeters at several channels that represent significant conveyance pathways throughout Breton Sound. Each site was calibrated to periodic acoustic Doppler current profiler measurements to yield discharges. Modeled discharges were compared against observed discharges. Several examples of these comparisons are depicted in Figures 4-10 through 4-13. It can be seen that the model simulates the general circulation of Breton Sound in a manner consistent with the observed circulation.

Figure 4-10. Discharge comparison at Site 2.

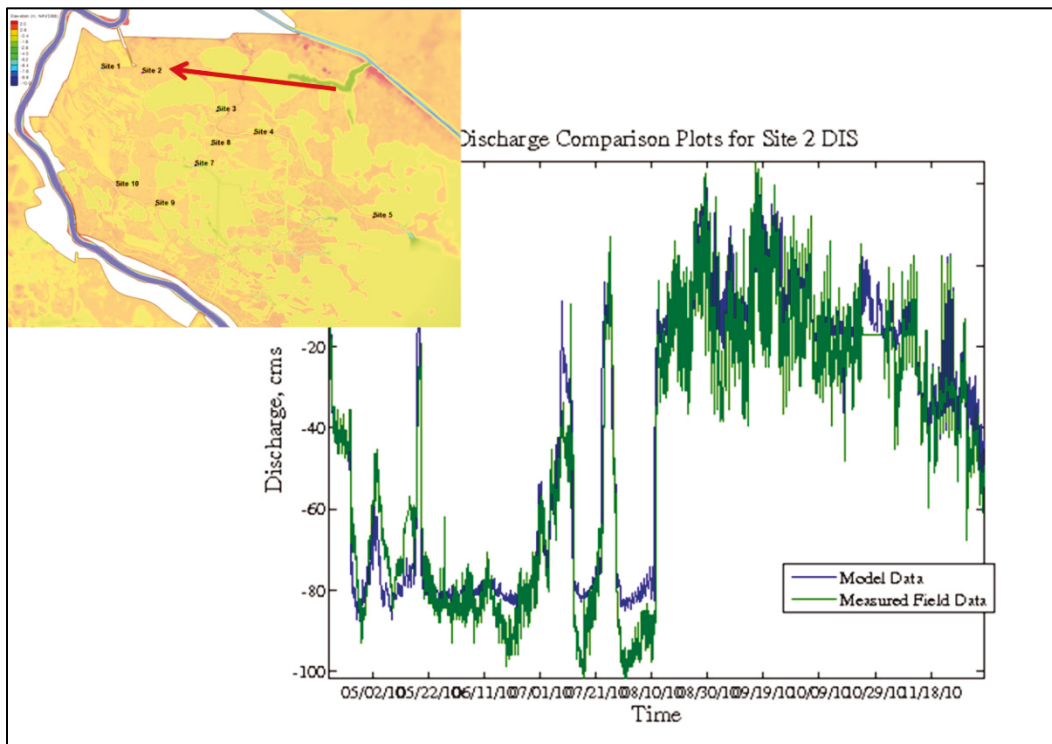


Figure 4-11. Discharge comparison at Site 3.

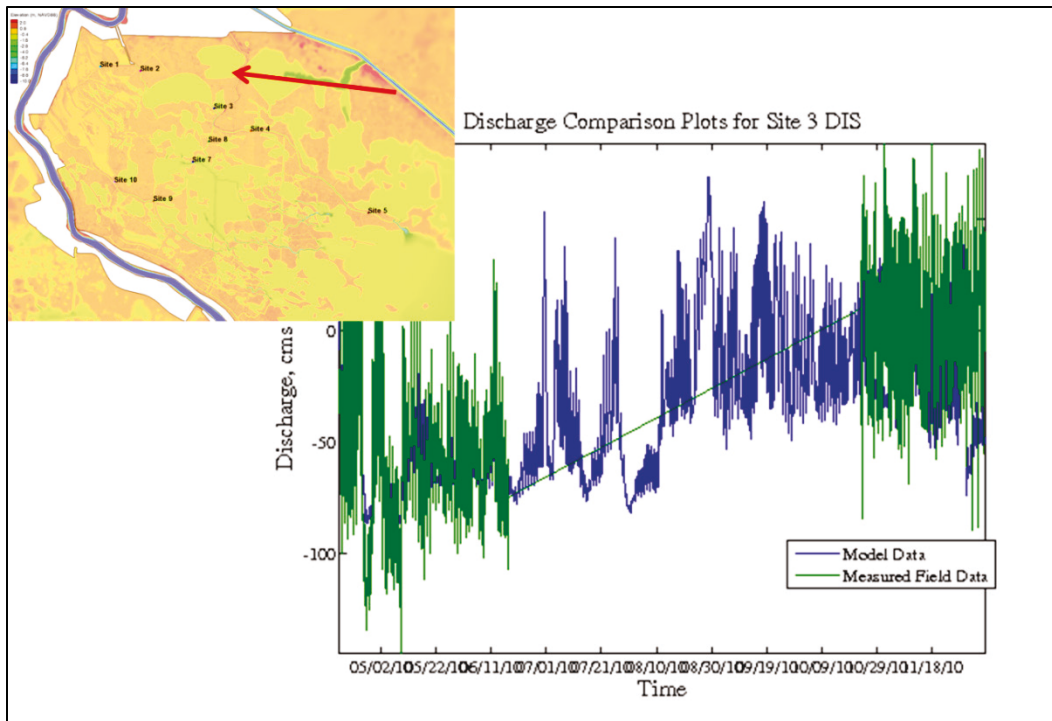


Figure 4-12. Discharge comparison at Site 5.

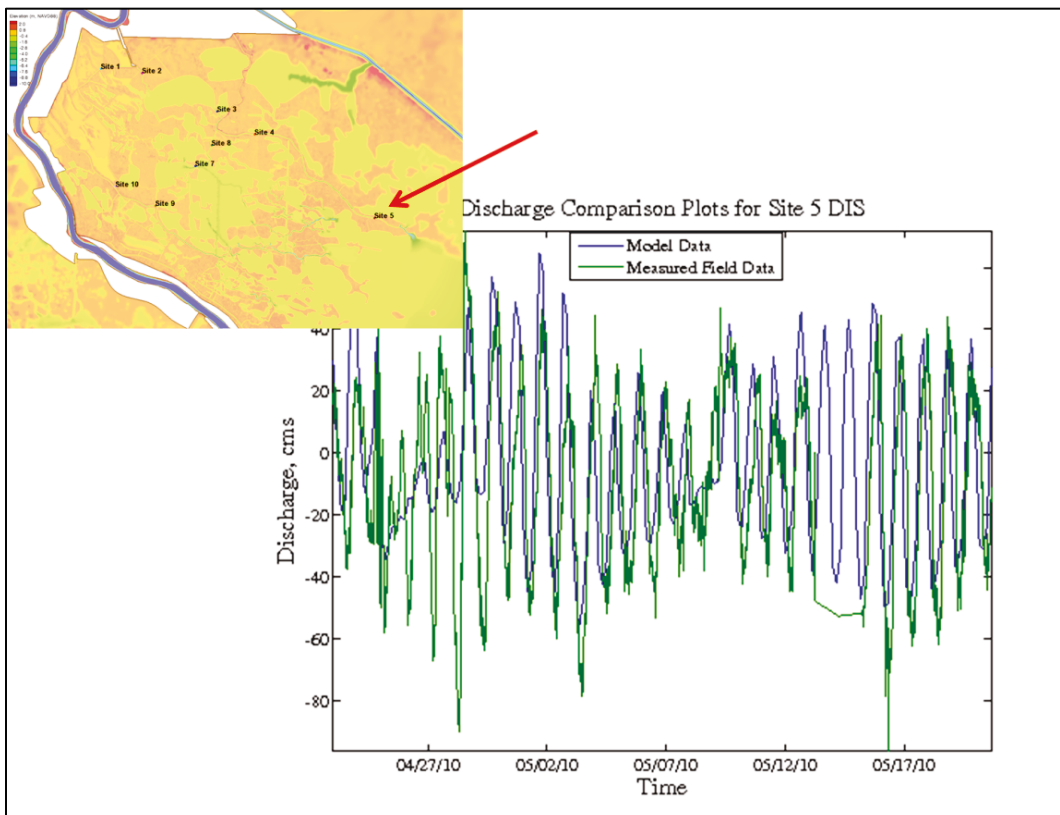
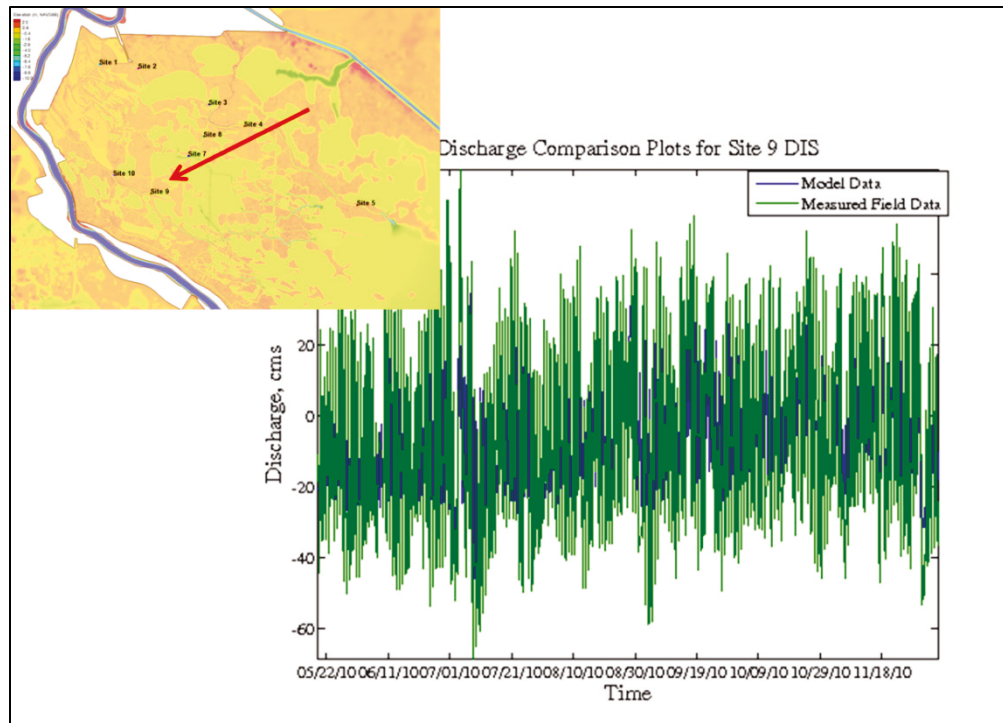


Figure 4-13. Discharge comparison at Site 9.



Salinity calibration and validation

Figure 4-14 through Figure 4-16 show snapshots (instantaneous images) of the modeled salinity contours for the spring (high river discharge), summer (falling river discharge) and fall (low river discharge), 2010. Several general features are of interest. Note that during high flow, the discharge emerging from Fort St. Philip and Baptiste Collette has a controlling influence on salinity in Breton Sound, not allowing any salinity from the Gulf to circulate into the Bay via wind driven currents. Also note how the discharge that emerges from Southwest Pass tends to jet into the Gulf of Mexico and induce a clockwise circulation between the river and Barataria Bay. This clockwise circulation is the primary means of entraining salt in Barataria Bay during high flow. Both of these phenomena can be observed in aerial imagery of the sediment plume emerging from Southwest Pass.

Figure 4-14. Color contour of spring (high river discharge) salinity.

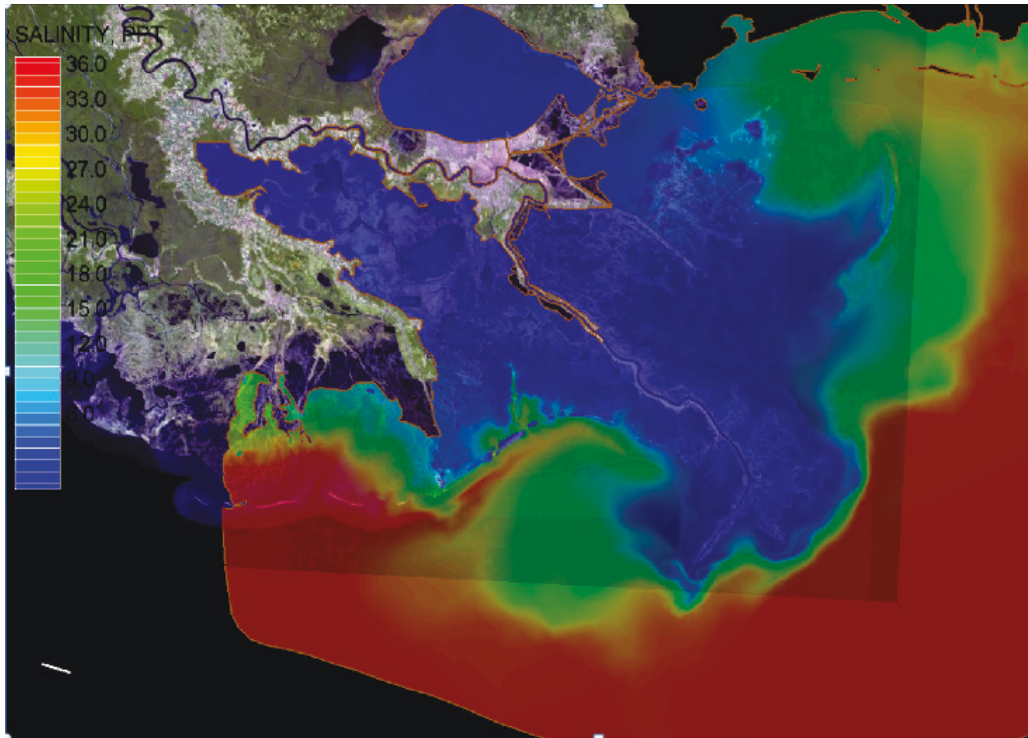


Figure 4-15. Color contour of summer (falling river discharge) salinity.

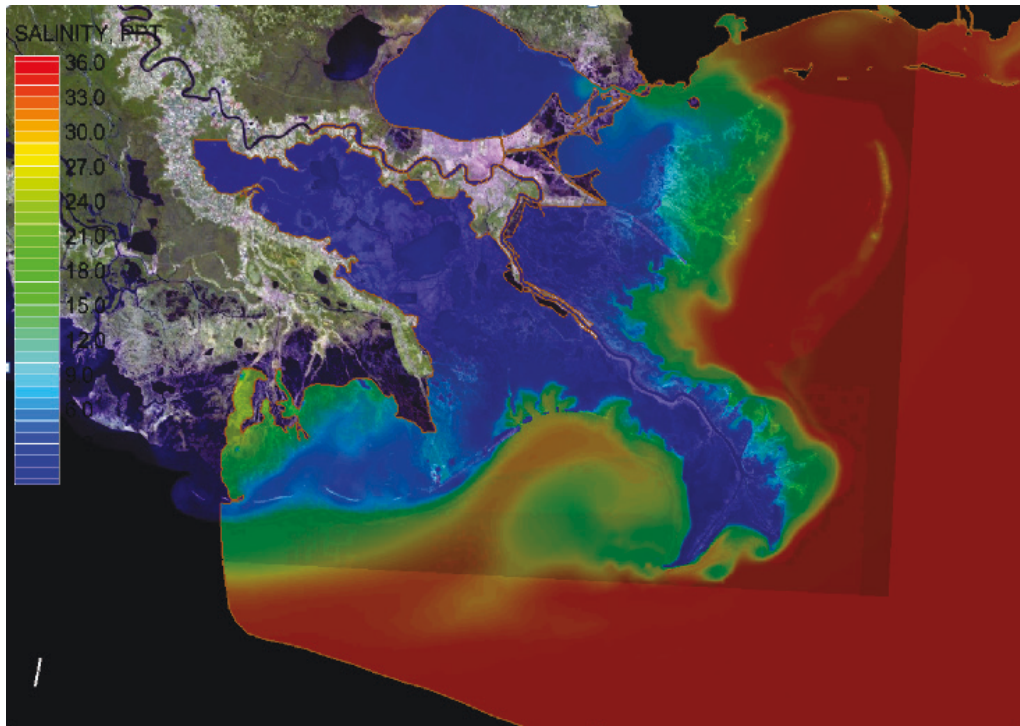


Figure 4-16. Color contour of fall (low river discharge) salinity.

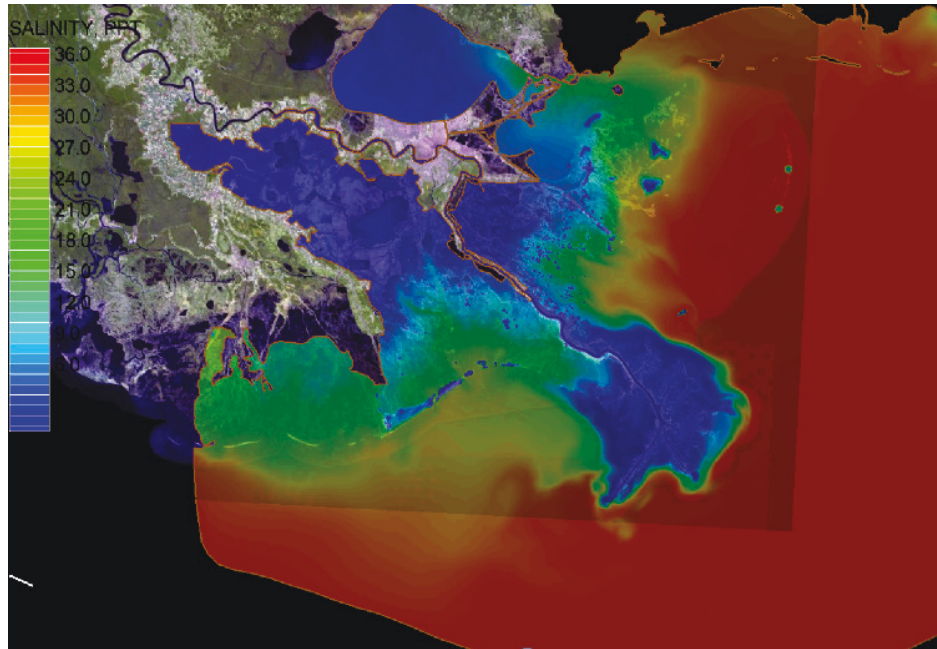


Figure 4-17 through Figure 4-19 depict the *calibration* results for salinity. In reality, however, there is no calibration for salinity as there is nothing to adjust. Salinity is a conservative substance, so there are no source or sink coefficients to tune. The mixing is prescribed by physically based equations, and the roughness and geometry are validated against hydrodynamic data. The calibration simulation is in reality just a simulation that aids in the refinement of the hydrodynamic calibration in that discrepancies in the salinity transport are indicative of errors in the hydrodynamics that are undetected in the hydrodynamic data.

It can be seen that the recovery of the salinity from fresh conditions is delayed in the model relative to the observations, although once the salinity does recover it tracks the observations quite well.

This delay in recovery appears to be due primarily to the fact that there are 3D features of the offshore circulation that are not represented in this depth-averaged model. In particular, the jet of fresh water emerging from Southwest Pass is a 3D feature in that it retains its integrity far into the Gulf (note that resolving this feature also requires very high 2D resolution, as the jet is narrow relative to the surrounding gulf). The 2D model tends to arrest its momentum (by forcing the momentum to mix vertically) and consequently forces too much fresh water north along the shoreline and into Barataria Bay.

Figure 4-17. Selected salinity calibration time series plots for Breton Sound.

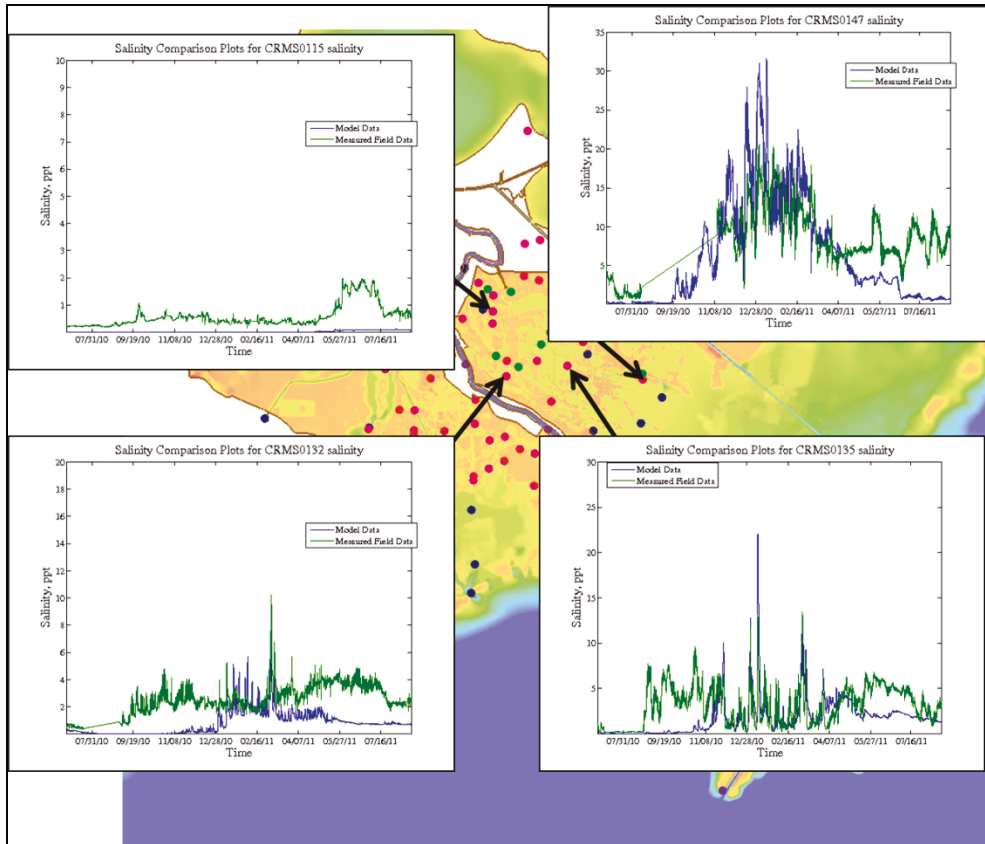


Figure 4-18. Selected salinity calibration time series plots for Barataria Bay.

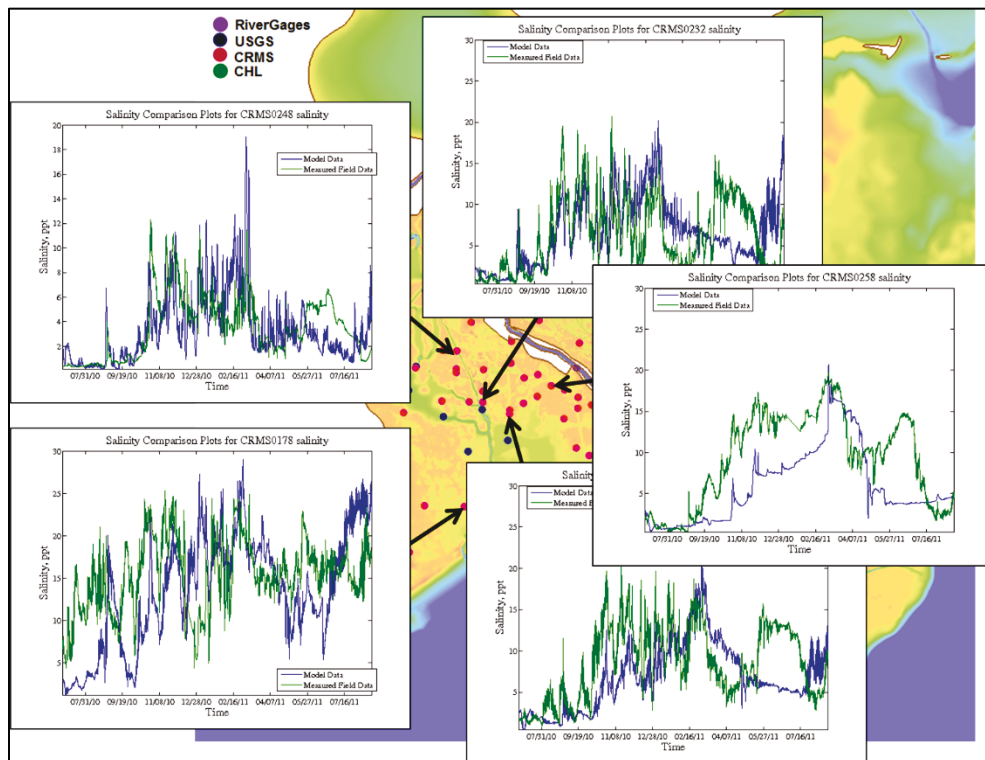


Figure 4-19. Statistical analysis of salinity calibration for all observation locations, by rank order (green is acceptable agreement, red is poor agreement).

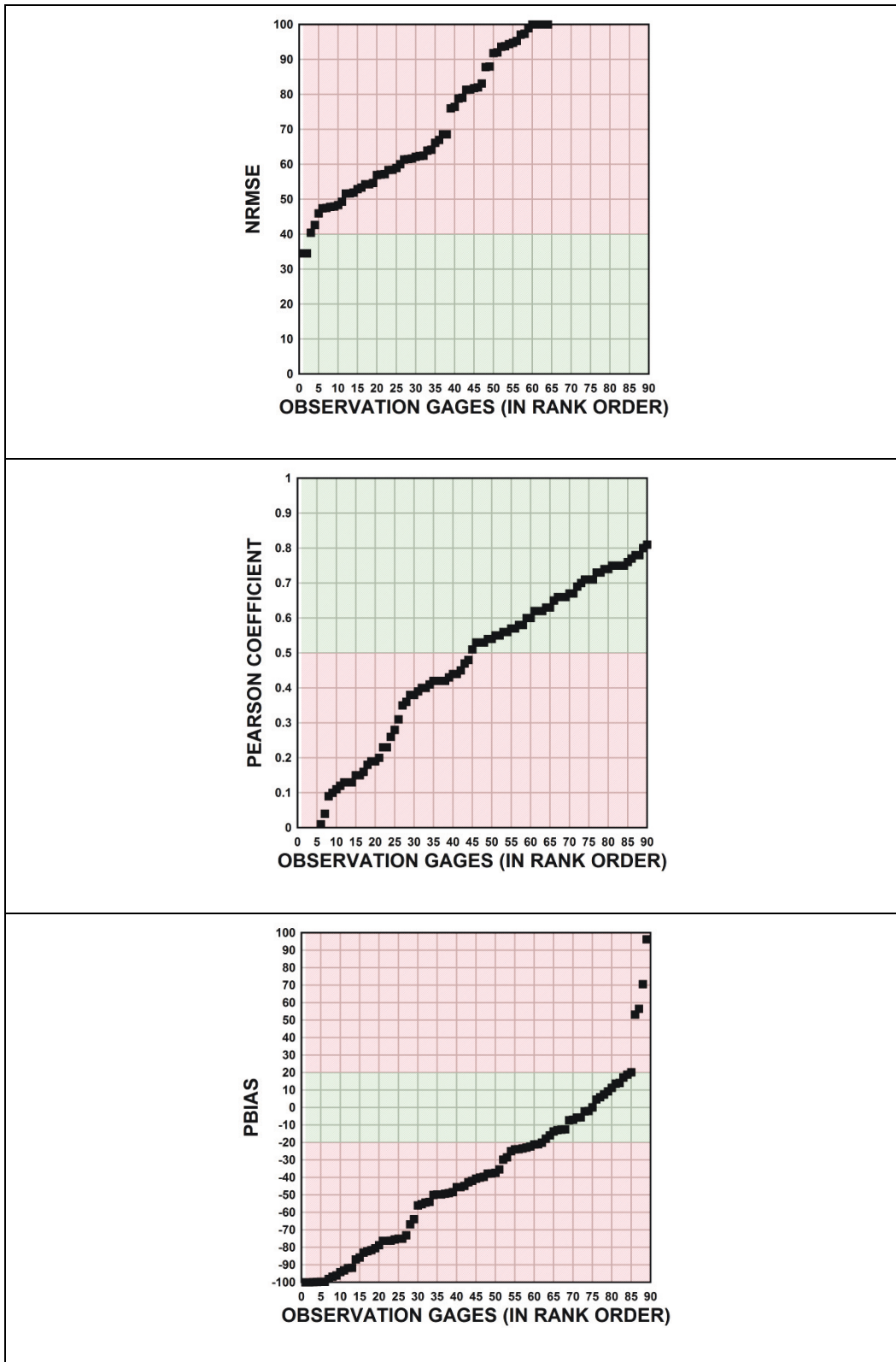


Figure 4-20 through Figure 4-22 depict the salinity validation period. Note that the agreement during this lower flow period is much better than for the earlier higher flow period. Hence, the model performs well with respect to circulation of salinity within the bays, but there are still pulses of fresh and saline water propagating in from the boundary that are either not modeled or appear to be delayed or displaced. This, again, is due primarily to the lack of highly resolved 3D modeling of the offshore circulation.

Figure 4-20. Selected salinity validation time series plots for Breton Sound.

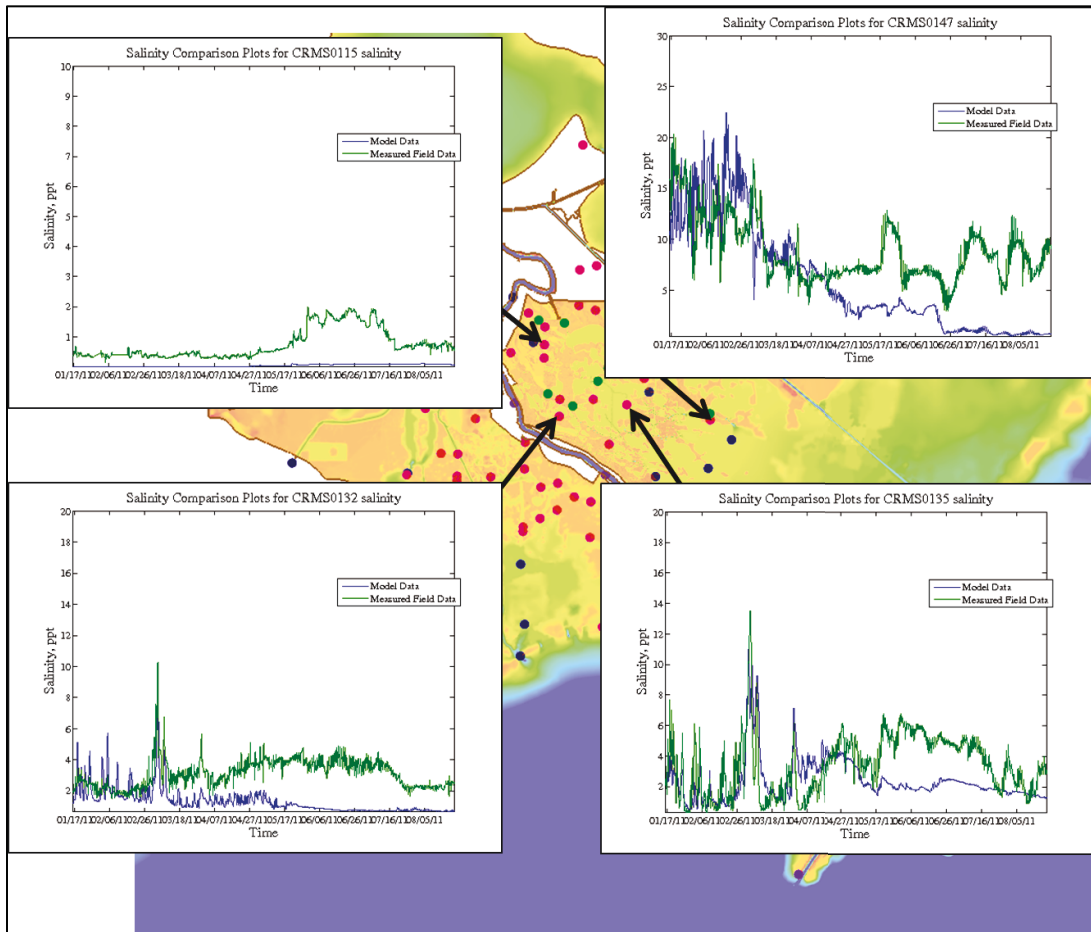


Figure 4-21. Selected salinity validation time series plots for Barataria Bay.

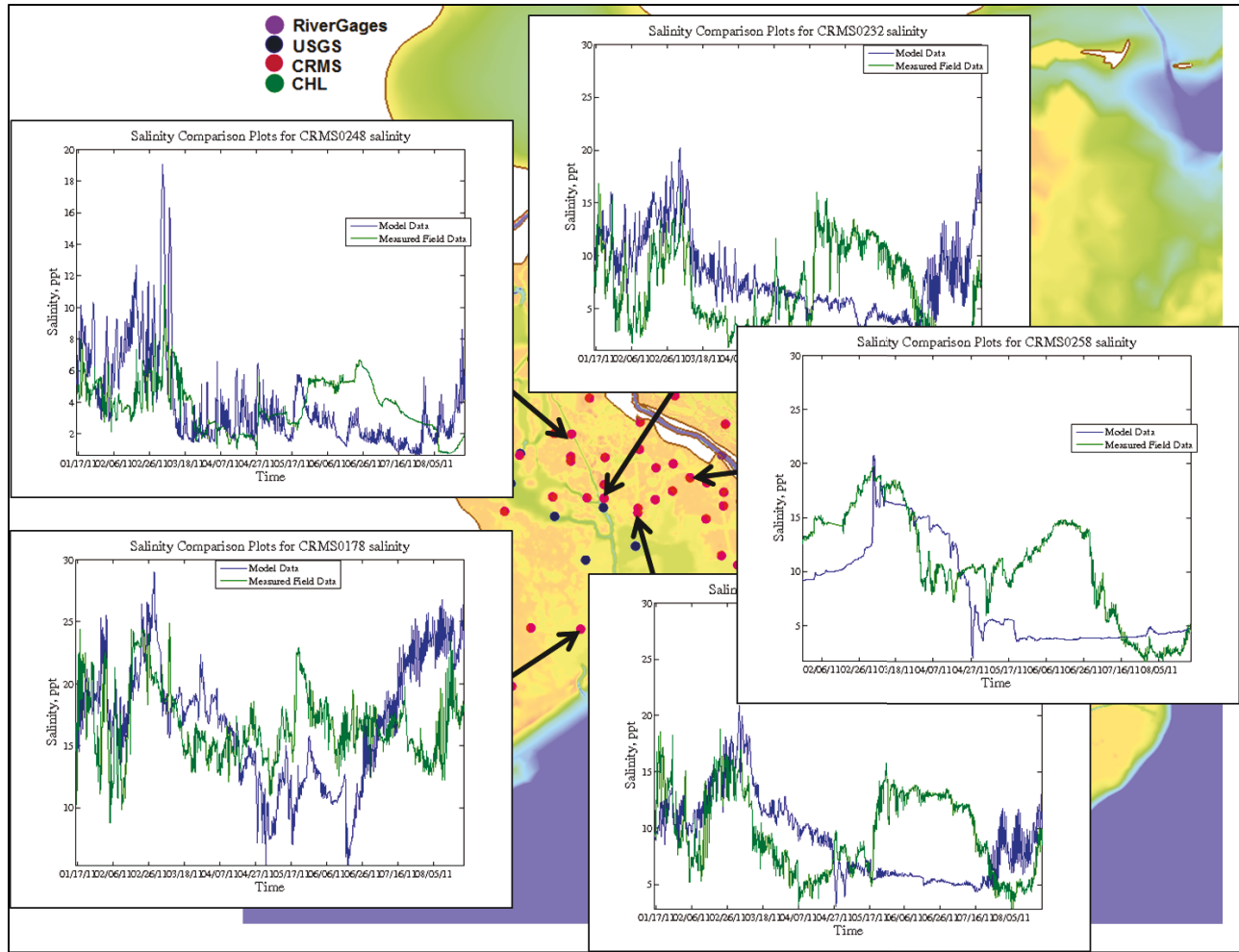
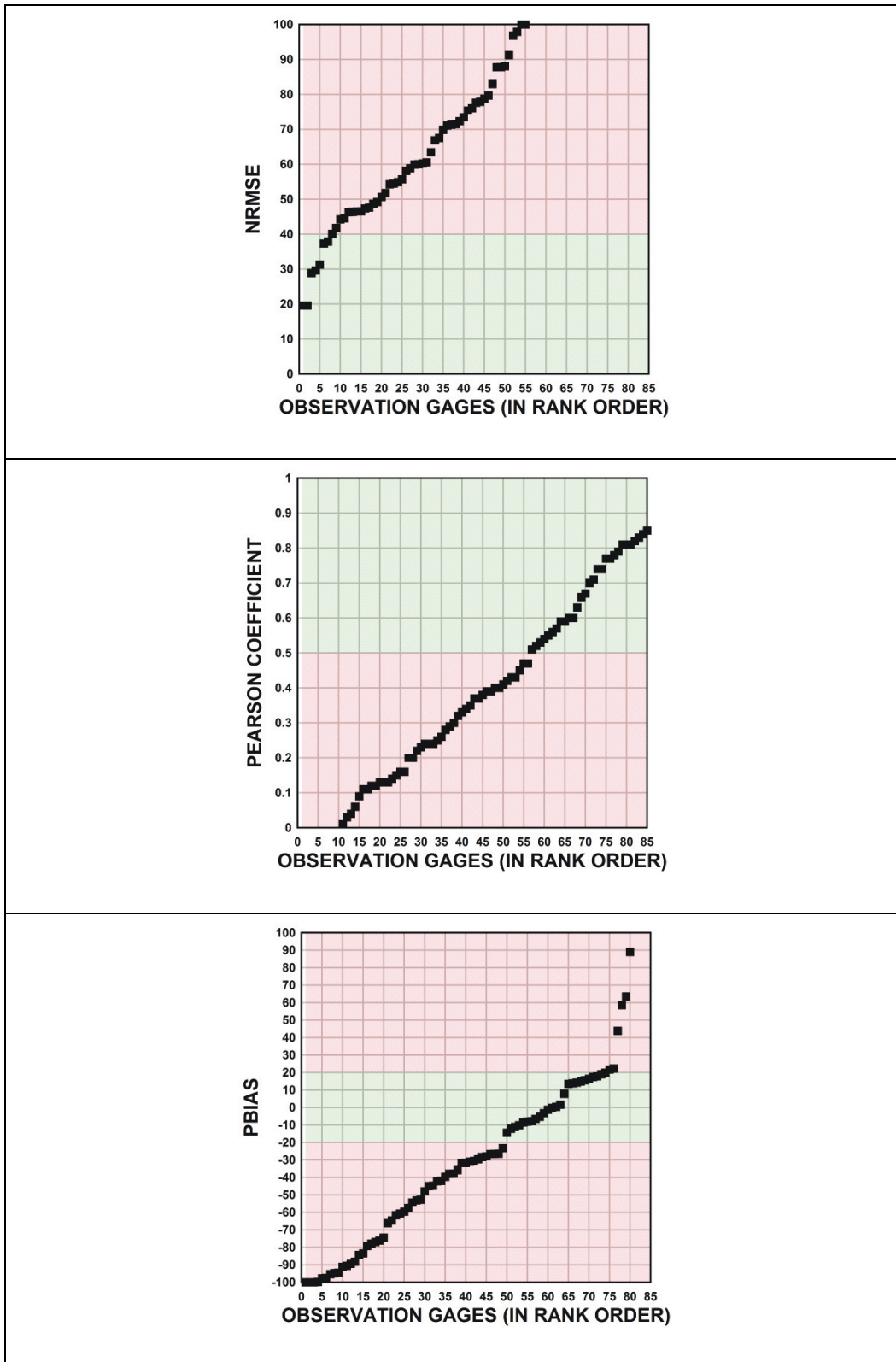


Figure 4-22. Statistical analysis of salinity validation for all observation locations, by rank order (green is acceptable agreement; red is poor agreement).



5 Morphology and Vegetation Validation

Vegetation validation

A cursory validation of the vegetation model was conducted whereby the model was allowed to grow to an equilibrium condition in Breton Sound, and the biomass results were compared to selected observations. The results are given in Figure 5-1 and Table 5-1. These results demonstrate that the model produces the proper spatial extent of vegetation and that the parameters selected for this application yield biomass values consistent with observations.

Figure 5-1. Modeled vegetation biomass in Breton Sound.

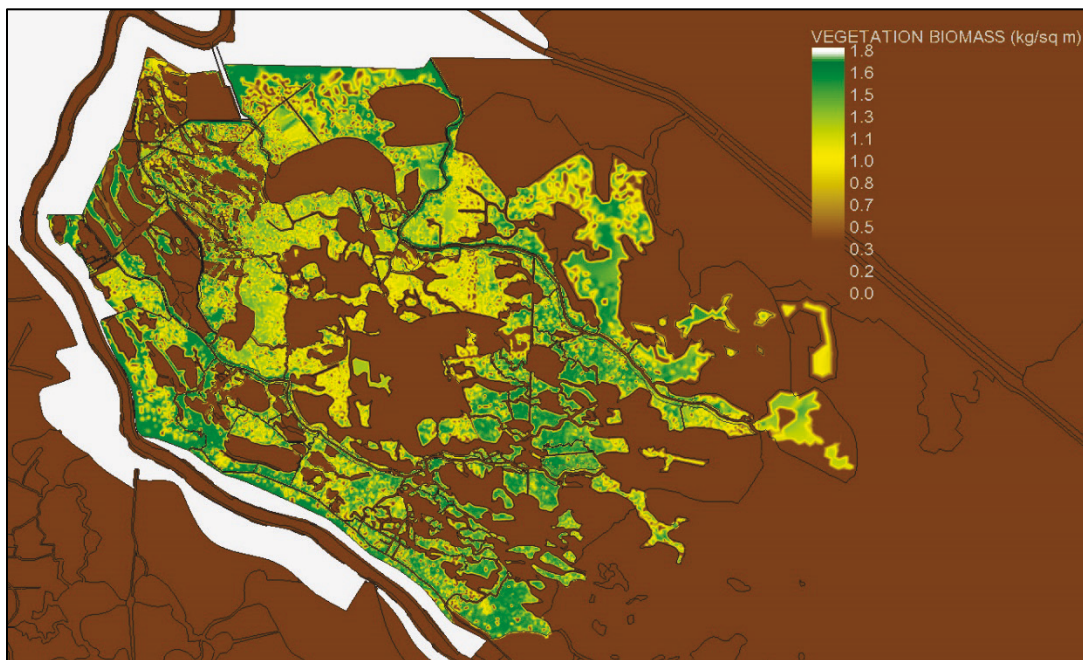


Table 5-1. Comparison between modeled and observed vegetation biomass at selected locations in Breton Sound.

Vegetation Biomass Compared to Day et al. (2012)	Observed (kg/m ²)	Modeled (kg/m ²)
Just Southwest of Big Mar	0.5–1.5	1.6
Northeast Breton Sound	0–1.2	1
Central Breton Sound	0.5–1.5	1.1
Southeast Breton Sound	0.2–1.2	1.5

Morphologic model validation: the Caernarvon delta

The Caernarvon delta was modeled from shortly after the 1993 opening of the Caernarvon Diversion until 2012. Figure 5-2 shows that the sediment boundary conditions chosen for this simulation yield sediment discharges through the diversion that are generally consistent with observations.

Figure 5-2. Comparison between modeled and observed sediment fluxes through Caernarvon Diversion.

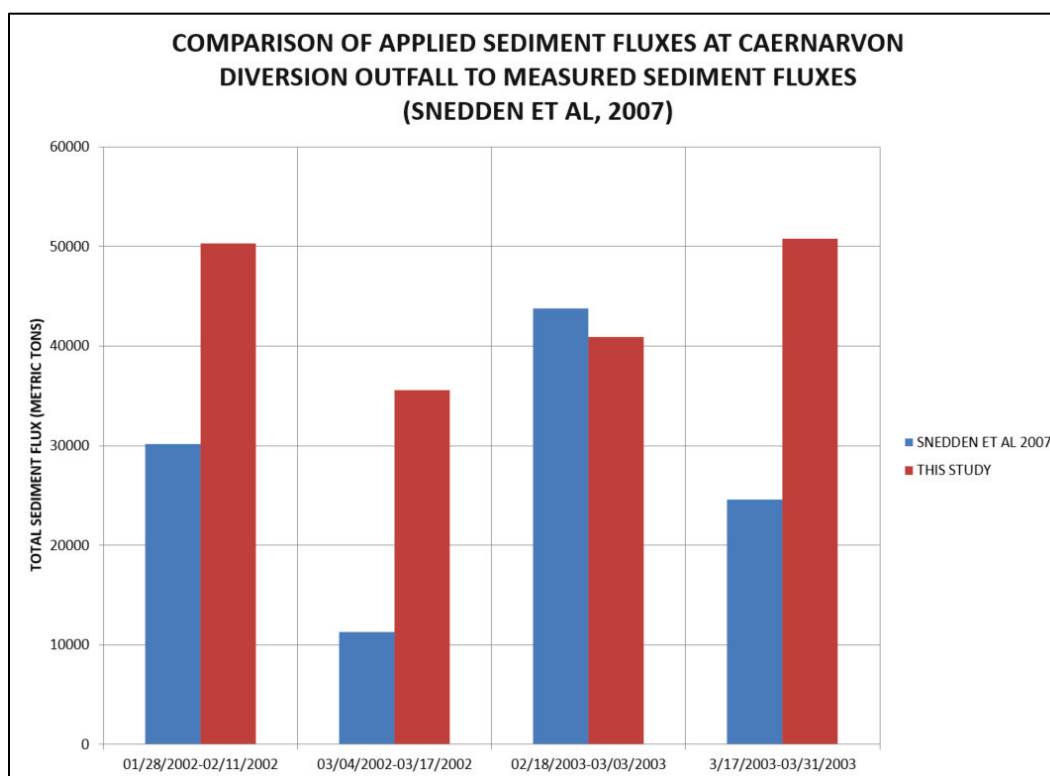


Figure 5-3 depicts a series of areal images that show the growth and shape of the delta. Figure 5-4 and Figure 5-5 show the modeled extent of the vegetation biomass (and hence the emergent delta) for two different model simulations: one with an assumed subsidence of 5 millimeters (mm)/year, and one with an assumed subsidence of 9 mm/year. These were chosen to characterize the influence of uncertainty in the rate of subsidence on the results. The model builds land in the same general size and configuration as the observed delta.

Figure 5-3. Observed growth of the Caernarvon delta (source: Lake Pontchartrain Foundation).



Figure 5-4. Modeled vegetation biomass at the Caernarvon Delta in 2012, assuming a subsidence of 5 mm/year.

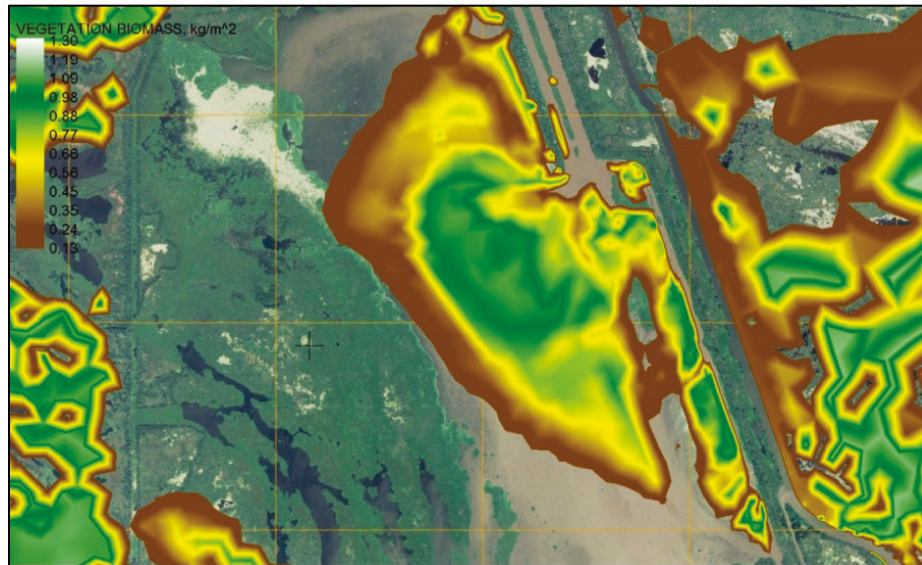


Figure 5-5. Modeled vegetation biomass at the Caernarvon Delta in 2012, assuming a subsidence of 9 mm/year.

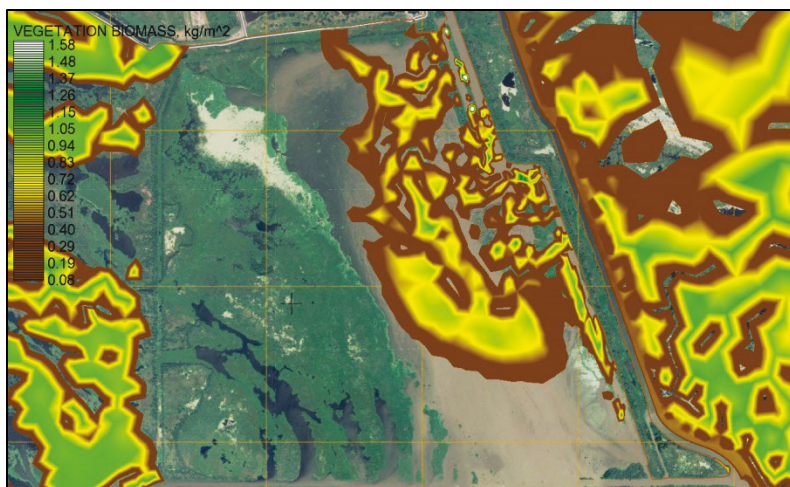


Figure 5-6 and Figure 5-7 depict both modeled and two observed characterizations of the surface area of the delta for both the 5 mm/year subsidence simulation and the 9 mm/year subsidence simulation. Several methods for characterizing land are given for the model results since there is no consistent definition for how this was done for the field observations. Note that the model reproduces both the date of initiation and rate of growth of the delta quite well.

Figure 5-6. Comparison between modeled and observed areal extent of the Caernarvon delta, assuming subsidence = 5 mm/year.

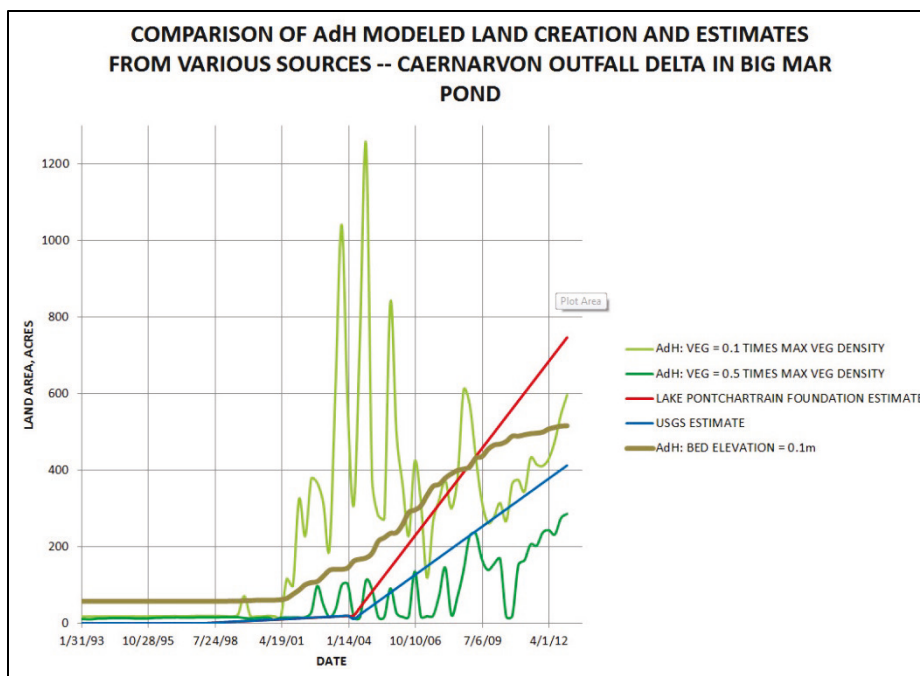
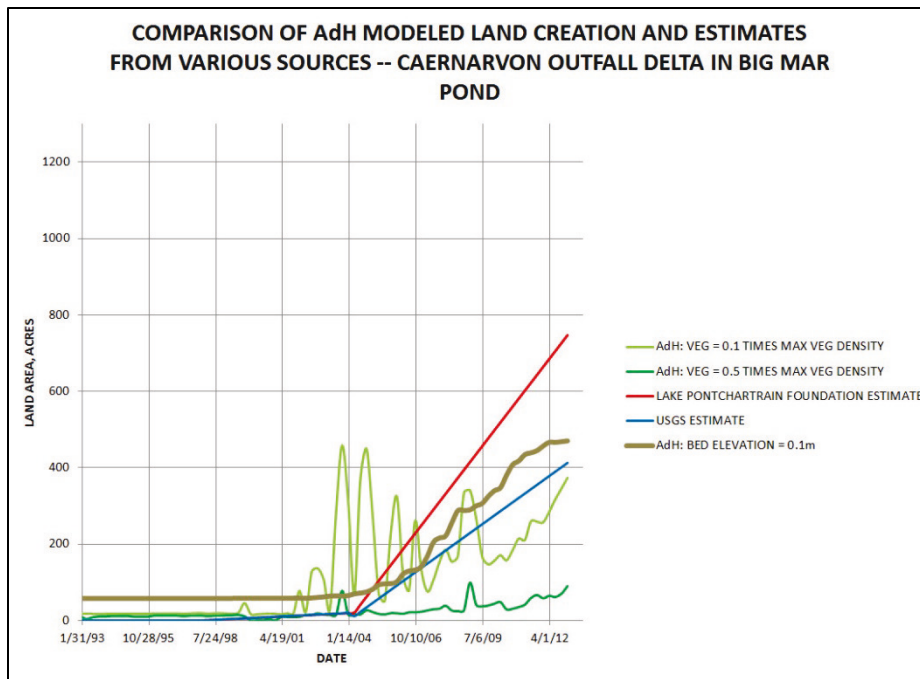


Figure 5-7. Comparison between modeled and observed areal extent of the Caernarvon delta, assuming subsidence = 9 mm/year.



Morphologic modeling validation: the West Bay delta

The West Bay Diversion was simulated from the date of its opening (2003) though 2012. Figure 5-8 shows the observed configuration of the delta in 2012 whereas Figure 5-9 shows the modeled configuration. Note the similarity in the pattern and areal extent of the delta.

Figure 5-8. Observed West Bay delta in October 2012.



Figure 5-9. Modeled West Bay delta in October 2012.

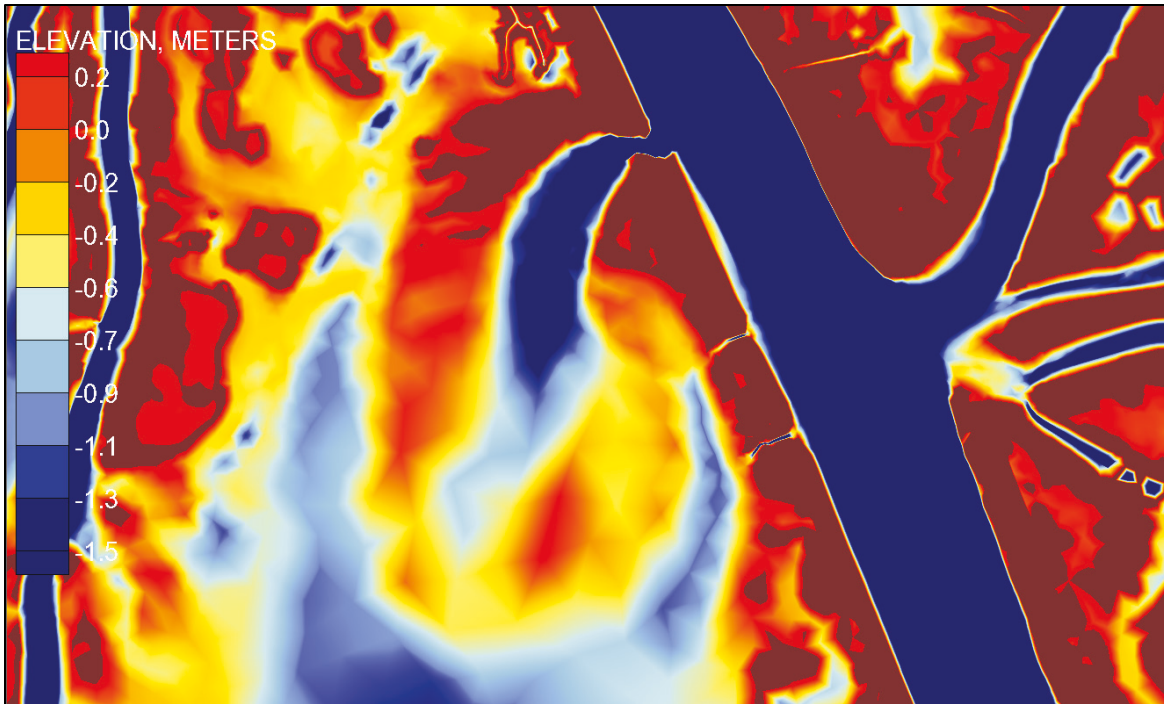
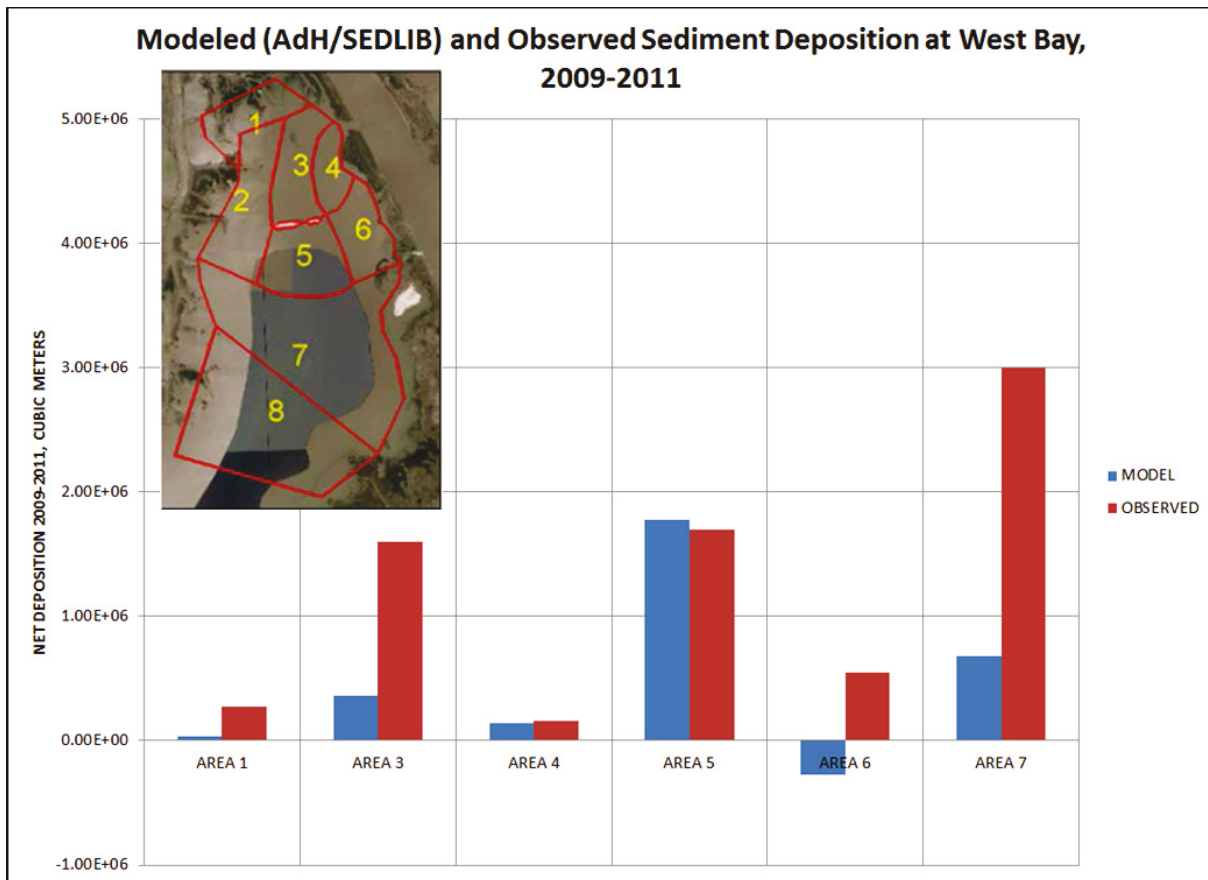


Figure 5-10 gives a quantitative comparison between the model and observed values of volumetric change for various pre-defined polygons between 2009 and 2011. The general agreement is very good, except in areas 3, 6, and 7. Two things are of note here. First, there were two islands constructed in area 7 during this time period that were not in the simulation. This is the primary reason for the large discrepancy between the modeled and observed values in that area. Second, the model widened a connection to the river that is not widened in the prototype (real world). This connection induced the scour seen in area 6.

Figure 5-10. Quantitative comparison between modeled and observed values of the growth of the West Bay delta between 2009 and 2011.



6 Sediment Diversion Scenario Analysis: Preliminary Screening Analysis and Initial Model Simulations

Introduction

The process of selecting the two sediment diversions that were carried forward into the final model simulations (the Mid-Breton and Mid-Barataria Diversions) entailed two separate steps: a preliminary screening analysis and an initial set of model simulations.

The preliminary screening analysis was performed before the models had been calibrated and validated. As such, the analysis was conducted with desktop tools and with unvalidated model simulations that were bracketed with large uncertainties. These tools were evaluated together to perform the initial screening analysis on five proposed diversions. This process screened out one of the major proposed diversions, and the largest proposed discharge scenario for another of the diversions.

The initial model runs were performed to develop quantitative analyses of the remaining four diversions. This process screened out two of these diversions, leaving the Mid-Breton and Mid-Barataria Diversions as the only remaining diversions.

Both of these analyses involved detailed and extensive work. However, only a brief summary is given in this report as the results of the analyses were ultimately superseded by the final scenario analyses, given in Chapters 7–9 of this report.

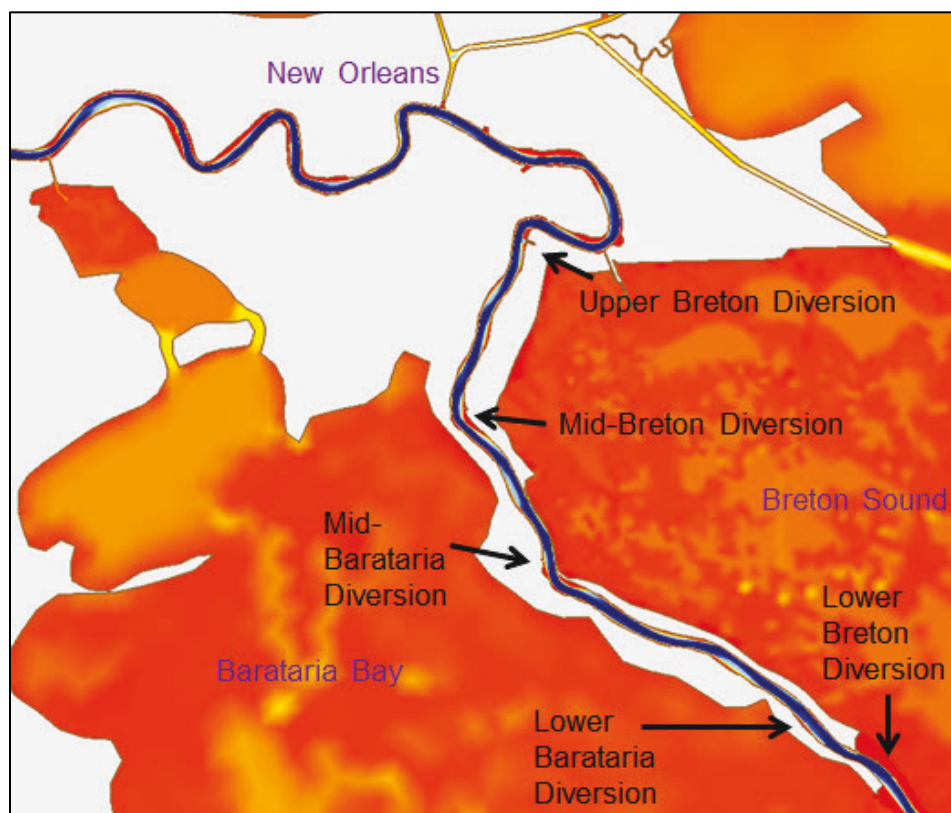
Also, note that the study partners (the State of Louisiana, CPRA) performed parallel desktop and modeling analyses for each of the tasks described above. At each stage, their analyses were compared and contrasted with the analyses presented here, and lessons learned from these comparisons were included in subsequent work by both partners. This report contains only the U.S. Army Corps of Engineers (USACE)

analyses. The CPRA efforts are documented in Baustain et al. 2018 and Sadid et al.¹

Screening analysis

The preliminary screening analyses evaluated five proposed diversions. The locations of these are depicted in Figure 6-1, and the water discharge rates associated with each proposed diversion are given in Table 6-1. These were evaluated using multiple methods of analysis. Two of the methods that were most instrumental in the screening process are presented here.

Figure 6-1. Locations of diversions evaluated in preliminary screening analysis.



¹ Sadid, K., F. Messina, H. Jung, E. Meselhe, S. Duke-Sylvester, and M. Baustian. In preparation. Morphologic and ecologic analysis of a proposed network of sediment diversions in the Mississippi River delta estuaries. *Earth Surface Processes and Landforms*. Special Issue. RCEM Symposium.

Table 6-1. Water discharges associated with each diversion in preliminary screening analysis.

Proposed Diversion	Discharge(s) (cms)	Notes
Upper Breton	7079 and 1416	
Mid-Breton	141.6	This diversion discharge was revised to 991 cms for the next phase of the analysis.
Mid-Barataria Diversions	7079 and 1416	
Lower Barataria Diversion	1416	
Lower Breton Diversion	1416	

To have a means to evaluate the potential of each diversion to build land, a desktop tool was developed for his study. The Diversion Accreted Marsh Life-cycle Analysis (DAMLAY) tool estimates the operational lifespan of the diversion, based on the available energy (head difference between the river side and the basin side of the diversion structure). It then estimates the total acreage of land that can be created in that time. The tool is a gross simplification of diversion operations and does not consider the potential for dredging the diversion outfall or other modifications. However, it is a useful screening tool for comparing between alternatives. The equations that comprise the tool are given in Appendix A.

A DAMLAY analysis was conducted for each proposed diversion. Each of the input parameters to the analysis was perturbed about a standard deviation of the estimated uncertainty in the parameter so that a Monte-Carlo-type analysis could be performed for each proposed diversion. This provided an estimate of the relative uncertainty of the results.

Figure 6-2 depicts the estimated head difference across the diversion structure at the onset of diversion operations. Note that for the two diversions with discharges of 7079 cms, the net available head is negative. This means that for the given channel width, the diversion cannot pass the design discharge. The design discharge results in too much backwater in the receiving basin, due to friction. To pass the design discharge, the channel would have to be widened significantly. This highlights the importance of the energy budget in the design of sediment diversions. Appendix B is derived from a Power-Point presentation that was presented to the Legacy Diversions conference at Southeastern Louisiana University on 6 October 2015 that explains how physics constrains the design and operation of diversions.

Figure 6-2. DAMLAY results: estimated net available head for the proposed diversions.

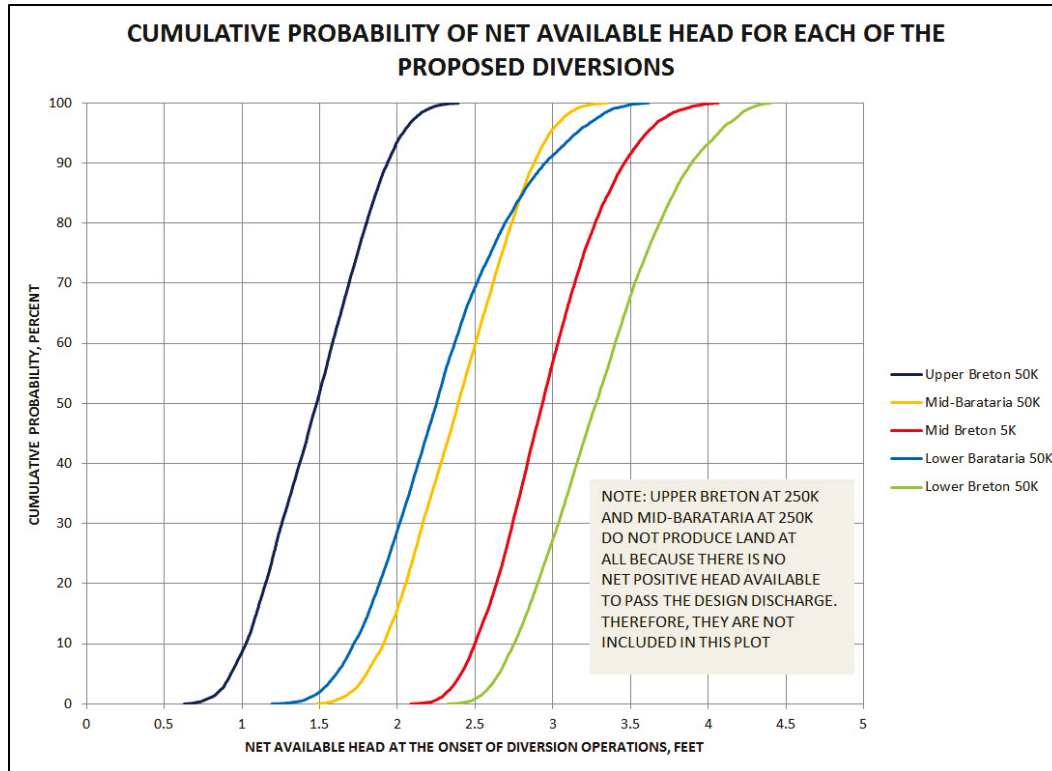


Figure 6-3 and Figure 6-4 depict the estimated life span of the diversions (i.e., elapsed time before maintenance dredging would be required to maintain the design discharge) and the estimated acres of land that would be created, respectively. The analysis shows that the median probability for land building for most of the diversions is between 2,000 and 10,000 acres. The large uncertainty associated with the Lower Breton and Lower Barataria Diversions in this analysis is associated with the large uncertainty in the amount of sand being delivered to those diversions. Counterintuitively, the Monte-Carlo realizations with lower sand concentration result in larger estimated acres of land. This is because high sand concentration results in significant deposition at the mouth of the diversion, which causes the friction to increase rapidly and shorten the lifespan of the diversion. This illustrates one of the physical constraints of a sediment diversion (also notes in Appendix B); a large sand load builds land, but it also increases friction. This must be considered in the diversion design.

Figure 6-3. DAMLAY results: estimated operational lifespan of the proposed diversions.

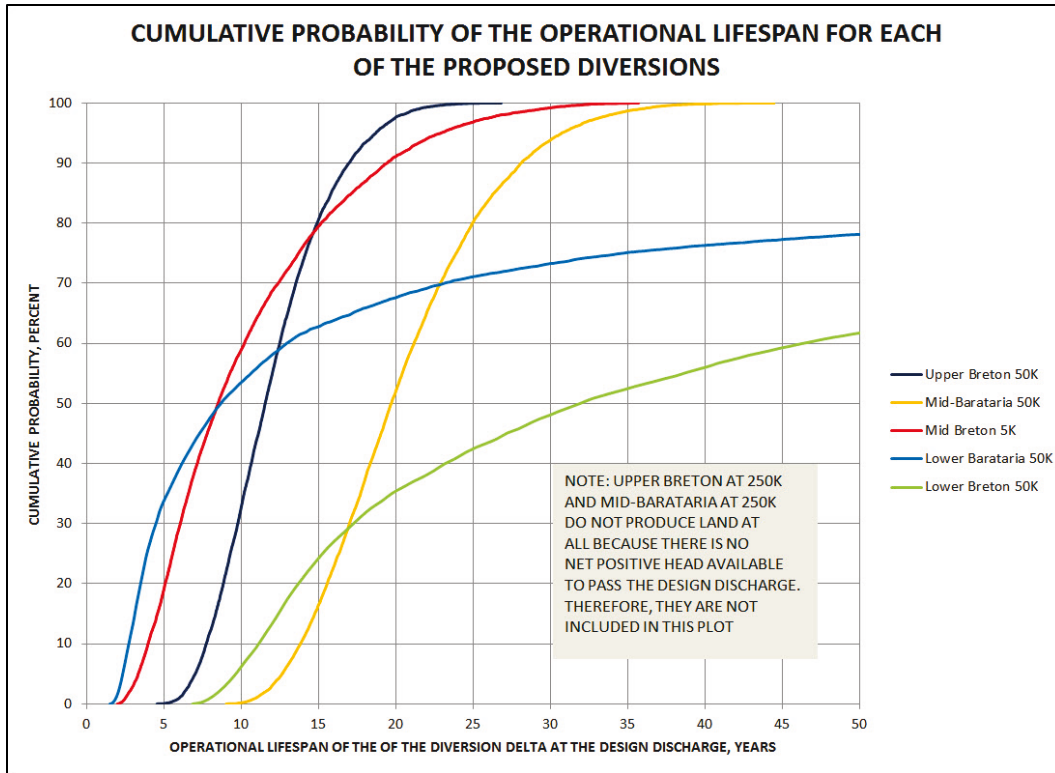
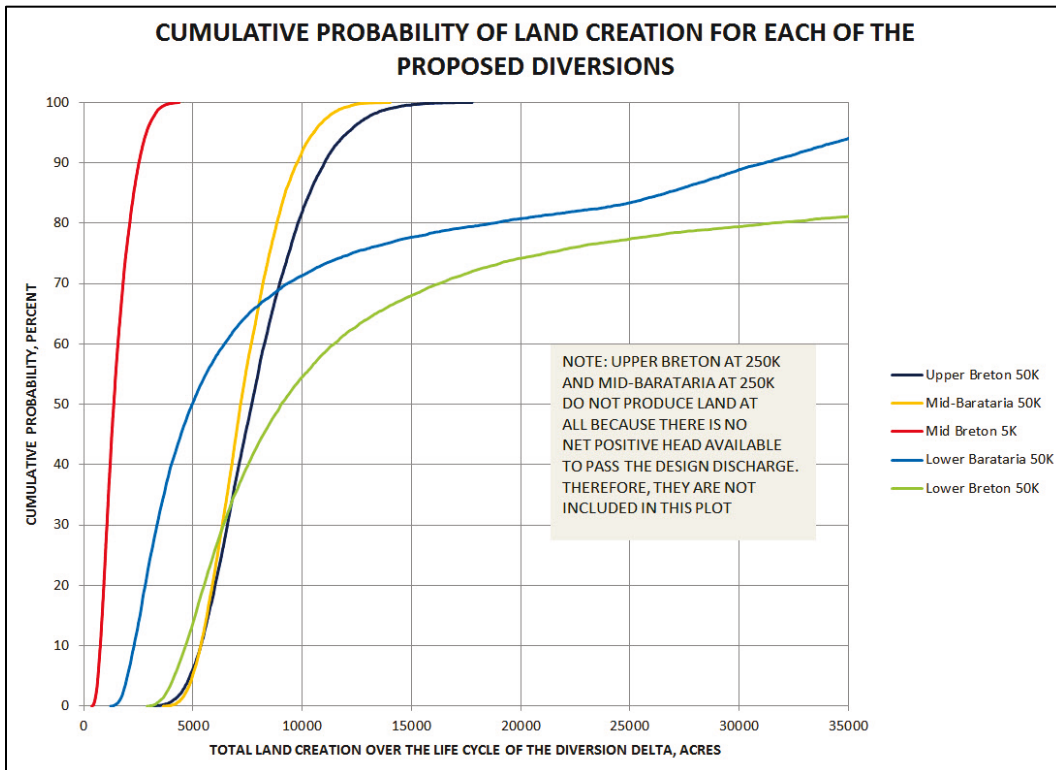


Figure 6-4. DAMLAY results: estimated acres of created land for the proposed diversions.



A second method of analysis that was used to screen the proposed diversions was a water surface elevation analysis, conducted using an uncalibrated AdH model. This analysis computed the water surface elevation increase that results from each diversion. To account for the fact that the friction (associated with marsh vegetation) had not yet been calibrated, a sensitivity analysis was included to estimate the change in water surface elevation for each diversion location and discharge, assuming *low* and *high* marsh friction. An example of the water surface elevation results for the Upper Breton Diversion is given in Figure 6-5, and a tabulation of the estimated water surface elevation increase associated with diversion operations at a distance of 1 kilometer (km) from the diversion mouth is given in Table 6-2. These results generally confirm the DAMLAY analysis of available head (i.e., the large (7079 cms) diversions result in very large water surface elevation increases in the receiving basins, due to friction.

Figure 6-5. Water surface elevation difference associated with the Upper Breton Diversion at 7079 cms.

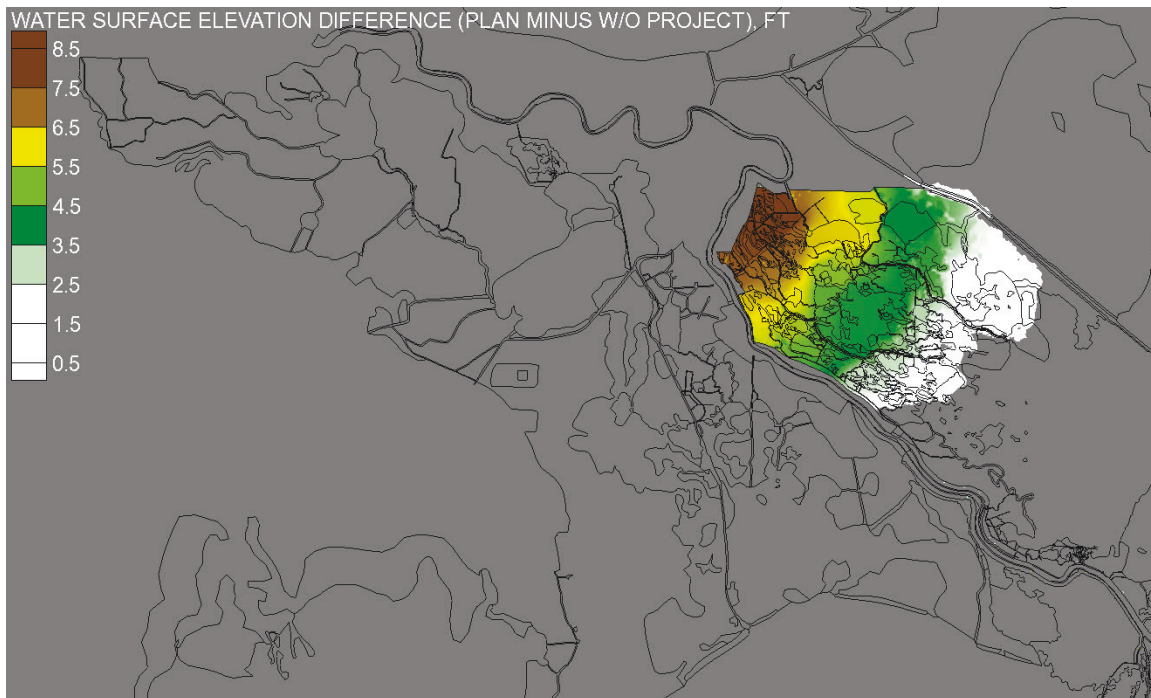


Table 6-2. Water surface elevation difference at a distance of 0.6 miles (1 km) from the diversion outlet.

	Water Surface Elevation at a Distance of 1 km from the Diversion Outlet: Low Estimated Marsh Friction (m)	Water Surface Elevation at a Distance of 1 km from the Diversion Outlet: High Estimated Marsh Friction (m)
Upper Breton Sound	1.87	3.22
Mid-Breton Sound	0.71	1.07
Mid-Barataria Bay, 50K max discharge	0.69	1.12
Mid-Barataria Bay, 250K max discharge	1.75	3.08
Lower Barataria Bay	0.65	0.99
Lower Breton Sound	0.41	0.44

After consideration of these and other analyses, it was decided that the Upper Breton Diversion would be removed from further consideration and that the large discharge scenario (7079 cms) would not be considered for the Mid-Barataria Diversion.

Initial model simulations

After the screening analysis eliminated the upper Breton Diversion and the largest discharge scenario for the Mid-Barataria Diversion from consideration, the remaining four diversions were then subjected to a full model analysis, including hydrodynamics, salinity, and morphological change. Unlike the previous screening analysis, this model analysis was conducted with models that had completed calibration and validation. A brief summary of those results and the lessons learned from the analysis that were carried forward into the final model scenario analyses (presented in Chapters 7–9 of this report) is given here.

For this analysis, the design discharges of some of the diversions were altered. The diversions analyzed are given in Table 6-3, together with the design discharges. Model simulations were conducted to investigate the influence of the diversions on the following three parameters of interest.

- Hydrodynamics (water surface elevation)
- Morphology (land building)
- Salinity

Table 6-3. Diversions and design discharges for initial model simulations.

Diversion	Design Discharge (cms)
Mid-Breton	991
Mid-Barataria	2124
Lower Barataria	1416
Lower Breton	1416

Detailed discussions of the applied boundary conditions and model results are deferred to Chapters 7–9, where the final scenario simulations are described. For this summary of the initial model simulations, only a brief description of the results is presented.

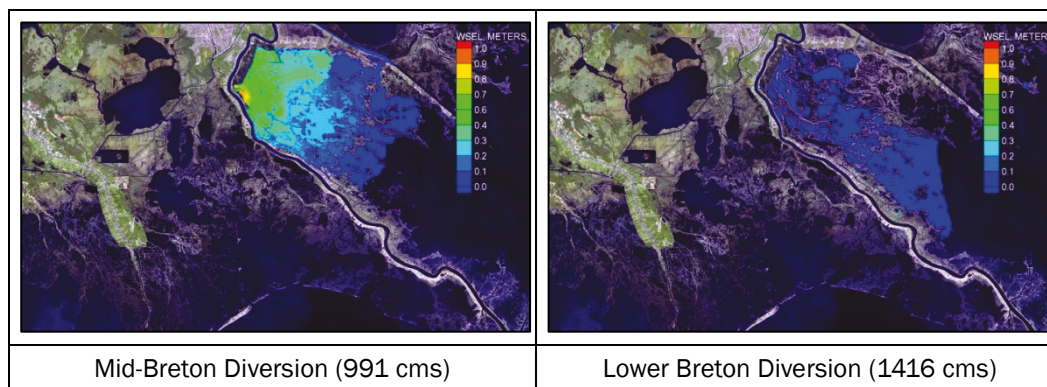
Hydrodynamics (water surface elevation)

Figure 6-6 depicts the water surface elevation differences associated with two of the diversions: the Mid-Breton Diversion, and the lower Breton Diversion. Note that the discharge from the Mid-Breton Diversion results in a much larger impact to the water surface elevation than does the discharge from the lower Breton Diversion. This is true, even though the discharge from the Mid-Breton Diversion is lower than the discharge from the lower Breton Diversion.

This difference is due to the difference in the friction resistance between the shallow (< 1 m deep), vegetated outfall of the Mid-Breton Diversion and the relatively deep (> 2 m), unvegetated outfall of the lower Breton Diversion. This difference is also consistent with the expected results from traditional analytic hydraulic analysis (see Appendix B).

These results demonstrate that diverting water into shallow, vegetated basins can result in significant water surface elevation impacts.

Figure 6-6. Water surface elevation impacts associated with the Mid-Breton and Lower Breton Diversions (contoured from 0 to 1 m of water surface elevation impact).



Morphology (land building)

Figure 6-7 depicts a map of the modeled land gain and land loss associated with 50 years of operation of the Mid-Breton Diversion. Figure 6-8 depicts a similar map for the Mid-Barataria Diversion. Although both images show significant land gain near the diversion site, both images show widespread land loss associated with the diversions. This land loss is attributable to the inundation associated with the diversions. This inundation retards the rate of growth of the wetland vegetation, which in turn hastens marsh collapse and causes an increase in land loss.

This association between inundation and land loss is discussed in much greater detail in the next three chapters, where the final results are presented. There is significant disagreement in the scientific literature concerning the response of wetland vegetation to the inundation associated with diversions, and this scientific debate is manifested in the discrepancies in modeled results. How this issue has been addressed in this study, and recommendations for addressing it in future studies, is discussed in the following chapters.

Figure 6-7. Modeled land gain and land loss associated with the Mid-Breton and Lower Breton Diversions.

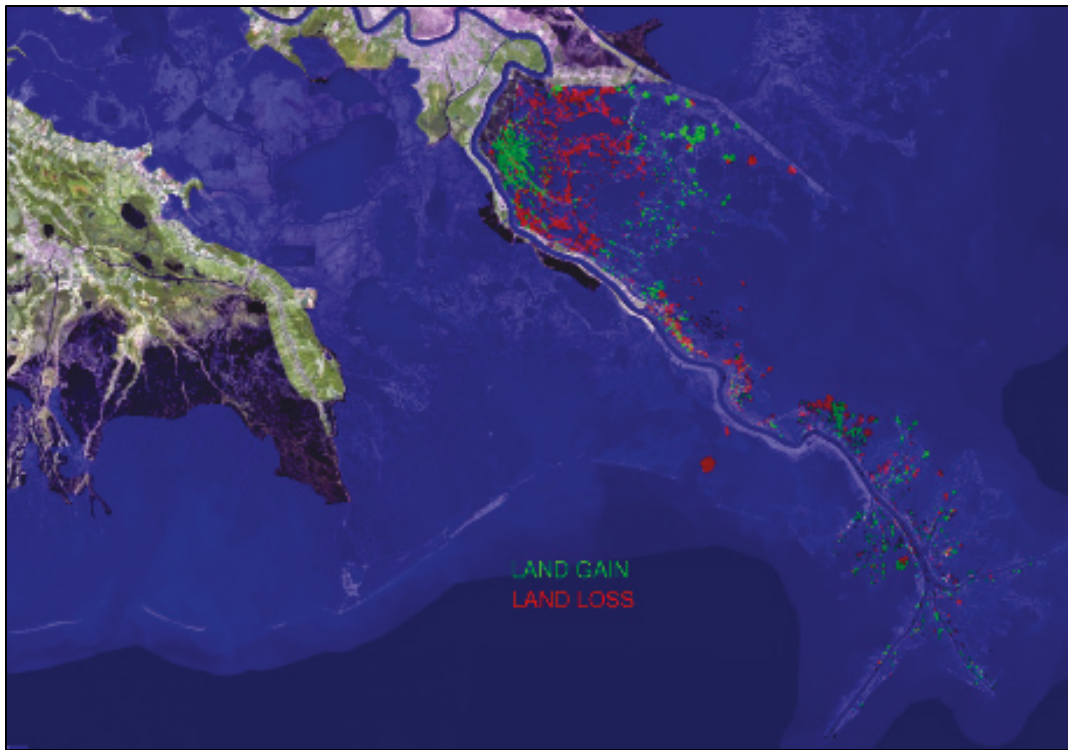
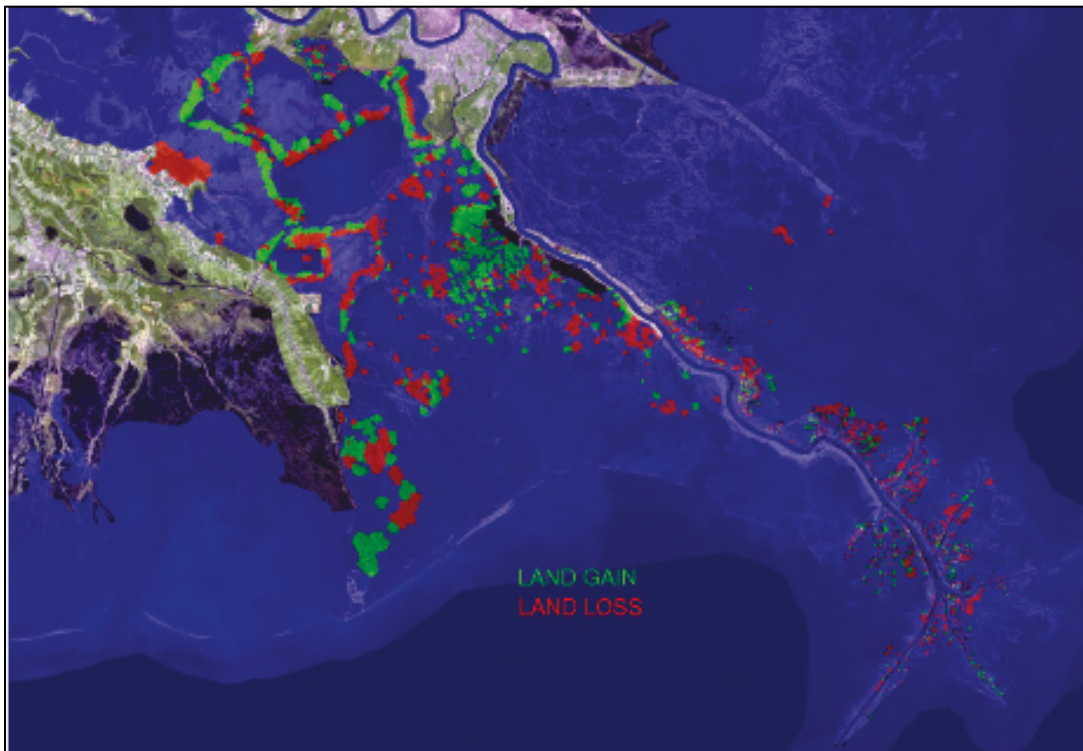


Figure 6-8. Modeled land gain and land loss associated with the Mid-Breton and Lower Breton Diversions.



Salinity

Figure 6-9 depicts the April through June average salinities for the analysis year 2020 for without project conditions. The contour intervals are chosen to highlight the delineation of salinity zones that were deemed ecologically significant by the study team. Figure 6-10 and Figure 6-11 depict the same time-averaging period for the operation of the Mid-Barataria and Mid-Breton Diversions, respectively. These plots show that the diversions have a significant and widespread influence on bay salinity during times of diversion operations. The consequences of this widespread influence will be discussed in more detail in Chapter 9.

Figure 6-9. Average April through June salinity for analysis year 2020, without project.

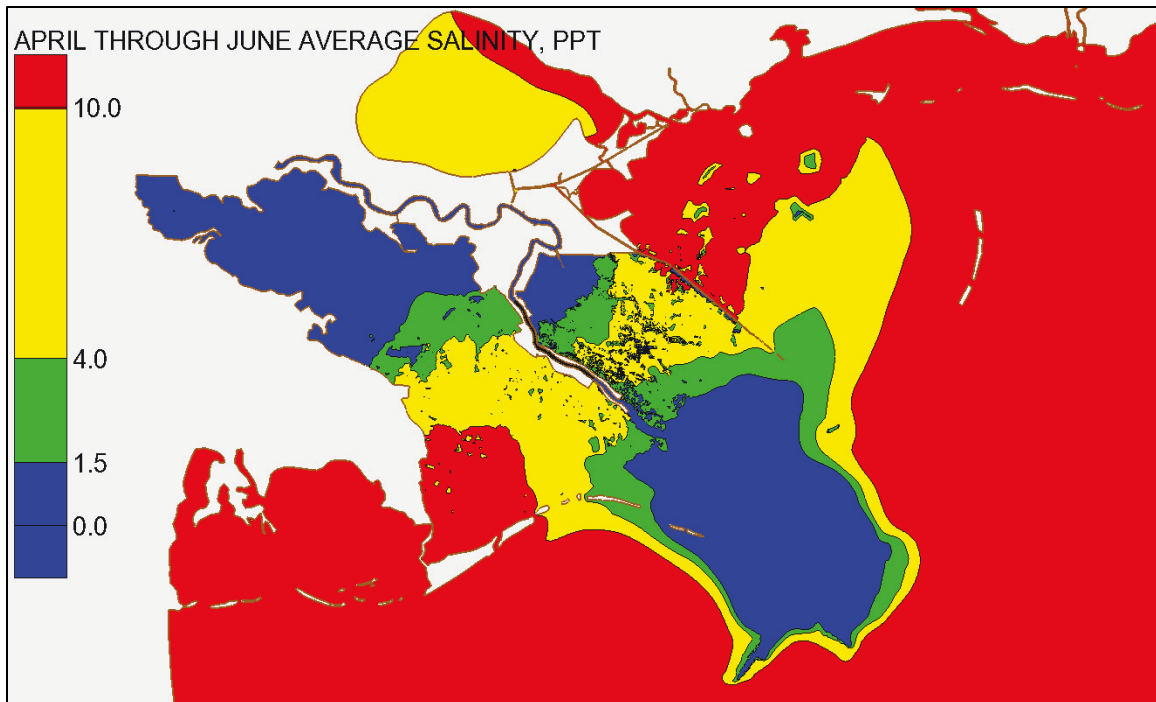


Figure 6-10. Average April through June salinity for analysis year 2020, Mid-Barataria Diversion operated at 75 kcfs.

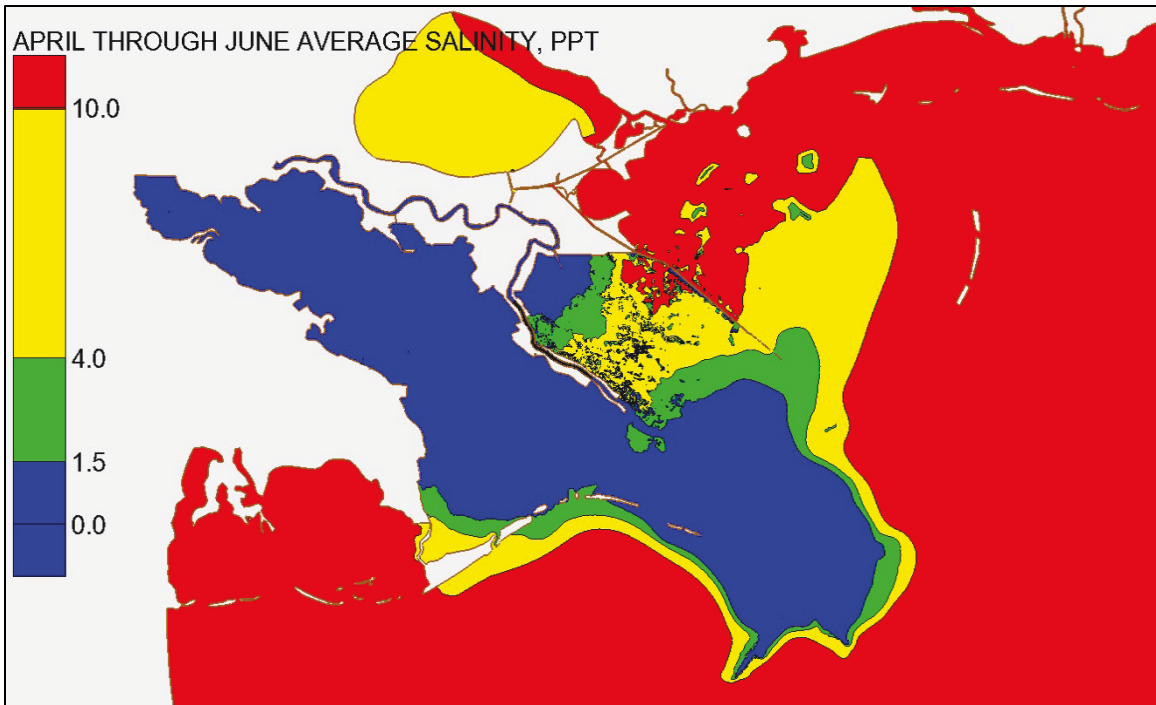
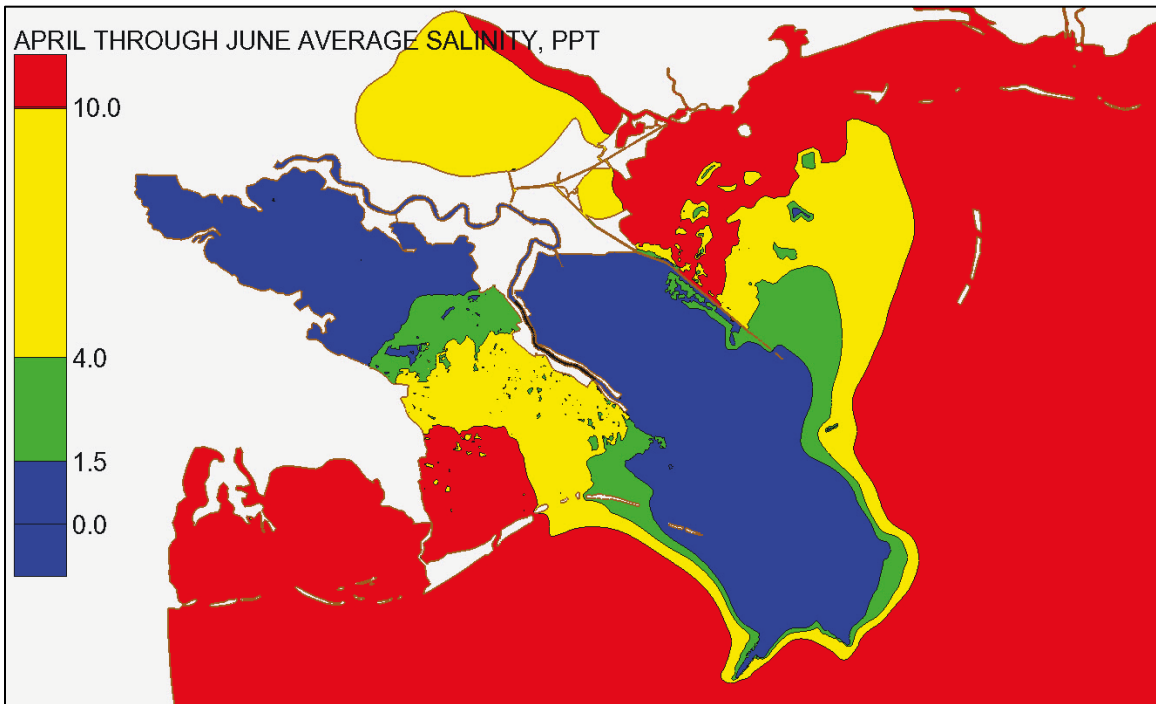


Figure 6-11. Average April through June salinity for analysis year 2020, Mid-Breton Diversion operated at 35 kcfs.



7 Sediment Diversion Scenario Analysis: Mid-Breton and Mid-Barataria Diversions; Selected Simulations and Morphologic Modeling Boundary Conditions

Selected simulations

The simulations selected for analysis included the following:

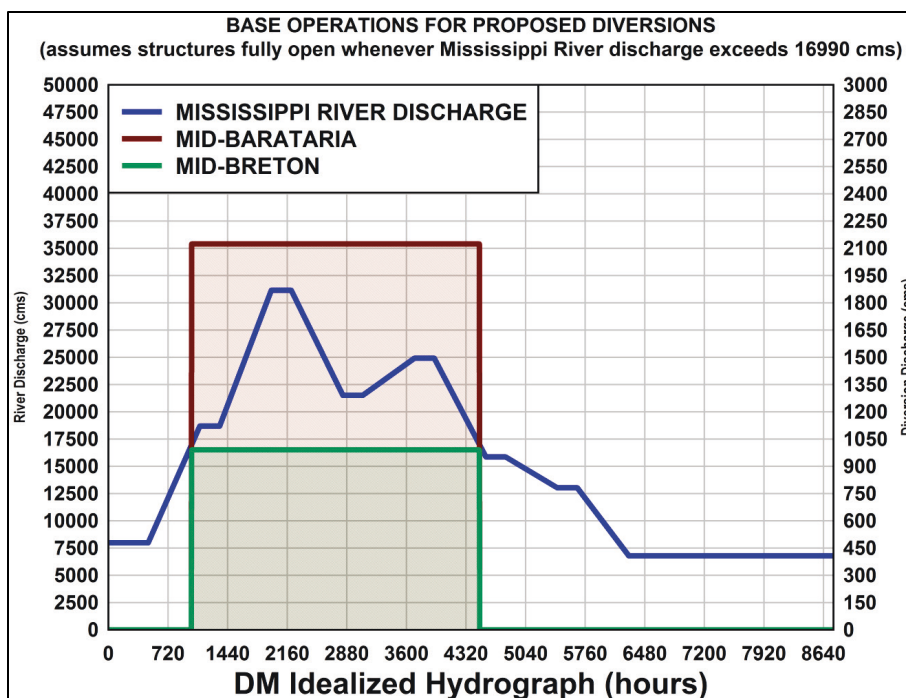
- Without project
- Mid-Barataria and Mid-Breton Diversions – base operations
- Mid-Barataria and Mid-Breton Diversions – base operations with closure of Bohemia Spillway and Fort St. Philip
- Mid-Barataria and Mid-Breton Diversions – optimized operations.

A myriad of different operational plans could be employed for the diversions, but for the purposes of this report, the USACE and CPRA agreed upon the base operations depicted in Figure 7-1. The base operations dictate that the structures will operate at full capacity) 991 cms (35,000 cfs) for Mid-Breton Diversion, and 2,124 cms (75,000 cfs), for the Mid-Barataria Diversion) whenever the river discharge (measured at Tarbert Landing) exceeds 16,990 cms (600,000 cfs).

The base operations with closure of Bohemia Spillway and Fort St. Philip was designed to assess the effects of the closure of these two existing outlets on downstream land building through existing outlets and, perhaps more significantly, the closure of these outlets on the salinity regime in Breton Sound. If closure of these passes resulted in increased salinity in Lower Breton Sound, it could potentially serve to mitigate any deleterious effects of the reduction in the salinity of Upper Breton Sound that would result from the operation of the Mid-Breton Diversion.

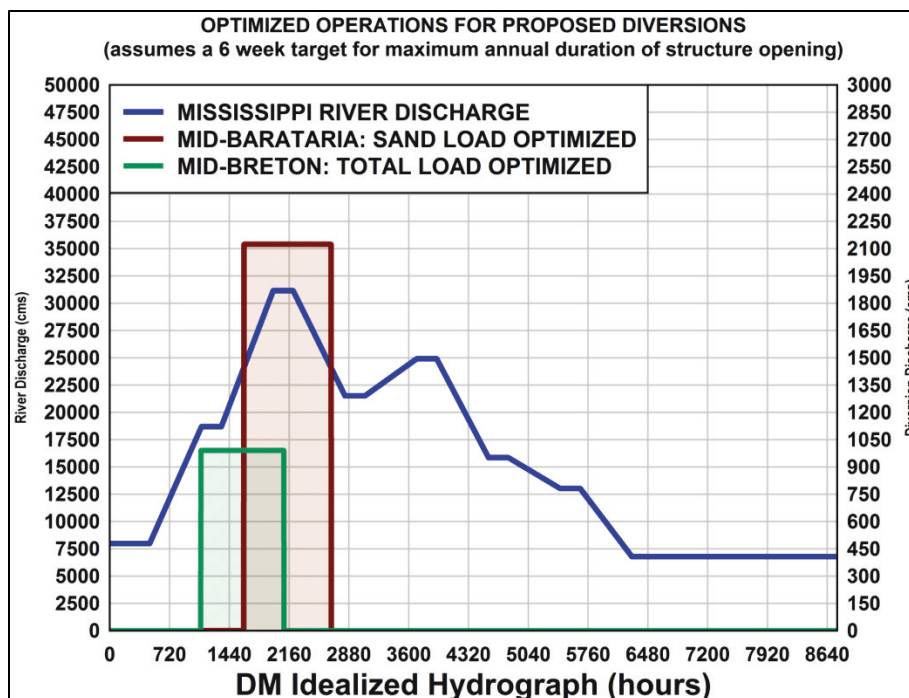
The optimized operations scenarios were designed as follows: a constraint of a maximum of 6 weeks of continuous operation was placed on the diversions, to mitigate inundation and salinity impacts. Then within this constraint, optimum operational schedules were determined that were designed to optimize either the diversion of sand load, or total (sand and fines) load. Appendix C details the methodology used to determine the optimization.

Figure 7-1. Base operations for diversion scenario simulations.



For this scenario analysis, it was decided to optimize the Mid-Breton Diversion for total load, since this diversion is already very efficient at diverting sand, and to optimize the Mid-Barataria Diversion for diverting sand load. These optimized operations are presented in Figure 7-2.

Figure 7-2. Optimized operations for diversion scenario simulations.



Morphologic modeling boundary conditions

The morphologic model is simulated for 50 years. This was done by applying a modified porosity factor of 9.266 (see Chapter 2 for a discussion of the Modified Porosity Factor), which allowed 50 years of morphologic simulation to be performed with just 5.4 years of true model simulation. The value of 9.266 was chosen such that an exact number of tides were contained in the scaled yearly simulation period ($365.25/9.266 = 39.42$ days of simulation for 1 scaled year). This is discussed in more detail in the subsection concerning the tidal boundary condition below.

Mississippi River inflow hydrograph

The applied Mississippi River hydrograph is depicted in both Figure 7-1 and Figure 7-2. This hydrograph is an idealized hydrograph, generated for this study (Sadid et al. 2018). It is an idealized typical hydrograph, resulting from a statistical synthesis of the observed Mississippi River hydrograph at Tarbert Landing. It is applied as a repeating hydrograph for each of the 50 simulated model years. The duration of the hydrograph is scaled down to the duration of the scaled year (39.42 days).

Tidal boundary condition

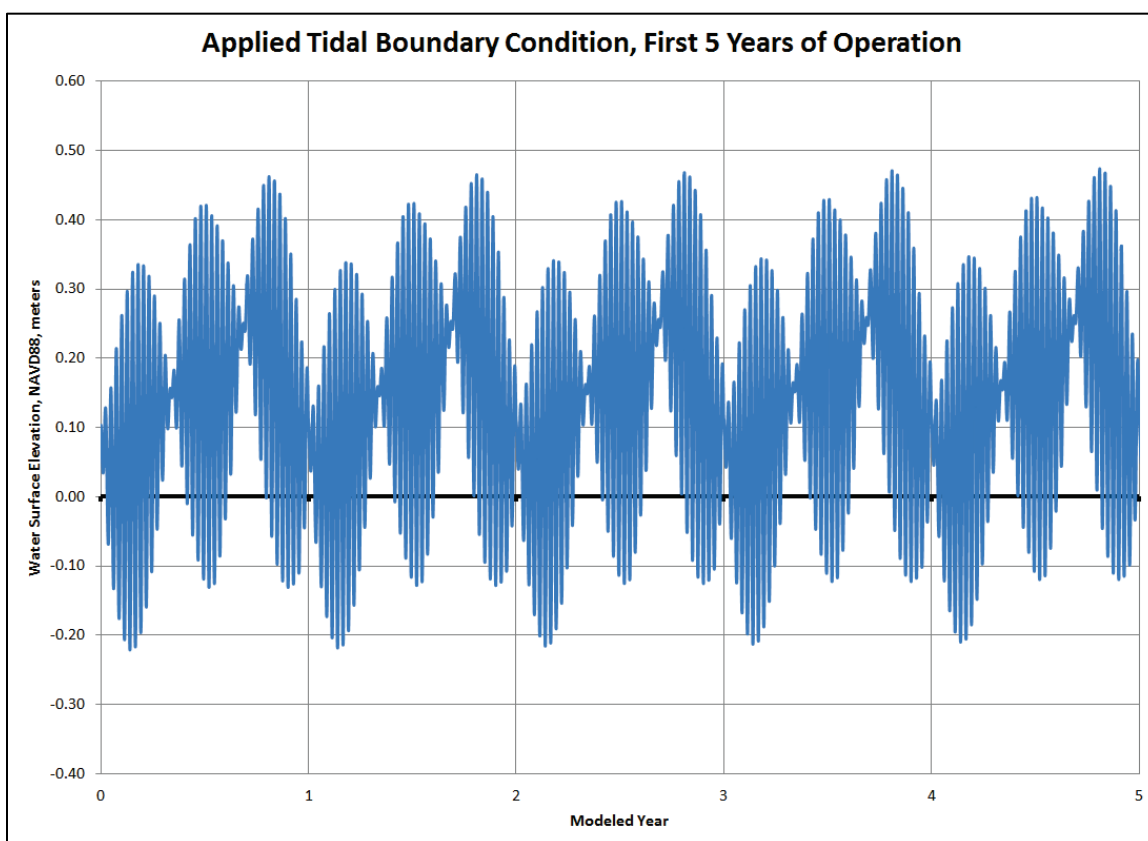
The applied tidal boundary condition is an idealized annual repeating tide, with an approximate rate of eustatic sea level rise for the project life superimposed on the signal. The tidal boundary condition is generated by summing three separate components, listed below.

1. The tidal signal, which is composed of the K1 and O1 components of the tide, as observed at Port Fourchon (note the components are adjusted for the model boundary by multiplying the amplitude by 1.056, and adjusted for the NAVD88 vertical datum by adding by 0.134 m) .
2. The seasonal variation in mean tide level, which is taken from observations at Port Fourchon.
3. The eustatic sea level rise associated with the National Research Council NRCI curve (the intermediate curve) as specified by the ETL 1100-2-1 (USACE 2014) guidance, “Procedures to Evaluate Sea Level Change: Impacts, Responses, and Adaptation.” The NRC curves are derived by assuming a constant acceleration of the rate of sea level rise, commencing in 1992. The acceleration associated with the NRCI curve yields in a

relative increase of sea level elevation between 1992 and 2100 of 0.5 meters.

Figure 7-3 depicts the first 5 years of this tidal condition, in scaled time coordinates (i.e., 1 year = 39.42 days). Note that, consistent with the guidance on using the modified porosity for tidal boundary conditions given in Chapter 2, the tidal boundary is not scaled by dilating the period of the tide but rather by reducing the number of tides per year. Hence, there are only three spring-neap cycles for each tidal *year* of the simulation.

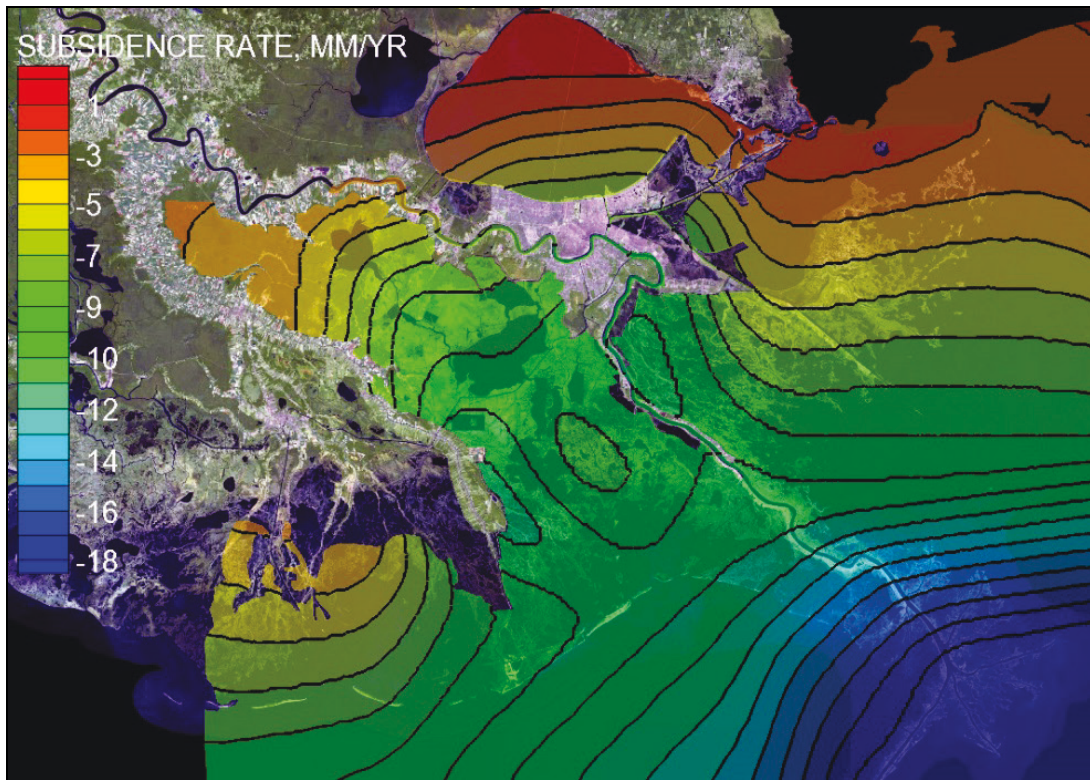
Figure 7-3. Applied tidal boundary condition for first 5 years of simulation.



Applied subsidence

Subsidence is applied as a spatially varying surface, based on a synthesis of available data developed by the project study team. The rate of subsidence is assumed constant with time. The subsidence surface is depicted in Figure 7-4.

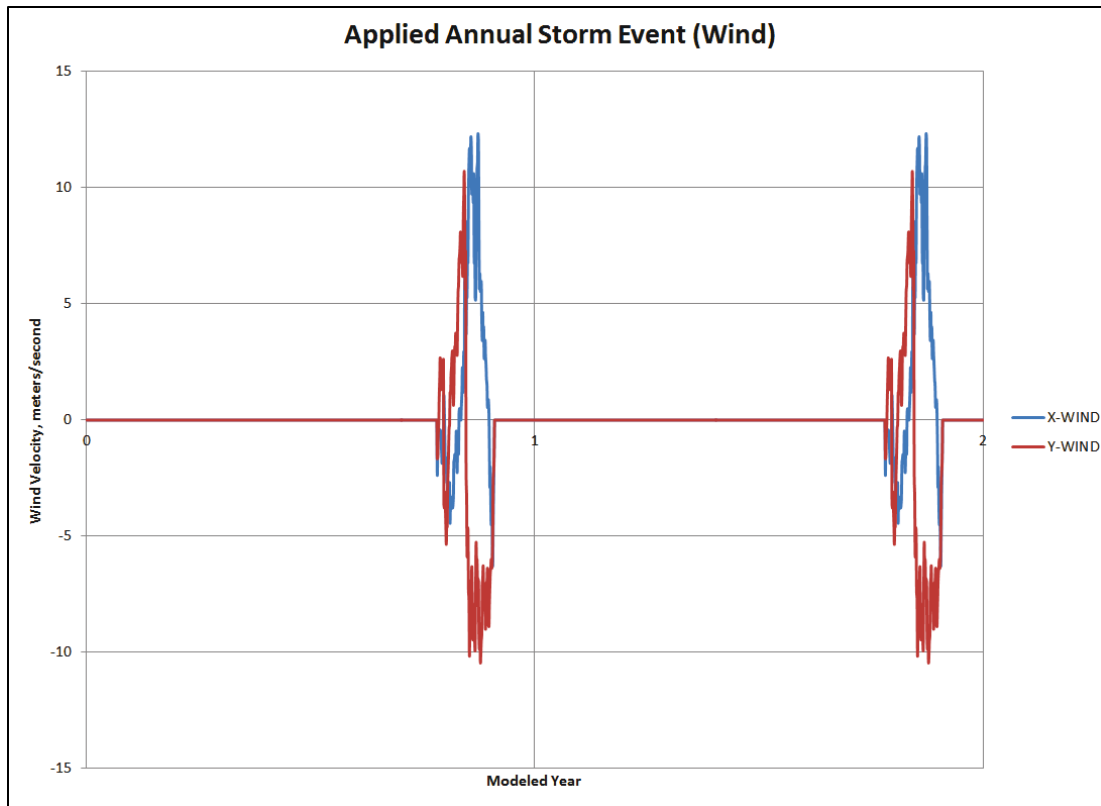
Figure 7-4. Applied spatially varying subsidence surface.



Applied annual idealized storm wind

To simulate the influence of the applied shear stresses, circulation, and inundation changes associated with storm events on the modeled marshes, an idealized storm was applied as an applied wind to the model simulation once per simulated year. The storm winds were taken from an observed event in Breton Sound. This event approximates typical storm conditions (not an extreme event). Figure 7-5 depicts the applied winds for the first 2 years of model simulation.

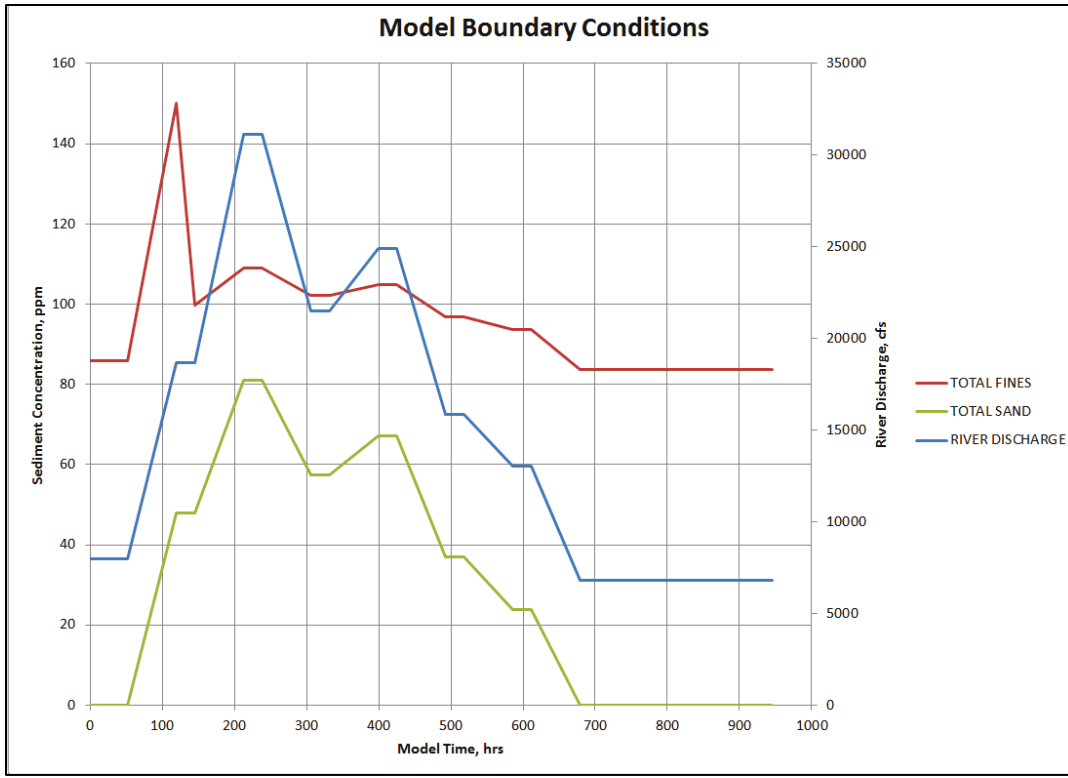
Figure 7-5. Applied storm (wind) condition for first 2 years of simulation.



Applied sediment inflow boundary conditions

The Mississippi River inflow boundary must have sediment boundary conditions assigned to it. The applied boundary conditions are depicted in Figure 7-6. These boundary conditions are taken from idealized sediment inflow conditions that were developed for this study by The Water Institute of the Gulf (TWIG). These were developed from statistical analysis of the observed sediment concentrations at Belle Chasse. The only modification to TWIG results is an increased fine sediment concentration associated with the first flush (the initial rise of the hydrograph). This was also generated from observed data at Belle Chasse and is a commonly observed property of the fine sediment concentration.

Figure 7-6. Applied sediment inflow boundary conditions.



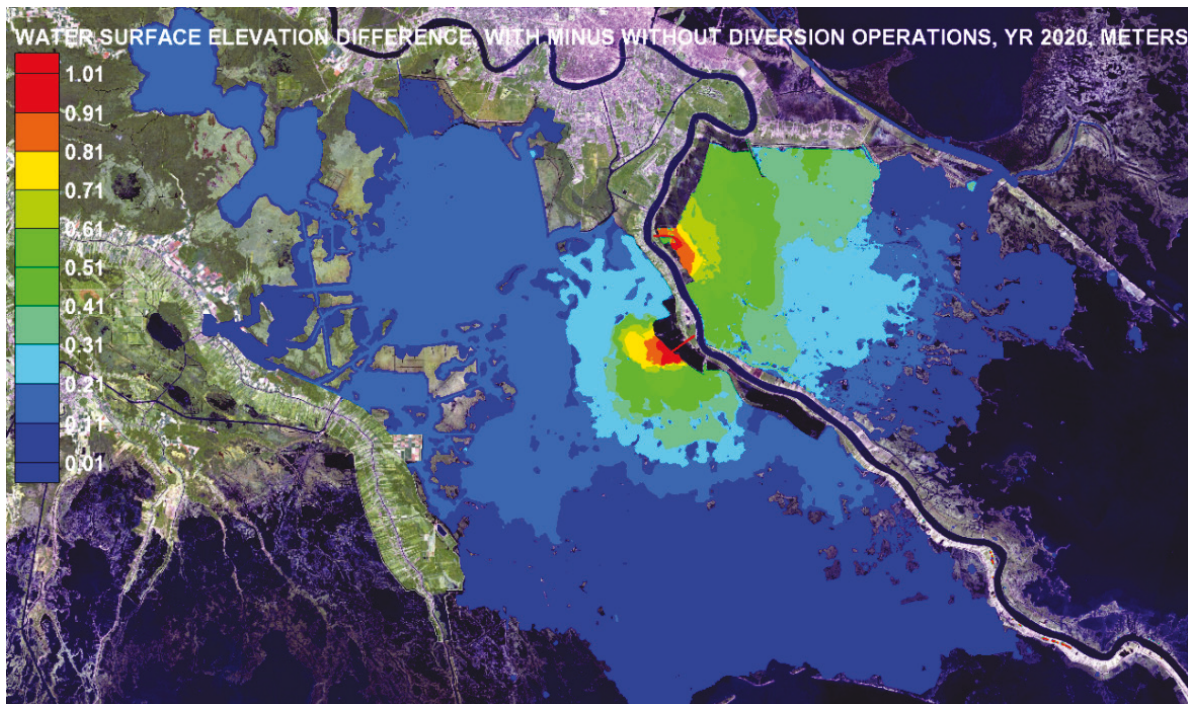
8 Sediment Diversion Scenario Analysis: Mid-Breton and Mid-Barataria Diversions; Water Surface Elevation and Morphologic Analyses

Water surface elevation impacts: Year 0

Figure 8-1 depicts the water surface elevation difference associated with the operation of the Mid-Breton Diversion at 991 cms (35,000 cfs), and the Mid-Barataria Diversion at 2124 cms (75,000 cfs). The model results are not contoured below 1 cm of difference. Any contoured results represent at least 1 cm of water surface elevation increase associated with the operation of the diversions.

The Mid-Breton Diversion shows widespread impacts, primarily due to the fact that the receiving basin is very shallow (< 1 m depth) and vegetated. The Mid-Barataria Diversion does not show as much significant impact as the Mid-Breton Diversion (even though the diversion discharge is much greater) because the receiving basin is somewhat deeper and there is more open water. However, the extent of the minimal impacts (~1 cm) is very widespread. This is because the diverted water flows both north and south of the diversion outlet. The northbound flow fills the available storage in northern Barataria Bay and then circulates back to the south and exits the Bay.

Figure 8-1. Water surface elevation difference with and without diversion operations for Year 2020 of the model simulation (Year 0 of the analysis).



Water surface elevation impacts: Year 50

Initially, the operation of the diversions induces some scour of the receiving basins. As time progresses, however, deposition of sands at the diversion outfalls induces a backwater effect that results in a gradual increase in the downstream water surface elevation. This increase in water surface elevation represents the increased potential energy required to convey water through the developing sand delta. This effect is especially pronounced for the Mid-Breton Diversion. Initially, the water surface elevation at the Mid-Breton outfall during diversion operations is about 1.1 meters. However, by the end of 50 years, this water surface elevation has risen to about 1.9 meters. If the water surface elevation at the outfall exceeds the maximum threshold for the downstream water surface elevation associated with the ability to operate the structure at maximum capacity, continued operation of the diversion would require dredging of the diversion outfall to alleviate the backwater effect. This effect should be taken into consideration when designing the diversion structures, and when preparing project-life cost estimates.

Qualitative analysis of sediment erosion and deposition and wetland vegetation

Figure 8-2 and Figure 8-3 depict the modeled bed displacement after 50 years of simulation associated with sand transport only, for base operations and optimum operations, respectively. Figure 8-4 and Figure 8-5 depict the modeled bed displacement after 50 years of simulation associated with fines transport only (silts and clays), for base operations and optimum operations, respectively.

The sand transport plots show deposition of sands near the diversion outlets. The Mid-Breton diversion shows more deposition than does the Mid-Barataria Diversion, even though it diverts less water. This is because the Mid-Breton Diversion is more efficient at diverting sand from the river than is the Mid-Barataria Diversion (Brown et al. 2018). The optimized operations simulations show significantly less deposition than do the base operations. This is to be expected since the duration of the operations (6 weeks) is much less than the duration of the base operations (~20 weeks). It must be remembered that *optimization* here refers not to the absolute maximum sediment delivery but rather to the maximum sediment delivery that can be attained within the constraint of 6 weeks of operation.

The fines transport plots show erosion of new channels for the Mid-Breton Diversion and both the erosion of new channels and the widening of existing channels for the Mid-Barataria Diversion. The plots also show deposition of fine sediments, much of it filling existing shallow lakes in the receiving basins. For the Barataria basin, there is also fine sediment deposition in the Barataria Waterway.

Figure 8-2. Bed elevation change associated with sands for base diversion operations after 50 years of operation.

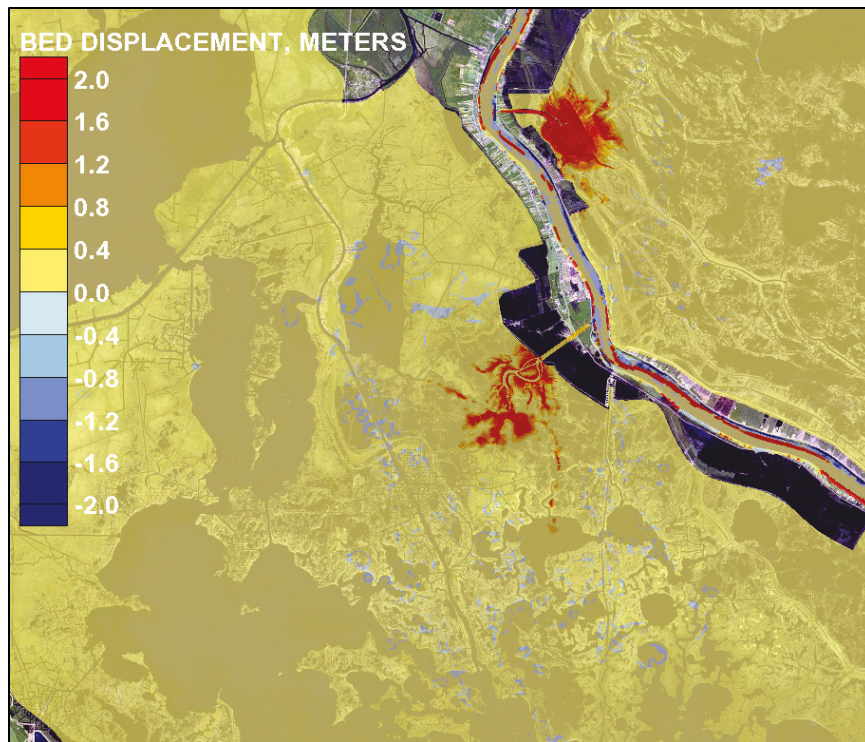


Figure 8-3. Bed elevation change associated with sands for optimized diversion operations after 50 years of operation.

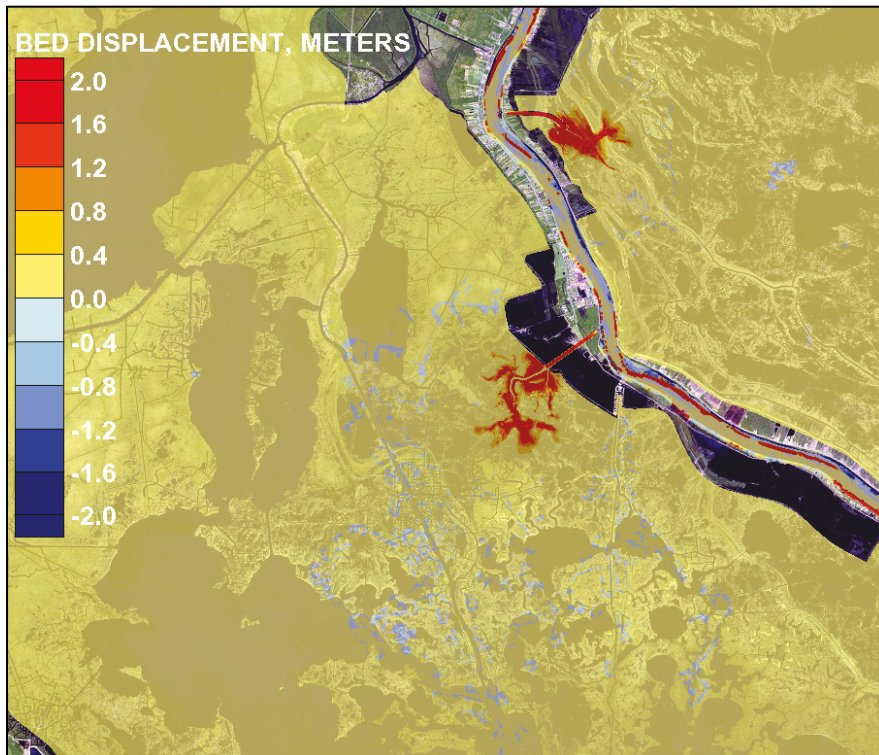


Figure 8-4. Bed elevation change associated with fines for base diversion operations after 50 years of operation.

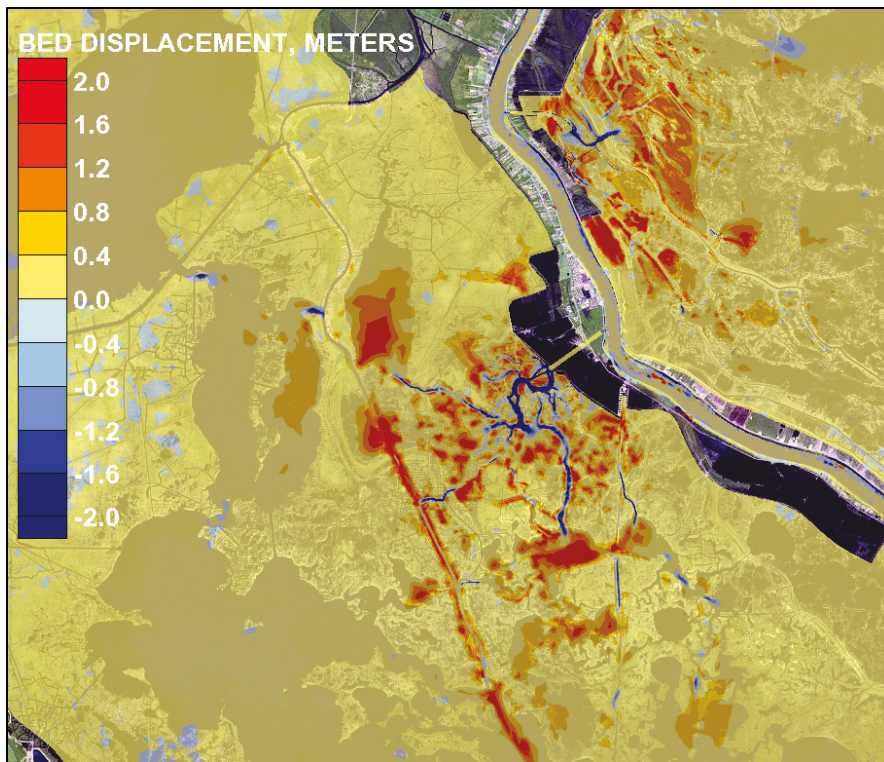


Figure 8-5. Bed elevation change associated with fines for optimized diversion operations after 50 years of operation.

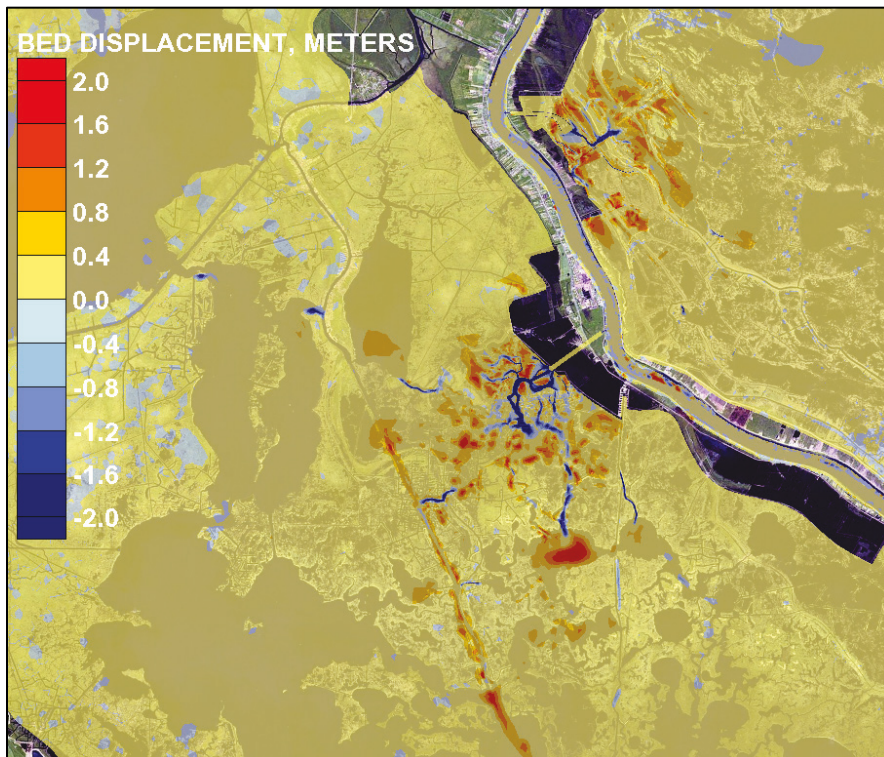


Figure 8-6 and Figure 8-7 depict the root mass distribution of the vegetation after 50 years of simulation for without project conditions and for base operation conditions, respectively. Figure 8-8 and Figure 8-9 depict the refractory organics (*muck* mass) distribution after 50 years of simulation for without project conditions and for base operation conditions, respectively. Note that in both cases, the operation of diversions adds vegetative mass near the diversion outlets (associated primarily with vegetative colonization of sand deposits) but, importantly, also results in a reduction in plant productivity for locations farther away from the diversion outlets where inundation effects are still present although there is little inorganic sediment deposition.

Figure 8-6. Root mass distribution for without project conditions after 50 years of simulation.

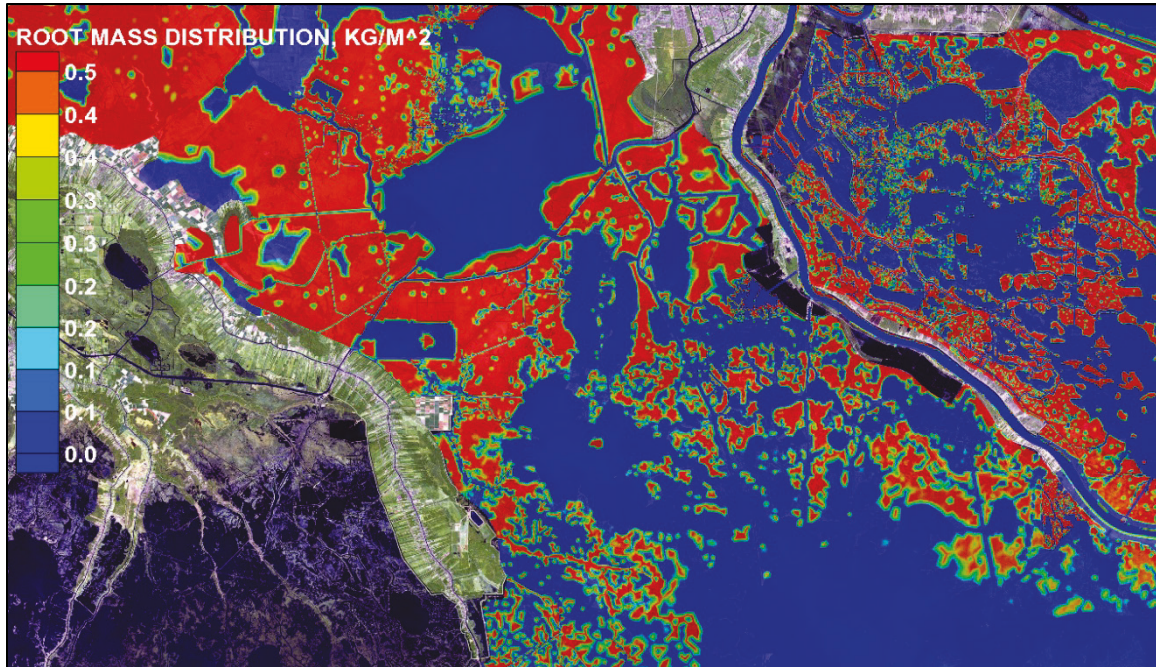


Figure 8-7. Root mass distribution for base diversion operation conditions after 50 years of simulation.

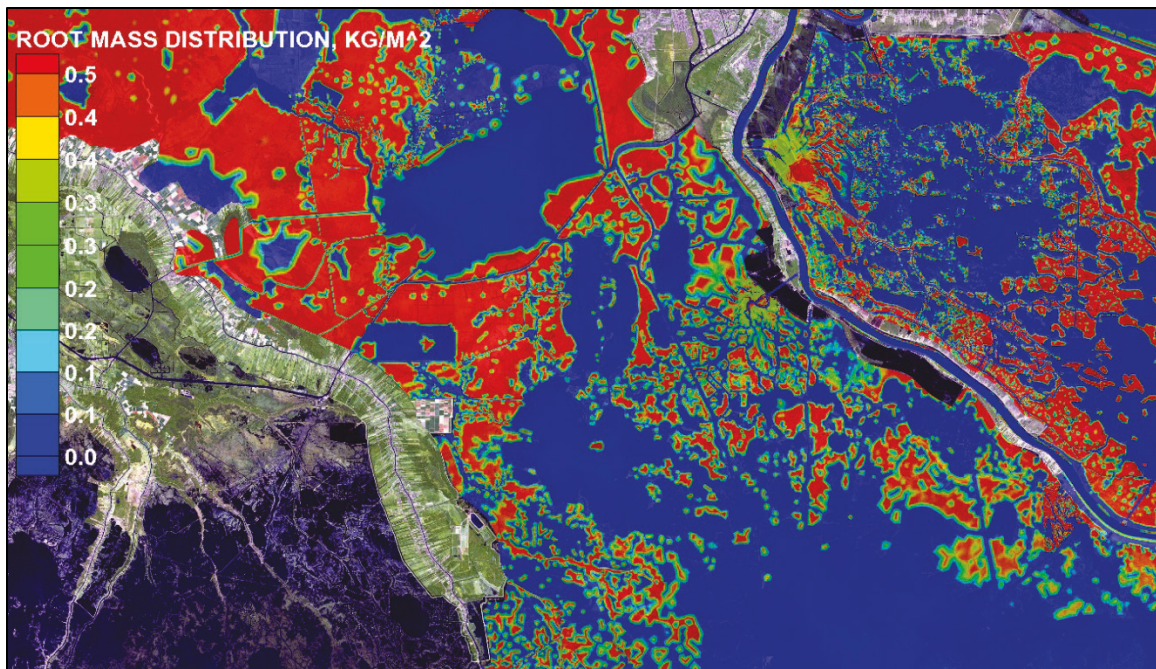


Figure 8-8. Refractory organics distribution for without project conditions after 50 years of simulation.

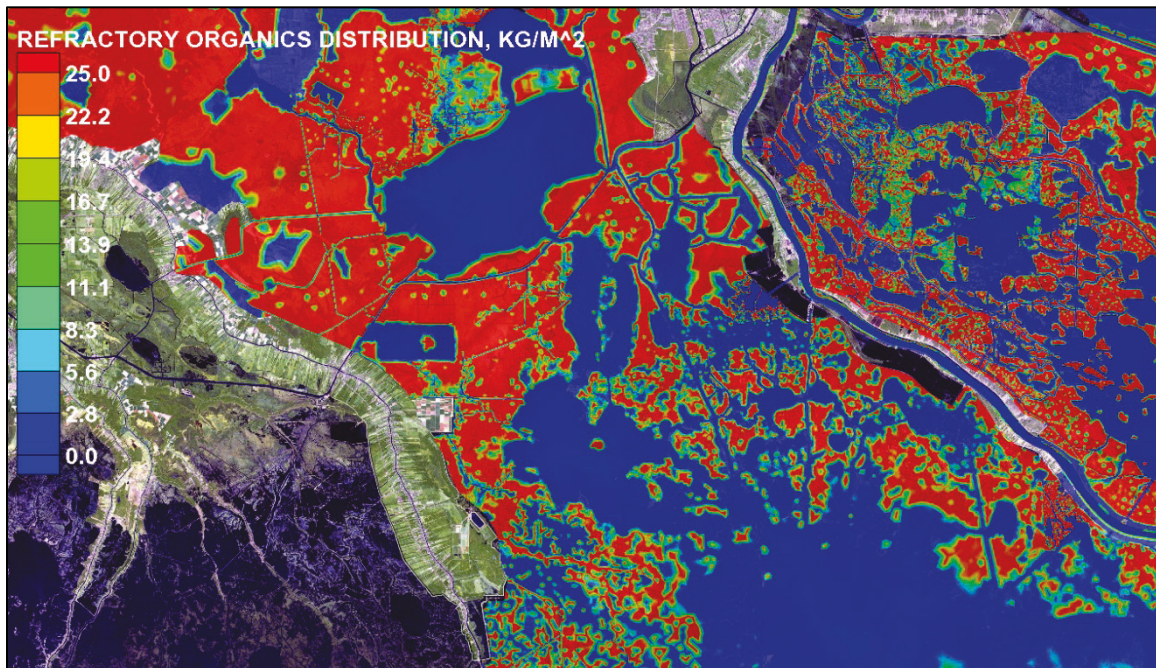
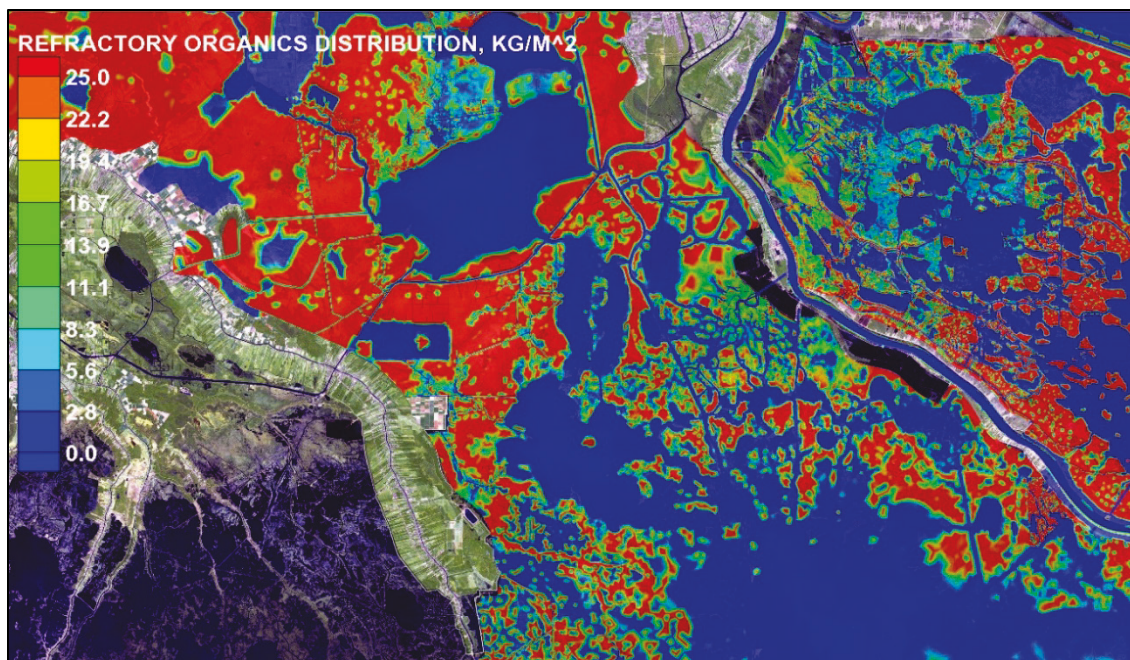


Figure 8-9. Refractory organics distribution for base diversion operation conditions after 50 years of simulation.



Quantitative analysis of the efficiency of optimization operations

The efficiency of the optimization operations can be determined by calculating the average concentration of the diverted sediment for optimized conditions and dividing this number by the average concentration for the diverted sediment for base conditions. This optimization efficiency index is a ratio that measures how much better the optimized operations are at diverting the sediment than the base operations are (a value of 1 indicates equal performance between optimized and base operations).

Table 8-1 lists the results of the optimization efficiency index calculations. The results show that the optimization for sands for the Mid-Barataria Diversion is very effective whereas the optimization for total load for the Mid-Breton Diversion is less effective. This is evidently due to the fact that the timing of the operations was somewhat early, since the fine sediment efficiency is actually greater for the Mid-Barataria Diversion than for the Mid-Breton Diversion (the operation of the Mid-Barataria Diversion is delayed relative to the Mid-Breton Diversion). Hence, the efficiency could be improved by carefully timing operations to coincide precisely with the arrival for the first flush sediments.

Table 8-1. Optimization efficiency indices for the Mid-Breton and Mid-Barataria optimization simulations.

	Optimization Efficiency Index – Sand Load	Optimization Efficiency Index – Fines Load	Optimization Efficiency Index – Total Load
Mid-Breton Diversion (optimized for total load)	1.29	1.07	1.16
Mid-Barataria Diversion (optimized for sand load)	3.45	1.19	1.72

Land gained and lost as a result of diversion operations

Land change maps

Figure 8-10 through Figure 8-13 are land change maps, after 50 years of simulation. The land changes are categorized in one of four ways. The categories and criteria for each are given in Table 8-2.

Table 8-2. Criteria for determination of land change categories for land change maps.

Land Change Category	Land Exists at This Location at Year 0 (2020)	Land Exists at This Location at Year 50 (2070) Without Project	Land Exists at This Location at Year 50 (2070) With Project (i.e., with diversions)
Land Created	NO	NO	YES
Land Saved	YES	NO	YES
Land Lost	YES	YES	NO
Land Not Created	NO	YES	NO

Figure 8-10 depicts the land change associated with without project conditions (i.e., the land change over 50 years that is expected if no diversions are implemented). The map shows widespread land loss due mostly to marsh collapse resulting from the inundation of wetlands and wetland erosion from wind-waves. There is some land gain, however, associated with land building at existing outlets, including some land building associated with the Fort St. Philips crevasse.

Figure 8-10. Modeled land change after 50 years – without project.

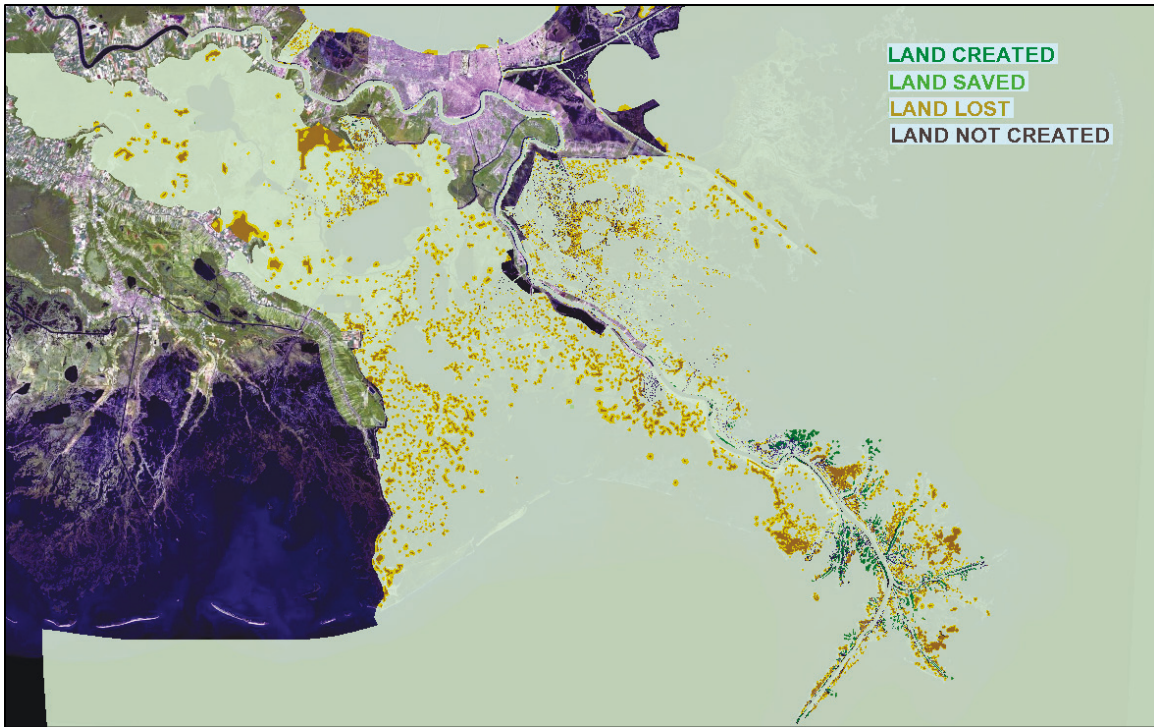
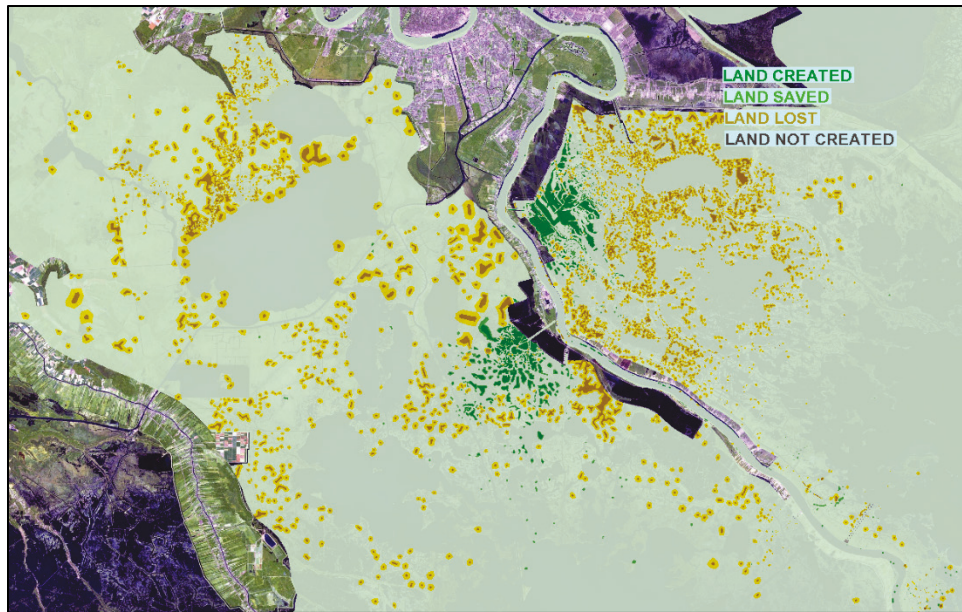


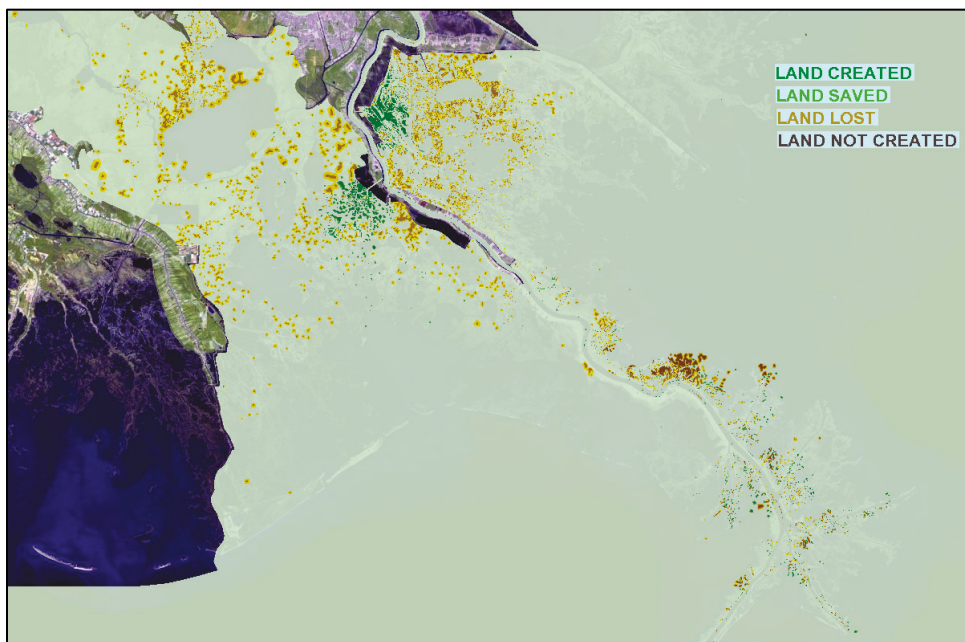
Figure 8-11, Figure 8-12, and Figure 8-13 depict the net land change associated with diversion operations associated with base operations, base operations with closure of Bohemia Spillway and Fort St. Philip, and optimized operations, respectively. Note that all of the maps show significant net land gain in the near vicinity of the diversion outlets and significant net land loss farther away from the outlets. The areas of land gain roughly correspond with the zones of significant sand deposition, whereas the areas of largest land loss correspond with areas where there is diversion induced inundation but not significant sediment from the diversion. These results are discussed in more detail in the discussion section of this chapter.

Figure 8-11. Modeled land change after 50 years relative to without project conditions – base operations.



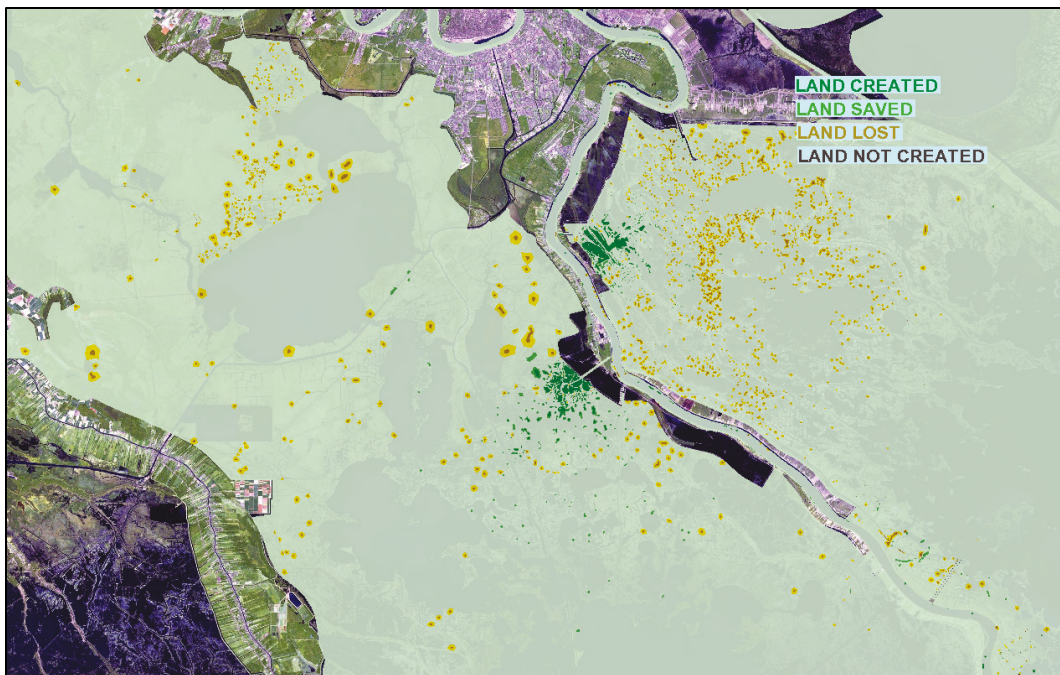
The maps show that the closure of the Bohemia Spillway and Fort St. Philip result in net land loss at the Fort St. Philip crevasse distributary, as would be expected. There is also some land gain associated with the outlets downstream, due to the increased stream power available to transport sediment through these passes and out onto the marsh surface.

Figure 8-12. Modeled land change after 50 years relative to without project conditions – base operations With Bohemia Spillway and Fort St. Philip closure.



The optimized operations show the same basic results as the base operations except that there is less net land gain and less net land loss, both due to the reduced duration of operations (the reduction in duration of operations results in less total sediment load, but also a smaller duration of diversion induced inundation on the existing marsh).

Figure 8-13. Modeled land change after 50 years relative to without project conditions – optimized operations.



Quantification of land change by regional polygon

For the purposes of this study, land is said to exist if the elevation of a given location exceeds a specified value for the elevation of the marsh surface. The specified value for the elevation of the marsh surface is 0 m NAVD88 in 2010. For every year thereafter, the elevation increases by the rate of eustatic sea level rise imposed as the model boundary condition. For these simulations, that is the intermediate rate (the NRCI curve).

The land change is quantified by regional polygons, which were selected as part of the Wetland Value Assessment analysis (WVA). These names and boundaries of these polygons are depicted in Figure 8-14.

Note that for this analysis, the Pontchartrain polygon is omitted (this was not by design; it was an inadvertent omission from the modeling). Hence, all totals reported here do **not** include totals from the Pontchartrain

polygon. However, since the project is not expected to have significant impacts within the Pontchartrain polygon (with respect to land change), this omission does not significantly influence the quantification of the impacts.

Figure 8-14. Polygons used for WVA.



Figure 8-15 depicts the total land gain and lost, relative to without project conditions, for the sum of all of the polygons (excluding Pontchartrain), broken out into land gained (primary from sediment deposition) and land lost (primarily from accelerated loss of marsh vegetation). This figure shows clearly how significant the land loss associated with inundation of the existing vegetation influences the results. For these model scenarios, none of the scenarios tested have a net land gain, due to the losses incurred from inundation of the vegetation. The one that performs the best is the optimization simulation; it builds less land, but the vegetation losses are also much less, resulting in a net value of near 0.

Figure 8-15. Acres of land gained and lost after 50 years of diversion operation.

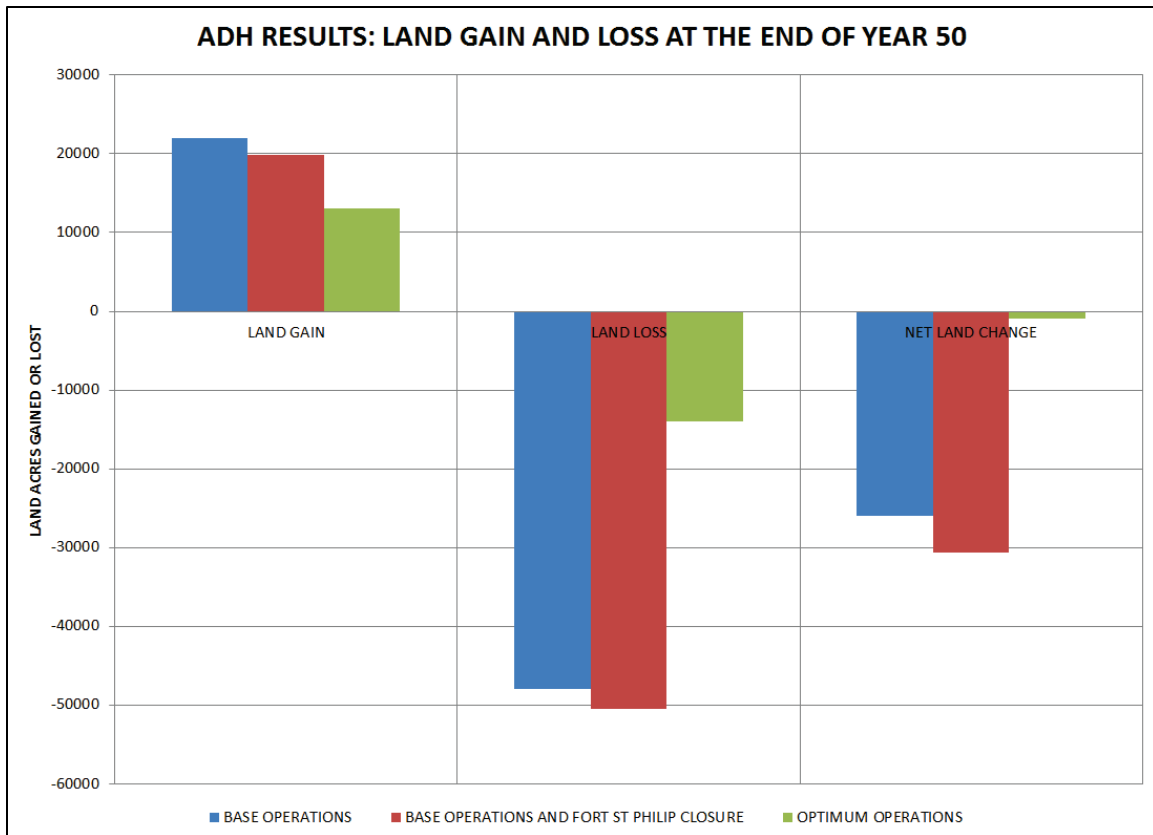


Figure 8-16, Figure 8-17, and Figure 8-18 depict time-histories of the net land change for the Breton, Barataria, and combined Birdsfoot and NWR polygons, respectively. Figure 8-19 depicts the same results for the sum of all of the polygons (except Pontchartrain). These plots further demonstrate the sensitivity of the vegetation model to the inundation associated with the diversions, especially in the Barataria polygon.

Figure 8-16. Time-history of wetland acres relative to without project conditions – Breton polygon.

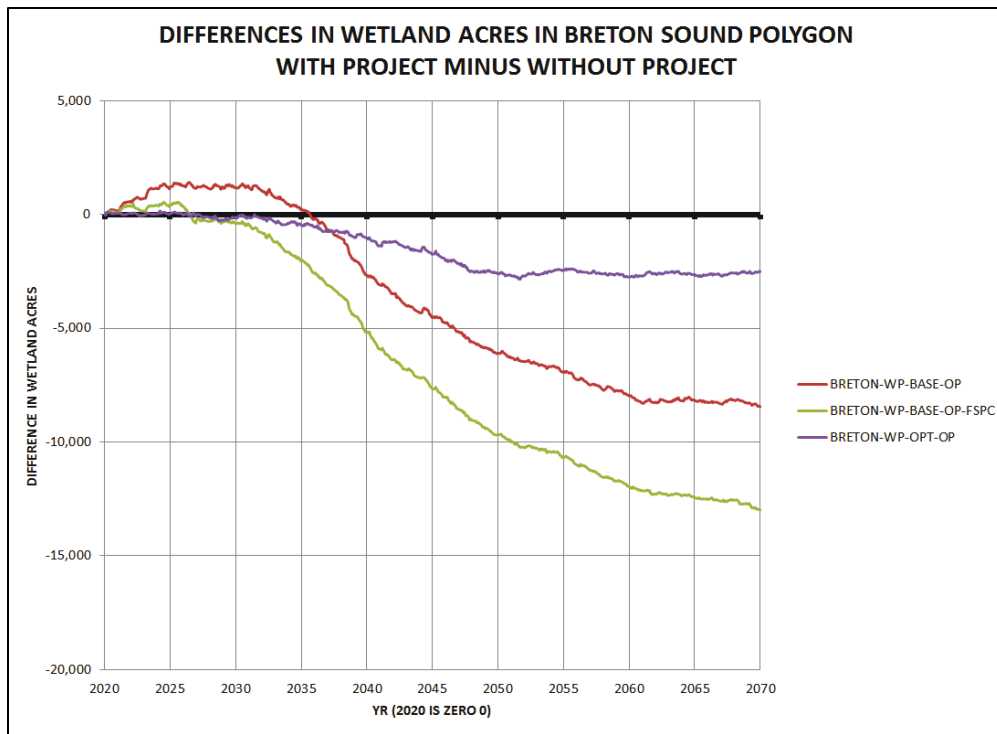


Figure 8-17. Time-history of wetland acres relative to without project conditions – Bataratia polygon.

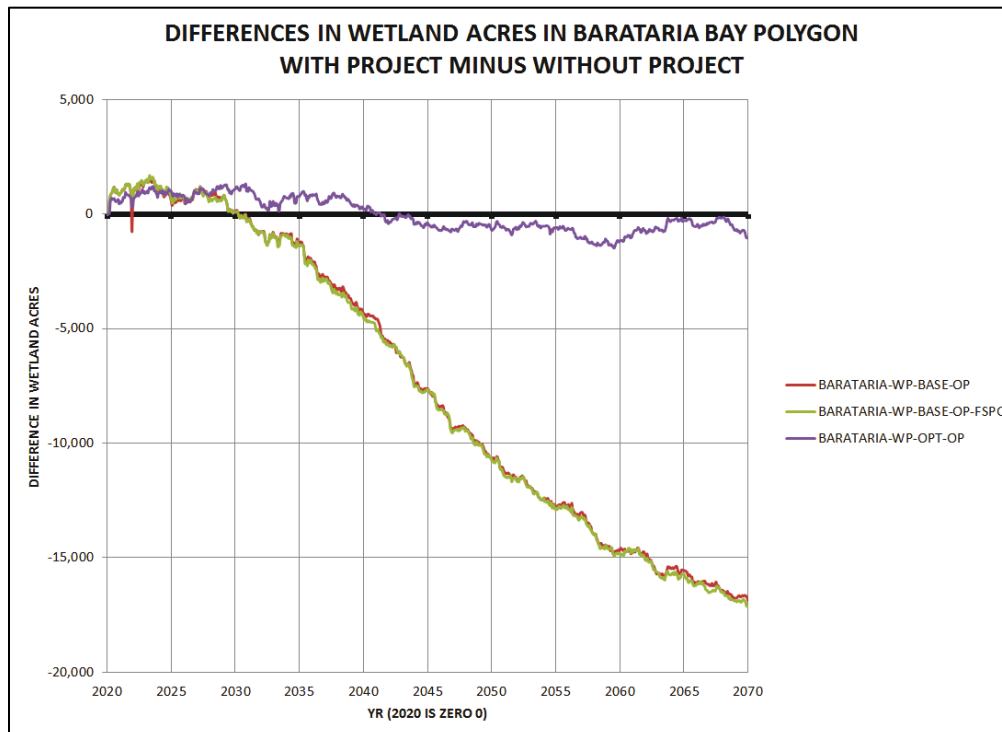


Figure 8-18. Time-history of wetland acres relative to without project conditions – Birdsfoot and NWR polygons.

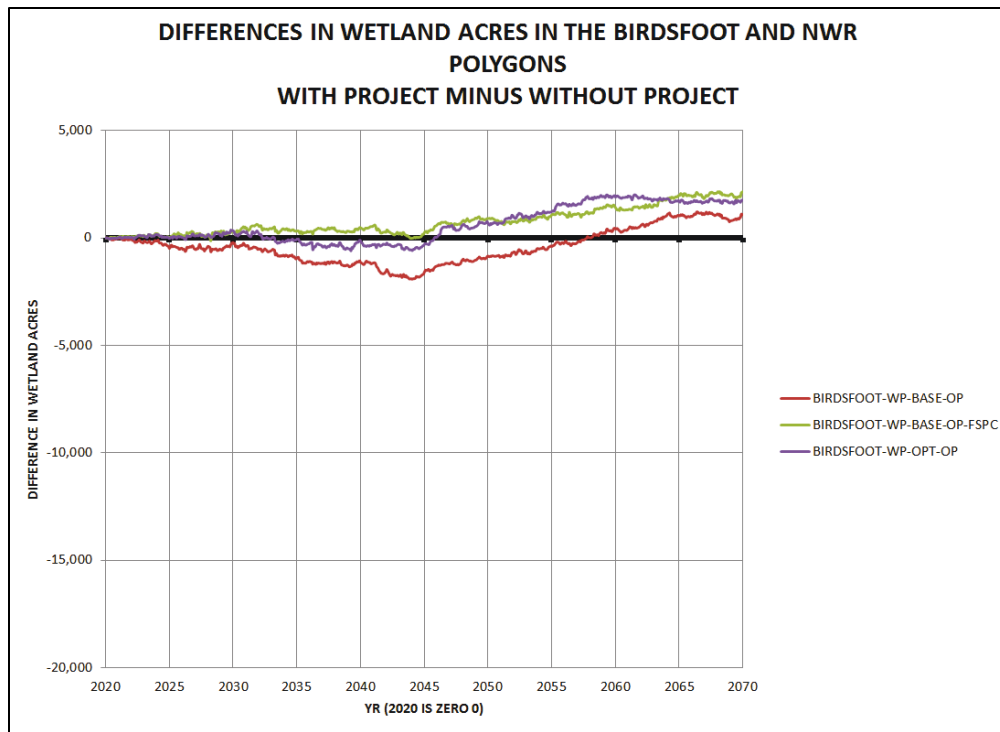
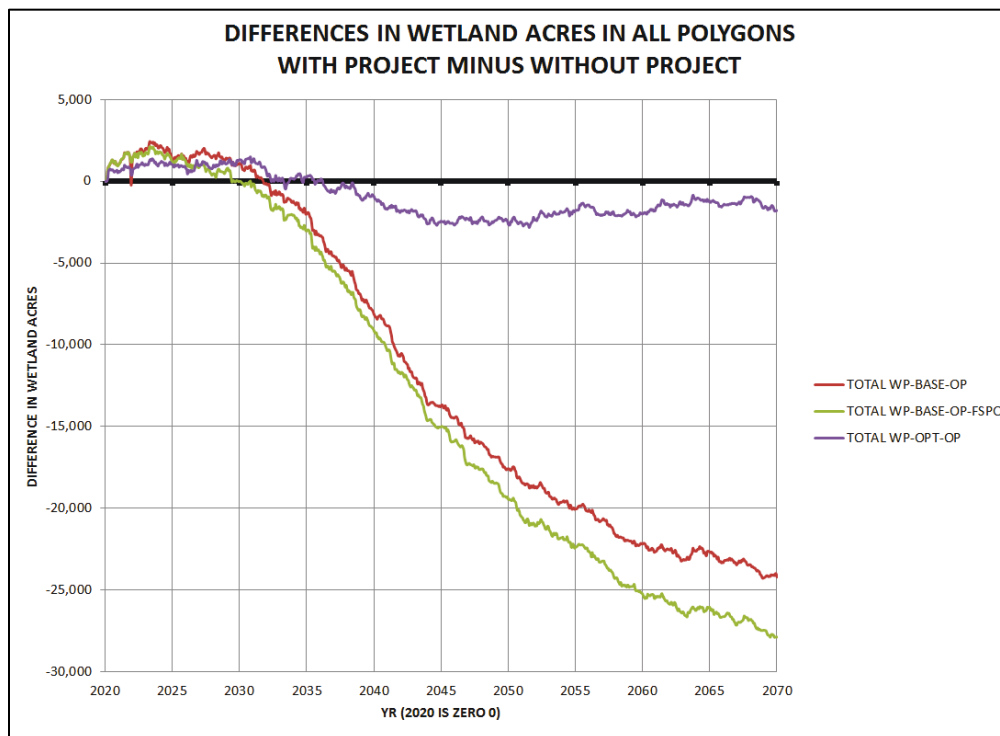


Figure 8-19. Time-history of wetland acres relative to without project conditions – all polygons (except Pontchartrain).



The means whereby inundation accelerates marsh loss in the model can be examined by selecting an example observation location in the marsh. At this location, plots can be generated depicting a time-history land elevation together with water surface elevation. Figure 8-20 depicts the sample location in the marsh. Figure 8-21 is the first 3 years of the time-history, and Figure 8-22 is the full 50 years of the time history. Figure 8-22 is shaded blue beneath the water surface elevation curve so that the point in time at which the land elevation becomes inundated is easily illustrated (this point in time occurs when the land elevation crosses into the blue region of the plot).

These plots illustrate how inundation can accelerate marsh collapse. The rate of accretion of the marsh surface is dramatically slowed when the diversion is in operation, so much so that the sinking of the surface due to subsidence results in a net loss of elevation. In the first few years of the analysis, during times when the diversion is not in operation, the rate of accretion of the marsh recovers to the without project rate. However, as time progresses, the time-integrated influence of this loss of elevation capital results in further reductions in the rate of growth, leading to a nonlinearly increasing loss of elevation capital. Eventually, the marsh surface sinks below the threshold for elevation growth, and marsh collapse occurs.

Figure 8-20. Location of observation point for time-history analysis of vegetation response to diversion-induced inundation.

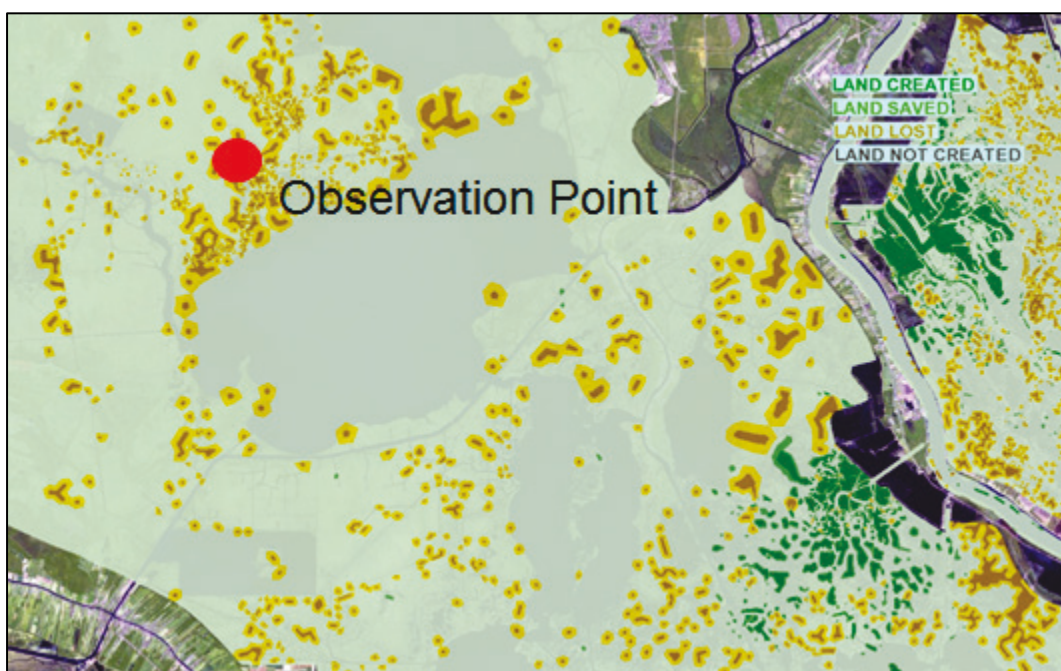


Figure 8-21. Time-history analysis of vegetation response to diversion-induced inundation – first 3 years.

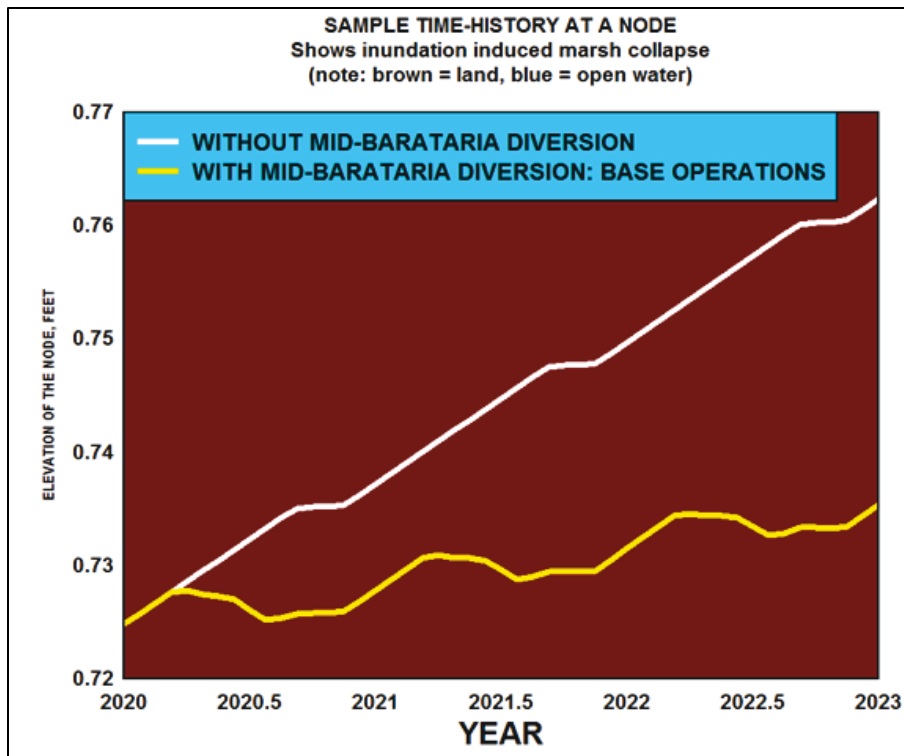
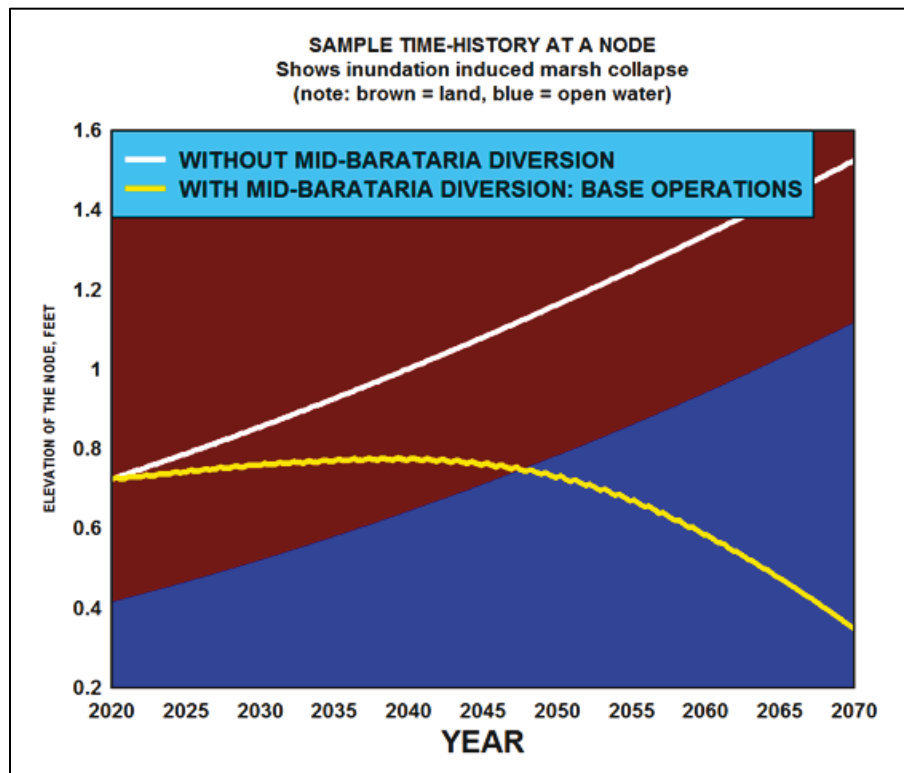


Figure 8-22. Time-history analysis of vegetation response to diversion-induced inundation – 50 years.



Discussion

Due to the computational expense of performing the morphologic simulations needed for these analyses, the Project Development Team (PDT) decided to defer any formal uncertainty analysis until the temporary selected plan had been determined (both the configuration and the operation of the proposed diversions). However, the results given here make clear that the response of the existing wetland vegetation to the inundation associated with the proposed diversions is the overwhelming source of uncertainty, with respect to the expected influence of the diversions on net acres of wetland in the receiving basins.

The vegetation model presented here (SEDLIB-VEG) is a relatively simple model for which the rate of growth of vegetation at any location is a function of only one variable: the local instantaneous depth. This is in contrast to the vegetation model used by TWIG for the CPRA analysis: LaVegMod (Baustain et al. 2018). That model is a highly complex, science-based model, allowing for multiple species of vegetation, and species switching.

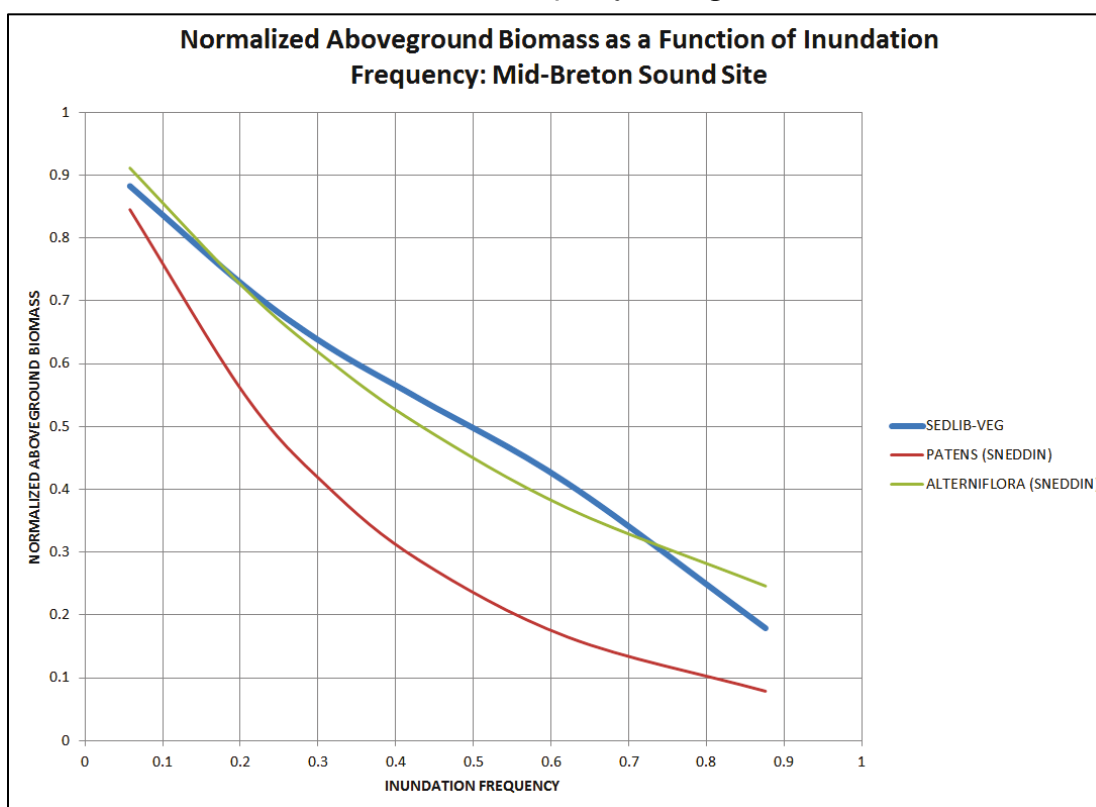
The SEDLIB-VEG model consistently showed more inundation impacts on existing vegetation than did the LaVegMod. There were extensive discussions between the federal and state partners concerning differences in the model results and means of reconciling them. These discussions resulted in some changes to the models that were included in the scenario analyses presented in this chapter. With respect to vegetation, both models were examined against what is known from the literature and from participating scientists to determine how they should be adjusted to better represent the expected response of wetland vegetation to inundation. However, the model results still yielded significantly different results.

The SEDLIB-VEG model implemented for this study showed good agreement with observed reductions in wetland productivity associated with inundation. Figure 8-23 depicts a comparison between the SEDLIB-VEG model results and observed correlations between inundation and primary productivity of *Spartina Alterniflora* and *Spartina Patens* (Snedden et al. 2015). The observations were taken from a *marsh organ* study, where the plantings of vegetation are established at several different predetermined elevations. The study also included synoptic observations of water surface elevation and salinity. Hence, this study is ideal for isolating the influence on inundation on wetland productivity. The fact

that the SEDLIB-VEG results demonstrate a similar degree of sensitivity to inundation to these observations adds confidence to the SEDLIB-VEG model.

However, in contrast to the LaVegMod model, the SEDLIB-VEG model is a relatively simple model and, crucially, does not allow for species switching. If new species are able to colonize the receiving basins, and these species are both more flood tolerant and are at least as productive as the species they replace, then the inundation impacts on land loss could be significantly mitigated (see Appendix D).

Figure 8-23. Comparison of Observed (Snedden et al. 2015) and SEDLIB-VEG modeled correlation between inundation frequency and vegetation root biomass.



The differences in these approaches are, at least in part, a result of differences in the characterization of inundation effects in the scientific literature. Basic plant biology dictates that inundation is a stressor for all wetland plant species (Mitsch and Gosselink 2007). This, in turn, means that these species only exist in these environments because of their ability to adapt to or tolerate various levels of inundation. Therefore, a first-order qualitative analysis indicates that there should be measurable impacts of inundation on existing wetland vegetation communities. Some literature

indicates significant deleterious inundation effects and/or little species transition (e.g., Snedden et al. 2015), whereas other literature indicates little or no inundation effects for some species (especially freshwater species), and/or robust species transition (e.g., Visser and Sandy 2009). The SEDLIB-VEG results tend to show significant vegetation impacts with no species switching, and the LaVegMod results show minimal impacts with species switching. Therefore, it is assumed that the SEDLIB-VEG results presented here, together with the model results associated with the LaVegMod simulations, grossly bracket the uncertainty associated with vegetation impacts. This, in turn, means that this range of uncertainty can only be narrowed with some clarification and/or consensus building within the wetland research community of scientists.

Note that the reason that the proposed diversions are associated with significant inundation of the receiving waters, and hence have potentially significant influence on the existing vegetation, is that they are diverting into existing coastal wetland systems, which are both shallow and vegetated. Although this approach permits the formation of land early in the project life, it also induces inundation effects (see Appendix B).

Although the proposed diversions are often characterized as being analogous to naturally occurring crevasse-splay sub-deltas, this is not entirely the case. Naturally occurring crevasse-splay sub-deltas typically form and develop in deeper, unvegetated embayments, where the energy gradient between the river and the receiving basin is significant enough to induce crevasse growth and development (Wells et al. 1984; and Appendix B).

Note that diverting into deeper, unvegetated embayments, such as typically occurs with crevasse-splay sub-deltas, dramatically mitigates inundation effects (Appendix B). Also, since there is typically little existing vegetation in such receiving waters, there is effectively no wetland-induced inundation influence on existing vegetation.

The West Bay Diversion is just such a diversion into a relatively deep, unvegetated receiving water. The history of this diversion is instructive. The West Bay Diversion was opened in 2003. It did not build any significant land for the first 7-8 years of its operation. This was because there was some initial scour of the existing bay bottom, the diverted sand was settling subaqueously, and the fines were not retained (they were

removed by wind wave erosion) (Barras et al. 2009). However, the introduction of constructed islands in the receiving basin in 2009 and 2010 allowed some of the finer sediments to be retained and to begin to build land. Also, after the flood of 2011, the sand deposition at the diversion outlet was significant enough to establish more land near the outlet (Kolker 2012). Hence, although initial results were not encouraging, land growth has continued since this 2011 event.

In this study, the Lower Breton Diversion is analogous to the West Bay Diversion in that it was designed to divert into a relatively deep, unvegetated basin. Because the modeling indicated that the initiation of land building would not commence until ~20 years after the initiation of operations (because the deposition would be occurring subaqueously until then), it was decided not to pursue that option further.

However, the fact that the Lower Breton Diversion would not have any significant impact on existing vegetation means that that uncertainty associated with this diversion would be much less than the uncertainty associated with the proposed diversions (Mid-Breton and Mid-Barataria).

Hence, both the existing West Bay Diversion and the (screened-out) Lower Breton Diversion are examples of diversions that more closely mimic the natural crevasse play process than do the proposed Mid-Breton and Mid-Barataria Diversions. This means that they require more time to commence land building than do the proposed diversions but also that they induce much less receiving basin inundation than do the proposed diversions.

These considerations should be taken into account as the formal uncertainty analyses of the proposed diversions are carried forward.

Also note that the influence of storms on wetland erosion is not considered in a robust fashion in these simulations. The AdH/SEDLIB simulations do include an annual storm that can induce erosion of the marsh surface. However, this storm is a *typical* annual storm and does not represent the effects of a large storm (such as a hurricane) on wetland erosion and the redistribution of sediments.

Since the proposed diversions increase the water surface elevation on the marsh surface, the waves associated with storms could potentially

penetrate much farther into the marsh interior when the diversions are in operation than they do without the diversions in operation. This effect could be mitigated for hurricanes since the diversions could be closed if a hurricane is approaching. However, large winter storms and other less predictable events could occur during diversion operations and expose the marsh to additional wave induced erosion. This effect should be considered in any future evaluation of the proposed diversions.

Finally, it should be noted that the work documented in this report was conducted as part of the MRHDMS. In May 2017, CPRA notified MVN of their intent to advance both the Mid-Barataria and Mid-Breton sediment diversions through the Department of the Army Section 10/404 permitting process and requested an orderly shutdown of the study. Pursuant to this objective, CPRA has invested significant efforts in seeking to address many of the outstanding issues that are discussed in this report. The results of these subsequent efforts are not documented here: this report only documents work undertaken as part of the MRHDMS.

9 Sediment Diversion Scenario Analysis: Mid-Breton and Mid-Barataria Diversions; Salinity Analysis

Model boundary conditions

It is not possible to use any type of numerical acceleration (such as modified porosity) to model salinity. However, since the residence time for the salinity is the same as the residence time of the water (on the order of months to years) it is not necessary to perform a cumulative analysis of all 50 years of the project duration. All that is necessary is to perform an analysis of a limited number of representative years in the period of investigation. For this study, three representative years were chosen: Years 0, 30, and 50 (2020, 2050, and 2070).

The model boundary conditions consisted of the same inflow conditions as those given for the morphological study (see previous chapter), except that they were modified such that the duration of the hydrograph was a full year (365 days). The wind and tide conditions, however, were not the same as the idealized boundary conditions used for the morphologic study. Rather, they were the same as those used for the verification simulations (see Chapter 3). This is because the salinity simulations require observed tide and wind conditions to realistically simulate the typical circulation of salt in the receiving waters.

Without project salinity: influence of relative sea level rise

Figure 9-1, Figure 9-2, and Figure 9-3 depict the modeled average annual salinity for without project conditions for year 0 (2020), year 30 (2050), and year 50 (2070), respectively. The encroachment of salinity induced by relative sea level rise is evident in this series of images. However, it must be noted that, for these simulations, the operation of Davis Pond and the Caernarvon Diversions are unaltered. The influence of this on the salinity is addressed in the discussion section of this chapter.

Figure 9-1. Modeled average annual salinity without project for Year 0 (2020).

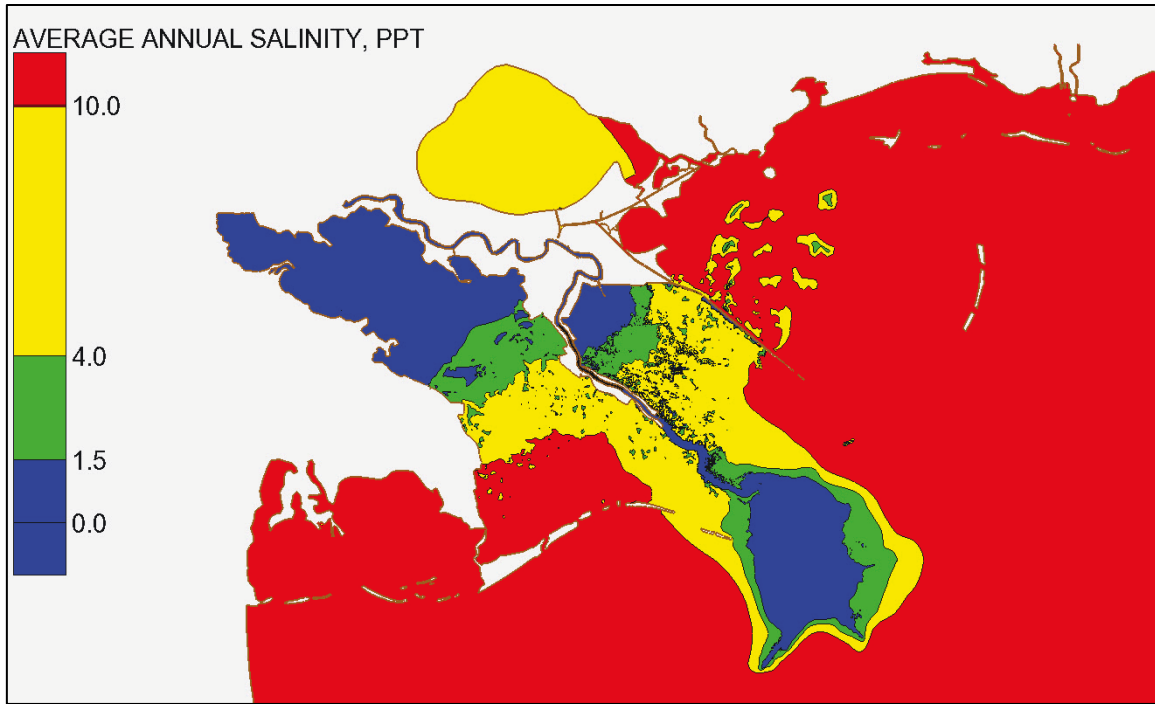


Figure 9-2. Modeled average annual salinity without project for Year 30 (2050).

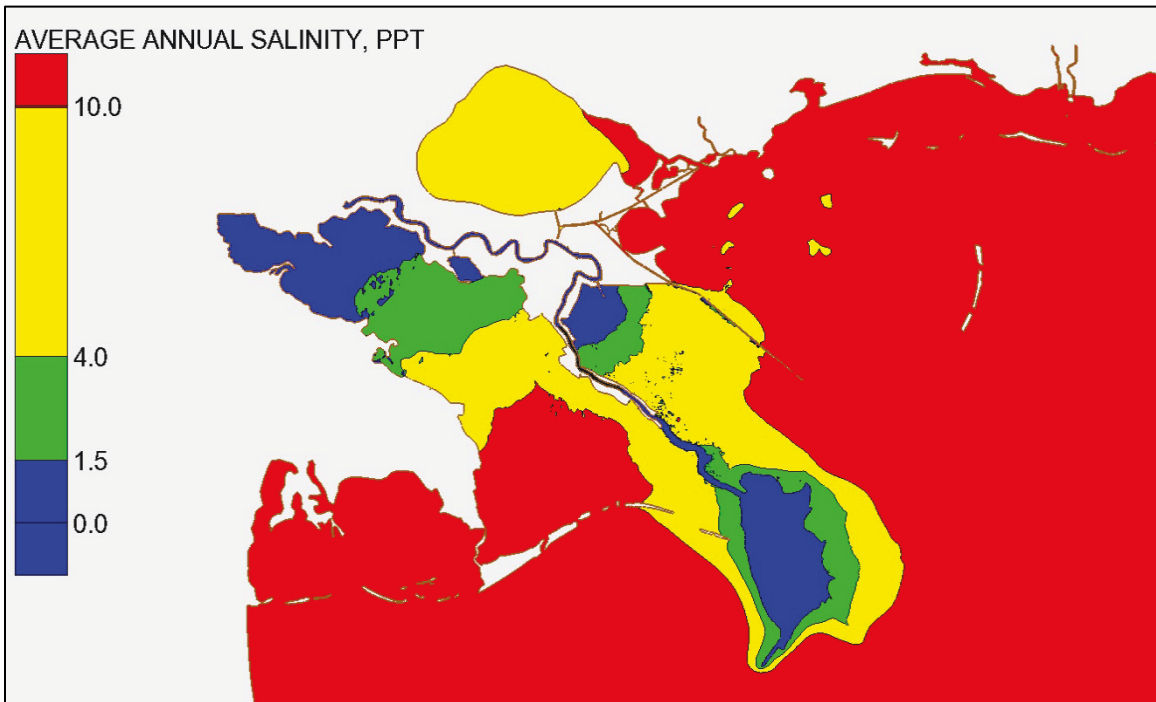
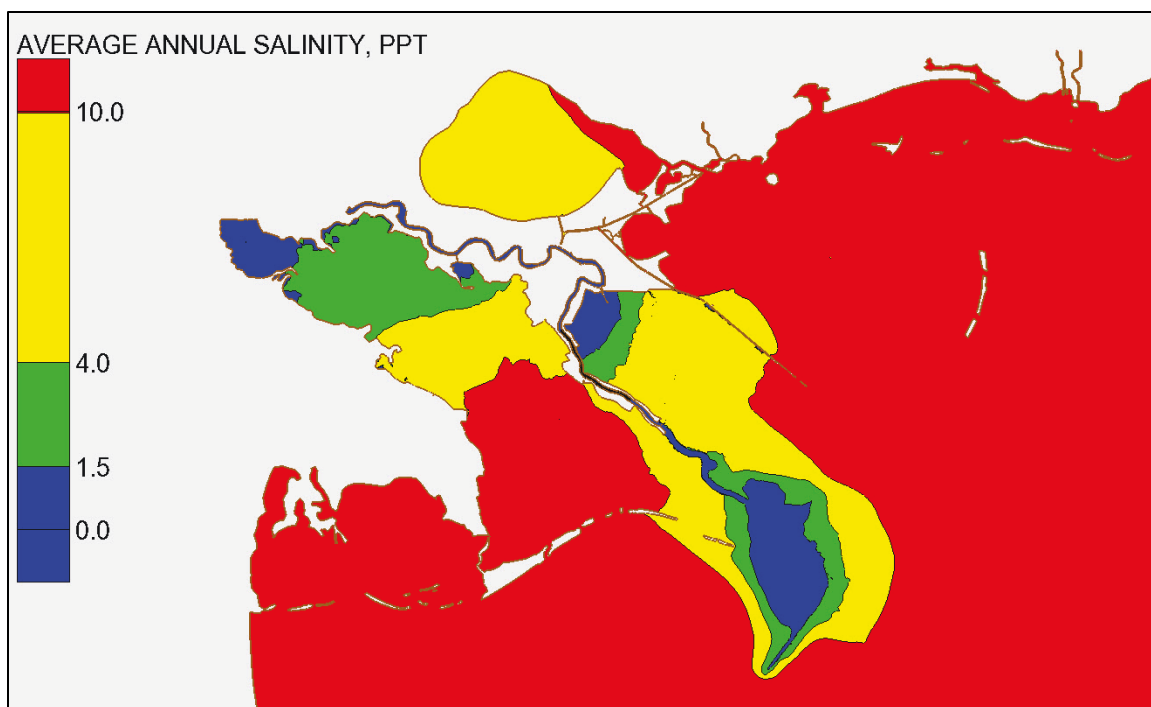


Figure 9-3. Modeled average annual salinity without project for Year 50 (2070).



Scenario analysis results for Year 0 (2020)

The salinity results for Year 0 are given in Figure 9-4 in the form of color contour plots of the percent of the year that the salinity exceeds five parts per thousand. This is a convenient way to determine the relative impacts of various proposed changes.

The results presented are as follows:

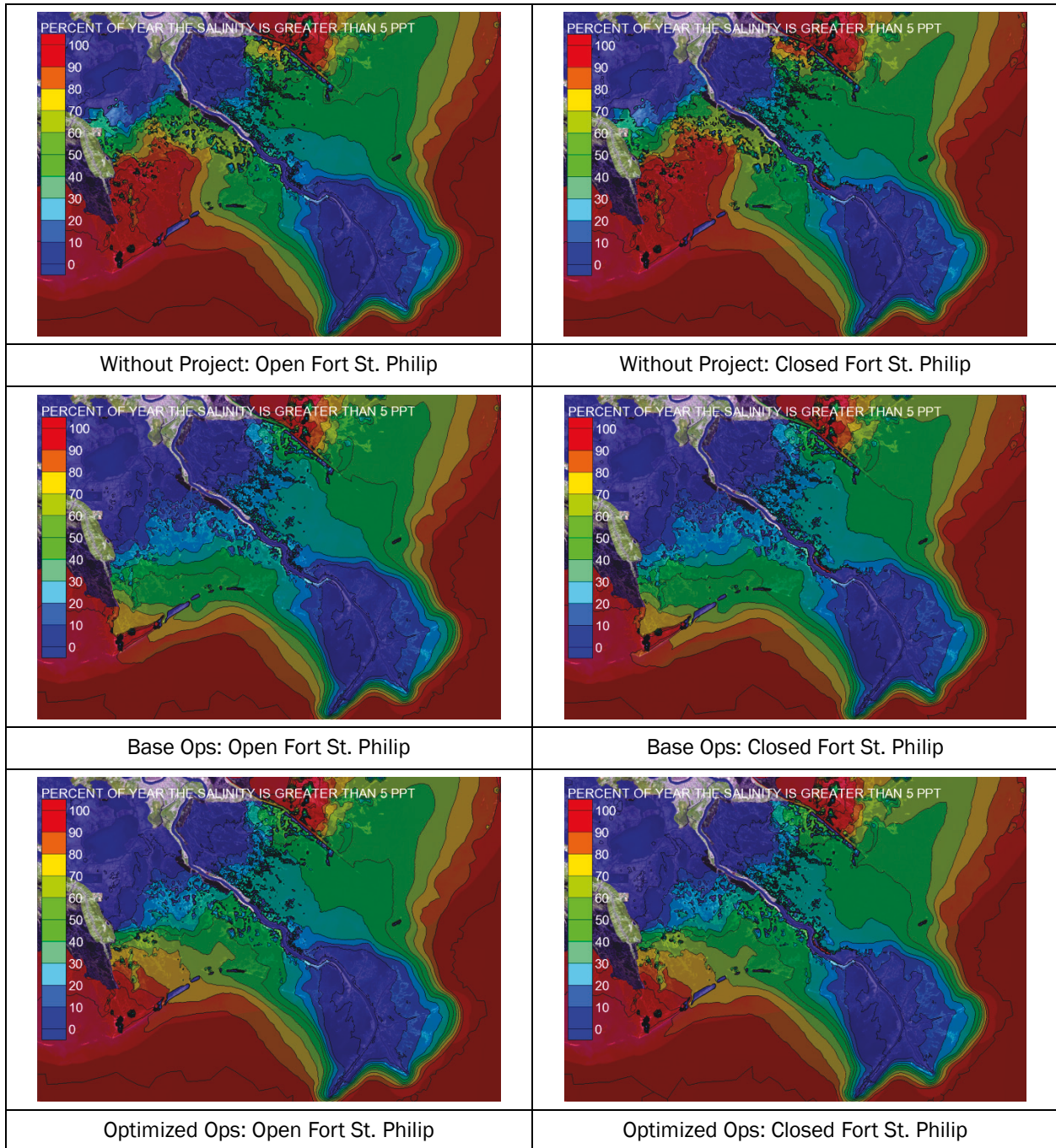
1. Without project, open Fort St. Philip
2. Without project, closed Fort St. Philip
3. With project, base operations (i.e., diversions open for ~4.5 months), open Fort St. Philip
4. With project, base operations (i.e., diversions open for ~4.5 months), closed Fort St. Philip
5. With project, optimized operations (i.e., diversions open for ~1.5 months), open Fort St. Philip
6. With project, optimized operations (i.e., diversions open for ~1.5 months), closed Fort St. Philip.

The results show that the closure of Fort St. Philip has effects both near field and far field, although the effects in southern Breton Sound are not as pronounced as might be supposed. This is because the prevailing offshore currents carry the freshwater emanating from Baptiste Collette and Cubits Gap northward. Thus, the same basic footprint of freshening is occupied regardless of opening or closure, but the size of the footprint is reduced.

This means that the degree to which the salinity increases as a result of Fort St. Philip closure is a statistical question. That is, for a given year, depending on the river discharge and winds, the probability of exceeding a given salinity threshold is higher with the closure than without it, but this does not mean that the target will be achieved for any given year.

The optimization operations appear to have a significant effect on salinity conditions. Specifically, there is some evidence that a significant zone of persistent mesohaline conditions is present in southwestern Baratavia Bay, for the optimization simulations. This mesohaline zone is essentially absent for the Base condition operations.

Figure 9-4. Salinity scenario results for Year 0 (2020).



Discussion

Some general characteristics of the salinity modeling are given below.

- Future relative sea level rise induces significant salinity intrusion into both Breton Sound and Barataria Bay. However, it must be noted that, for these simulations, the operation schedules for Caernarvon Diversion and the Davis Pond Diversion are unaltered over the 50 year simulation. If these diversions, which are designed as salinity control structures, were operated such that the diversion of fresh water increased over time in response to the encroachment salinity associated with sea level rise, the salinity intrusion associated with sea level rise could be significantly reduced.
- The receiving waters tend to freshen significantly during diversion operations. However, when operations cease, the recovery of salinity is not significantly influenced by residual diverted fresh water but instead is almost entirely determined by prevailing offshore conditions (i.e., the wind-driven circulation of the offshore, together with the river discharge, controls the salinity exchange with Breton Sound and Barataria Bay). If winds drive salinity into the bays shortly after operations cease, the recovery is rapid. However, if calm conditions exist, recovery of salinity can be delayed for weeks or months.

There is one important technical concern that has not been fully addressed (as of the writing of this report) by either the AdH model application (presented here) or the Delft3D model application used in depth-averaged mode (the model used by CPRA). It has to do with the influence of river discharge from Southwest Pass on the salinity of lower Barataria Bay.

Aerial photography shows clearly that the Mississippi River discharge at Southwest Pass jets far into the Gulf so that the fresh water associated with this jet enters Barataria Bay from the west. This is a result of recirculation of this buoyant fresh water jet associated with a clockwise gyre between Barataria Bay and Southwest Pass. (Falcini et al. 2012). This behavior can only be accurately modeled with a highly resolved 3D model, as it requires dense resolution both in the horizontal and vertical directions in order to properly simulate the behavior.

The AdH and the Delft3D models are both applied in depth-averaged mode. The depth averaging tends to force the plume alongshore in a counterclockwise direction towards Barataria Bay rather than out into the

Gulf (in a depth-averaged model, the momentum of the plume is diffused over the entire depth, so it does not tend to jet into the gulf). This tendency to force southwest pass discharge alongshore in a counterclockwise direction causes an over-freshening of Barataria Bay in the models.

To cope with this modeling limitation, the AdH and Delft modeling teams took different approaches. The AdH modelers reduced the offshore turbulent mixing to values associated with typical riverine turbulent mixing ($\sim 0.1 \text{ m}^2/\text{sec}$) and added significant horizontal resolution in the offshore (both base resolution and adaptive mesh resolution) to resolve the jet as much as possible within a 2D model. This greatly improved the ability of the model to properly resolve salinity in Lower Barataria Bay, but the model still tended to overfreshen the southeast portion of the Bay, due to the inability for the model to fully resolve the buoyant plume and thereby eliminate the alongshore counterclockwise freshwater transport.

The Delft modeling team elected to add very high diffusion to the offshore ($\sim 200 \text{ m}^2/\text{sec}$), thereby ensuring that the fresh water emerging from Southwest Pass is well mixed with ambient salt water before it interacts with Barataria Bay. This results in good comparisons between the model and observed data in South Barataria Bay. However, it does so by using diffusion to compensate for the inability to resolve the clockwise buoyant jet.

This means that, when diversions are introduced into the Delft3D model (as applied for this study), the diversion water is subject to the same elevated mixing in the offshore as is the water that emerges from Southwest Pass. Hence, there is the potential for artificial diffusive entrainment of salt water into Lower Barataria Bay resulting from the elevated diffusion coefficients in the offshore.

Overall, this means that there is significant uncertainty associated with the salinity response to diversions in Lower Barataria Bay due to the differing mitigation strategies employed by the modelers to cope with inherent model limitations. This uncertainty must be taken into consideration in future phases to fully evaluate diversion impacts on salinity.

10 Summary and Conclusions

Calibration and validation

The AdH model was calibrated and validated against observations of water surface elevation, discharge, and salinity.

For water surface elevation, the qualitative comparisons of the modeled and observed data show good agreement, especially with respect to the ability to simulate both tidal and sub-tidal amplitudes of water surface elevation variation. However, there is a vertical offset in water surface elevation that is evident throughout Barataria Bay. It is possible that this may be due to a systematic offset in the vertical elevation of the observation stations in Barataria Bay or a systematic error in the applied vertical tidal datum at the tidal boundary in the model. As of the writing of this report, there is no direct evidence that can be used to confirm either hypothesis.

The quantitative statistical analyses of these data indicate that approximately half of the observation locations show statistically acceptable agreement, with acceptable being defined according to a set of standards established for this project (Meselse and Rodrigue 2013).

The water surface elevation validation data are very similar to those associated with the calibration data. Of note, however, is the storm-induced increase in water surface elevation, which appears in each of the data sets. The good agreement between the model and field is further verification that the vegetative roughness is well calibrated for inundation events as well. This is important, as the roughness will partly determine the spatial extent of inundation associated with the introduction of diversions.

Modeled discharges were compared against observed discharges. The model simulates the general circulation of Breton Sound in a manner consistent with the observed circulation.

The model performs well with respect to circulation of salinity within the bays, but the model is somewhat deficient at modeling the offshore circulation. This is thought to be due primarily to the depth-averaged assumption employed in the modeling, since the relatively fresh water emerging from the Mississippi River tends to be transported as a buoyant

jet near the surface of the receiving water in the Gulf and is not quickly mixed over the depth.

The model was verified for morphologic modeling by comparison of model hindcasts to the observed development of the Caernarvon and West Bay Diversion deltas.

With respect to the Caernarvon delta, the model builds land in the same general size and configuration as the observed delta. The model reproduces both the date of initiation and rate of growth of the delta quite well.

With respect to the West Bay Diversion, there is significant similarity in the pattern and areal extent of the delta development between modeled and observed deltas. The general agreement between the model and observed values of volumetric change for various pre-defined polygons within the West Bay Delta is generally good, with some exceptions that are most likely due mainly to differences between modeled and observed external conditions. Two things are of note here. First, there were two islands constructed in the Delta during this time period that were not in the simulation. This is the primary reason for the large discrepancy between the modeled and observed values in that area. Second, the model widened a small connection to the river that is not widened in the prototype. This resulted in differences in the observed accumulation of sediment in the polygons adjacent to this widened connection.

Morphologic modeling

The simulations selected for analysis included the following:

- Without project
- Mid-Barataria and Mid-Breton Diversions – base operations
- Mid-Barataria and Mid-Breton Diversions – base operations with closure of Bohemia Spillway and Fort St. Philip
- Mid-Barataria and Mid-Breton Diversions – optimized operations.

All of the morphologic modeling results show net land gain in the near vicinity of the diversion outlets and net land loss farther away from the outlets. The areas of land gain roughly correspond with the zones of significant sand deposition whereas the areas of largest land loss correspond with areas where there is diversion induced inundation, but not significant sediment input from the diversion.

The optimized operations show the same basic results as the base operations except that there is less net land gain and less net land loss, both due to the reduced duration of operations (the reduction in duration of operations results in less total sediment load but also a smaller duration of diversion-induced inundation on the existing marsh).

Quantitative analysis of the net land change associated with the operations of the diversions shows that none of the scenarios tested have a net land gain, due to the losses of land incurred from inundation of the vegetation. The scenario that performs the best is the optimization simulation; it builds less land than the base simulation, but the vegetation losses are also much less, resulting in a net value of near 0.

Note that the vegetation model presented here (SEDLIB-VEG) is a relatively simple model for which the rate of growth of vegetation at any location is a function of only one variable: the local instantaneous depth. This is in contrast to the vegetation model used by TWIG for CPRA: LaVegMod (Baustain et al. 2018). That model is a highly complex, science-based model, allowing for multiple species of vegetation, and species switching.

The differences in these approaches are, at least in part, a result of differences in the characterization of inundation effects in the scientific literature. Basic plant biology dictates that inundation is a stressor for all wetland plant species (Mitsch and Gosselink 2007). This, in turn, means that these species only exist in these environments because of their ability to adapt to or tolerate various levels of inundation. Therefore, a first-order qualitative analysis indicates that there should be measurable impacts of inundation on existing wetland vegetation communities. Some literature indicates significant deleterious inundation effects and/or little species transition (e.g., Snedden et al. 2015) whereas other literature indicates little or no inundation effects for some species (especially freshwater species) and/or robust species transition (e.g., Visser and Sandy 2009). However, since the SEDLIB-VEG results tend to show significant vegetation impacts with no species switching and the LaVegMod results show minimal impacts with species switching, it is assumed that the range of model results presented here grossly bracket the uncertainty associated with vegetation impacts. This, in turn, means that this range of uncertainty can only be narrowed with some clarification and/or consensus building within the wetland research community of scientists.

Note that the reason that the proposed diversions are associated with significant inundation of the receiving waters, and hence have potentially significant influence on the existing vegetation, is that, unlike most naturally formed crevasse-splay sub-deltas (which tend to form in open water), these diversions are designed to divert into existing coastal wetland systems that are both shallow and vegetated. Although this approach permits the formation of land early in the project life, it also induces inundation of the existing wetland vegetation and a concomitant increase in uncertainty with respect to the predicted net land change throughout the project life (see Appendix B).

Also note that, since the proposed diversions increase the water surface elevation on the marsh surface, the waves associated with storms could potentially penetrate much farther into the marsh interior when the diversions are in operation than they do without the diversions in operation. This effect should be considered in any future evaluation of the proposed diversions.

Salinity modeling

Some general characteristics of the salinity modeling are given below.

- Future relative sea level rise induces significant salinity intrusion into both Breton Sound and Barataria Bay. However, it must be noted that, for these simulations, the operation schedules for Caernarvon Diversion and the Davis Pond Diversion are unaltered over the 50 year simulation. If these diversions, which are designed as salinity control structures, were operated such that the diversion of fresh water increased over time in response to the encroachment salinity associated with sea level rise, the salinity intrusion associated with sea level rise could be significantly reduced.
- The receiving waters tend to freshen significantly during diversion operations. However, when operations cease, the recovery of salinity is not significantly influenced by residual diverted fresh water but instead is almost entirely determined by prevailing offshore conditions (i.e., the wind-driven circulation of the offshore, together with the river discharge, control the salinity exchange with Breton Sound and Barataria Bay). If winds drive salinity into the bays shortly after operations cease, the recovery is rapid. However, if calm conditions exist, recovery of salinity can be delayed for weeks or months.

- The optimization operations appear to have a significant effect on salinity conditions. Specifically, there is some evidence that a significant zone of persistent estuarine conditions is present in Southwestern Barataria Bay for the optimization simulations. This mesohaline zone is essentially absent for the Base condition operations.

Note that that there is significant uncertainty associated with the salinity response to diversions in Lower Barataria Bay, due to the differing mitigation strategies employed by the modelers to cope with inherent model limitations associated with depth-averaging in the offshore. This uncertainty must be taken in to consideration in future phases to fully evaluate diversion impacts on salinity.

Finally, it should be noted that the work documented in this report was conducted as part of the MRHDMS. In May 2017, CPRA notified MVN of their intent to advance both the Mid-Barataria and Mid-Breton sediment diversions through the Department of the Army Section 10/404 permitting process and requested an orderly shutdown of the study. Pursuant to this objective, CPRA has invested significant efforts in seeking to address many of the outstanding issues that are discussed in this report. The results of these subsequent efforts are not documented here; this report only documents work undertaken as part of the MRHDMS.

References

- Alishahi, M. R., and R. B. Krone. 1964. *Suspension of Cohesive Sediments by Wind-Generated Waves*. Technical Report HEL-2-9. University of California, Berkeley: Hydraulic Engineering Laboratory.
- Allison, M. A., C. R. Demas, B. A. Ebersole, B. A. Kleiss, C. D. Little, E. A. Meselhe, N. J. Powell, T. C. Pratt, and B. M. Vosburg. 2012. A water and sediment budget for the lower Mississippi-Atchafalaya River in flood years 2008-2010: implications for sediment discharge to the oceans and coastal restoration in Louisiana. *Journal of Hydrology* 432(3):84–97.
- Allison, M. A., and J. A. Nittrouer. 2004. *Assessing Quantity and Quality of Sand Available in the Lower Mississippi River Channel for Coastal Marsh and Barrier Island Restoration in Louisiana*. Final Technical Report for Governor's Applied Coastal research and Development Program.
- Barras, J. A., W. C. Padgett, and C. B. Sanders. 2009. *Aerial and Bathymetric Spatial Change Analysis of the West Bay Sediment Diversion Receiving Area, Louisiana*. For U.S. Army Engineer District, New Orleans (MVN) Report. U.S. Army Corps of Engineers.
- Baustian, M. M., E. A. Meselhe, H. Jung, K. Sadid, S. M. Duke-Sylvester, J. M. Visser, M. A. Allison, L. C. Moss, C. Ramatchandirane, D. S. van Marend, M. Jeuken, and S. Bargu. 2018. Development of an integrated biophysical model to represent morphological and ecological processes in a changing deltaic and coastal ecosystem. *Environmental Modelling & Software* 109: 402–419. <https://doi.org/10.1016/j.envsoft.2018.05.019>
- Bernard, B. 1992. *Depth-Average Numerical Modeling for Curved Channels*. Technical Report HL-92-9. Vicksburg, MS: U.S. Army Engineer Research and Development Center.
- Brown, G. L. 2008. Approximate profile for nonequilibrium suspended sediment. *Journal of Hydraulic Engineering* 134(7):1010–1014.
- Brown, G. L. 2012a. A quasi-3d suspended sediment model using a set of correction factors applied to a depth averaged advection diffusion equation. In *Proceedings, IIHR 3rd International Shallow Flows Symposium, University of Iowa, 2012*.
- Brown, G. L. 2012b. Modification of the bed sediment equations of Spasojevic and Holly (1993) to account for variable porosity, variable grain specific gravity, and nonerodable boundaries. In *Proceedings, IIHR 3rd International Shallow Flows Symposium, University of Iowa, 2012*.
- Brown, G. L., J. V. Letter, Jr., R. E. Heath, R. McAdory, L. L. Wehmeyer, and B. L. Gunkel. 2013. *A Simplified Analytic Investigation of the Riverside Effects of Sediment Diversions*. ERDC/CHL CHETN-VII-13. Vicksburg, MS: U.S. Army Engineer Research and Development Center. <http://acwc.sdp.sirsi.net/client/search/asset/1030340>

- Brown, G. L., J. N. Tate, K. Pevey, C. P. Richards, C. P. Price, and B. A. Kleiss. 2018. *Mississippi River Hydrodynamic Study: Multi-Dimensional Modeling: AdH/SEDLIB Multi-Dimensional Model Study*. <http://www.mvd.usace.army.mil/Missions/Mississippi-River-Science-Technology/Mississippi-River-Hydro/>
- Christensen, B. A. 1972. Incipient motion on cohesionless channel banks. *Sedimentation: Symposium to Honor Professor H.A. Einstein*. Edited by H. W. Shen. Fort Collins, CO.
- Darby, F. A. 2006. *Belowground Biomass of Spartina alterniflora: Seasonal Variability and Response to Nutrients*. PhD dissertation, Louisiana State University and Agricultural and Mechanical College.
- Day, J., R. Lane, M. Moerschbaeche, R. DeLaune, I. Mendelssohn, J. Baustian, and R. Twilley. 2012. Vegetation and soil dynamics of a Louisiana estuary receiving pulsed Mississippi River water following Hurricane Katrina. *Estuaries and Coasts* 36(4):665–682. DOI 10.1007/s12237-012-9581-0. <https://link.springer.com/content/pdf/10.1007%2Fs12237-012-9581-0.pdf>.
- Egiazaroff, L. V. 1965. Calculation of non-uniform sediment concentration. *Journal of Hydraulics Division ASCE* 91(HY4):225–248.
- Fagherazzi, S., M. L. Kirwan, S. M. Mudd, G. R., Guntenspergen, S. Temmerman, A. D'Alpaos, J. van de Koppel, J. M. Rybczyk, E. Reyes, C. Craft, and J. Clough. 2012. Numerical models of salt marsh evolution: Ecological, geomorphic, and climatic factors. *Rev. Geophys.* 50(1). doi:10.1029/2011RG000359.
- Falcini, F., N. S. Khan, L. Macelloni, B. P. Horton, C. B. Lutken, K. L. McKee, R. Santoleri, S. Collela, L. Chunyan, G. Volpe, M. D-Emidio, A. Salusti, and D. Jerolmack. 2012. Linking the historic 2011 Mississippi River flood to coastal wetland sedimentation. *Nat. Geosci.* 5: 803–807.
- Gliński, J., J. Horabik, and J. Lipiec, eds. 2011. *Encyclopedia of Agrophysics*. Springer Science+Business Media B.V. DOI 10.1007/978-90-481-3585-1 2011
- Heath, R. E., G. L. Brown, C. D. Little, T. C. Pratt, J. J. Ratcliff, D. D. Abraham, D. Perkey, N. B. Ganesh, K. Martin, and D. P. May. 2015. *Old River Control Complex: Sedimentation Investigation*. ERDC/CHL TR-15-8. Vicksburg, MS: U.S. Army Engineer Research and Development Center.
- Huang, P. T., M. Patel, M. C. Santagata, and A. Bobet. 2009. *Classification of Organic Soils*. Final Report. FHWA/IN/JTRP-2008/2. Project No. C-36-36TT. Joint Transportation Research Program. Indiana Department of Transportation and Purdue University.
- Jarvis, J. C. 2010. *Vertical Accretion Rates in Coastal Louisiana: A Review of the Scientific Literature*. ERDC/EL TN-10-5. Vicksburg, MS: U.S. Army Engineer Research and Development Center.
- Kirwan, M. L., and G. R. Guntenspergen. 2012. Feedbacks between inundation, root production, and shoot growth in a rapidly submerging brackish marsh. *Journal of Ecology* 100: 764–770.

- Kleinhans, M. G., and L. C. van Rijn. 2002. Stochastic prediction of sediment transport in sand-gravel bed rivers. *Journal of Hydraulic Engineering* 128(4):412–425.
- Kolker, A. S. 2012. Depositional dynamics in a river diversion receiving basin: the case of the West Bay Mississippi River Diversion. *Estuar. Coast. Shelf Sci.* 106:1–12.
- Krone, R. 1962. *Flume Studies of the Transport of Sediment in Estuarial Shoaling Process*. University of California, Berkeley: Hydraulic Engineering Laboratory and Sanitary Engineering Research Laboratory.
- Lane, R. R., J. W. Day, G. P. Kemp, and D. M. Demcheck. 2001. The 1994 experimental opening of the Bonnet Carre Spillway to divert Mississippi River water into Lake Pontchartrain, Louisiana. *Ecological Engineering* 17(2001): 411–422
- Lane, R. R., J. W. Day, and B. Thibodeaux. 1999. Water quality analysis of a freshwater diversion at Caernarvon, Louisiana. *Estuaries* 22: 327–336.
- Lewis, J. W., G. L. Brown, and S. K. Ayres. 2017. *Investigation of Discharge Measurement of the Lower Mississippi River below Natchez, MS*. MRG&P Tech Note No. 3. Vicksburg, MS: U.S. Army Engineer Research and Development Center.
- Lick, W. 2009. *Sediment and Contaminant Transport in Surface Waters*. Boca Raton, FL: CRC Press, Taylor & Francis Group.
- Lindquist, D. C., and R. M. Summer. 2007. *Coastal Restoration Annual Project Reviews: December 2007*. Baton Rouge: Louisiana Dept. of Natural Resources.
- Louisiana Coastal Area. 2004. *Louisiana Coastal Area, Louisiana: Ecosystem Study*. Final report. USACE, New Orleans District.
- McKay, S. K., J. C. Fischenich, S. J. Smith, and R. Paille. 2010. Quantifying benefits of flow diversion to coastal marshes. *I: Theory. Louisiana Coastal Area Ecosystem Restoration Projects Study, Vol. 3*. Final Integrated Feasibility Study and Environmental Impact Statement for the Convey Atchafalaya River Water to Northern Terrebonne Marshes and Multipurpose Operation of Houma Navigation Lock, Appendix M, Annex 3. New Orleans, LA: U.S. Army Corps of Engineers and Coastal Protection and Restoration Authority,
- Meselhe E. A., and M. D. Rodrigue. 2013. *Models Performance Assessment Metrics and Uncertainty Analysis*. Final Report. Prepared for the Louisiana Coastal Protection and Restoration Authority.
- Mitsch, W. J., and J. G. Gosselink. 2007. *Wetlands*, 4th ed. New York: John Wiley.
- Snedden, G. A., J. E. Cable, C. Swarzenski, and E. Swenson. 2007. Sediment discharge into a subsiding Louisiana deltaic estuary through a Mississippi River diversion. *Estuarine, Coastal and Shelf Science* 71(1–2):181–193.
- Snedden, G. A., K. Cretini, and B. Patton. 2015. Inundation and salinity impacts to above-and belowground productivity in *Spartina patens* and *Spartina alterniflora* in the Mississippi River deltaic plain: Implications for using river diversions as restoration tools. *Ecol Eng* 81: 133–139.

- Stansby, P. K. 2004. A mixing length model for shallow turbulent wakes. *Shallow Flows*, edited by Jirka and Uijtewaal. London: Taylor and Francis Group.
- U.S. Army Corps of Engineers (USACE). 2014. *Procedures to Evaluate Sea Level Change: Impacts, Responses, and Adaptation*. ETL 1100-2-1. Washington, DC: U.S. Army Corps of Engineers.
http://www.publications.usace.army.mil/Portals/76/Publications/EngineerTechnicalLetters/ETL_1100-2-1.pdf
- van Rijn, L. C. 1984. Sediment transport, part I: Bed load transport. *J. Hydr. Engrg.* 110(10): 1431–1456. DOI: [10.1061/\(ASCE\)0733-9429\(1984\)110:10\(1431\)](https://doi.org/10.1061/(ASCE)0733-9429(1984)110:10(1431))
- Visser, J. M., and E. R. Sandy. 2009. The effects of flooding on four common Louisiana marsh plants. *Gulf Mex. Sci.* 27(2009): 21–29.
- Walton R., and B. A. Christensen. 1980. Friction factors in storm surges over inland areas. *J. Waterw. Port, Coastal Ocean Div., Am. Soc. Civ. Eng.* 106(2): 261–271.
- Wamsley, T. V. 2013. *Land Building Models: Uncertainty in and Sensitivity to Input Parameters*. ERDC/CHL CHETN-VI-44. Vicksburg, MS: U.S. Army Engineer Research and Development Center.
- Wells, J. T., S. J. Chinburg, and J. M. Coleman. 1984. *The Atchafalaya River Delta, Report 4: Generic Analysis of Delta Development*. Report HL 82–15. Vicksburg, MS: U.S. Army Engineer Research and Development Center.
- Wright, S., and G. Parker. 2004. Flow resistance and suspended load in sand-bed rivers: simplified stratification model. *Journal of Hydraulic Engineering* 130(8):796–805.

Appendix A: DAMLAY Theoretical Development

Diversion Accreted Marsh Lifecycle Analysis (DAMLAY): Theoretical Development

Gary L Brown

06-2017

The Energy Budget Constraint for a Sediment Diversion

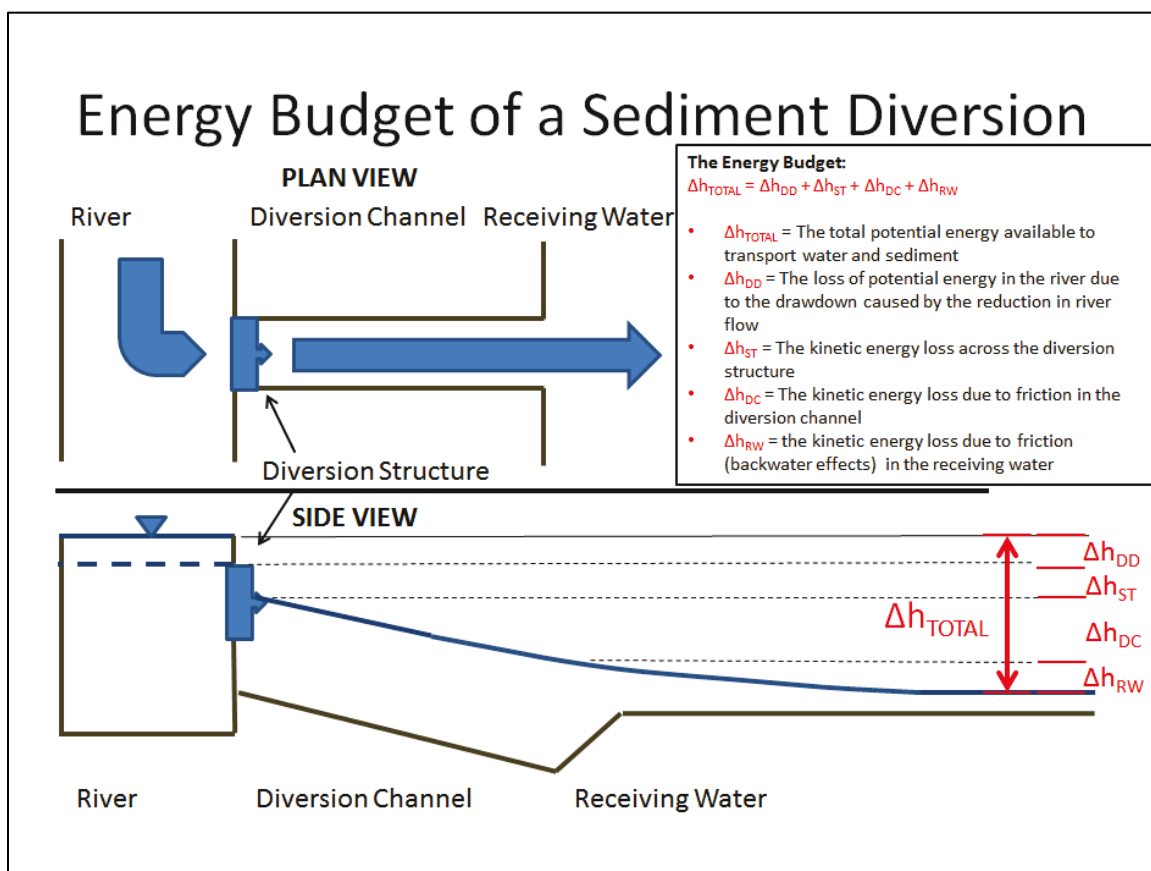
The operation of any sediment diversion is constrained by the total mechanical energy available to move water and sediment from the river to the receiving water. For subcritical river flows, this total available energy can be approximated to a high degree of accuracy by the potential energy difference between the river and the receiving water (i.e. the water surface elevation difference).

There are 4 basic energy sinks associated with a water and sediment diversion. These are illustrated in Figure 1. If the combined energy loss associated with these 4 sinks exceeds the total available energy, the diversion cannot be operated as designed.

This paper gives analytic techniques to approximately quantify these 4 sinks for a given diversion design. This paper also gives analytic methods to optimize the diversion width (for minimum energy loss) and the diversion discharge (for maximum sediment discharge over the life-cycle of the diversion).

Note that, for convenience, the energy losses are expressed in terms of the potential energy (water surface elevation difference) rather than the total energy (the potential and kinetic energy). Since the potential energy and total energy are essentially equal at the upstream and downstream ends of the analysis (the kinetic energy is assumed to be zero in the river and the receiving water), we can use the potential energy losses for the intermediate calculations if we are careful to account for the conversion of some of this potential energy to kinetic energy. This is accounted for in the equation for the energy loss at the structure.

Figure A1. The Energy Budget of a Sediment Diversion.



Simplifying Assumptions

- The river and the diversion channel are wide, rectangular channels
- The receiving water is a wide basin of uniform depth and uniform roughness
- Manning's equation is valid
- Sediment concentration can be expressed as a power law function of the shear stress
- The water and sediment discharges for the diversion are constant over time, when the diversion is in operation (note that these equations do not require that the diversion is in continuous operation, only that the water and sediment discharge do not vary when it is in operation)

Diversion Outfall Preliminary Design Theoretical Development: Drawdown in River

If the river is at uniform flow, the drawdown can be accurately estimated with a simple application of Manning's Equation. However, if the river is

flowing under non-uniform flow conditions (as is the case with the Lower Mississippi River, where backwater conditions prevail), it is necessary to include an additional approximation to account for the slope of the energy grade line.

The drawdown can be found by expressing the discharge ratio in terms of Manning's Equation:

$$\frac{Q_R - Q_D}{Q_R} = \left(\frac{h_{R,DD}}{h_R} \right)^{5/3} \left(\frac{S_{R,DD}}{S_R} \right)^{1/2} \quad (1)$$

The slope ratio is unknown and must be approximated. For a backwater curve, this is done as follows:

For a Froude number $\ll 1$, (as is most often the case for large lowland rivers) the velocity head is small relative to the pressure and gravity heads and can be neglected. Hence, for this case, the slope of the energy grade line is approximately equal to the slope of the water surface.

Assume that the elevation of the water surface associated with a backwater curve approaching the sea can be approximated with an exponential function, and that the inclusion of a diversion can be approximated by a translation of the x-coordinate of the exponential function, as follows:

$$\begin{aligned} \eta_R - \eta_{MSL} &= e^x \\ \eta_{R,DD} - \eta_{MSL} &= e^{x-x_D} \end{aligned} \quad (2)$$

Since the derivative (slope) of the exponential function is equal to the function itself, it follows that, at a given x-coordinate, the ratio of the water surface slopes (and hence the energy grade line slopes) is equal to the ratio of the water surface elevations. I.e.

$$\frac{S_{R,DD}}{S_R} \cong \frac{\eta_{R,DD} - \eta_{MSL}}{\eta_R - \eta_{MSL}} = \frac{\eta_R - \eta_{MSL} - \Delta h_{DD}}{\eta_R - \eta_{MSL}} \quad (3)$$

Substituting 3 into 1, and noting that $h_{R,DD} = h_R - \Delta h_{DD}$ and $\delta_D = Q_D/Q_R$, we get the following:

$$1 - \delta_D = \left(1 - \frac{\Delta h_{DD}}{h_R}\right)^{5/3} \left(1 - \frac{\Delta h_{DD}}{\eta_R - \eta_{MSL}}\right)^{1/2} \quad (4)$$

This equation can be solved for Δh_{DD} iteratively. The choice of which Δh_{DD} to solve for is dependent on the relative sizes of $\eta_R - \eta_{MSL}$ and h_R .

$$\left(\frac{(\eta_R - \eta_{MSL})}{h_R} < \frac{1}{2} \right) \rightarrow \Delta h_{DD} = (\eta_R - \eta_{MSL}) \left(1 - \frac{(1 - \delta_D)^2}{\left(1 - \frac{\Delta h_{DD}}{h_R}\right)^{10/3}} \right) \quad (5)$$

$$\left(\frac{(\eta_R - \eta_{MSL})}{h_R} > \frac{1}{2} \right) \rightarrow \Delta h_{DD} = h_R \left(1 - \frac{(1 - \delta_D)^{3/5}}{\left(1 - \frac{\Delta h_{DD}}{(\eta_R - \eta_{MSL})}\right)^{3/10}} \right) \quad (6)$$

Note that 6 approaches the uniform flow relationship for large $\eta_R - \eta_{MSL}$, which is consistent with the asymptotic shape of the backwater curve.

Diversion Outfall Preliminary Design Theoretical Development: Local Energy Loss at the Diversion Structure

The local energy loss at the diversion structure can be estimated by applying Bernoulli's equation across the structure, and noting that the kinetic energy on the upstream side of the structure is assumed equal to 0:

$$\Delta h_{ST} = \frac{1}{2g} \left(\frac{Q_D}{w_{DC} h_{DC}} \right)^2 + \frac{\zeta_{ST}}{2g} \left(\frac{\psi_{ST} Q_D}{w_{DC} h_{DC}} \right)^2 \quad (7)$$

Diversion Outfall Preliminary Design Theoretical Development: Friction Loss in the Diversion Channel

Express the sediment concentration in the river and the diversion channel in terms of the shear stress using a generic power law formula

$$C_R = \alpha \tau_R^\beta \quad (8)$$

$$C_{DC} = \alpha \tau_{DC}^\beta \quad (9)$$

Define the sediment diversion efficiency as the ratio of the concentration in the diversion to the concentration in the river

$$\varepsilon_D \equiv \frac{C_{DC}}{C_R} = \left(\frac{\tau_{DC}}{\tau_R} \right)^\beta \quad (10)$$

Solve 10 for τ_{DC} .

$$\tau_{DC} = \varepsilon_D^{1/\beta} \tau_R \quad (11)$$

Bed shear stress can be expressed in terms of the hydraulic slope as follows:

$$\tau = \rho g h S \quad (12)$$

Substituting 12 into 11 yields an expression for the hydraulic slope in the diversion channel:

$$S_{DC} = \frac{h_R}{h_{DC}} \varepsilon_D^{1/\beta} S_R \quad (13)$$

Using this slope and known roughness, inflow and depth values, Manning's equation can be used to solve for the diversion channel width (Note, for convenience, we use the form of Manning's Equation given by Christensen (1970) that expresses the roughness in terms of an equivalent roughness height).

$$w_{DC} = \frac{Q_D}{M_{DC} h_{DC}^{5/3} S_{DC}^{1/2}} \quad (14)$$

$$M_{DC} = \frac{K_n}{n_{DC}} = \frac{8.25 \sqrt{g}}{k_{DC}^{1/6}} \quad (15)$$

The diversion channel velocity and Froude number can then be found as follows:

$$u_{DC} = \frac{Q_D}{h_{DC} w_{DC}} \quad (16)$$

$$\mathbb{F}_{DC} = \frac{u_{DC}}{\sqrt{gh_{DC}}} \quad (17)$$

The water surface elevation and the invert elevation at the structure are found as follows:

$$\eta_{ST} = \eta_{RW.MAX} + L_{DC}S_{DC} \quad (18)$$

$$z_{ST} = \eta_{ST} - h_{DC} \quad (19)$$

An equation for the head loss in the diversion channel can be developed by solving 14 for h_{DC} , substituting into 13, and approximating the head loss in the channel as equal to the product of the hydraulic slope in the channel with the channel length. This results in the following equation (note that the width is kept separate from the rest of the terms for convenience, since later in this analysis we will seek an optimization of the width):

$$\Delta h_{DC} = \phi_{DC} w_{DC}^{6/7} \quad (20)$$

$$\phi_{DC} = L_{DC} \left[\left(\frac{M_{DC}}{Q_D} \right)^{3/5} h_R \varepsilon_D^{1/\beta} S_R \right]^{10/7}$$

Diversion Outfall Preliminary Design Theoretical Development: Friction Loss in the Receiving Water

Write the energy equation for a differential radial distance dr . Assume the velocity head can be neglected (i.e. assume subcritical flow)

$$h_{RW} = h_{RW} + dh_{RW} + S_{RW} dr \quad (21)$$

Assume Manning's equation is valid, and assume a constant radial distribution of discharge away from the diversion outfall, at a constant spreading angle of θ . Express Manning's equation in terms of the equivalent sand roughness height, after Christensen (1970)

$$Q_D = M_{RW} h_{RW}^{5/3} S_{RW}^{1/2} (2\theta r) \quad (22)$$

$$M_{RW} = \frac{K_n}{n_{RW}} = \frac{8.25\sqrt{g}}{k_{RW}^{1/6}} \quad (23)$$

Combine 21 and 22 and separate the differential values.

$$h_{RW}^{10/3} dh = \frac{-1}{4} \left(\frac{Q_D}{M_{RW} \theta} \right)^2 \frac{1}{r^2} dr \quad (24)$$

Integrate 24 and solve for h_{RW} .

To solve for the integration constant, assume $h_{RW}=h_{RW.0}$ at $r=\infty$. Then, find the solution for $h_{RW.MAX}$ by setting $r = (1/2) w_{DC}$ (the radial location of the diversion channel mouth). This yields the depth at the diversion mouth when the diversion is flowing, which is the maximum depth in the receiving water.

$$h_{RW.MAX} = \left[h_{RW.0}^{13/3} + \frac{13}{6} \left(\frac{Q_D}{M_{RW} \theta} \right)^2 \frac{1}{w_{DC}} \right]^{3/13} \quad (25)$$

Now render 25 dimensionless using convenient dimensionless groups

$$\begin{aligned} H_{RW.MAX} &= \left[1 + \frac{\lambda_{RW}}{w_{DC}} \right]^{3/13} \\ H_{RW.MAX} &= \frac{h_{RW.MAX}}{h_{RW.0}} \\ \lambda_{RW} &= 0.0318 K_{RW.C}^2 K_{RW.F}^{1/3} \\ K_{RW.C} &= \sqrt{\frac{1}{g} \frac{Q_D}{\theta h_{RW.0}^2}} \\ K_{RW.F} &= \frac{k_{RW}}{h_{RW.0}} \end{aligned} \quad (26)$$

Finally, the energy loss associated with the backwater effect in the receiving basin can be expressed as follows:

$$\Delta h_{RW} = h_{RW.0} (H_{RW.MAX} - 1) \quad (27)$$

Diversion Outfall Preliminary Design Theoretical Development: Optimum Diversion Width

We can find the width that minimizes the combined energy loss in the diversion channel and the receiving water by solving for the derivative of the sum of these head losses with respect to the diversion channel width and setting it equal to 0.

$$\frac{d(\Delta h_{DC} + \Delta h_{RW})}{dw_{DC}} = 0 = \frac{d(\Delta h_{DC})}{dw_{DC}} + \frac{d(\Delta h_{RW})}{dw_{DC}} \quad (28)$$

If we substitute the expressions for the head loss given in 20 and 27, differentiate with respect to w_{DC} , and solve for w_{DC} , the resulting equation yields the diversion channel width that minimizes the energy loss for the diversion channel-receiving water system. The equation must be solved by iteration (use a very large value as the first guess for $w_{DC.OPT}$)

$$w_{DC.OPT} = \left[\frac{7}{26} \frac{\lambda_{RW} h_{RW.0}}{\phi_{DC}} \left(1 + \frac{\lambda_{RW}}{w_{DC.OPT}} \right)^{-10/13} \right]^{7/13} \quad (29)$$

Diversion Outfall Preliminary Design Theoretical Development: Optimum Diversion Discharge

If we assume the water discharge and sediment discharge are constant over time, the total volume of sediment discharged by the diversion over its life-cycle is given by this equation:

$$V_{S,D} = C_D Q_D T_D \quad (30)$$

If we assume the rate of change of the depth at the channel outfall is a linear function of time (i.e. the head loss associated with sediment deposition causes a linear increase in the depth) the time T_D in equation 30 can be expressed in terms of the initial depth at the outfall and the critical depth $h_{RW.MAX.CR}$, defined as the maximum depth for which the diversion can pass the design discharge.

$$V_{S,D} = C_D Q_D K_{RW} (h_{RW.MAX.CR} - h_{RW.MAX.I}) \quad (31)$$

$$h_{RW.MAX.CR} = h_{RW.0} + \eta_R - \eta_{RW.0} - \Delta h_{DD} - \Delta h_{ST} - \Delta h_{DC} \quad (32)$$

The optimum discharge can be estimated by taking the derivative of the sediment volume with respect to discharge, and setting it equal to 0.

$$\begin{aligned} \frac{dV_{S.D}}{dQ_D} = 0 = \frac{dC_D}{dQ_D} Q_D K_{RW} (h_{RW.MAX.CR} - h_{RW.MAX.I}) \\ + C_D K_{RW} (h_{RW.MAX.CR} - h_{RW.MAX.I}) - \frac{dh_{RW.MAX}}{dQ_D} C_D K_{RW} Q_D \end{aligned} \quad (33)$$

Recognizing that, for constant Q_D and C_D , $dC_D/dQ_D=0$, and canceling C_D and K_D (which appear in all terms), we get the following equation:

$$(h_{RW.MAX.CR} - h_{RW.MAX.I}) = -\frac{dh_{RW.MAX}}{dQ_D} Q_D \quad (34)$$

Note that the fact that C_D and K_D drop out of the equations means that the optimum discharge is independent of both the concentration of the inflow and the rate of change of the depth in the outfall.

Now, we can render the depth terms dimensionless by dividing through by $h_{RW.O}$.

$$(H_{RW.MAX.CR} - H_{RW.MAX.I}) = -\frac{dH_{RW.MAX.I}}{dQ_D} Q_D \quad (35)$$

Finally, we substitute 26 into 35 for $H_{RW.MAX.I}$, differentiate with respect to Q_D , and solve for $\lambda_{RW.OPT}$.

$$\lambda_{RW.OPT} = w_D \frac{13}{7} \left[H_{RW.MAX.CR} \left(1 + \frac{\lambda_{RW.OPT}}{w_D} \right)^{10/13} - 1 \right] \quad (36)$$

The equation must be solved by iteration. Start with $\lambda_{RW.OPT}=0$. Once $\lambda_{RW.OPT}$ is known, the optimum Q_D can be found by substituting $\lambda_{RW.OPT}$ into 26 and solving for Q_D .

Alternatively, we can solve for $H_{RW.MAX.CR}$ in terms of λ_{RW} and plot a design curve.

$$H_{RW.MAX.CR} = \frac{\left(1 + \frac{7}{13} \frac{\lambda_{RW.OPT}}{w_D}\right)}{\left(1 + \frac{\lambda_{RW.OPT}}{w_D}\right)^{10/13}} \quad (37)$$

Diversion Outfall Preliminary Design Theoretical Development: project life and maximum potential land gain

The first part of this technical note consists of the development of some simple analytic expressions for estimating the terms of the energy budget for a sediment diversion from a river into a receiving water. These relationships establish the estimated energy budget at the onset of diversion operations. However, in order to estimate the expected project life of a diversion, it is necessary to develop an estimate of how the energy budget of the diversion changes over time.

As soon as diversion operations are initiated, the sand transported by the diversion will begin to deposit in the receiving water, generally in the near vicinity of the diversion channel mouth. Eventually, this deposited sand becomes emergent, and a distributary channel network begins to develop.

The evolution and character of these delta networks have been studied by many researchers. But, for this simple analysis, it is only necessary to note the following:

- The diversion channel is designed as a live bed stable channel (i.e. there is no net erosion or deposition of sand in the channel)
- The distributary network is, by definition, a network of channels that distribute the sediment from the diversion channel to the wetland.
- Therefore, the distributary network, however it evolves, should retain roughly the same sediment transport capacity as the diversion channel.
- This capacity diminishes with distance from the head of the distributary delta, due to the fact that some fraction of the sediment being transported is deposited to form the delta.

The increase in the water surface elevation at the diversion mouth is largely determined by the energy loss associated with friction in the distributary channels of the delta. I.e.

$$\Delta h_{DN} = \int_0^{L_{DN}} S_{DN} dl \quad (38)$$

If we assume that the conveyance of the distributary channel network is similar to the conveyance of the diversion channel, then we can assume that the slope of the energy grade for the distributary channel network is approximately equal to the slope of the energy grade line for the diversion channel. Then, can be written more simply as follows:

$$\Delta h_{DN} = S_{DC} L_{DN} \quad (39)$$

If we take the derivative of with respect to time, we can express the rate of change of the head loss in terms of the rate of growth of the distributary network, or, more simply, the distributary channel network length velocity.

$$\frac{d(\Delta h_{DN})}{dt} = S_{DC} \frac{dL_{DN}}{dt} = S_{DC} u_{L,DN} \quad (40)$$

To develop a simple expression for $u_{L,DN}$, we assume that the ratio of $u_{L,DN}$ to the water velocity (u) is equal to the ratio of the rate of sand deposition to the water discharge. If we assume that all of the sand is deposited to form the channel boundary, the rate of sand deposition is just equal to the sediment discharge, converted to units of volumetric deposition. i.e.

$$\frac{u_{L,DN}}{u} = \frac{1}{s(1-p_{SAND})} \frac{Q_S}{Q} = \frac{C_{SAND}}{s(1-p_{SAND})} \quad (41)$$

Note that the ratio of the sediment discharge to the water discharge is just the concentration, so the equation is further simplified to reflect this.

The concentration is at a maximum value at the head of the distributary delta. As sediment is transported into the delta, some fraction of the sediment is deposited to form the delta. If we approximate this delta growth as simply the extension of the diversion channel, it can be shown that the spatial gradient of the concentration can be related to the rate of deposition as follows:

$$uh \frac{dC}{dx} = -s(1-p_{SAND}) \frac{d\eta}{dt} \quad (42)$$

Next, note that the spatial gradient of the concentration can be transformed to a temporal term by invoking the distributary channel network velocity $u_{L,DN}$.

$$\frac{dC}{dx} = \frac{dC}{dt} \frac{dt}{dx} = \frac{dC}{dt} \frac{1}{u_{L,DN}} \quad (43)$$

Combining 41-43, we get the following equation.

$$\frac{h}{C} \frac{dC}{dt} = -\frac{d\eta}{dt} \quad (44)$$

This can be integrated to get the following:

$$C = C_o e^{-\frac{\eta}{h}} \quad (45)$$

Substituting 45 and 40 into 41 yields an expression for $d\eta/dt$.

$$\frac{d\eta}{dt} = \frac{Su}{s(1-p_{SAND})} C_o e^{-\frac{\eta}{h}} \quad (46)$$

This can be integrated with respect to time, with the integration constant defined by noting that $\eta=0$ at $t=0$.

$$\eta_T = h \ln \left(\frac{SuC_o}{hs(1-p_{SAND})} t + 1 \right) \quad (47)$$

Finally, the water velocity can be expressed in terms of the water discharge and the diversion channel dimensions (remember that we are assuming that the total conveyance of the distributary network is relatively constant, and hence the water velocity remains constant throughout the distributary network).

$$\eta_T = h_{DC} \ln \left(\frac{S_{DC} Q_{DC} C_o}{h_{DC}^2 w_{DC} s (1-p_{SAND})} t + 1 \right) \quad (48)$$

The project life can be estimated by setting the displacement at time t equal to the total head available for diversion operations (ie. the net

available energy from the energy budget at the onset of operations) and solving for Δt_{PL} . I.e.

$$\Delta t_{PL} = \frac{h_{DC}^2 W_{DC} S (1 - p_{SAND})}{Q_{DC} S_{DC} C_o} \left(e^{\frac{\Delta h_{NET}}{h_{DC}}} - 1 \right) \quad (49)$$

Finally, the maximum expected surface area of land that can be built over this project life can be estimated by assuming that (a) all of the diverted sediment is used to build land, and (b) all of the land is vegetated as soon as the depth reaches some threshold depth necessary for growth.

Using these assumptions, the maximum land created can be estimated as follows.

$$A_{CL} = \frac{C_{SED} Q_D \Delta t_{PL}}{s (1 - p_{SED}) (h_{RW.o} + h_{RSLR} - h_{PP})} \quad (50)$$

Note that, if it is desired to assume that some fraction of the silt and clay sized sediment does not get retained in the wetland, that can easily be done by simply reducing the contribution of the silt and clay concentrations to both C_{SED} and the estimate of p_{SED} .

Acknowledgements

Linda Crandall proofread and corrected the mathematics in this document. Her contribution is greatly appreciated.

Reference

Christensen, B. A., "Manning's n For Cast-In-Place Concrete Pipe; Discussions by Bent A. Christensen, and R. Sakthivadivel, S. Seetharaman and M.V. Somasundaram", Journal of the Hydraulics Division, Proceedings of the American Society of Civil Engineers, Vol. 96, No. HY3., March, 1970.

Symbols

Subscripts

- I = Initial
- CL = Created land
- D = Diversion
- DC = Diversion Channel

- DD = Drawdown in the River Due to the Diversion
- DN = Distributary Network of Channels in the Delta
- MAX = Maximum
- MSL = Mean Sea Level
- OPT = Optimum
- PP = Primary productivity
- PL = Project Life
- R = River
- RSLR = Relative Sea Level Rise
- RW = Receiving Water
- SAND = property associated with sand sediment classes only
- SED = property associated with all sediment classes (sand, silt, and clay)
- ST = Diversion Structure
- o = Baseline conditions (i.e. without the diversion in operation)

Variables and Parameters

- A = the surface area
- C = the cross-sectional-averaged sediment concentration
- g = the acceleration due to gravity
- h = the water depth
- H = the normalized water depth
- k = the equivalent sand roughness height
- K_n = Manning's constant
- l = length coordinate
- L = the total length of a channel or channels
- n = Manning's n
- p = porosity
- Q = the water discharge
- r = the radial distance away from the diversion into the outfall area
- s = specific gravity
- S = the hydraulic slope
- t = the time coordinate
- T = the total elapsed time
- u = the cross-sectional-averaged velocity
- u_L = the length velocity, or rate at which a distributary channel in a delta extends into the basin

- V_s = the total sediment volume associated with the diversion
- w_{DC} = the width of the diversion channel
- z = the bed elevation
- α = the coefficient in the concentration power law equation
- β = the exponent in the concentration power law equation
- ϵ_D = the sediment diversion efficiency
- ζ = local energy loss coefficient
- η = the water surface elevation
- ρ = the water density
- θ = the spreading angle of the diversion outflow
- τ = the bed shear stress
- ψ = the contraction coefficient
- F_D = the Froude number in the diversion channel

Appendix B: Physics of Diversions

The following document is a summary of the slide presentation associated with a talk given at the Legacy Diversion Workshop at Southeastern Louisiana University, October 6 and 7, 2015.

The Physics of Diversions: The Energy Budget Constraint on Diversion Operation and Design

Gary L Brown
Engineer Research and Development Center
USACE

Diversion Design Based on Volumetric and Geometric Arguments

Several researchers have discussed criteria for designing diversions to optimize land building potential. Some common criteria that emerge from these analyses are:

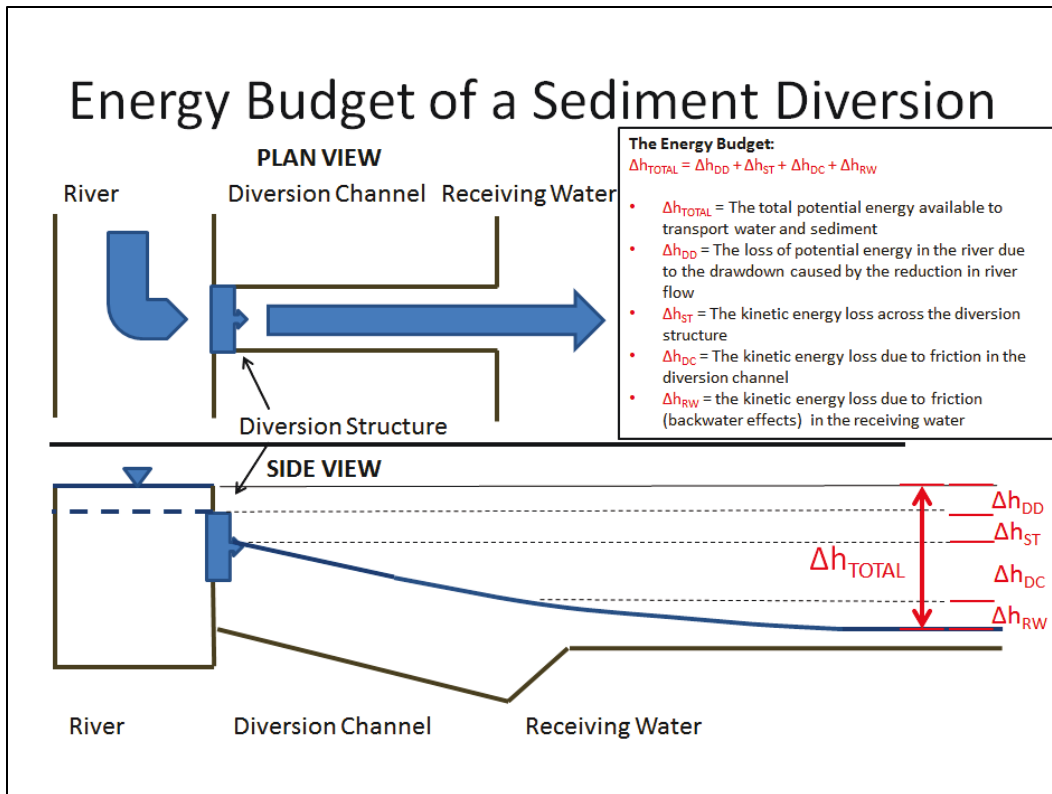
- Large Diversions (e.g. Dean et al., 2014) which maximize the emergent footprint of the diversion deposit
- Sediment (sand) rich diversions, to maximize land building potential and minimize potential downstream deposition in the river (e.g. Brown et al., 2013)
- Diversions into shallow receiving basins, to hasten emergence and maximize the emergent footprint.

Diversion Design Constrained by Physics

However, an examination of energy conservation principles (founded in traditional hydraulics) demonstrates that the energy budget of the diversion acts as a constraint on optimization criteria derived solely from volumetric and geometric arguments.

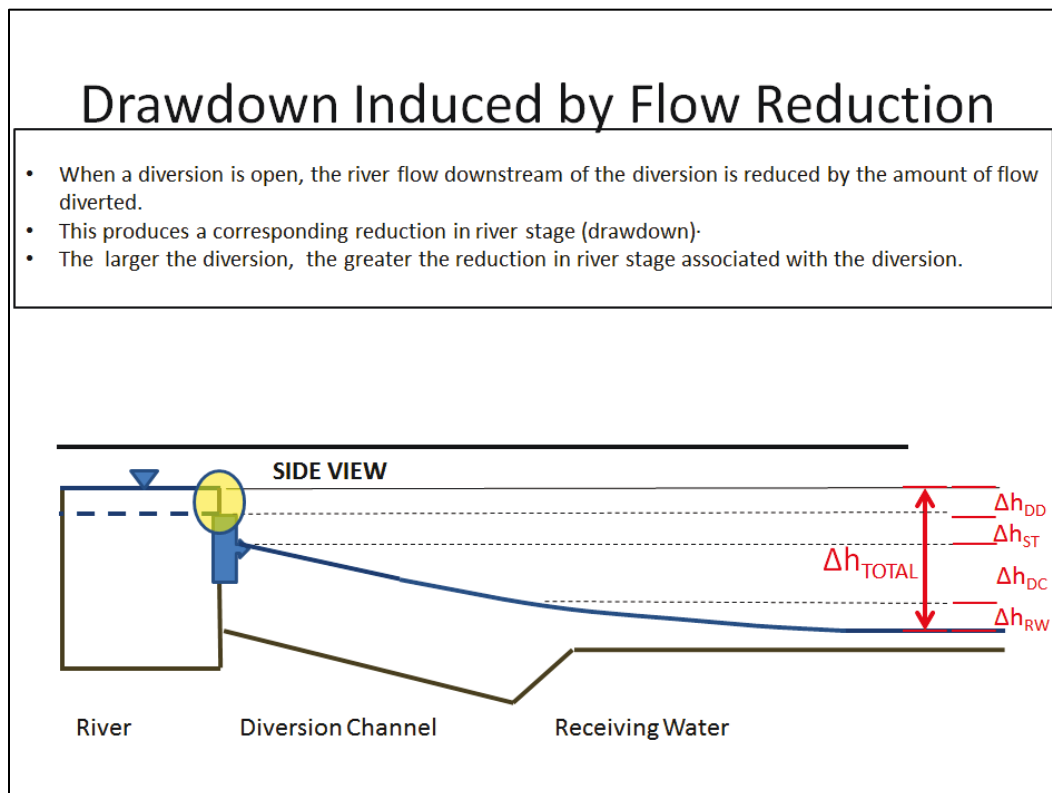
The following figures illuminate the basics of this energy budget and demonstrate how it both bounds what is possible with respect to diversion design and influences the life cycle of crevasse splay deltas.

Energy Budget of a Sediment Diversion



Drawdown Induced by Flow Reduction

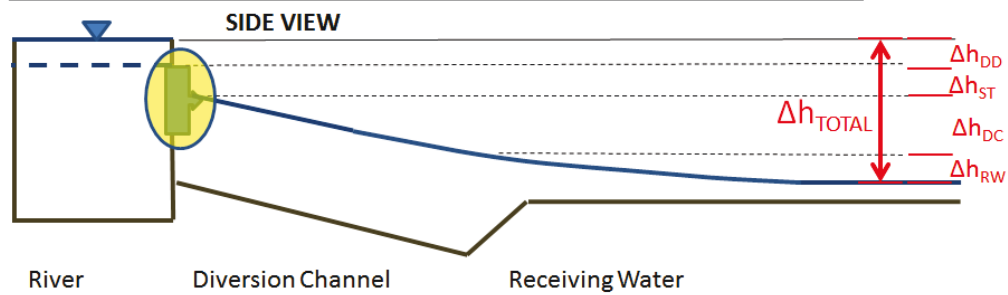
- When a diversion is open, the river flow downstream of the diversion is reduced by the amount of flow diverted.
- This produces a corresponding reduction in river stage (drawdown).
- The larger the diversion, the greater the reduction in river stage associated with the diversion.



Energy Loss at the Diversion Structure

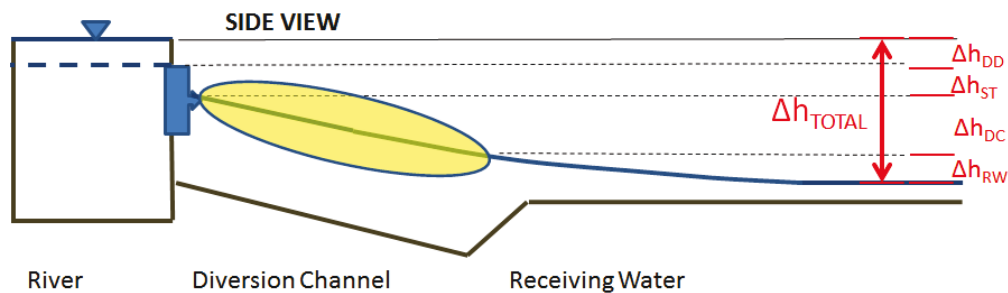
- Energy losses at the diversion structure are typically associated with drag, flow separation, flow contraction, and flow expansion as water passes through the structure
- These losses can be minimized with design specifications that limit their magnitude and number.

$$\Delta h_{ST} = \frac{\zeta_{ST}}{2g} \left(\frac{\psi_{ST} Q_D}{w_{DC} h_{DC}} \right)^2$$



Energy Loss in the Diversion Channel

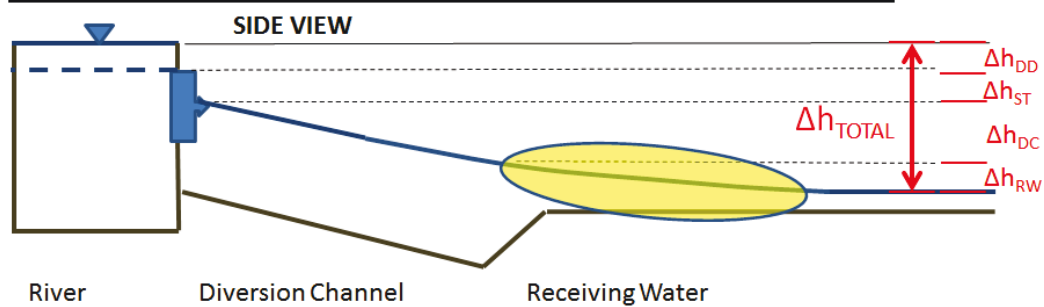
- The diversion channel must be designed with sufficient shear stress to transport the diverted sand.
- Therefore, diversions with higher concentrations of sand require a higher velocity diversion channel than do diversions with lower concentrations of sand.
- This results in more energy loss, or a “steeper” water surface slope in the channel.



Energy Loss in the Channel Receiving Basin

- As water exits the diversion, it forms a jet of water into the receiving basin.
- If the receiving basin is relatively shallow, this exiting water tends to pile up, forming a “dome” of water with a maximum elevation at the channel outfall.
- This “backwater” effect is more pronounced for larger discharges than it is for smaller discharges.
- It is also more pronounced for narrow channels than it is for wide channels

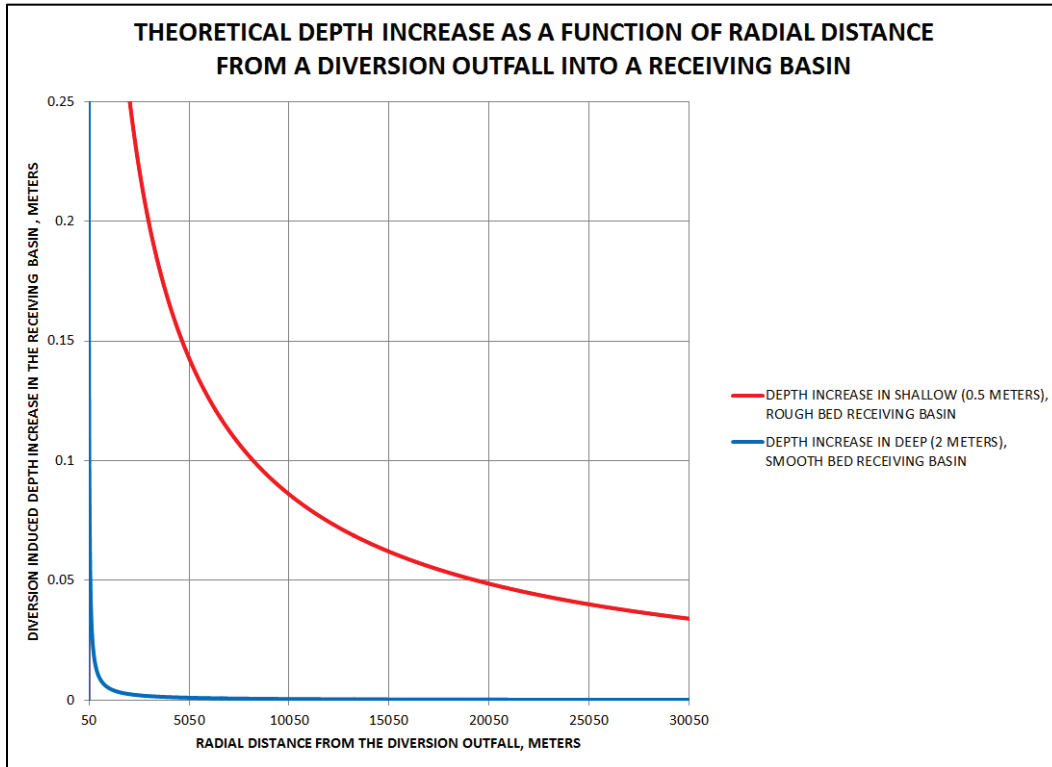
$$h_{RW,r} = h_{RW,0} \left[1 + 0.00492 \left(\frac{Q_D}{h_{RW,0}^2 \sqrt{gr}} \right)^2 \left(\frac{k_{RW}}{h_{RW,0}} \right)^{\frac{1}{3}} \right]^{3/13}$$



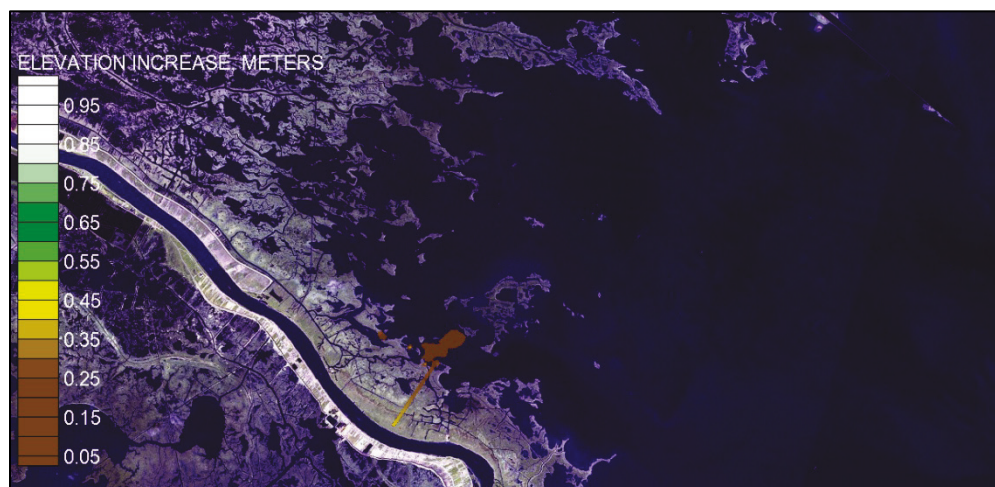
Diversion-induced Inundation in the Receiving Basin. The following figure provides a closer look at the terms that comprise the analytic equation for diversion induced inundation in the receiving basin. This equation is derived from the conservation of mass and energy for radial flow into a receiving basin with uniform depth.

$$h_{RW,r} = h_{RW,0} \left[1 + 0.00492 \left(\frac{Q_D}{h_{RW,0}^2 \sqrt{gr}} \right)^2 \left(\frac{k_{RW}}{h_{RW,0}} \right)^{\frac{1}{3}} \right]^{3/13}$$

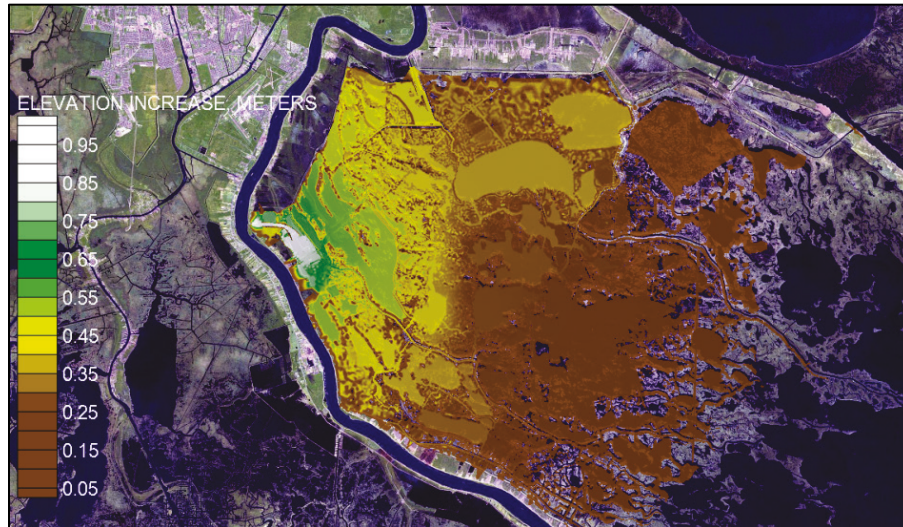
The following plot demonstrates the sensitivity of the depth in the receiving basin to changes in the depth and roughness of the receiving basin.



These theoretical observations are also observed in numerical analysis (see below), and in field observations. Specifically, Snedden et al., (2007) have demonstrated a statistically significant correlation between Caernarvon Discharge (max ~8000 cfs) and water level at a site ~5 km distant from the diversion channel outfall



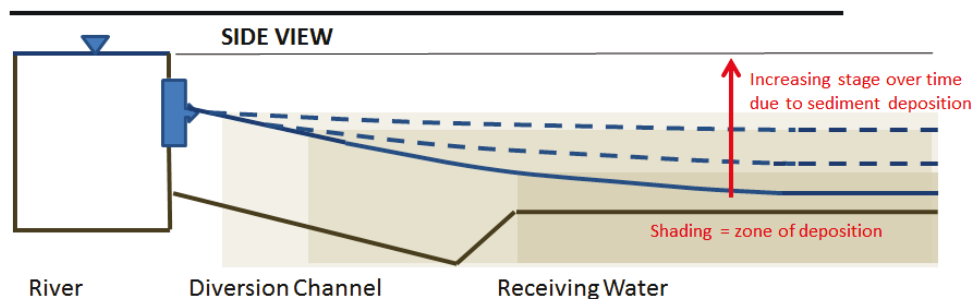
Numerical (AdH) results for inundation associated with diversion discharge (50 kcfs) into a relatively deep (~2m), un-vegetated receiving basin.



Numerical (AdH) results for inundation associated with diversion discharge (35 kcfs) into a relatively shallow (<1m), vegetated receiving basin.

Functional Life of the Diversion

- As time progresses, deposition in the diversion outfall will become emergent land and begin to obstruct flow. This will induce an increase in the water surface elevation at the downstream end, and an upstream extension of the zone of deposition.
- When the water surface elevation increases to the point where the diversion can no longer pass the design flow, the diversion can no longer be operated at full capacity.

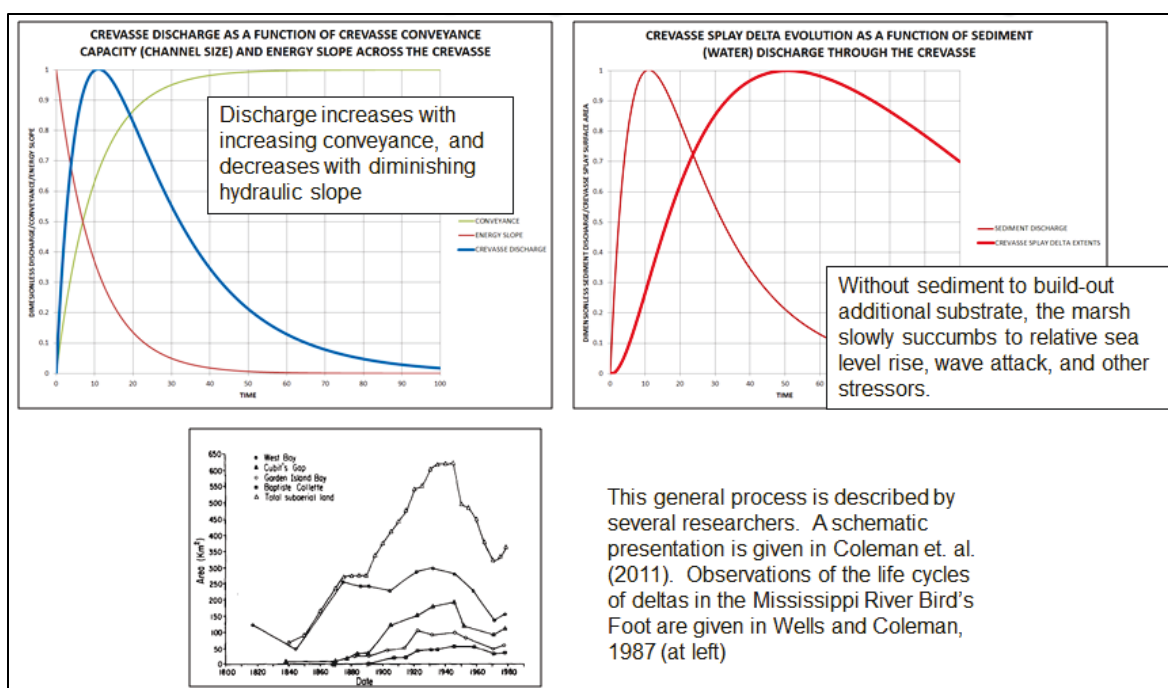


Adjusting Diversion Design to Account for Energy Constraints

We can now revisit the recommendations for diversion design optimization based exclusively on volumetric and geometric considerations and include the influence of the energy constraint.

- Large Diversions maximize the emergent footprint of the diversion deposit.
 - However, they also increase inundation in the outfall (magnitude and extent).
- Sediment (sand) rich diversions maximize land building potential and minimize potential downstream deposition in the river.
 - However, they also require a (hydraulically) steeper channel to convey the sediment to the receiving basin.
 - Also, the deposited sediment will more rapidly increase the downstream water level (due to backwater effects), eventually resulting in a loss of capacity to divert the design discharge
- Diversions into shallow receiving basins hasten emergence and maximize the emergent footprint.
 - However, shallow basins induce greater inundation (magnitude and extent) for a given design discharge

How Energy Principles Influence the Crevasse Splay Delta Life Cycle



Appendix C: Optimization of Diversion Operations

Proposed Optimized Operational Rules for Delta Management Scenario Simulations

Gary L Brown

2/15/16

Objective

The objective of these optimization exercises is to develop a set of operational rules for the Mid Breton and Mid-Barataria diversions that are designed to build as much (or possibly more) land than the original operational rules, while limiting the operational duration (and hence inundation and salinity impacts) to the greatest extent possible. Note that these are not intended to be design level operational rules: these would be much more complex. Rather, this exercise is intended to address one specific question: is it feasible to achieve similar or greater land building capability while significantly reducing inundation and freshwater impacts or would a significant reduction in the duration of operations necessarily result in a significant reduction in land gain.

Constraints

The constraints are given as follows:

- The targeted land gain should be equal to or greater than the land gain associated with the baseline operational rules
- The duration of operations should be limited such that the salinity and inundation impacts are significantly reduced relative to the baseline operational rules.

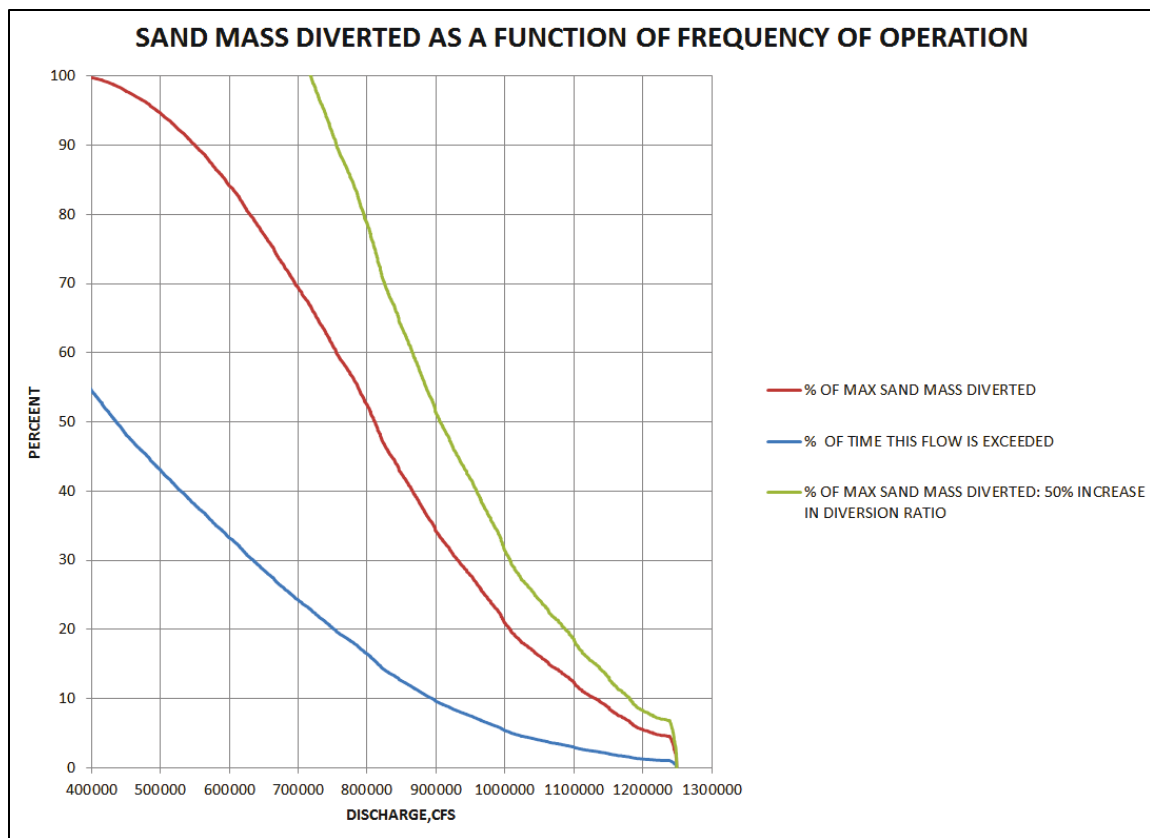
Methodology

The methodology employed in this optimization process is an extension of the methods used by Allison et al. (2013) in their paper on designing diversions to maximize sediment capture. I will refer to this paper in the following discussion.

Diversions of Sand

Figure 1 is an analysis of the sand transport regime at Belle Chasse. A 50-year hydrograph (extracted from the HEC-6T hydrograph) was plotted as a percent exceedance, in order to depict the discharge in terms of the average annual duration for which that discharge is exceeded (the blue curve). Then, the percent exceedance of discharge was integrated against the sand rating curve at Belle Chasse given in Allison et al. (2012) and normalized (the red curve). This shows the fraction of the total sand load that is associated with a river discharge greater than the one selected.

Figure 1. Percent exceedance and Normalized Cumulative Sediment Mass Analysis of Belle Chasse Data.



We can use this plot to investigate the discharge threshold and available sand load associated with a desired average annual operational duration (and, consequently, if we assume that we have a diversion with a diversion ratio that is constant, we can also investigate how much we can divert). For example, from Figure 1, if we decided to operate the diversion for 20% of the year, this corresponds to an operational trigger of 750,000 cfs, and

we can expect to divert about 57% of the total amount of sand we would divert if we left the diversion open at the design discharge all the time.

Note that for the 600,000 cfs threshold (used in the baseline runs) the average duration of operations is 33% of the year, and the fraction of available sand diverted is 84%. If we seek to reduce the duration of operation to about 15% of the year (about a month) we get an operational threshold of 820,000 cfs, but we only divert about 46% of the total sediment load – a dramatic reduction. Hence, we cannot achieve comparable sand diversion volumes with significant reductions in the duration of operations.

However, if we abandon the assumption of a constant diversion ratio, it may be possible to achieve comparable results. The green curve is the fraction of the total sand load diverted, assuming that the diversion ratio for the optimized rules is 50% greater than for the baseline rules. In this case, it can be seen that for an operational threshold of 820,000 cfs, we divert 70% of the total sand load – which is comparable to the baseline operations.

Hence, if we can develop strategies to maximize the operational efficiency of the diversion (with respect to sand transport) we may be able to achieve similar land building capability with much shorter operational duration.

Figure 2 shows the modeled sand concentrations in the Mississippi River and passing through the Mid-Breton Diversion, associated with the first 2 years of the AdH Delta Management simulations. Figures 3 and 4 show the same data plotted against the discharge, in order to illustrate the hysteresis in the sand concentration over the hydrograph.

Several things can be noted from these figures:

- The sand concentration in the Mississippi River varies non-linearly with the discharge
- The diverted sand is more significantly nonlinear, indicating an increased diversion ratio associated with mobilization of the lateral bar
- There is a pronounced hysteresis associated with the river hydrograph. The Mississippi River hydrograph shows elevated concentrations associated with the rising limb. The diversion hydrograph is less clear

but shows a significant rising limb concentration bias near the peak flows.

These observations together indicate that focusing the diversion operations for a shorter duration near the peak of the hydrograph may improve the diversion efficiency in two ways.

1. It will cause the scour of the lateral bar to coincide with the peak sediment discharge in the river, resulting in a maximum diversion ratio
2. The shorter duration will allow more time for the lateral bar to recharge, which should mitigate any multi-year degradation trend for the bar associated with diversion operations.

Figure 2. Sand Concentrations for First 2 Years of AdH Delta Management Simulations.

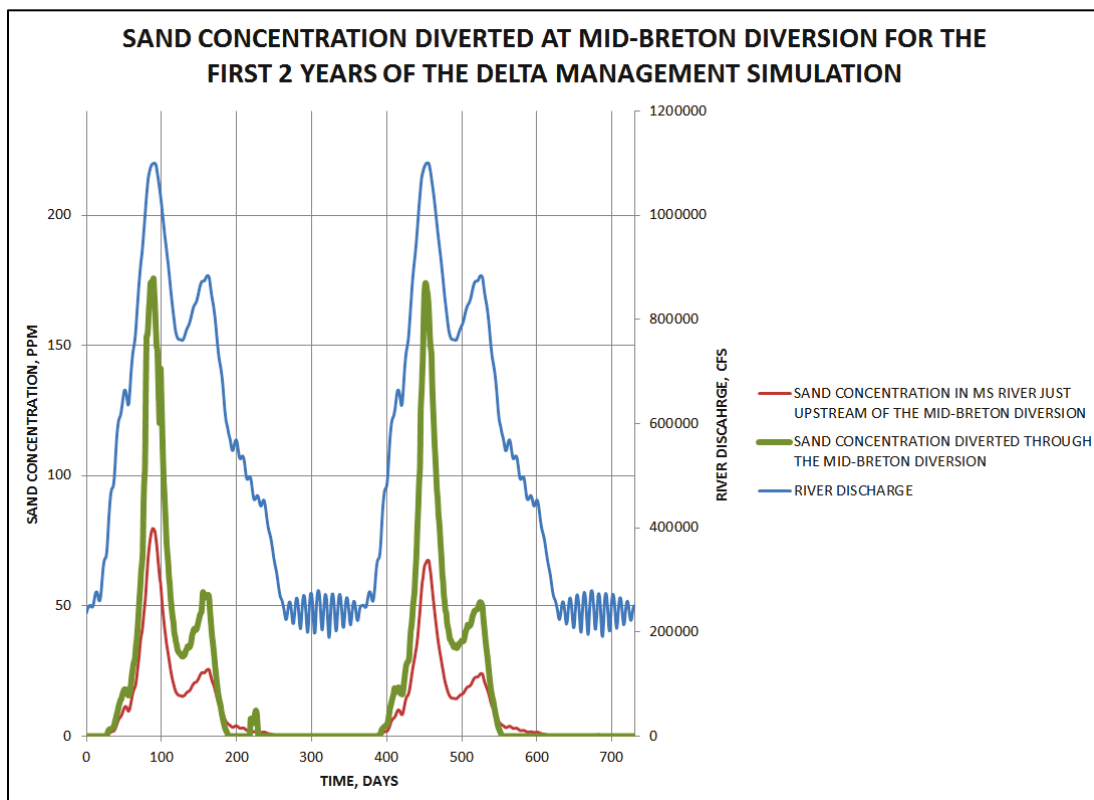


Figure 3. Hysteresis in the Sand Concentration in the Mississippi River.

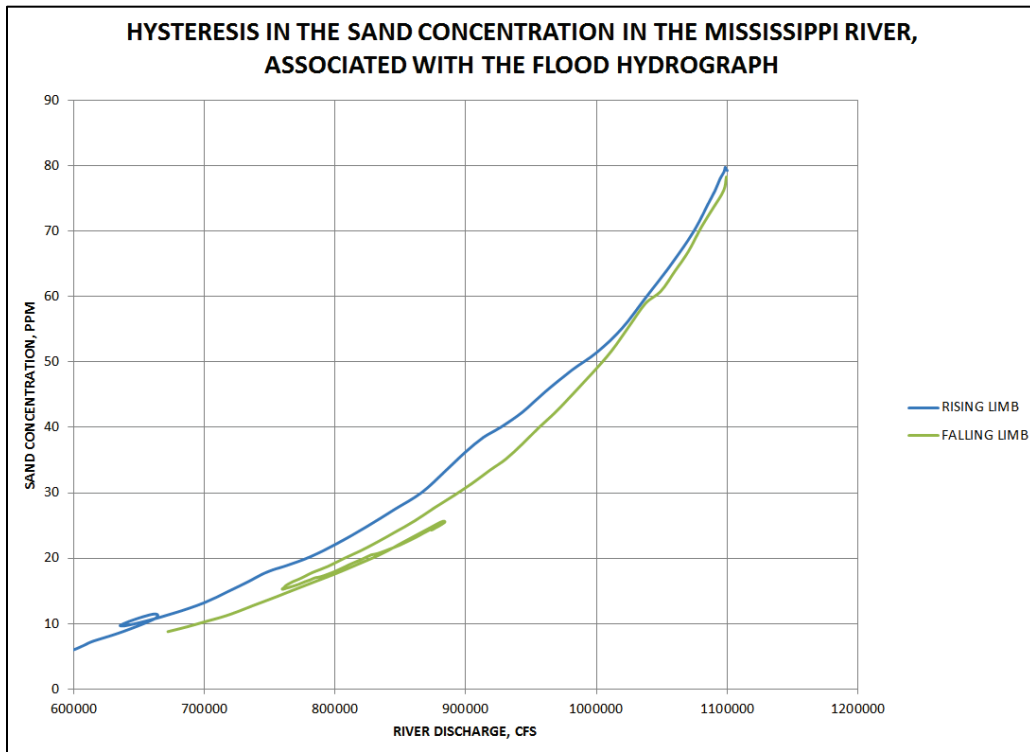
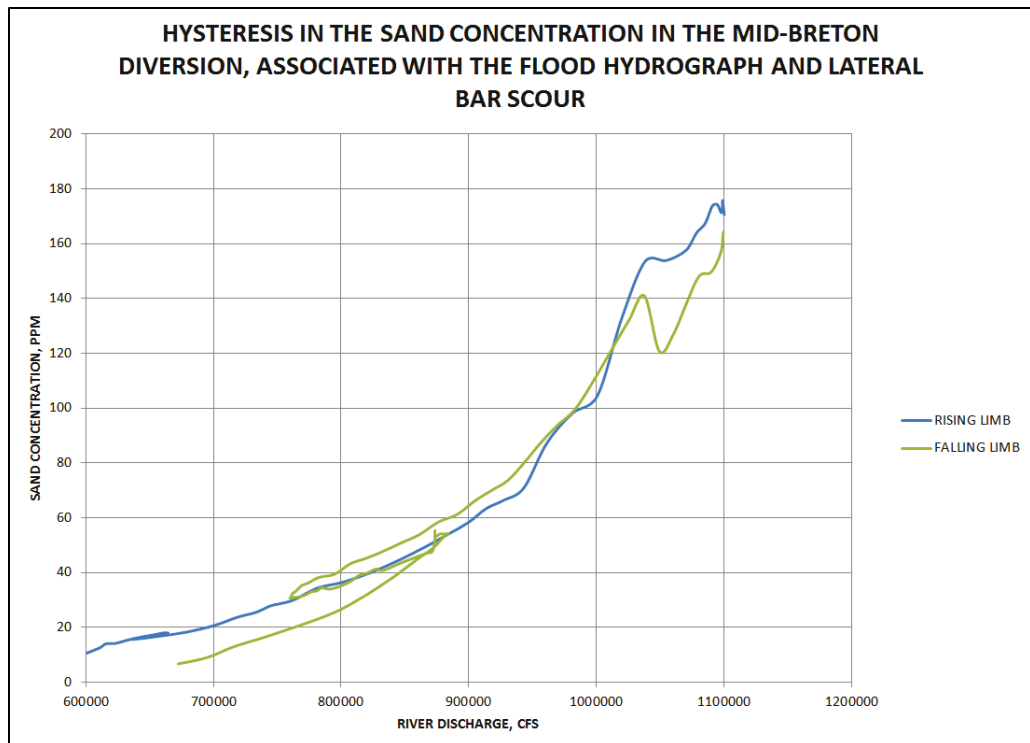


Figure 4. Hysteresis in the Sand Concentration in the Mid-Breton Diversion.



Diversions of Fines

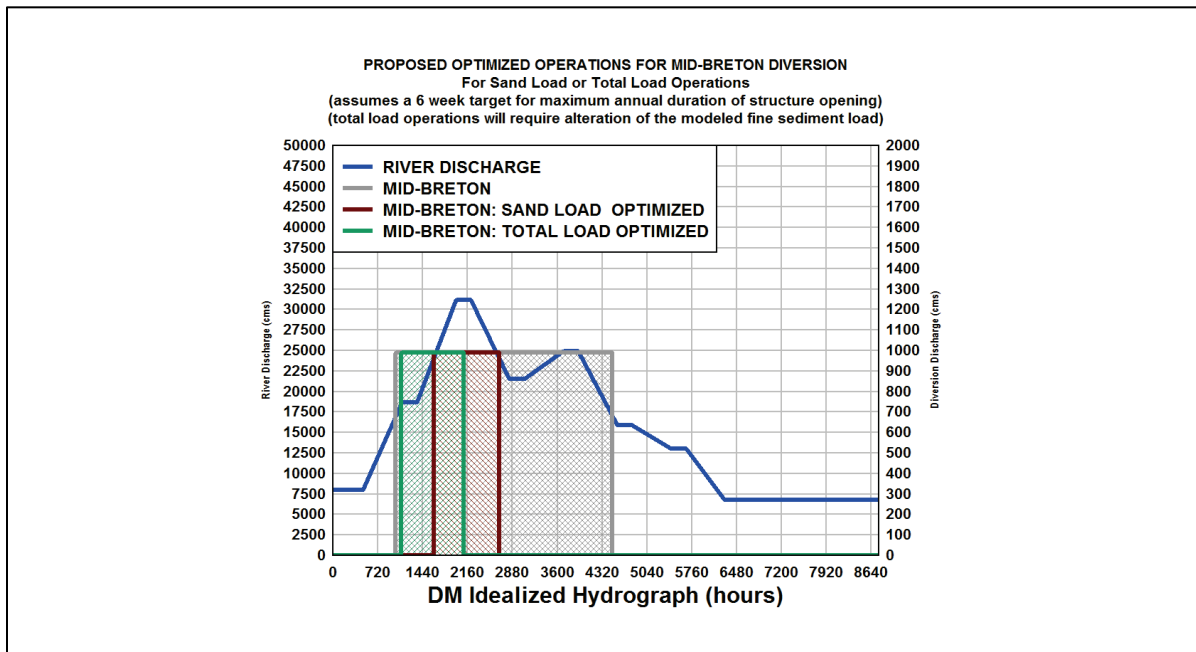
It is not possible to significantly alter the diversion efficiency of fines, so the strategies employed above are not helpful. However, if we recognize that a significant fraction of the fines are transported in the first flush of the sediments associated with the rising limb of the hydrograph, designing operations to capture this first slush should allow us to capture a significant portion of the available fine sediment.

Allison et al. (2013) have shown that the 600,000 cfs threshold is a good indicator of when the first flush of fine sediments are present in the river. Hence, an operational plan that shifts operations to the front side of the hydrograph will be able to capture the first flush of fine sediments, and still take advantage of the high sand transport associated with the rising limb and the peak.

Proposed Optimized Operational Scenarios

In Figure 5, I have presented two proposed operational scenarios: one for sand optimization, and one for sand and fines. For reference, I have also depicted the baseline operational rules (in grey).

Figure 5. Proposed Optimized Diversion Operations.



I assumed a target duration of operations of 6 weeks. This is a somewhat arbitrary duration, based loosely on the analysis of Figure 1.

The sand optimization is designed to initiate operations at 850,000 cfs (again, based loosely on the analysis of Figure 1).

The fines optimization is designed to initiate operations at 600,000 cfs. However, it is shifted somewhat to the right to ensure that at least half of the peak discharge is included in the operational window.

The selection of which operational plan to investigate is up to the PDT. However, it should be noted that, if we choose to investigate the total load optimization, we must design a revised fine sediment inflow hydrograph for our model runs, to include a first flush peak.

Appendix D: SEDLIB-VEG Cohort Analysis: Influence of Vegetation Species Switching on Inundation Response in the Breton and Barataria Basins and the Birdsfoot

Gary L Brown

06/20/16

Introduction

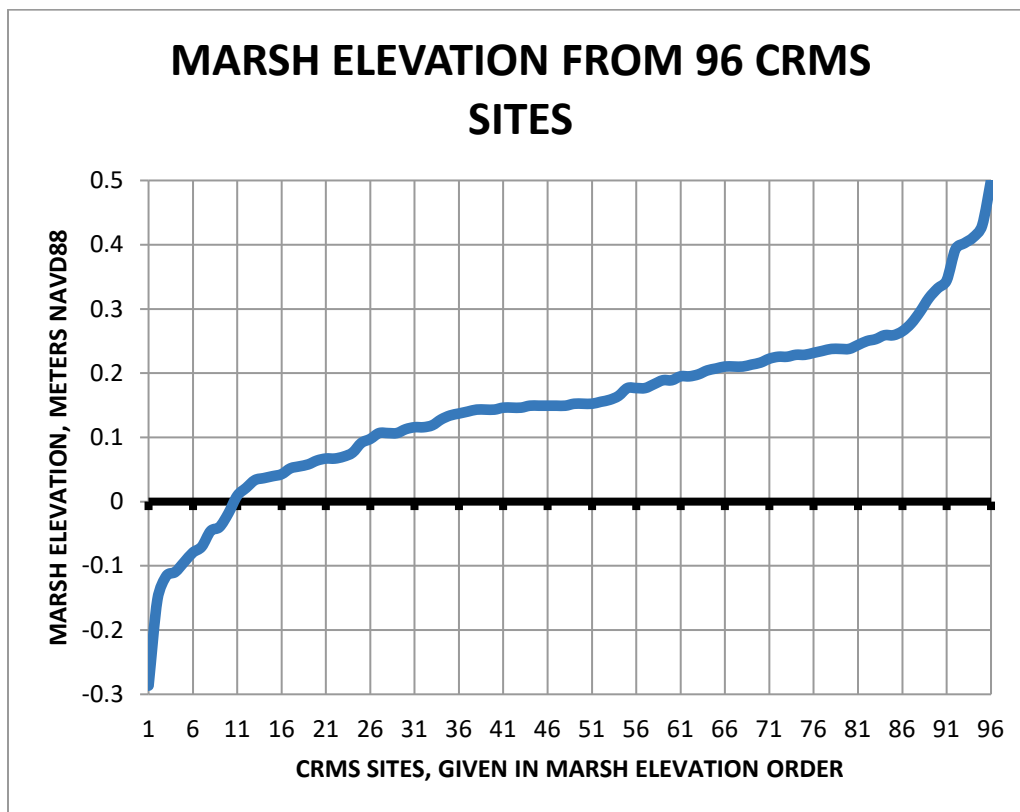
In order to investigate the sensitivity of SEDLIB-VEG results to various perturbations in the parameters that inform the model, it is useful to select a “cohort” of locations within the domain and perform SEDLIB-VEG simulations at each of these locations.

For this analysis, a cohort consisting of 96 CRMS marsh observation stations within Breton and Barataria basins and the Birdsfoots were selected. The number of cohort points was then tripled to 288 sites, by generating duplicate sets of points with elevation +/- 0.01 m. These points were analyzed for various perturbations of the parameters that determine the primary productivity of the vegetation. This analysis was then used to develop a set of indices that can be used to evaluate the relative influence of species switching on model results.

Methods

The elevation of the marsh surface for of each of the 96 CRMS stations used in this analysis are given as a hypsometric plot in Figure 1.

Figure 1. Hypsometric Plot of Marsh Elevation for each CRMS site.



Each of these stations were subjected to 60 years of analysis (2010-2070, assuming spinup in the first 10 years). A time varying water surface elevation boundary condition was applied. This water surface elevation boundary condition consisted of 3 superimposed parts:

- Annual variation
- Relative Sea Level Rise (assuming an average subsidence rate of 5 mm/yr, and ESLR acceleration given by NRCI).
- Diversion induced inundation (for the with-project simulations only: based on the base operations from the Delta Management simulations)

The initial water surface elevation (in 2010) is estimated from CRMS data.

Figure 2 depicts the first 5 years of this applied boundary condition, showing the difference between the with-project and without-project conditions (for this Figure, the 0.1m inundation case is shown). Figure 3 shows the applied boundary condition for the entire 60 years of simulation time.

Figure 2. Applied Water Surface Elevation Boundary Condition: First 5 years.

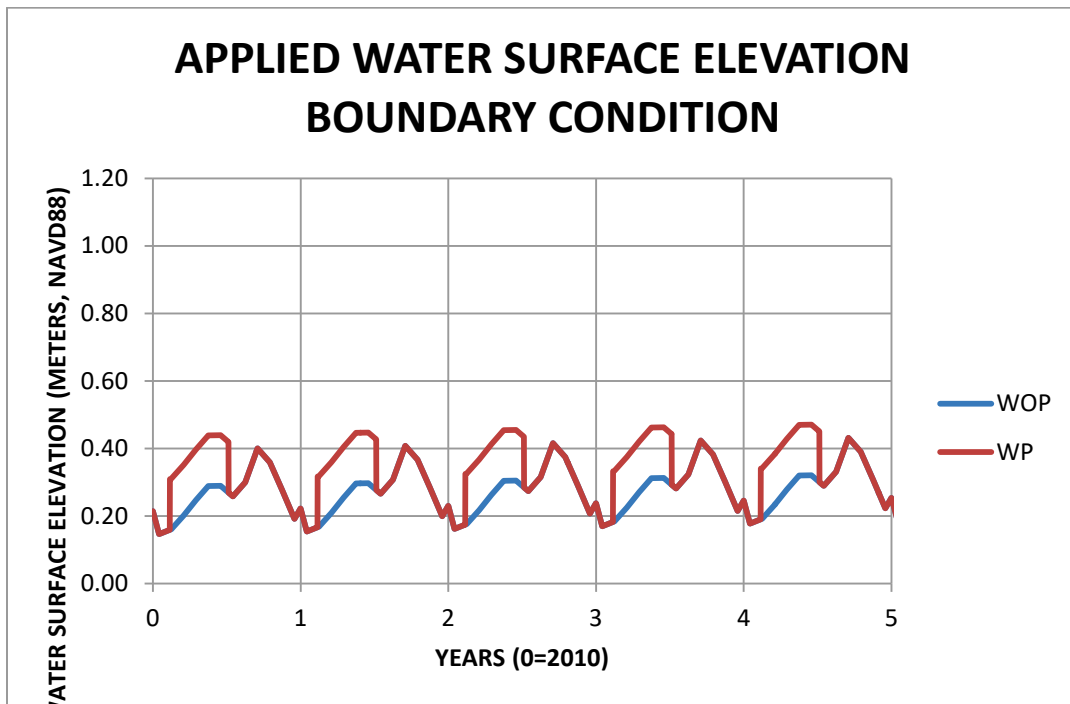
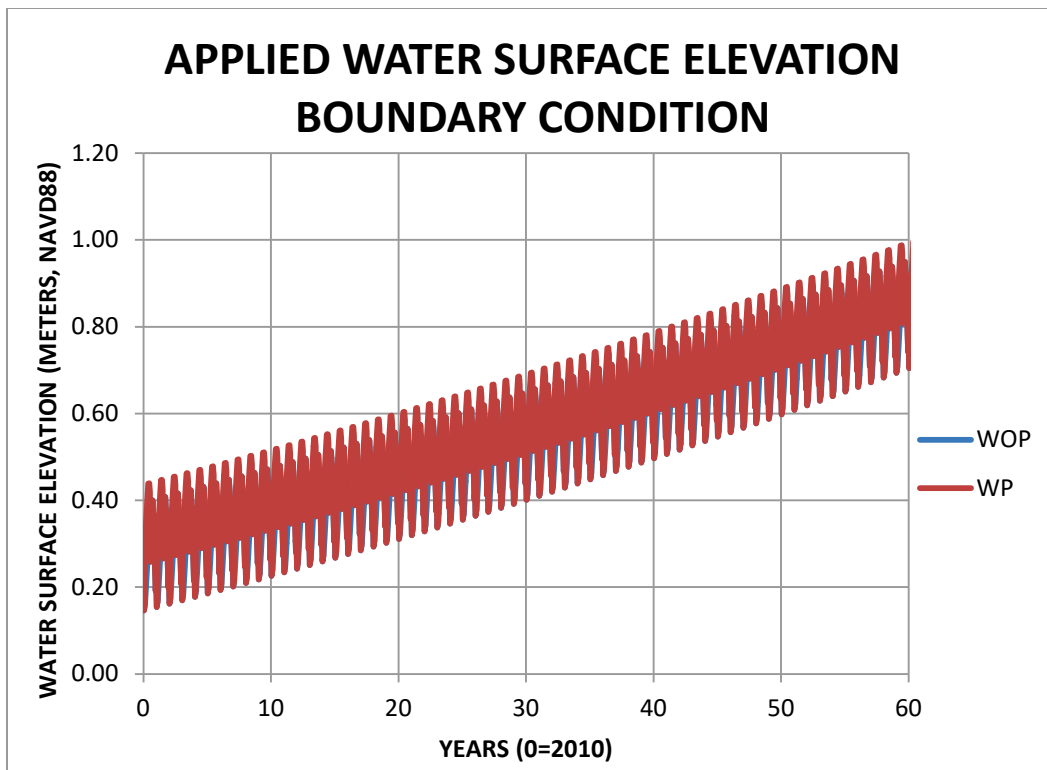


Figure 3. Applied Water Surface Elevation Boundary Condition: entire model simulation duration



The local depth is computed at each time-step within the model. It is computed using the following equation:

$$h = \eta - (z + \Delta) \quad (1)$$

where h is the depth, η is the water surface elevation, z is the initial bed elevation, and Δ is the cumulative bed displacement.

In order to investigate the influence of vegetation species switching on the model results, a series of simulations were conducted for which the parameters that influence marsh productivity were subjected to perturbation. Each of these simulations was conducted for both with project and without project conditions.

The three parameters that are perturbed for this exercise are given in the following equation, which is the equation in SEDLIB-VEG responsible for determining the aboveground productivity of the vegetation:

$$v_{src} = v_{src.m} \left(1 - \frac{h}{h_{ldep}} \right) : 0 \leq h \leq h_{ldep} \quad (2)$$

Where v_{src} is the aboveground productivity, $v_{src.m}$ is the maximum above ground productivity, h is the depth, and is the h_{ldep} limiting depth for vegetation growth.

Table 1 gives all of the simulations used for this analysis. Note that each of these is simulated for both with and without project conditions.

Table 1. Matrix of Sensitivity Simulations for Vegetation Aboveground Productivity Parameters.

Simulation	h_{ldep} (m)	$v_{src.m}$ ($g\ m^{-2}\ yr^{-1}$)	Diversion induced inundation (m)
1	0.2	1261	0.05
2	0.4	1261	0.05
3	0.6	1261	0.05
4	0.2	946	0.05
5	0.4	946	0.05
6	0.6	946	0.05
7	0.2	631	0.05

Simulation	h_{dep} (m)	$V_{src,m}$ ($g\ m^{-2}\ yr^{-1}$)	Diversion induced inundation (m)
8	0.4	631	0.05
9	0.6	631	0.05
10	0.2	1261	0.1
11	0.4	1261	0.1
12	0.6	1261	0.1
13	0.2	946	0.1
14	0.4	946	0.1
15	0.6	946	0.1
16	0.2	631	0.1
17	0.4	631	0.1
18	0.6	631	0.1
19	0.2	1261	0.15
20	0.4	1261	0.15
21	0.6	1261	0.15
22	0.2	946	0.15
23	0.4	946	0.15
24	0.6	946	0.15
25	0.2	631	0.15
26	0.4	631	0.15
27	0.6	631	0.15
28	0.2	1261	0.2
29	0.4	1261	0.2
30	0.6	1261	0.2
31	0.2	946	0.2
32	0.4	946	0.2
33	0.6	946	0.2
34	0.2	631	0.2
35	0.4	631	0.2
36	0.6	631	0.2

Results

The simulations were performed for with and without project conditions. The simulations were performed for 60 years (2010-2070). For each

simulation, the total number of marsh locations that are classified as land in 2070 was recorded. The criteria used to classify a location as land is the same criteria that has been selected for the Delta Management simulations: i.e. a marsh elevation threshold is established and indexed to ESLR, and any location with an elevation greater than the marsh elevation threshold (for that year) is assumed to be land. Using these criteria, the marsh elevation threshold for 2010 is 0 m NAVD88, and for 2060 is 0.264 m NAVD88.

Table 2 gives the results for both the with and without project simulations. For reference, the simulation number and relevant parameters are given as well. The results are given as the number of marsh locations that are defined as land in 2070.

For each simulation, the initial number of marsh locations that are defined as marsh is 277, out of a total of 288 locations evaluated.

Table 2. Results of Sensitivity Simulations (NOTE: initial number of land locations = 277).

Simulation	h_{dep} (m)	$V_{src,m}$ ($g\ m^{-2}\ yr^{-1}$)	Diversion induced inundation (m)	WOP – number of land locations	WP- number of land locations
1	0.2	1261	0.05	150	125
2	0.4	1261	0.05	231	221
3	0.6	1261	0.05	262	260
4	0.2	946	0.05	124	116
5	0.4	946	0.05	213	202
6	0.6	946	0.05	255	250
7	0.2	631	0.05	106	93
8	0.4	631	0.05	176	157
9	0.6	631	0.05	216	213
10	0.2	1261	0.1	150	117
11	0.4	1261	0.1	231	214
12	0.6	1261	0.1	262	258
13	0.2	946	0.1	124	104
14	0.4	946	0.1	213	192
15	0.6	946	0.1	255	243

Simulation	h_{dep} (m)	$V_{src,m}$ ($g\ m^{-2}\ yr^{-1}$)	Diversion induced inundation (m)	WOP – number of land locations	WP- number of land locations
16	0.2	631	0.1	106	85
17	0.4	631	0.1	176	139
18	0.6	631	0.1	216	208
19	0.2	1261	0.15	150	111
20	0.4	1261	0.15	231	208
21	0.6	1261	0.15	262	256
22	0.2	946	0.15	124	97
23	0.4	946	0.15	213	184
24	0.6	946	0.15	255	234
25	0.2	631	0.15	106	78
26	0.4	631	0.15	176	128
27	0.6	631	0.15	216	200
28	0.2	1261	0.2	150	108
29	0.4	1261	0.2	231	199
30	0.6	1261	0.2	262	253
31	0.2	946	0.2	124	95
32	0.4	946	0.2	213	169
33	0.6	946	0.2	255	226
34	0.2	631	0.2	106	75
35	0.4	631	0.2	176	123
36	0.6	631	0.2	216	192

Synthesis of Results: Vegetation Species Switching Index (VSSI)

It is useful to present these results as an index, normalized by the results associated with the parameters that have been used in the AdH Delta Management Model. This index can be used to estimate the effects of species switching on inundation induced land loss.

For this analysis, it is assumed that the parameters used in the Delta Management model characterize the species that are currently in the marsh, and also characterize the species that will be in the marsh in the future without project condition (i.e., there is no species switching over time without the influence of the project). Hence this index estimates how

species switching induced by diversions will impact the response of the wetlands to inundation, relative to how those same wetlands respond to inundation without species switching.

The Vegetation Species Switching Index (VSSI) is calculated as follows:

$$VSSI_n = \frac{N_{L.WP.n} - N_{L.WOP.ADH-DM}}{N_{L.WP.ADH-DM} - N_{L.WOP.ADH-DM}} \quad (3)$$

Where N_L is the number of land locations, and the subscript ADH-DM indicates results using the parameters that have been used in the ADH-DM modeling (i.e the parameters associated with simulations 1, 10, 19, and 28).

So, for example, the VSSI for simulation 5 is: $(202-150)/(125-150) = -2.08$.

A VSSI greater than 1 indicates more inundation wetland loss, a value less than 1 indicates less. A negative value (as seen above) indicates that the influence of species switching results in a net increase in land over the without project condition (i.e. the species switching saves land that would otherwise have been lost without the project).

The results are given in Figures 4-7. Figure 4 represents the results for simulations 1-9, Figure 5 represents the results for simulations 10-18, Figure 6 represents the results for simulations 19-27, and Figure 7 represents the results for simulations 28-36.

Figure 4. VSSI results for inundation depth = 0.05 m.

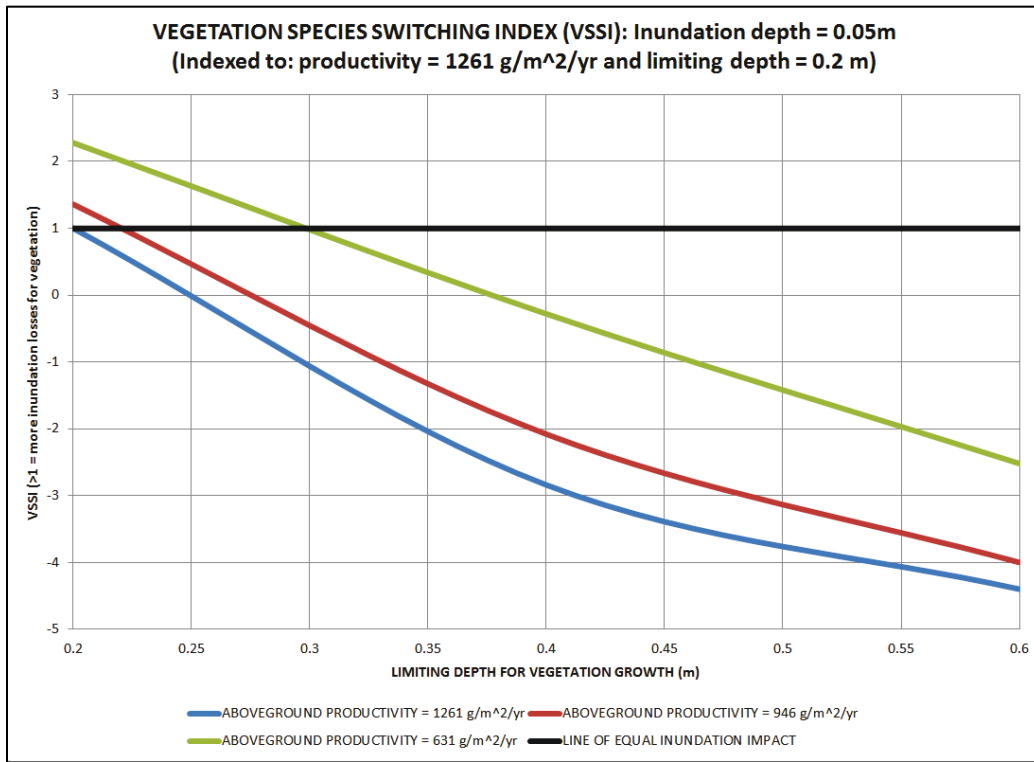


Figure 5. VSSI results for inundation depth = 0.1 m

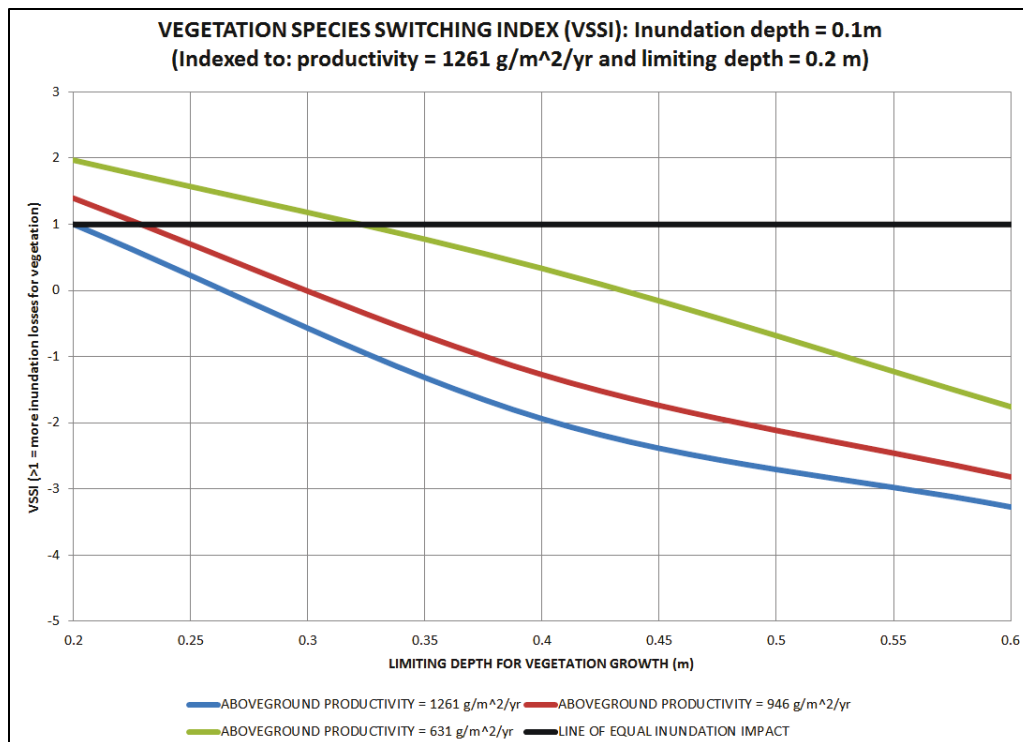


Figure 6. VSSI results for inundation depth = 0.15 m.

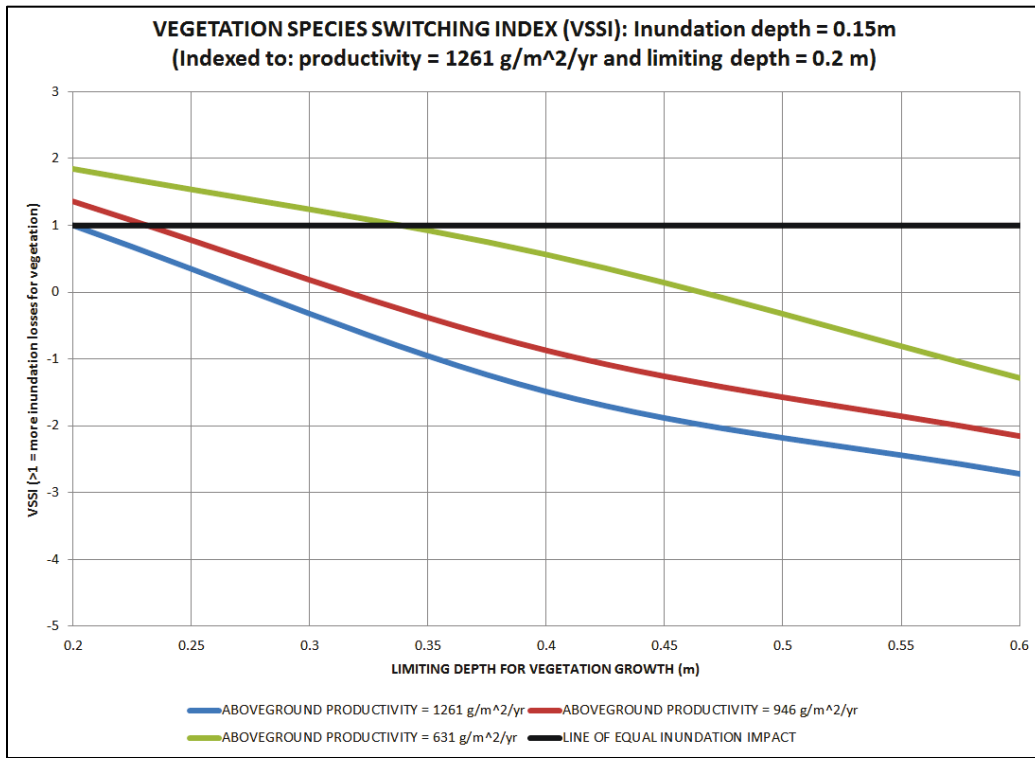
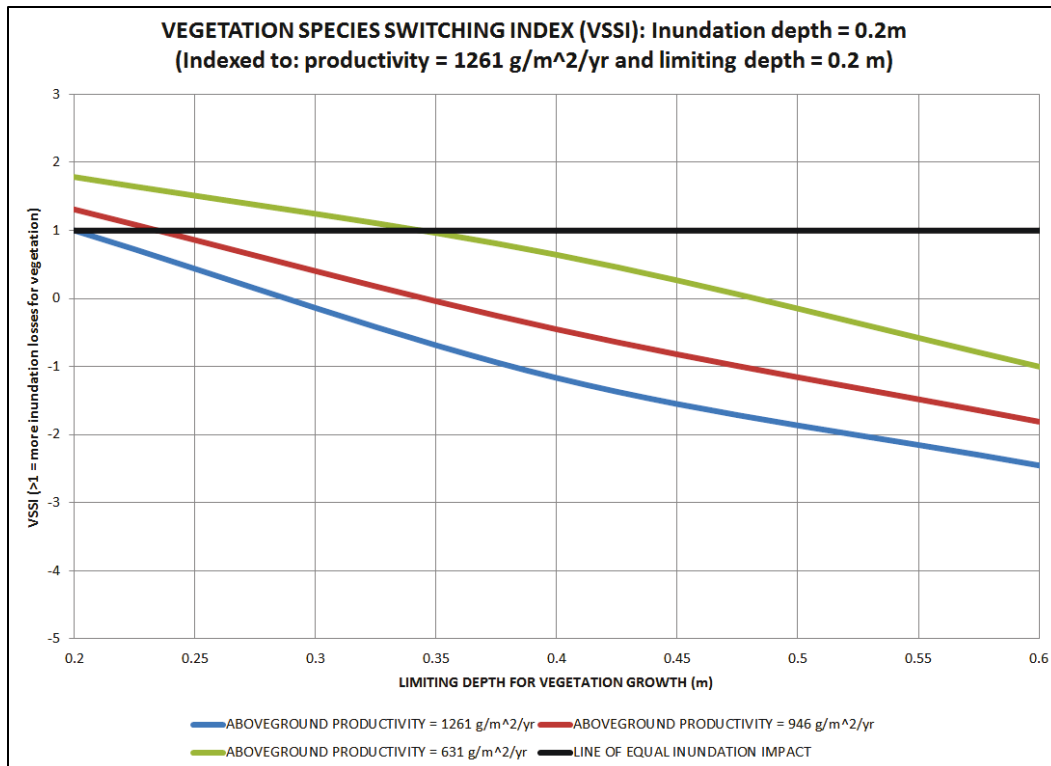


Figure 7. VSSI results for inundation depth = 0.2 m.



The results indicate that the dominant parameter in determining the sensitivity of the vegetation to inundation is the limiting depth parameter. This means that if the species switch to a vegetation type that is more inundation tolerant, there is a high likelihood that the inundation impacts will be significantly mitigated. This is true even if the aboveground productivity of the new vegetation type is significantly less than the productivity of the existing type.

It should be noted that this analysis is gross in nature and is intended to be a first estimate of how species switching might influence inundation losses. For example, there is no time lag for species switching in this analysis, and any such time lag could mitigate the benefits of species switching. Also, belowground productivity has not been considered (i.e. the root-to-shoot ratio was not perturbed in this analysis) and it is the combination of aboveground and belowground productivity that is ultimately responsible for the accretion of the marsh surface.

Further steps in using this analysis might include the following:

- Develop a projected species density and distribution model (or estimates) and calculate spatially averaged values of the vegetation parameters as they change over time.
- Using these values, reference the VSSI plots given above (or create new ones) to generate better estimates of the potential impacts on land loss.
- Using these analyses, select a set of parameters (possibly time varying) that can be used in an AdH-DM simulation, to determine sensitivity to changes in vegetation.

This procedure would allow for an investigation of the potential influence of vegetation switching on the modeled results, by using the SEDLIB cohort model and VSSI indices to refine the sensitivity runs to be used in AdH-DM.

REPORT DOCUMENTATION PAGE

*Form Approved
OMB No. 0704-0188*

The public reporting burden for this collection of information is estimated to average 1 hour per response, including the time for reviewing instructions, searching existing data sources, gathering and maintaining the data needed, and completing and reviewing the collection of information. Send comments regarding this burden estimate or any other aspect of this collection of information, including suggestions for reducing the burden, to Department of Defense, Washington Headquarters Services, Directorate for Information Operations and Reports (0704-0188), 1215 Jefferson Davis Highway, Suite 1204, Arlington, VA 22202-4302. Respondents should be aware that notwithstanding any other provision of law, no person shall be subject to any penalty for failing to comply with a collection of information if it does not display a currently valid OMB control number.
PLEASE DO NOT RETURN YOUR FORM TO THE ABOVE ADDRESS.

1. REPORT DATE March 2019		2. REPORT TYPE Final Report		3. DATES COVERED (From - To)	
4. TITLE AND SUBTITLE Mississippi River Hydrodynamic and Delta Management Study: Delta Management Modeling; AdH/SEDLIB Multi-Dimensional Model Validation and Scenario Analysis Report				5a. CONTRACT NUMBER	
				5b. GRANT NUMBER	
				5c. PROGRAM ELEMENT NUMBER	
6. AUTHOR(S) Gary L. Brown, Jennifer N. McAlpin, Kimberly C. Pevey, and Phu V. Luong, Cherie R. Price, and Barbara A. Kleiss				5d. PROJECT NUMBER 142871	
				5e. TASK NUMBER	
				5f. WORK UNIT NUMBER	
7. PERFORMING ORGANIZATION NAME(S) AND ADDRESS(ES) (see reverse)				8. PERFORMING ORGANIZATION REPORT NUMBER ERDC/CHL TR-19-2	
9. SPONSORING/MONITORING AGENCY NAME(S) AND ADDRESS(ES) U.S. Army Corps of Engineers, New Orleans District 7400 Leake Ave. New Orleans, LA 70118				10. SPONSOR/MONITOR'S ACRONYM(S) USACE MVN	
				11. SPONSOR/MONITOR'S REPORT NUMBER(S)	
12. DISTRIBUTION/AVAILABILITY STATEMENT Approved for public release; distribution is unlimited.					
13. SUPPLEMENTARY NOTES					
14. ABSTRACT This report details the process of developing and validating a multi-dimensional hydrodynamic, salinity, sediment transport, and coastal wetland morphology model of the Lower Mississippi River Delta. This model has been developed to run various sediment diversion scenarios. The results of these scenario analyses are documented in this report. The morphologic modeling results for the diversion scenario analyses show net land gain in the near vicinity of the diversion outlets and net land loss farther away from the outlets. The areas of land gain roughly correspond with the zones of sand deposition whereas the areas of largest land loss correspond with areas where there is diversion-induced inundation but not significant deposition of sediment from the diversion. The modeling results indicate that diversion-induced inundation results in a reduction in plant productivity, which induces an acceleration of land loss. Significant uncertainty exists with respect to the response of the existing wetland vegetation to diversion-induced inundation. The magnitude of this uncertainty can only be narrowed with further consensus building within wetland science. With respect to salinity, the receiving waters tend to freshen significantly during diversion operations. However, when operations cease, the recovery of salinity is almost entirely determined by prevailing offshore and/or riverine conditions.					
15. SUBJECT TERMS Geomorphology, Hydrodynamic—Models, River engineering—Mississippi River Delta (La.) Deltas Salinity Reserve (La.) Mexico, Gulf of, Sediment transport, Wetland hydrology, Wetlands					
16. SECURITY CLASSIFICATION OF:			17. LIMITATION OF ABSTRACT	18. NUMBER OF PAGES	19a. NAME OF RESPONSIBLE PERSON
a. REPORT	b. ABSTRACT	c. THIS PAGE			Gary L. Brown
Unclassified	Unclassified	Unclassified	SAR	172	19b. TELEPHONE NUMBER (Include area code) 601-634-4417

7. PERFORMING ORGANIZATION NAME(S) AND ADDRESS(ES)
(continued)

Coastal and Hydraulics Laboratory
U.S. Army Engineer Research and Development Center
3909 Halls Ferry Road
Vicksburg, MS 39180-6199

USACE New Orleans District
7400 Leake Ave.
New Orleans, LA 70118

USACE Mississippi Valley Division
1400 Walnut Street
Vicksburg, MS 39180